Chapter 10: Superconductivity

References:

1. C. Kittel ; Introduction to solid state physics
2. M. Tinkham: Introduction to superconductivity
3. Paul Hansma, Tunneling Spectroscopy

Table of Contents

Periodic Table of Superconductivity

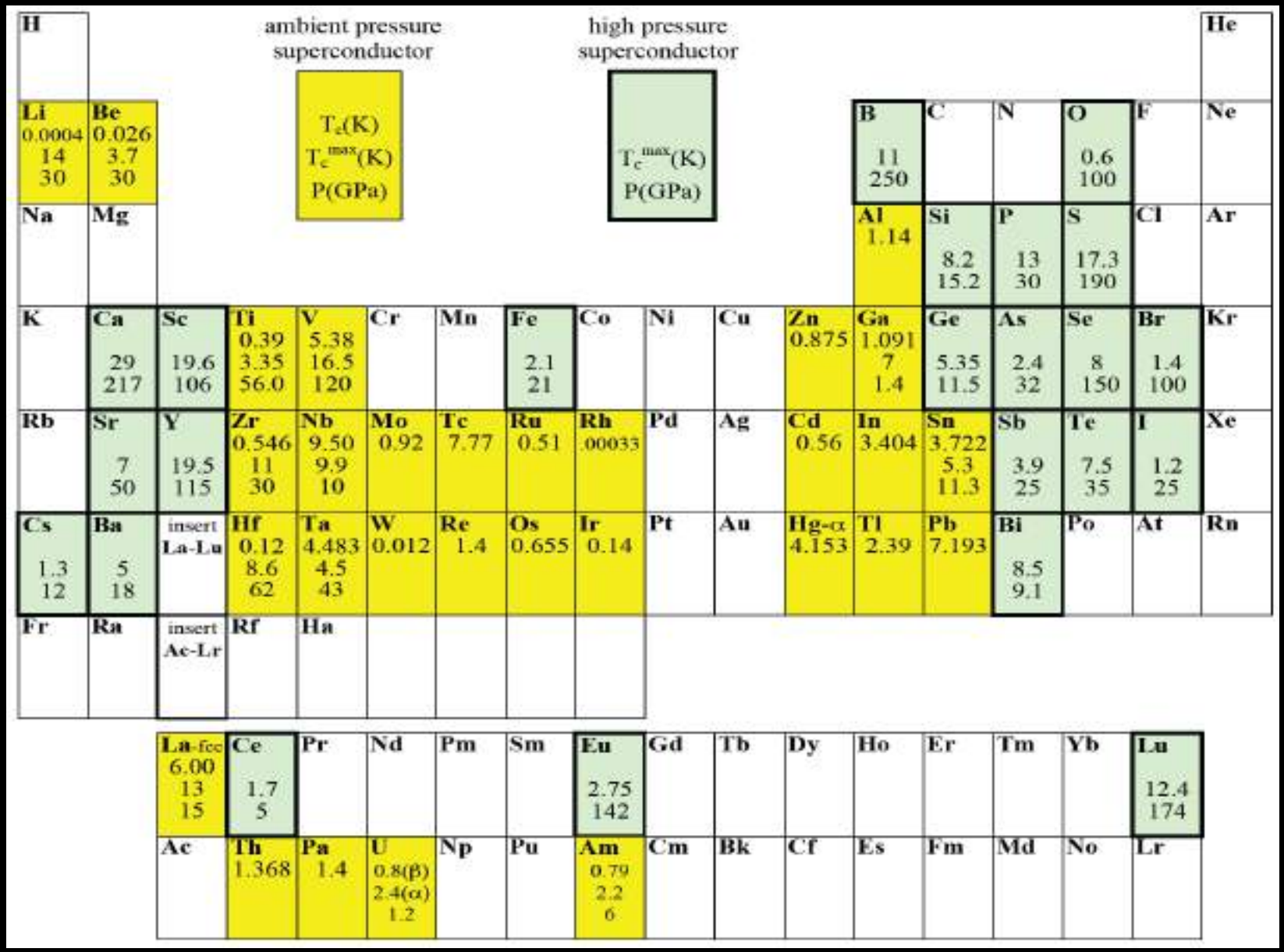

M. Debessai *et al.*, J. Phys.: Conf. Series 215, 012034 (2010).

Experimental Survey of Superconductivity Phenomenon

Helium Liquefaction in 1908

July 10, 1908

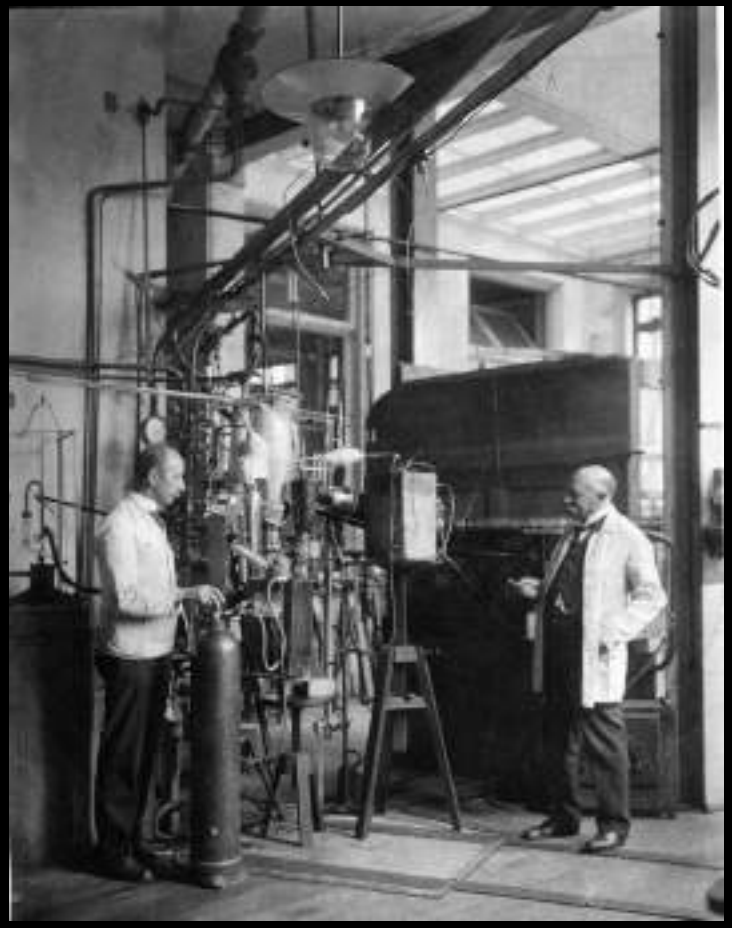

© LeidenInstitute of Physics

Heike Kamerlingh Onnes

Nobel Prize, 1913

"Door meten tot weten"
(Knowledge through measurement)

WHAT IS A SUPERCONDUCTOR?

1. **Zero resistance**
2. **Complete expulsion of magnetic flux**

Discovery of Superconductivity in 1911

April 8, 1911

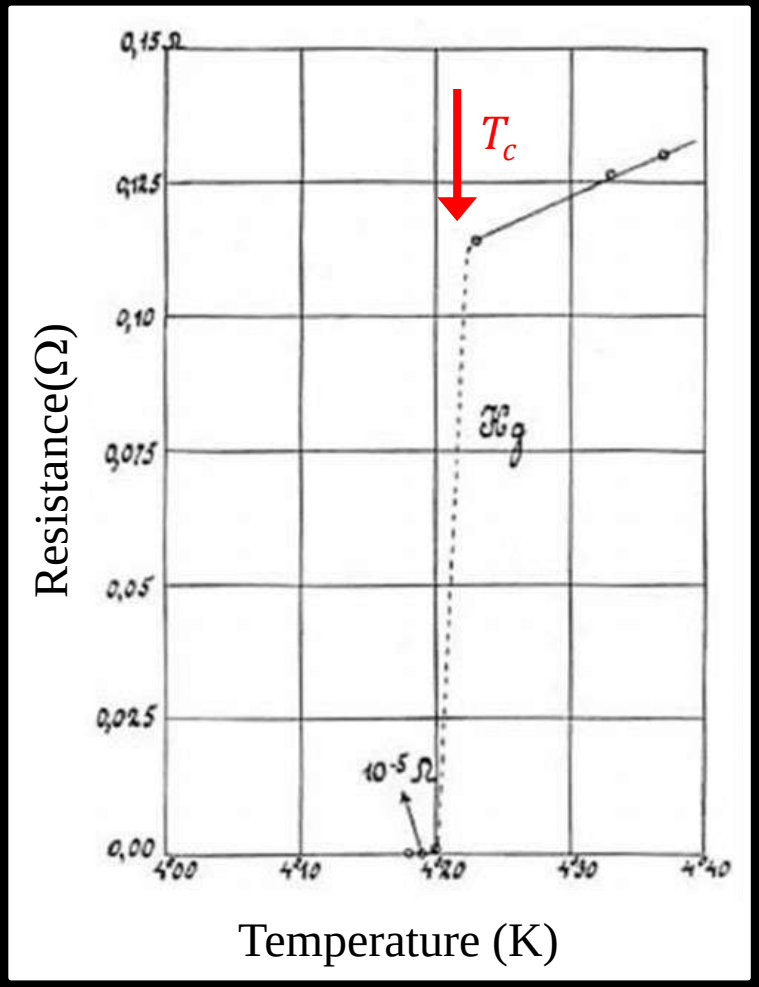

Heike Kamerlingh Onnes

Nobel Prize, 1913

"Door meten tot weten"
(Knowledge through measurement)

H. Kamerlingh Onnes, *Commun. Phys. Lab. Univ. Leiden. Suppl.* **29** (Nov. 1911).

SUPERCONDUCTIVITY

Type of material	What happens in a wire?	Result
Conductor	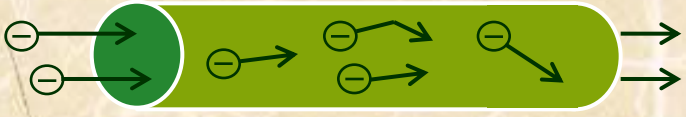 Electrons flow easily (like water through a garden hose)	Collisions cause dissipation (heat)
Insulator	 Electrons are tightly bound no flow (like a hose plugged with cement)	No current flow at all
Superconductor	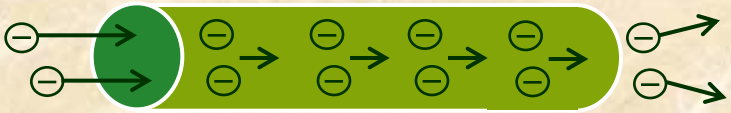 Electrons bind into pairs and cannot collide (a frictionless hose)	No collisions No dissipation No heat No resistance

HOW SMALL IS THE RESISTANCE?

Copper Cylinder

1) Induce current
2) Current decays in about 1/1000 second

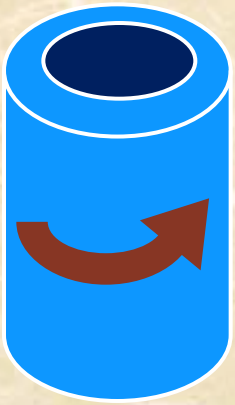

Superconducting Cylinder

1) Induce current
2) Current does not decay
   (less than 0.1% in a year)
   so, resistance is smaller than copper

$$\text{by } \frac{\text{1000 years}}{\text{1/1000 second}}$$

i.e., at least 1 trillion times!

The Meissner Effect in 1933

Perfect diamagnetism

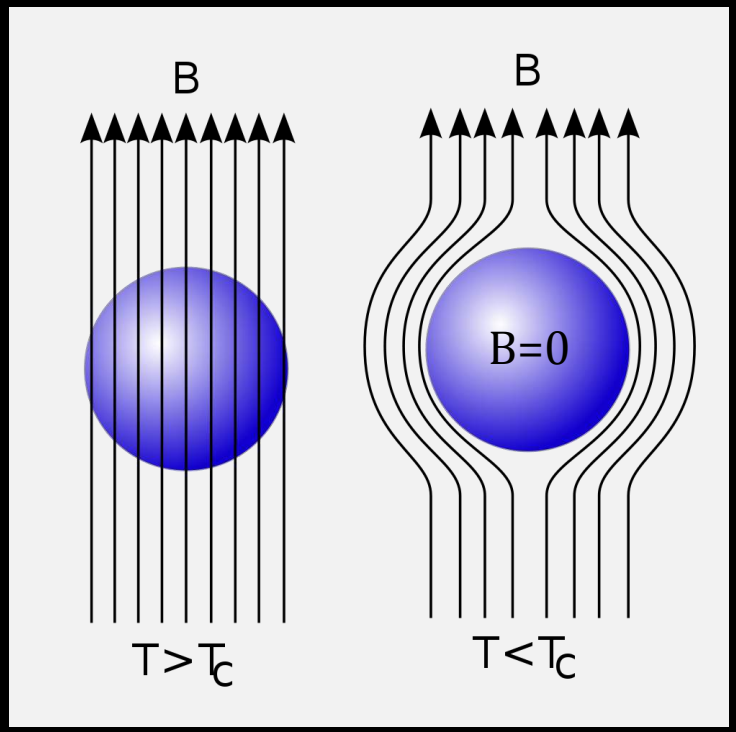

Walther Meißner

Robert Ochsenfeld

Meissner Effect

$$B = Ba + 4\pi M = 0 \; ; \qquad \frac{M}{Ba} = -\frac{1}{4\pi}$$

Eq.(1)

Perfect Diamagnetism

The magnetic properties cannot be accounted for by the assumption that a superconductor is a normal conductor with zero electrical resistivity.

The result $B = 0$ cannot be derived from the characterization of a super-conductor as a medium of zero resistivity.

From Ohm's law, $\mathbf{E} = \rho\mathbf{j}$, we see that if the resistivity ρ goes to zero, while $\mathbf{j}$ is held finite, then $\mathbf{E}$ must be zero. By a Maxwell equation $d\mathbf{B}/dt$ is proportional to curl $\mathbf{E}$, so that zero resistivity implies $d\mathbf{B}/dt = 0$. This argument is not entirely transparent, but the result predicts that the flux through the metal cannot change on cooling through the transition. **The Meissner effect contradicts this result, and suggests that perfect diamagnetism is an essential property of the superconducting state.**

Type I superconductor

Type II superconductor

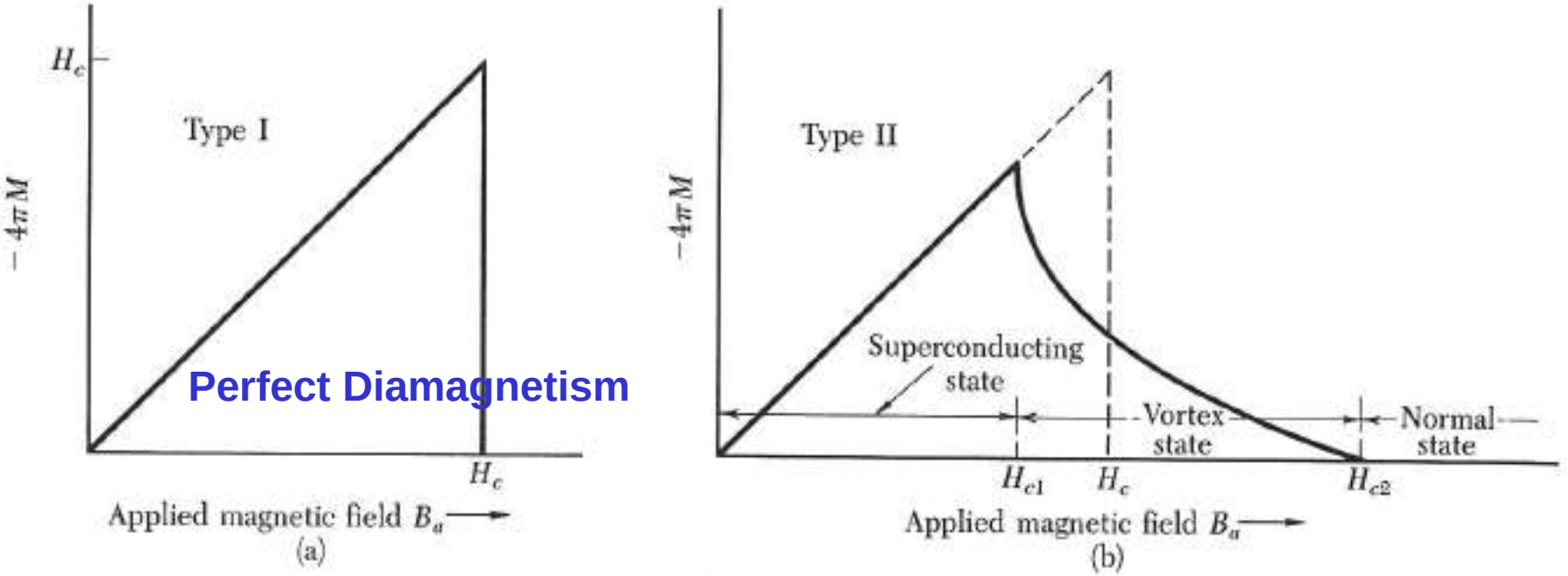

Figure 4 (a) Magnetization versus applied magnetic field for a bulk superconductor exhibiting a complete Meissner effect (perfect diamagnetism). A superconductor with this behavior is called a type I superconductor. Above the critical field H_c the specimen is a normal conductor and the magnetization is too small to be seen on this scale. Note that minus $4\pi M$ is plotted on the vertical scale: the negative value of M corresponds to diamagnetism. (b) Superconducting magnetization curve of a type II superconductor. The flux starts to penetrate the specimen at a field H_{c1} lower than the thermodynamic critical field H_c. The specimen is in a vortex state between H_{c1} and H_{c2}, and it has superconducting electrical properties up to H_{c2}. Above H_{c2} the specimen is a normal conductor in every respect, except for possible surface effects. For given H_c the area under the magnetization curve is the same for a type II superconductor as for a type I. (CGS units in all parts of this figure.)

Basic Properties of Superconductors

Zero electrical resistance + Meissner effect

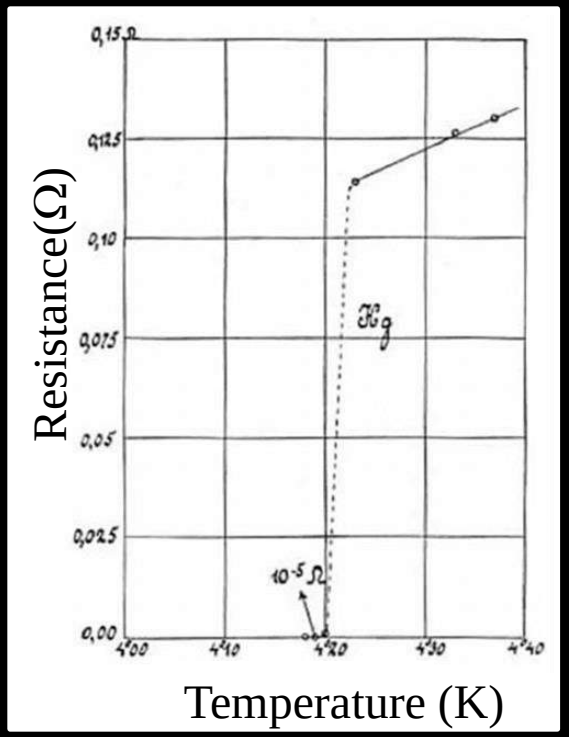

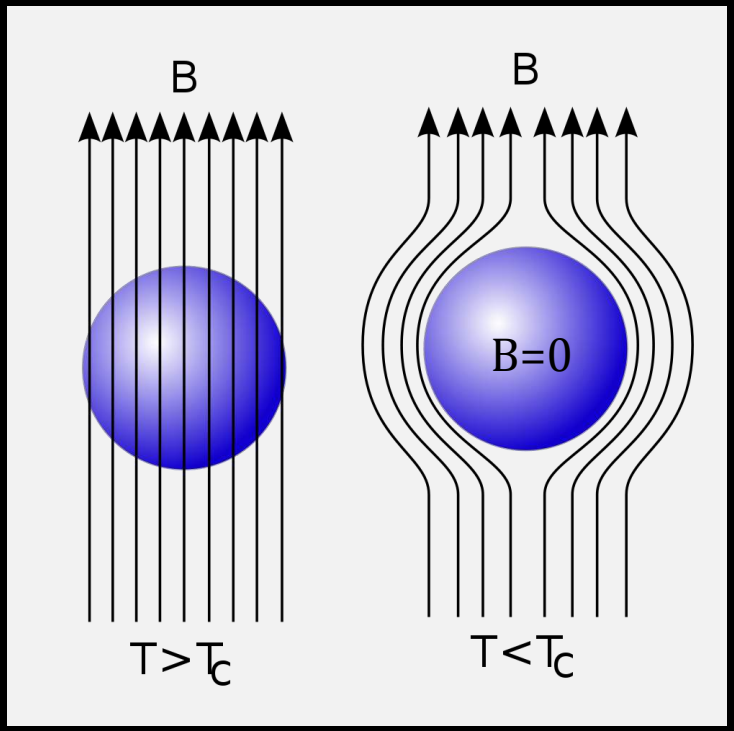

Type I & II Superconductors

Type I : Al, Pb…

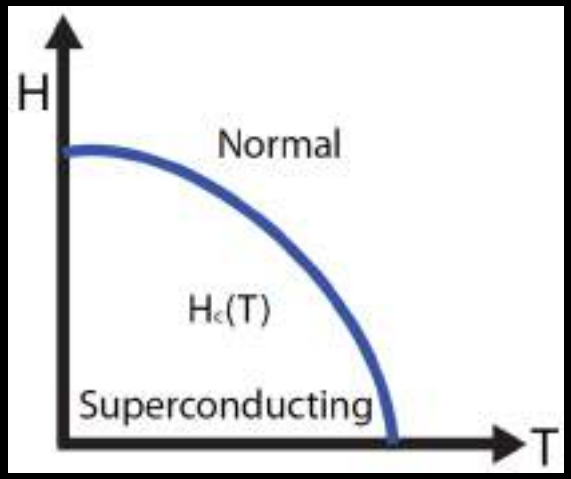

Type II : Nb, NbTi, Nb_3Sn and HTSC

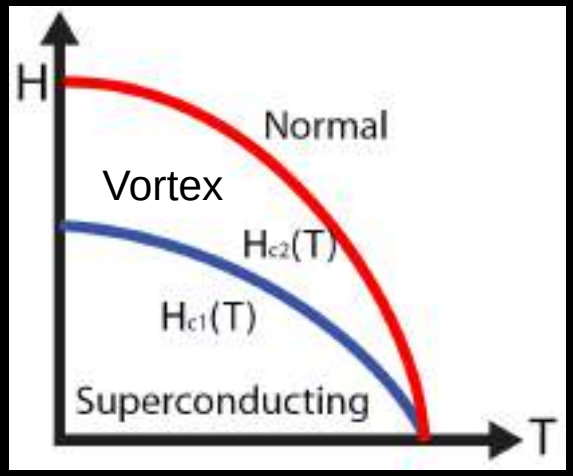

Lev V. Shubnikov

found type-II SC in Pb-Bi alloy in 1935.

J. N. Rjabinin, L.W. Schubnikow, Physikalische Zeitschrift der Sowjetunion 7, 122 (1935)

Superconducting Vortices in type II SC

Decoration image of vortex lattice

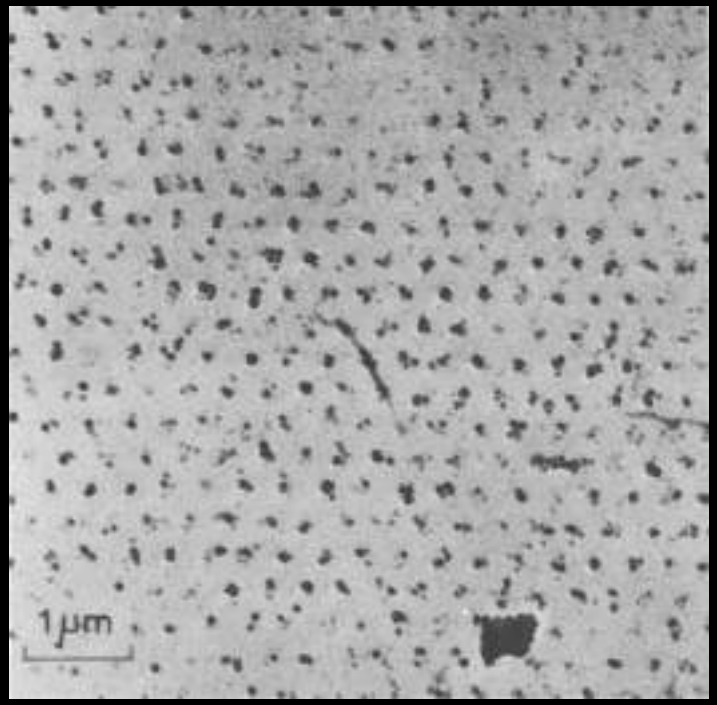

U. Essmann and H. Trauble, Physics Letters 24A, 526 (1967)

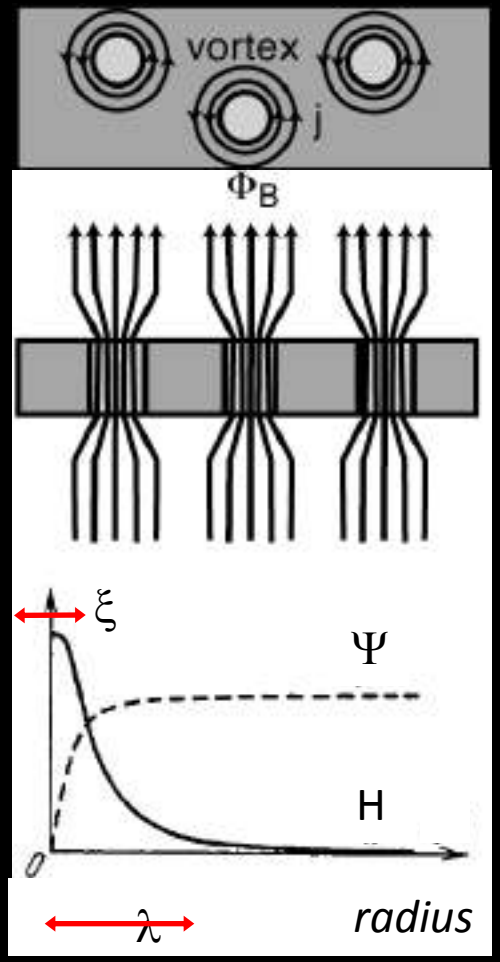

Alexei A. Abrikosov

Nobel Prize 2003

A. A. Abrikosov, Doklady Akademii Nauk SSSR 86, 489 (1952)
A. A. Abrikosov, Sov. Phys. JETP **5**,1174 (1957)

Why Superconductivity is so fascinating ?

- Fundamental SC mechanism
- Novel collective phenomenon at low temp
- Applications

Bulk: - Persistent current, power storage
- Magnetic levitation
- High field magnet, MRI

Electronics:
- SQUID magnetometer
- Josephson junction electronics

POSSIBLE IMPACT OF SUPERCONDUCTIVITY

- **Energy**
  - Superconductivity generators & motors
  - Power transmission & distribution
  - Energy storage systems
  - Magnets for fusion power
  - Magnets for magneto-hydrodynamic power

- **Transportation**
  - Magnets for levitated trains
  - Electro-magnetic powered ships
  - Magnets for automobiles

- **Health care**
  - Magnetic resonance imaging

Normal Metallic State

Electrons in wave-like states in momentum-space (k-space)

Free electron gas

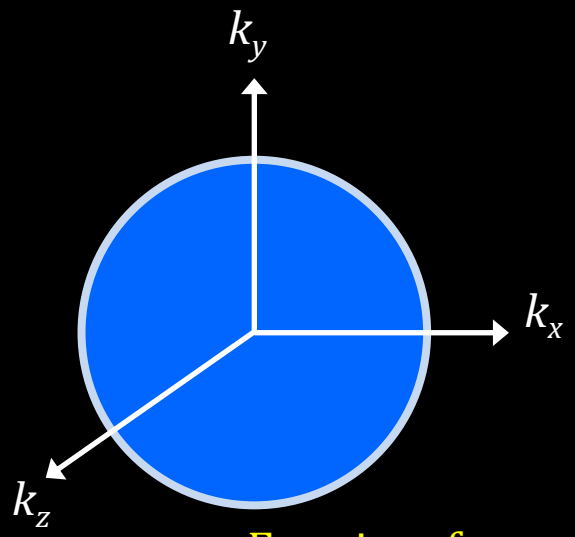

Fermi surface

Fermi liquid

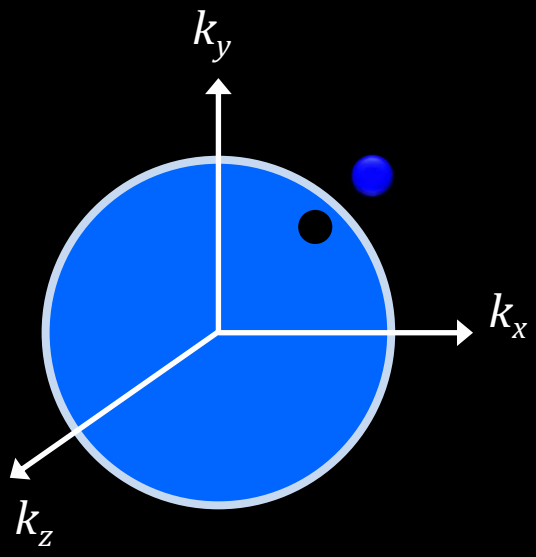

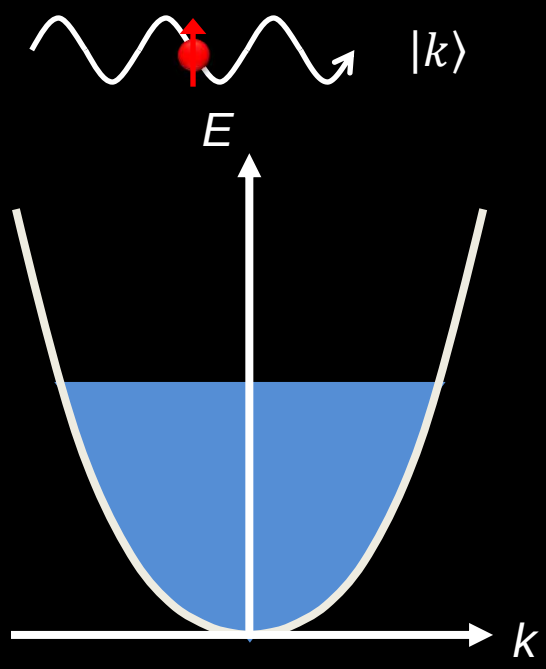

$$p = \hbar k = h/\lambda$$

$$E = \frac{\hbar^2 k^2}{2m}$$

BCS Theory in 1957 for Low T_c Superconductivity

Cooper Pairs

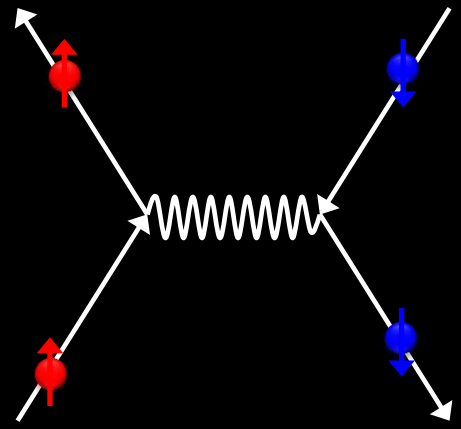

Exchange boson:
Lattice Vibration Mode

Microscopic theory for SC

John Bardeen

Leon Cooper

Robert Schrieffer

Nobel Prize 1972

J. Bardeen, L. N. Cooper, and J. R. Schrieffer, Phys. Rev. **108**, 1175 (1957)

Superconducting Ground State

Normal state

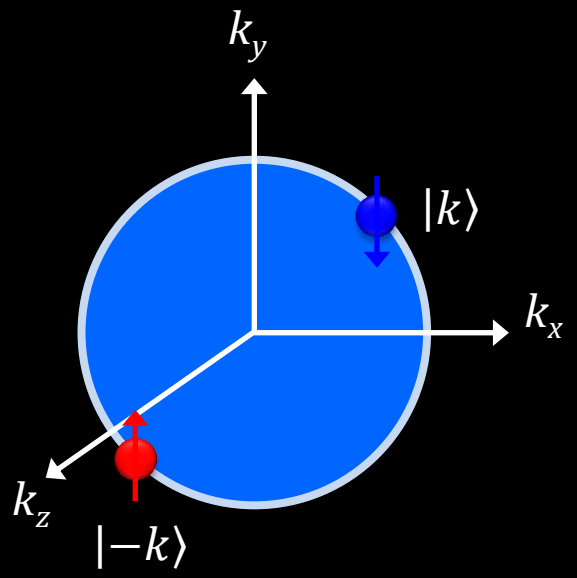

Cooper Pairs

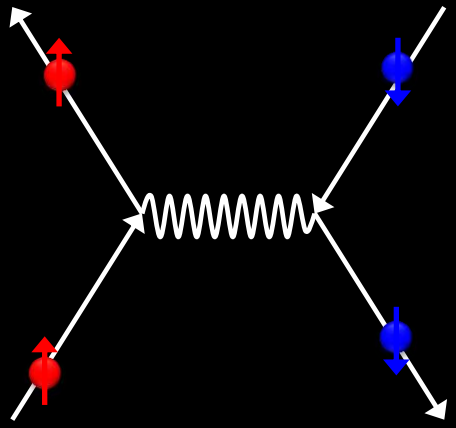

Exchange boson:
Lattice Vibration Mode

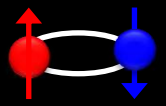

- Spin singlet
- L=0; S=0
- Binding energy: Δ

Superconducting ground state

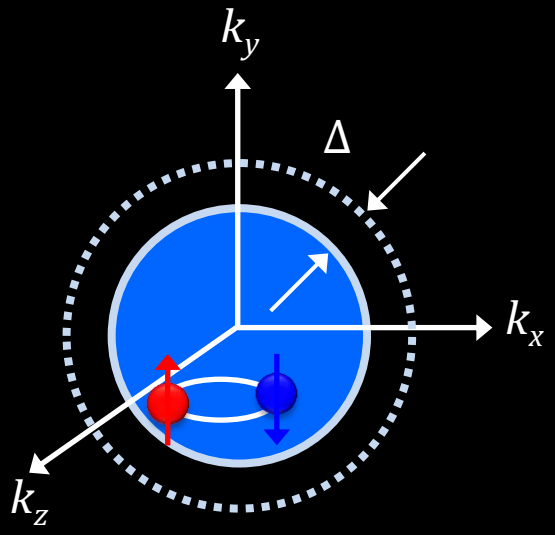

Fundamental Mechanism

The superconducting state is an ordered state of the conduction electrons of the metal.

Electron-Phonon Coupling

Cooper Pair formed by two electrons ***k,*** and ***–k*** with opposite spins near the Fermi level, as coupled through **phonons** of the lattice

The nature and origin of the ordering was explained by Bardeen, Cooper, and Schrieffer.[3]

BCS Theory, 1957

J. Bardeen, L. N. Cooper, and J. R. Schrieffer, Phys. Rev. **106**, 162 (1957); **108**, 1175 (1957).

The Discovery of Superconductivity

- Early 90's -- elemental *SP* metals like *Hg, Pb, Al, Sn, Ga*, etc.
- Middle 90's -- transitional metals, alloys, and compounds like Nb, NbN, Nb_3Sn, etc.
- Late 90's -- perovskite oxides

Table 2 Superconductivity of selected compounds

Compound	T_c, in K	Compound	T_c, in K
Nb_3Sn A-15	18.05	V_3Ga	16.5
Nb_3Ge	23.2	V_3Si	17.1
Nb_3Al	17.5	$YBa_2Cu_3O_{6.9}$ HTSC	90.0
NbN B1	16.0	Rb_2CsC_{60}	31.3
K_3C_6O	19.2	La_3In	10.4

A-15 compound A_3B, with T_c = 15-23 K

In the so called β–W structure
With three perpendicular linear chains of ***A*** atoms on the cubic face, and B atoms are at body centered cubic site,
With the presence of a sharp peak of *N(E) at* E_F

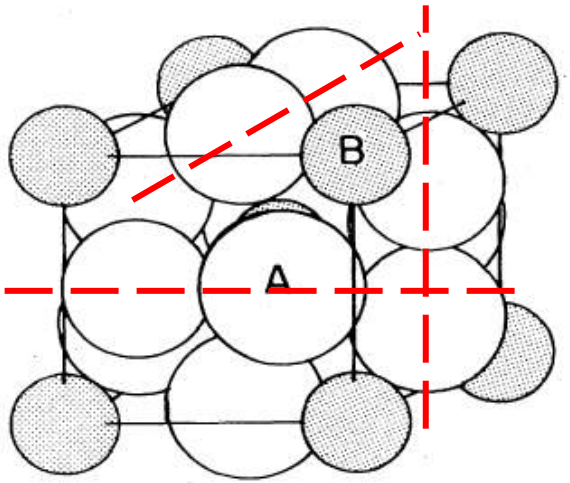

FIG. 1. The A-15 (or β-W) crystal structure for the compound formula A_3B. For the high T_c superconductors, A is a transition metal (usually V or Nb) and B is usually (but not always) a nontransition metal (e.g., Si, Ge, Sn, Al, Ga).

1973 discovery of Nb_3Ge, 23K !
how about Nb_3Si ??

Low temperature Superconductors

-- Mediated by Electron phonon coupling

-- McMillian formula for T_c

$$T_c = \frac{\Theta_D}{1.45} \exp\left\{ - \left[\frac{(1+\lambda_{ep})}{\lambda_{ep} - \mu^*(1+0.62\lambda_{ep})} \right] \right\}$$

λ : electron phonon coupling constant

μ^* : Coulomb repulsion of electrons

$\lambda \propto N(0) < I^2 > / \omega^2$

Are electrons or phonons more important?

The Phonon Spectrum of the low T_c A-15 compound Nb_3Al

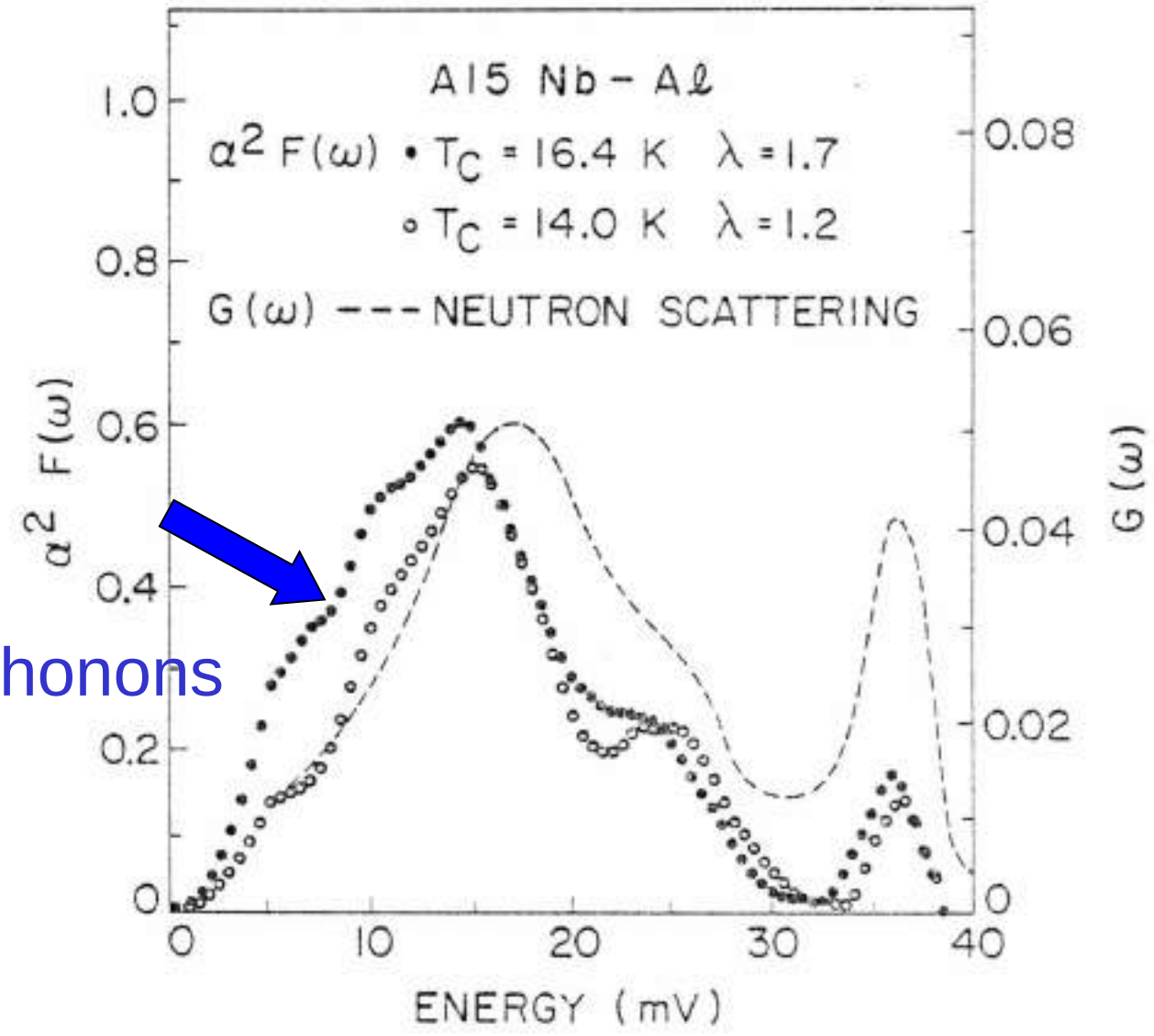

Soft Phonons

History of Conventional SC

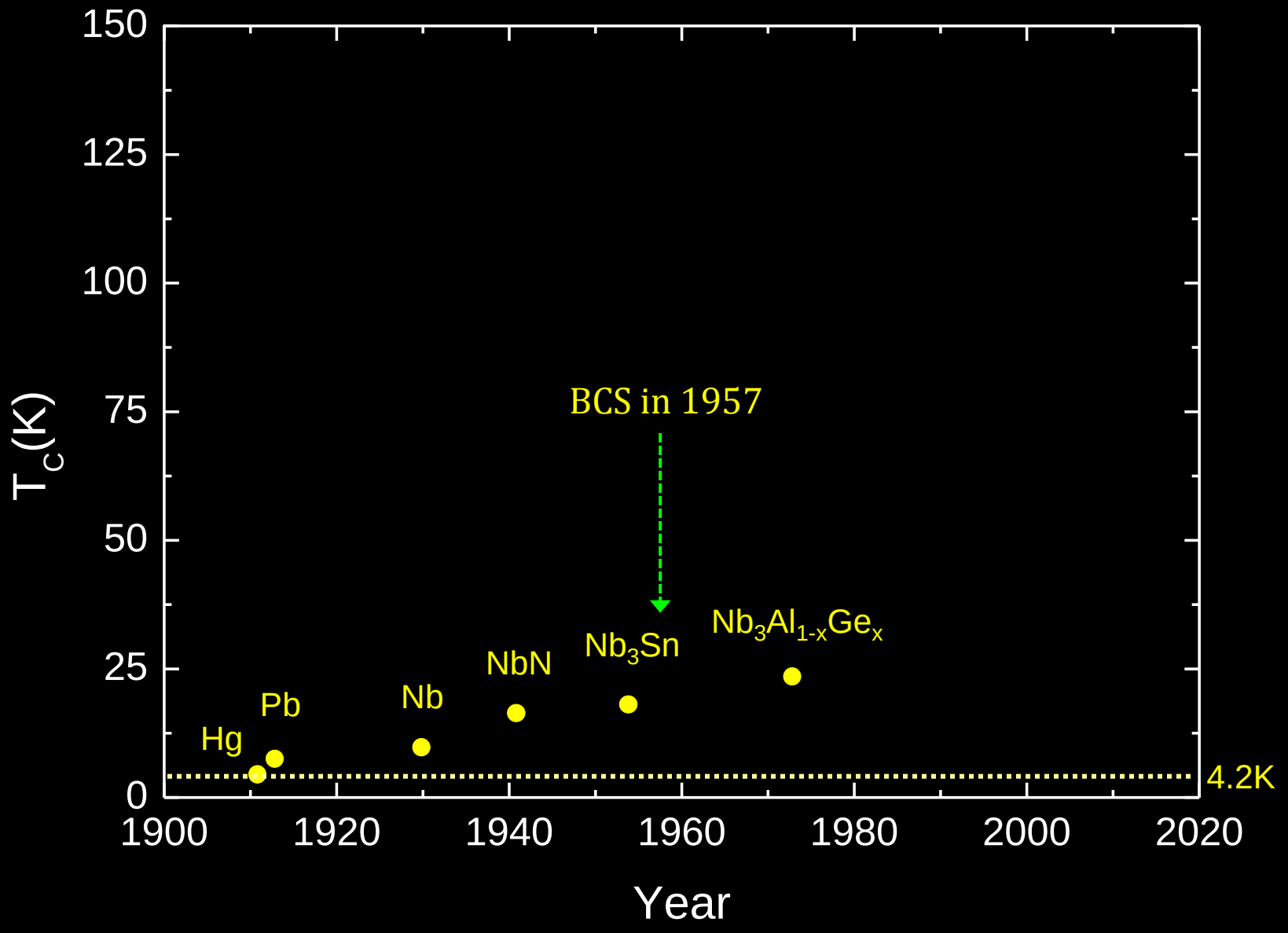

History of Conventional SC

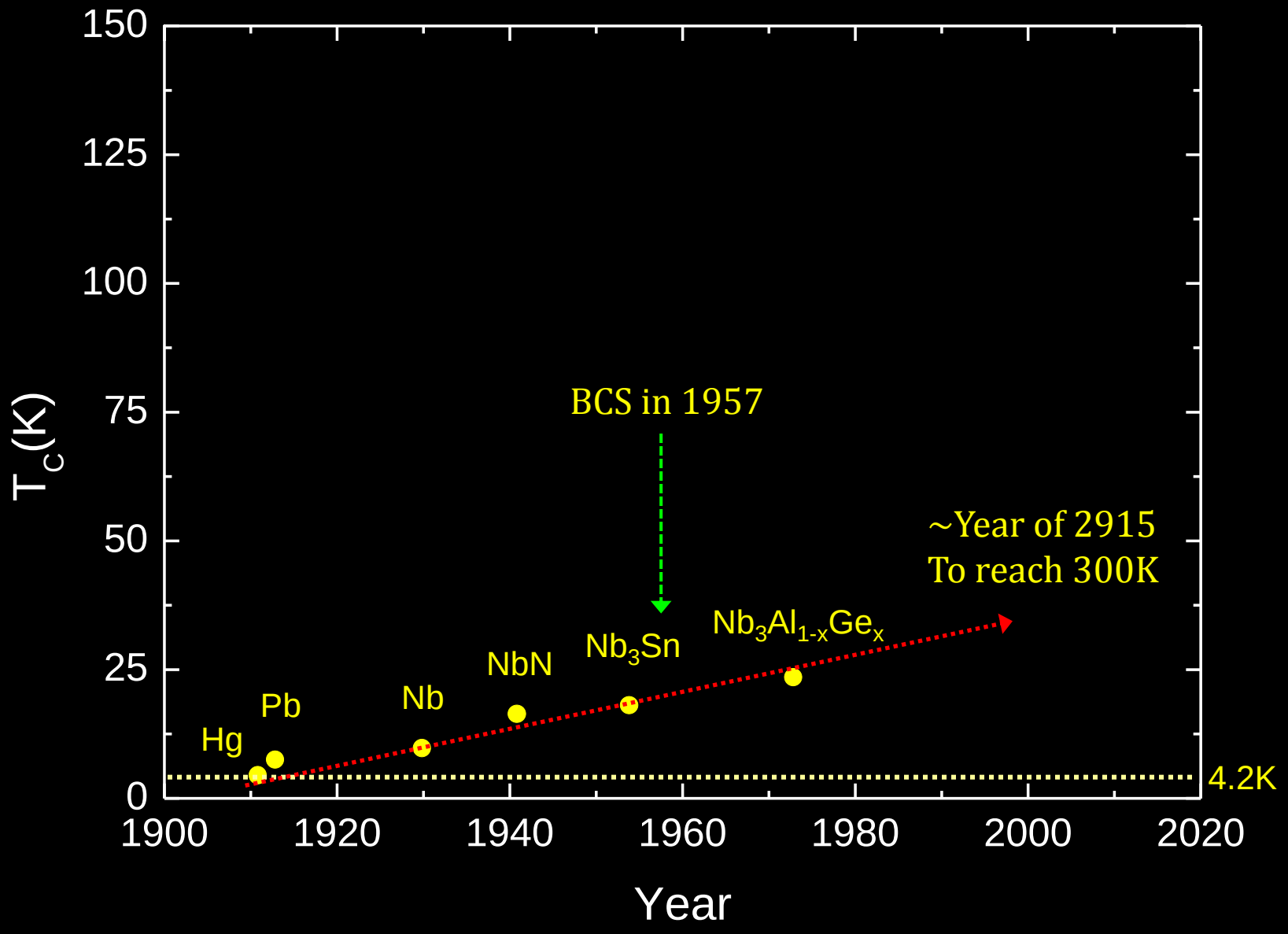

Can we raise the T_c higher than 30K?

Are we reaching the limitation of the BCS Theory ?

Matthias's Rules for Searching High T_C SC

Bernd Matthias

1. Stay away from insulators; transition metals are better.
2. There are favorable electron/atom ratios.
3. High symmetry is good; cubic symmetry is best.
4. Stay away from Oxygen
5. Stay away from magnetism
6. Stay away from theorists.

W. E. Pickett , Physica B **296**, 112 (2001)
I. I. Mazin, Nature **464**, 183 (2010)

A legacy of Superconductivity

Stanford, April, 2015

The Beginning of Unconventional SC: Heavy Fermion SC

Enormous effective mass of their charge carriers. This is achieved by a sharp spike in the DOS at the Fermi surface, to as much as 1000 times the density of states in Cu.

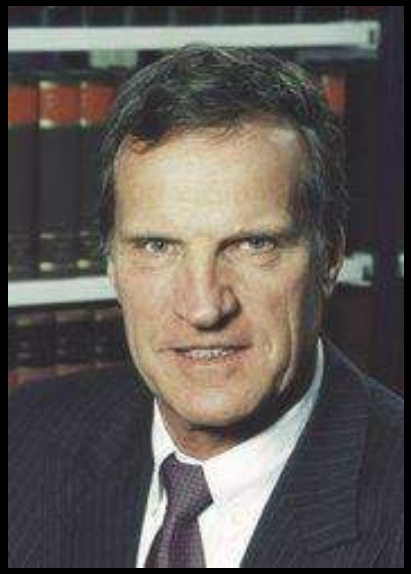

Frank Steglich

F. Steglich *et al.*, Phys. Rev. Lett. 43, 1892 (1979)

Breakthrough in late 1986
By Bednorz and Muller

Start the HTSC Era !

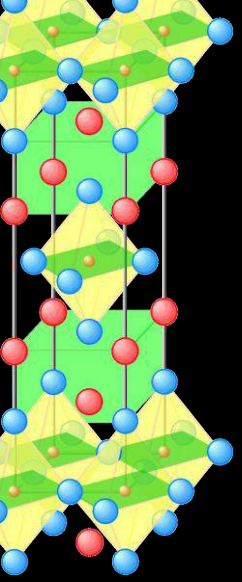

Discovery of High T_c Cuprates

Possible High T_c Superconductivity in the Ba – La – Cu – O System

J.G. Bednorz and K.A. Müller
IBM Zürich Research Laboratory, Rüschlikon, Switzerland

Received April 17, 1986

Z. Phys. B – Condensed Matter 64,189 (1986)

$La_{2-x}Ba_xCuO_4$, T_c=30K

J. Georg Bednorz

K. Alex Müller

Nobel Prize 1987

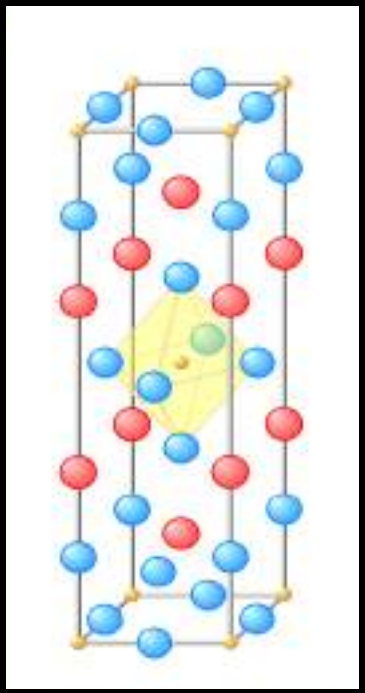

Discovery of High T_c Cuprates

$T_c > 77K$!

朱經武

吳茂昆

M. K. Wu *et al.*, PRL **58**, 908 (1987)

$YBa_2Cu_3O_{7-\delta}$, T_c~93K

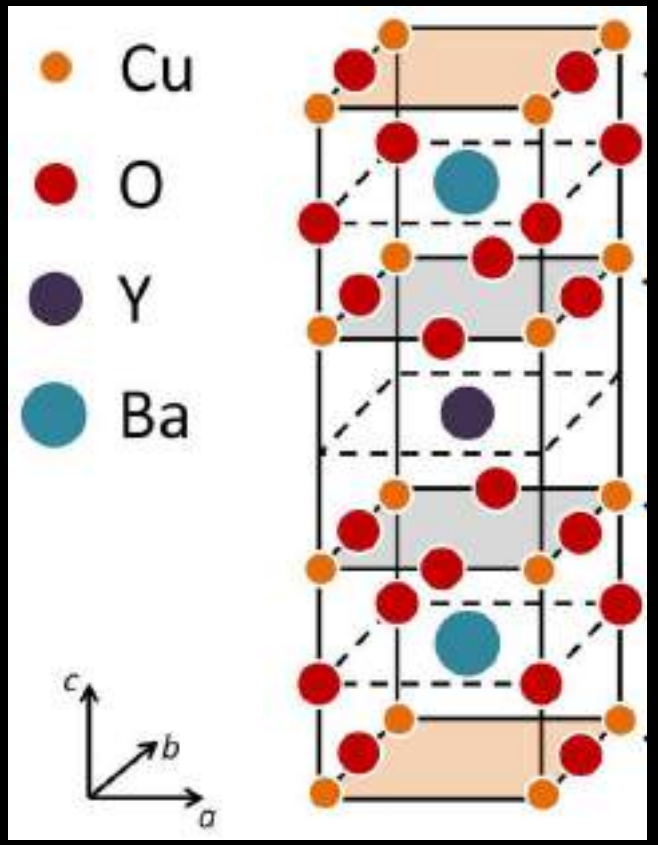

High Temperature Superconductor $YBa_2Cu_3O_7$

(90K)

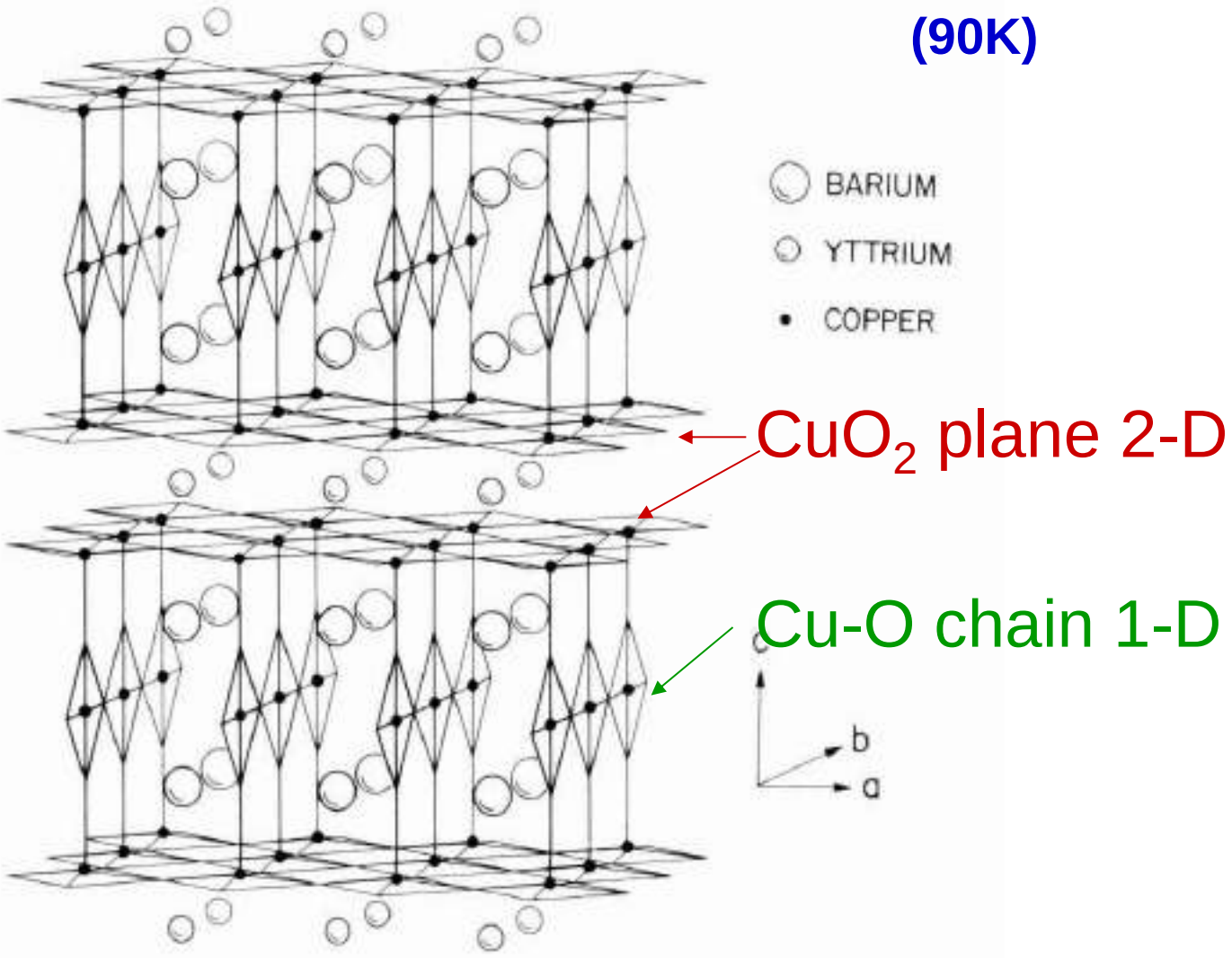

Invention of Oxide Molecular Beam Epitaxy For HTSC Single Crystal Films.

Woodstock of Physics - March Meeting 1987

"The stores and the bars were all 'Physicists welcome,' " said Paul M. Grant, who headed the superconductivity research at I.B.M.'s Almaden Research Center in San Jose. He recalled a discotheque in Chelsea with a long line of people waiting to get in. "The bouncers took anybody that had a physical society badge on to the front," Dr. Grant recalled, "and we got in gratis. Can you imagine what a culture shift? We had a hell of a good time." – NY Times

$La_{2-x}Ba_xCuO_4$

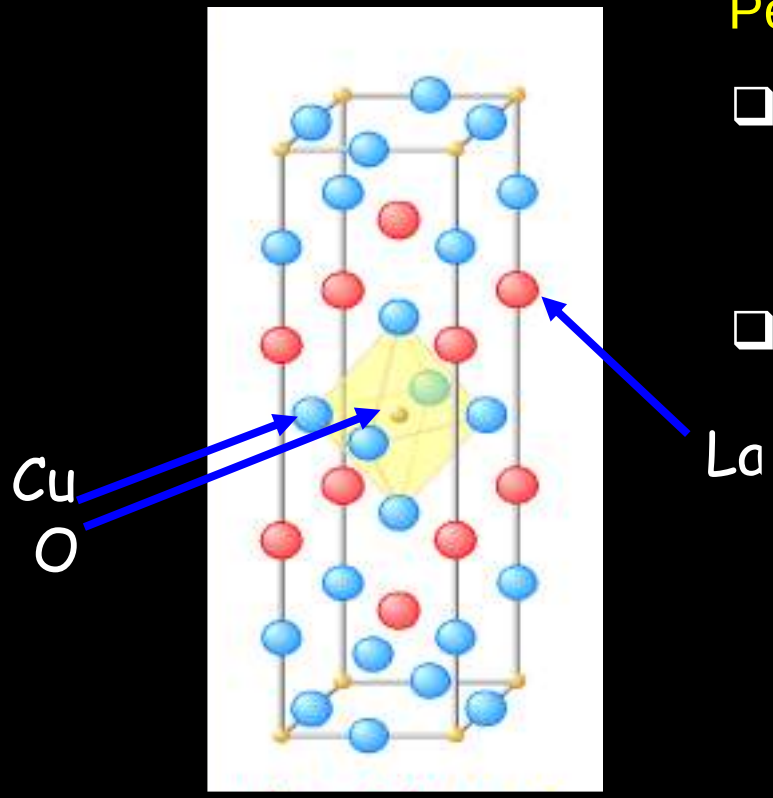

Perovskite oxide structure

- At small x cation doping, Antiferromagnetic Mott Insulator
- For SC state, the Tc is maximum at x = 0.15

Z. Phys. Rev. **B 64** 189 (1986)

$La_{2-x}Ba_xCuO_4$

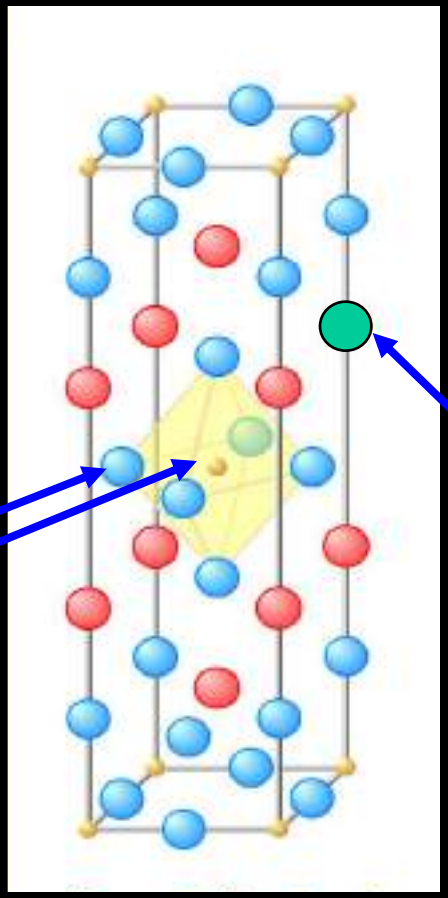

Each Ba atom substituted for the captures, and electron from CuO_2 plane leaving *p* holes per unit cell

Z. Phys. Rev. **B 64** 189 (1986)

High T_c Cuprate Superconductors (CuSC)

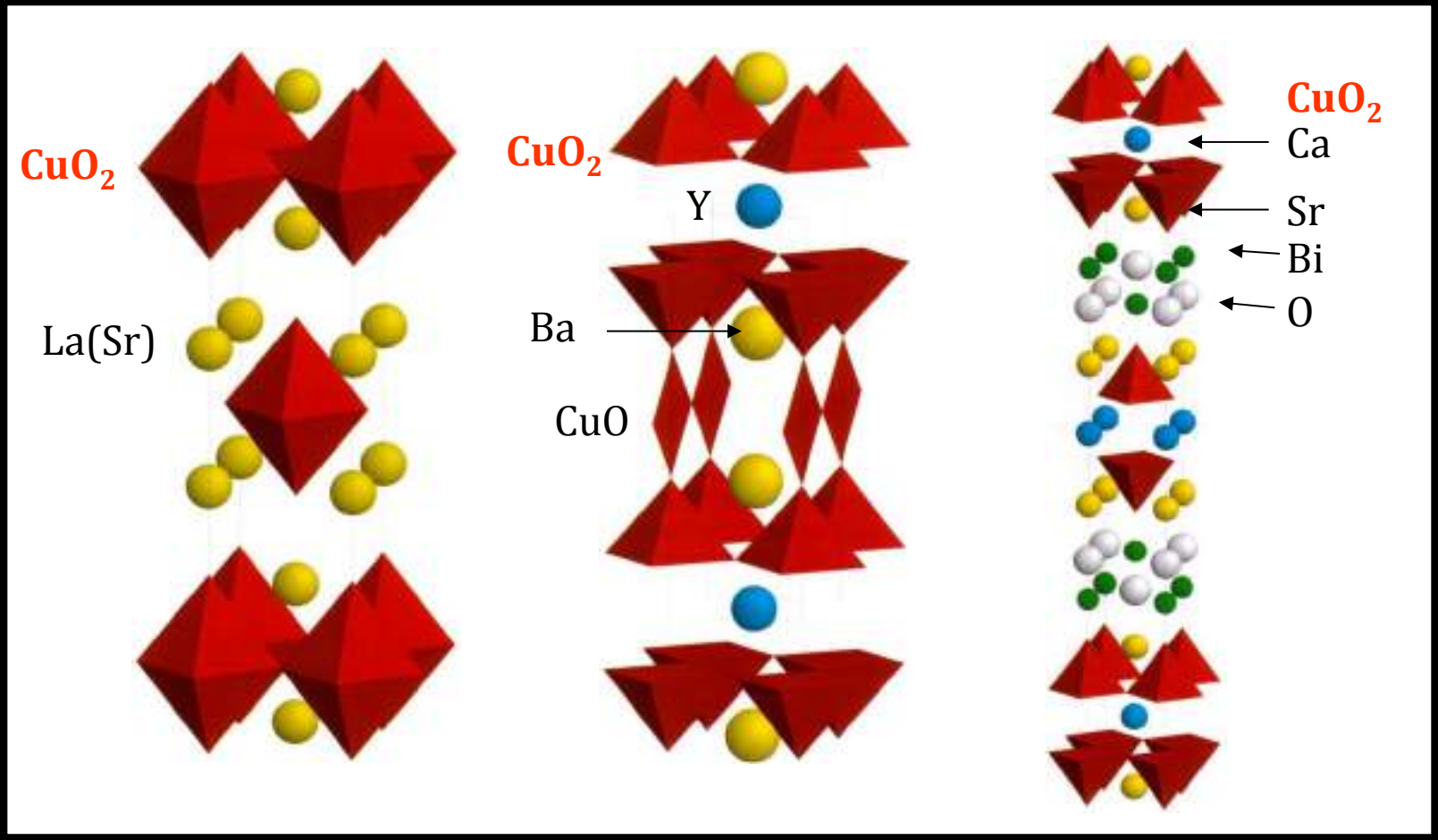

$La_{2-x}Sr_xCuO_4$
(LSCO)

($T_c^{max} \sim 40$ K)

$YBa_2Cu_3O_y$
(YBCO)

($T_c^{max} \sim 93$ K)

$Bi_2Sr_2CaCu_2O_y$
(Bi2212 or BSCCO)

($T_c^{max} \sim 95$ K)

History of Superconductors

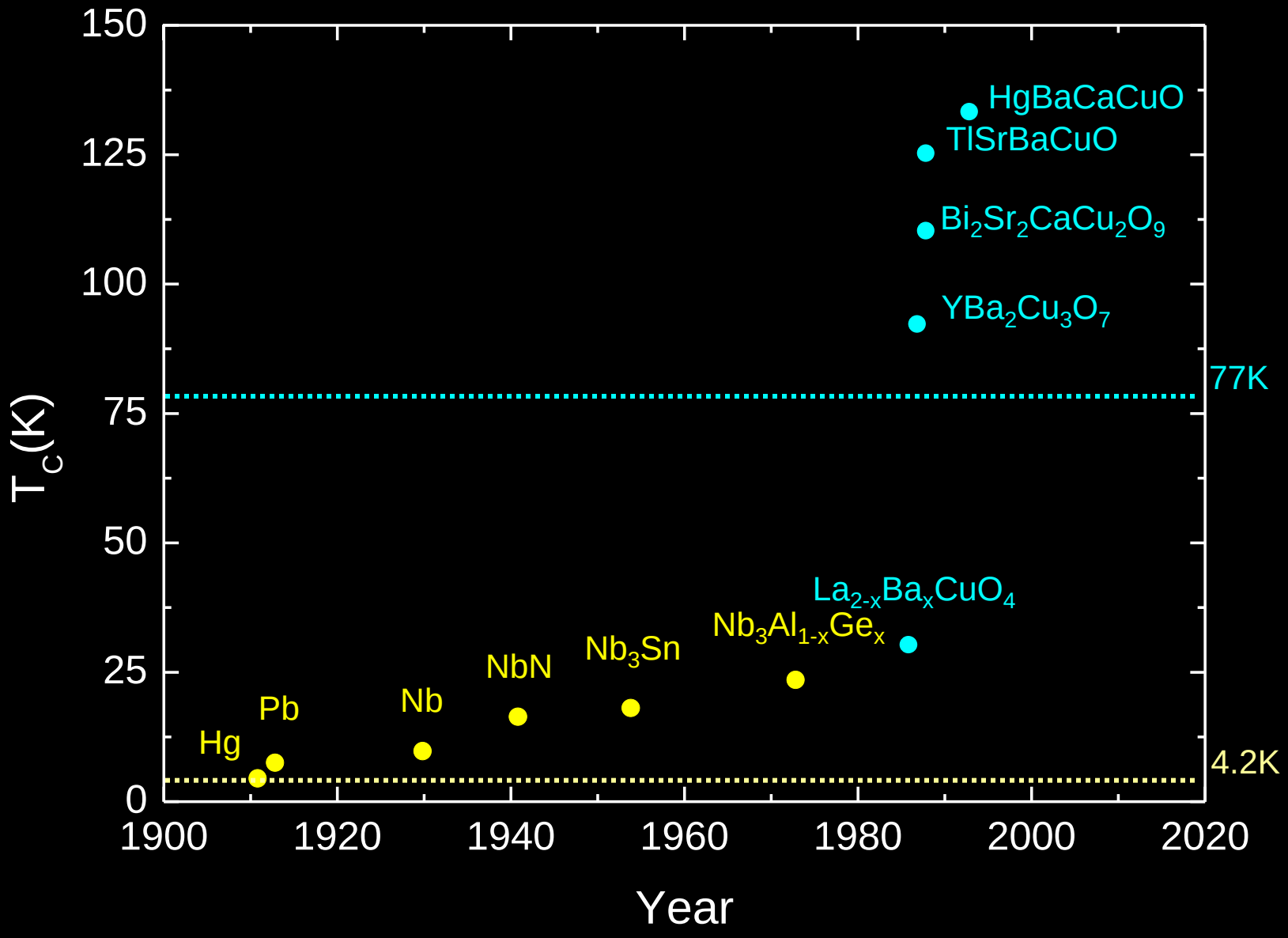

Honorable Mention : MgB_2 in 2001

T_c=39K
Two superconducting gaps
Strong sp^2 bonding and hybridization
E_{2g} phonon and σ bond coupling leads to high T_c

Jun Akimitsu
秋光純

©青山学院大学

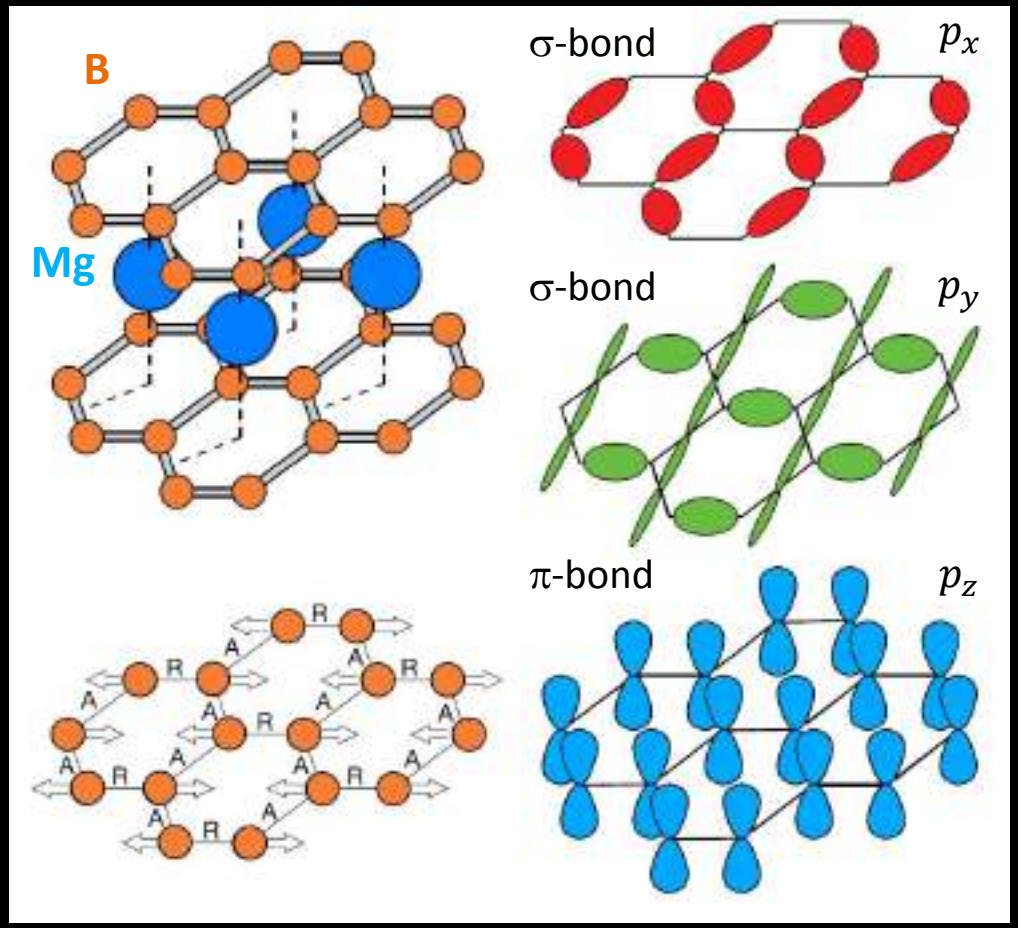

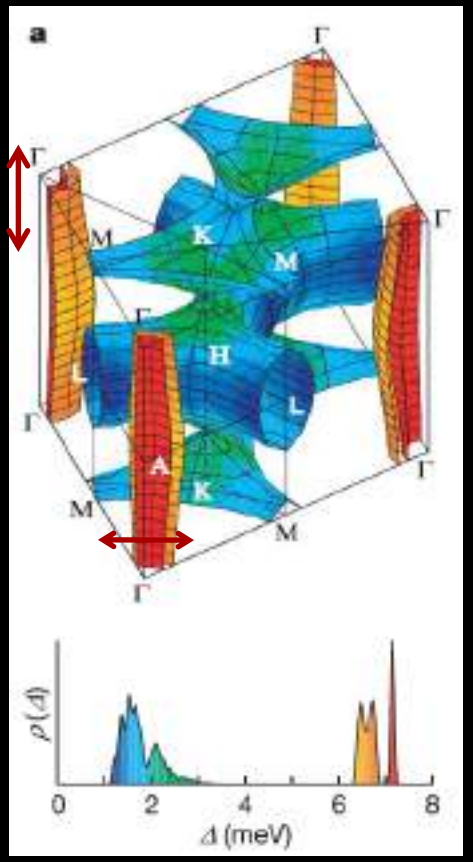

J. Nagamatsu *et al.*, Nature 410, 63 (2001)
Amy Liu *et al.*, PRL 87, 087005 (2001)
H.J. Choi *et al.*, Nature 418, 758 (2002)

The Discovery of Fe-based Superconductors (FeSC) in 2006

2006 : $LaFeP(O_{1-x}F_x)$: T_C~5K

2007 : LaNiPO: T_C~3K

2008 : $LaFeAs(O_{1-x}F_x)$, T_C~26K

Hideo Hosono

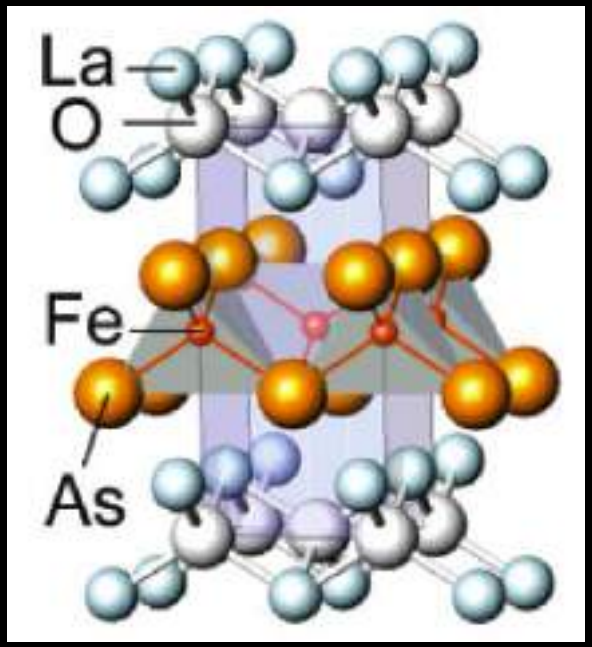

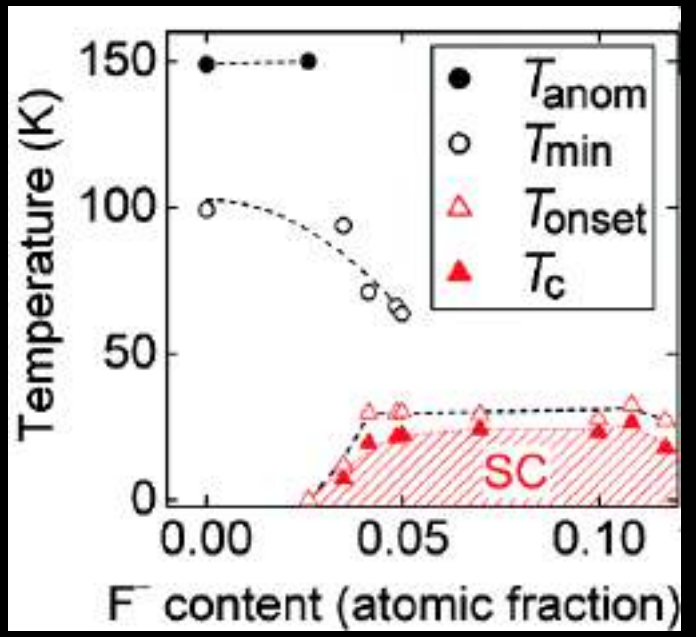

Y. Kamihara *et al.*, JACS. **128**, 10012 (2006)
T. Watanabe *et al.*, JACS. **46**, 7719 (2007)
Y. Kamihara *et al.*, JACS. **130**, 3296 (2008)

History of Conventional and High T_C Superconductors

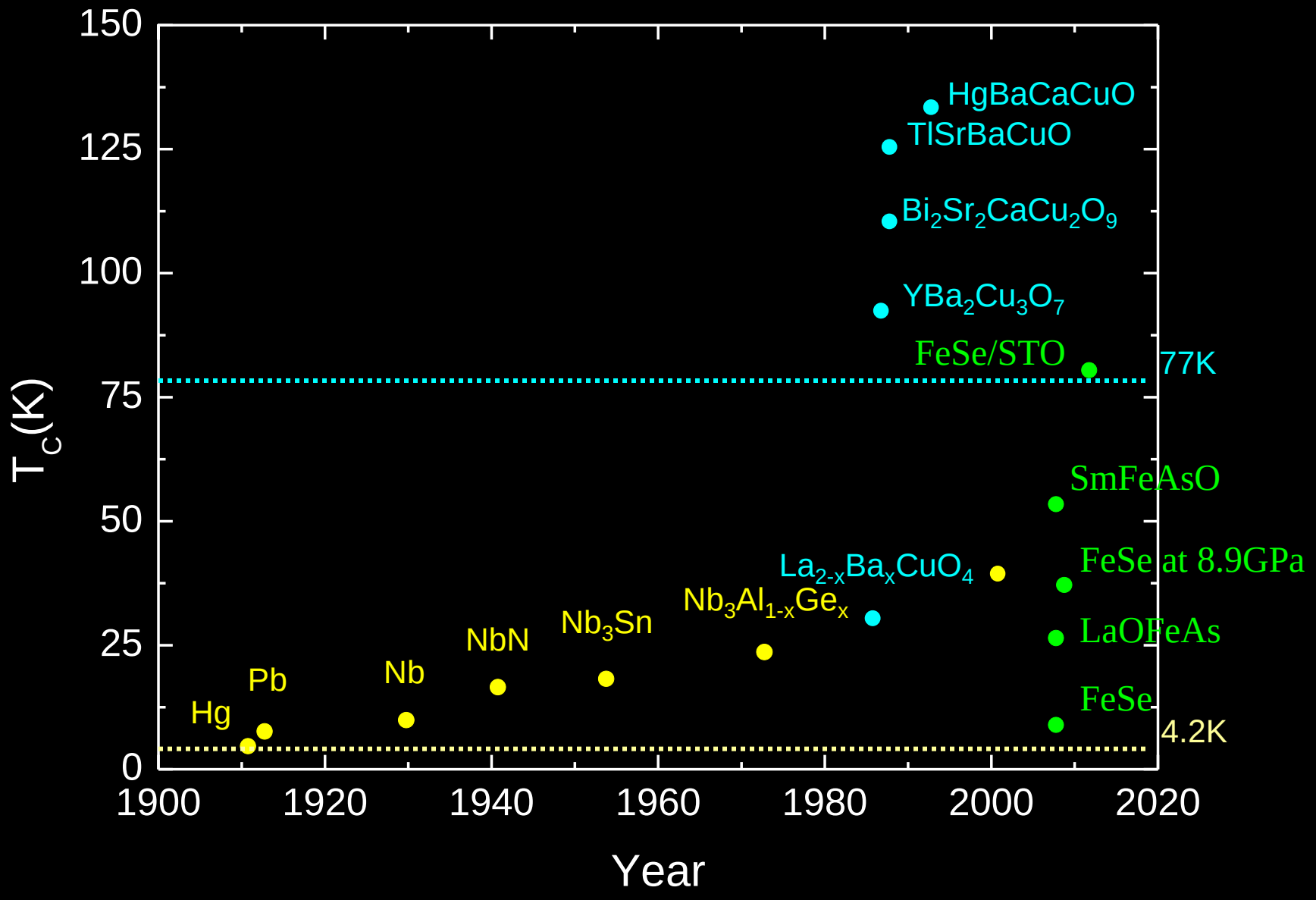

Honorable Mention : H_3S in 2015

T_C=203K under High Pressure
Likely H-rich H_3S
Conventional BCS superconductor ?

Mikhail Eremets

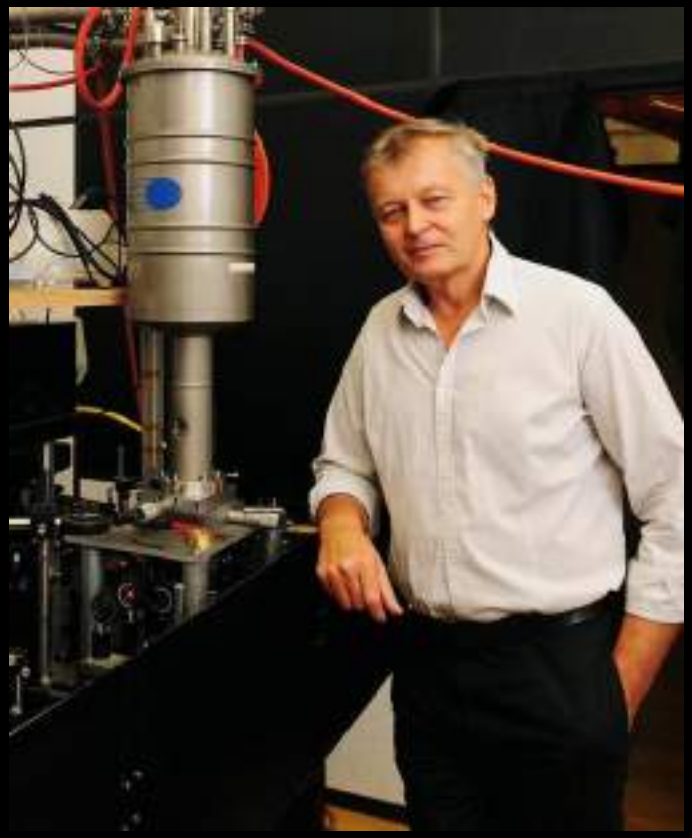

© Max-Planck-Institut für Chemie

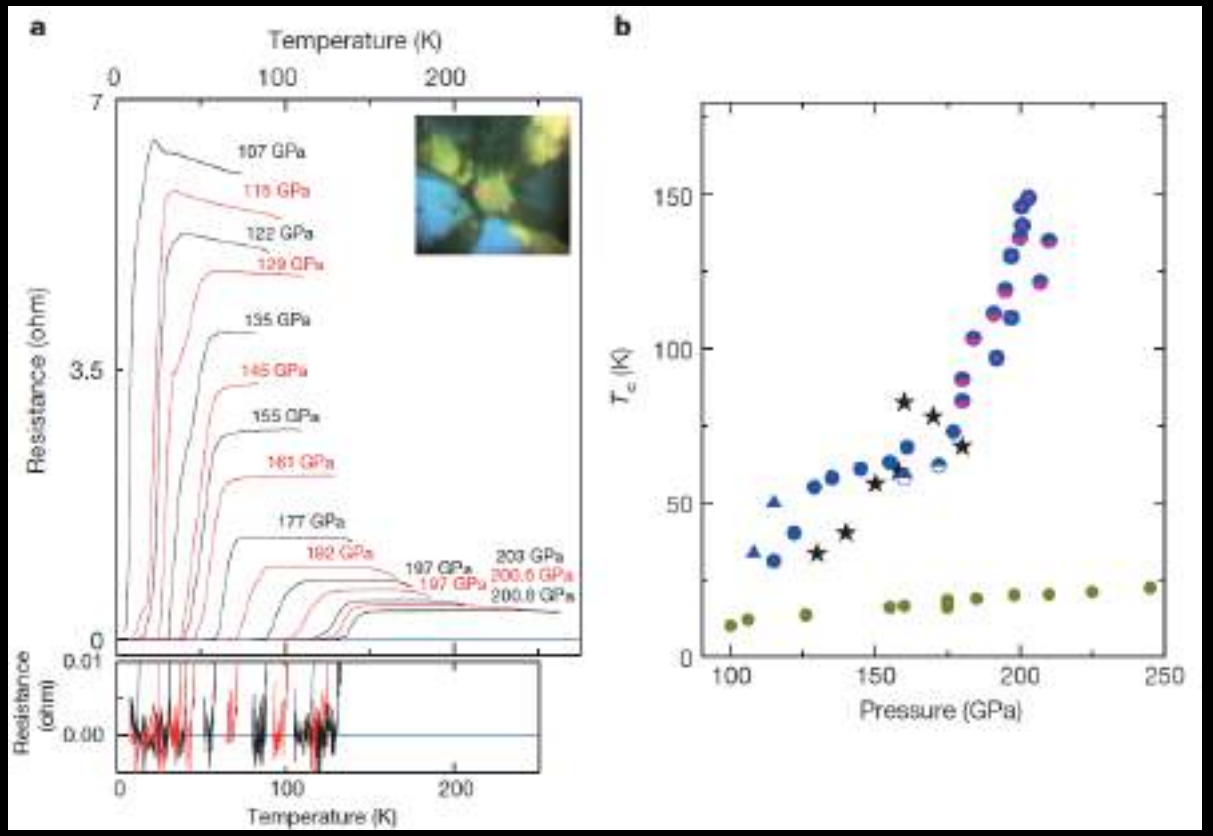

A. P. Drozdov *et al.*, Nature 525, 73 (2015)

- The results are the work of Mikhail Eremets, Alexander Drozdov and their colleagues at the Max Planck Institute for Chemistry in Mainz, Germany in 2015. They find that when they subject samples of hydrogen sulfide to extremely high pressures — around 1.5 million atmospheres (150 Gigapascals) — and cool them below 203 K, the samples display the classic hallmarks of superconductivity: zero electrical resistance and the Meissner effect.

- Other hydrogen compounds may be good candidates for high T_c too. For instance, compounds that pair hydrogen with *Pt, K, Se, Te,* instead of sulfur.

- Zhang in Dallas and Yugui Yao of the Beijing Institute of Technology in China predict that substituting 7.5% of the sulfur atoms in hydrogen sulfide with phosphorus, and upping the pressure to 2.5 million atmospheres (250 GPa) could raise the superconducting transition temperature all the way to 280 K, above water's freezing point.

Will all non magnetic metal become SC at low T?

(I) Destruction of Superconductivity by Magnetic Impurities

It is important to eliminate from the specimen even trace quantities of foreign paramagnetic elements

(II) Destruction of Superconductivity by Magnetic fields

At the critical temperature the critical field is zero: $H_c(T_c)=0$

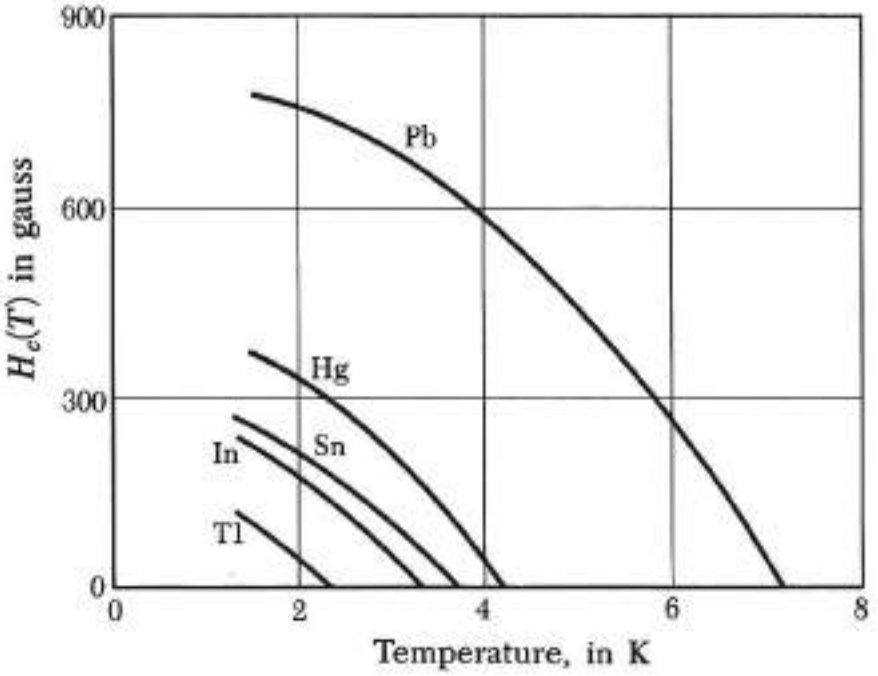

Figure 3 Experimental threshold curves of the critical field $H_c(T)$ versus temperature for several superconductors. A specimen is superconducting below the curve and normal above the curve.

Type I superconductor

Type II superconductor

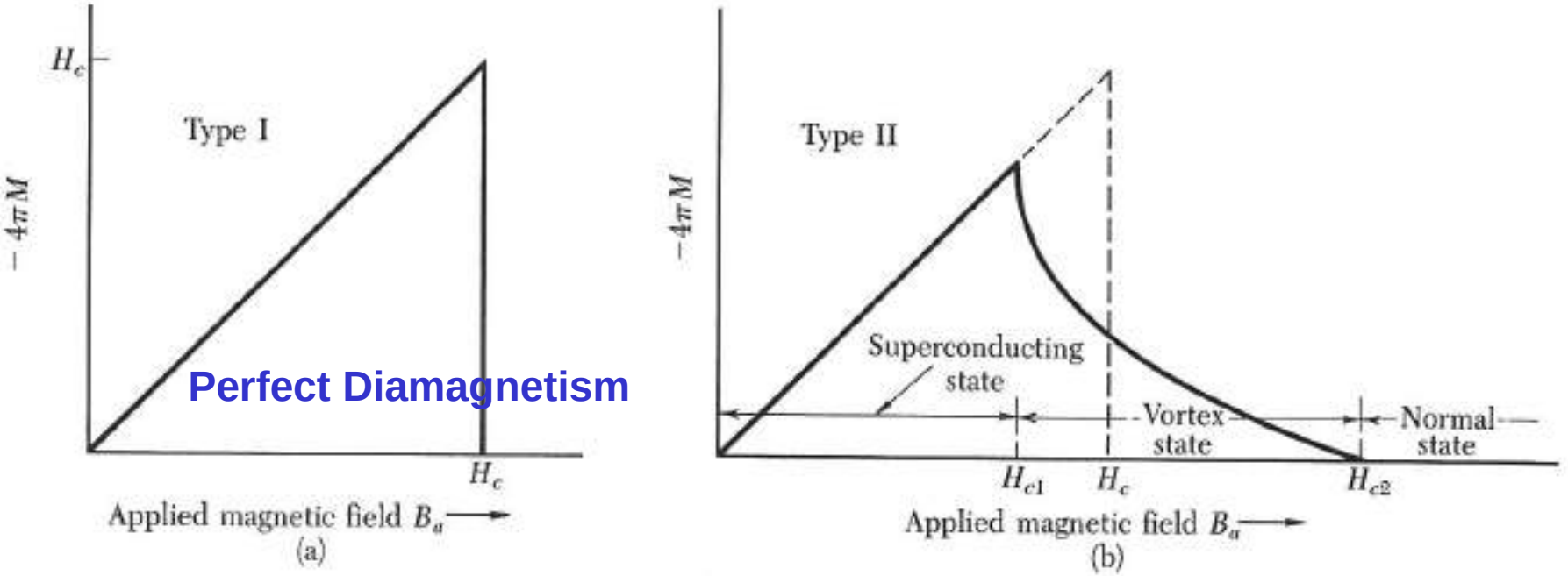

Figure 4 (a) Magnetization versus applied magnetic field for a bulk superconductor exhibiting a complete Meissner effect (perfect diamagnetism). A superconductor with this behavior is called a type I superconductor. Above the critical field H_c the specimen is a normal conductor and the magnetization is too small to be seen on this scale. Note that minus $4\pi M$ is plotted on the vertical scale: the negative value of M corresponds to diamagnetism. (b) Superconducting magnetization curve of a type II superconductor. The flux starts to penetrate the specimen at a field H_{c1} lower than the thermodynamic critical field H_c. The specimen is in a vortex state between H_{c1} and H_{c2}, and it has superconducting electrical properties up to H_{c2}. Above H_{c2} the specimen is a normal conductor in every respect, except for possible surface effects. For given H_c the area under the magnetization curve is the same for a type II superconductor as for a type I. (CGS units in all parts of this figure.)

Type II Superconductors

1. A good type **I** superconductor excludes a magnetic field until superconductivity is destroyed suddenly, and then the field penetrates completely.

2. (a) A good type **II** superconductor excludes the field completely up to a field $\boldsymbol{H}_{c1}$.

   (b) Above $\boldsymbol{H}_{c1}$ the field is partially excluded, but the specimen remains electrically superconducting.

   (c) At a much higher field, $\boldsymbol{H}_{c2}$, the flux penetrates completely and superconductivity vanishes.

   (d) An outer surface layer of the specimen may remain superconducting up to a still higher field $\boldsymbol{H}_{c3}$.

3. An important difference in a type **I** and a type **II** superconductor is in the mean free path of the conduction electrons in the normal state. are type **I**, with $\boldsymbol{\kappa} < 1$, will be type **II**. is the situation when $\boldsymbol{\kappa} = \boldsymbol{\lambda} / \boldsymbol{\xi} > 1$.

1. A superconductor is type **I** if the surface energy is always positive as the magnetic field is increased, For $H < H_c$

2. And type **II** if the surface energy becomes negative as the magnetic field is increased. For $Hc_1 < H < Hc_2$

The free energy of a bulk superconductor is increased when the magnetic field is expelled. However, a parallel field can penetrate a very thin film nearly uniformly (Fig. 17), only a part of the flux is expelled, and the energy of the superconducting film will increase only slowly as the external magnetic field is increased.

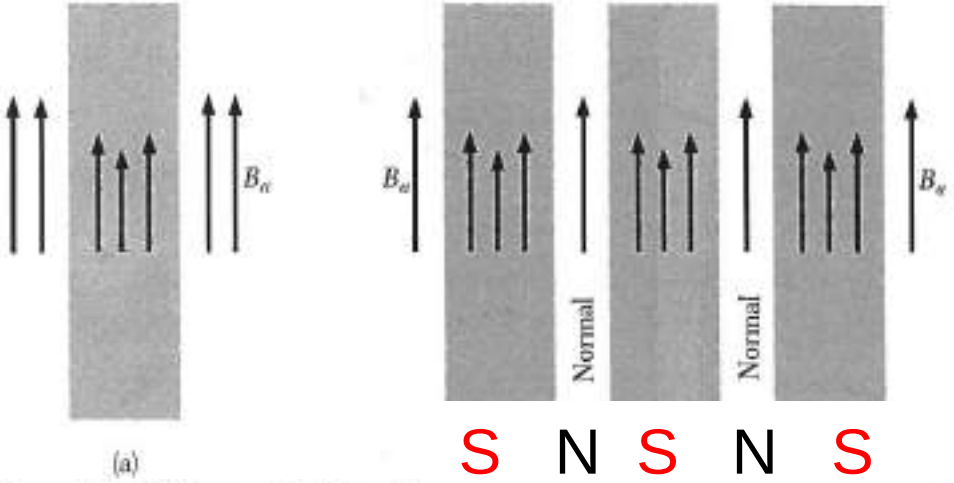

Figure 17 (a) Magnetic field penetration into a thin film of thickness equal to the penetration depth λ. The arrows indicate the intensity of the magnetic field. (b) Magnetic field penetration in a homogeneous bulk structure in the mixed or vortex state, with alternate layers in normal and superconducting states. The superconducting layers are thin in comparison with λ. The laminar structure is shown for convenience; the actual structure consists of rods of the normal state surrounded by the superconducting state. (The *N* regions in the vortex state are not exactly normal, but are described by low values of the stabilization energy density.)

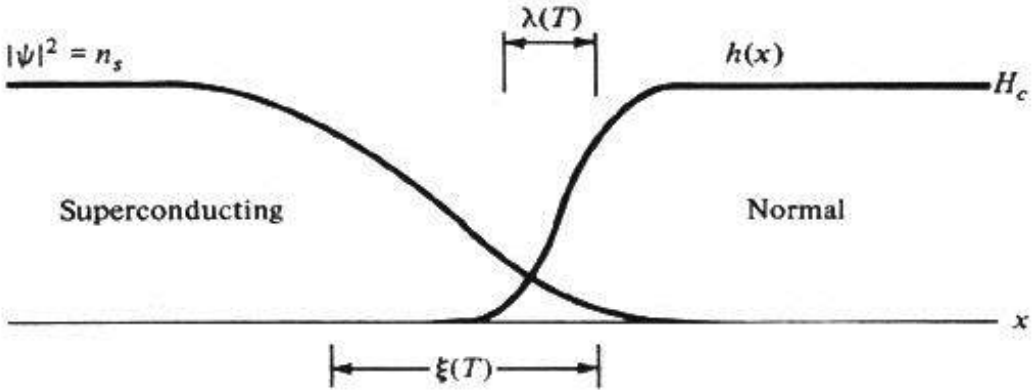

FIGURE 1-4
Interface between superconducting and normal domains in the intermediate state.

$$\kappa = \frac{\lambda_{\text{eff}}(T)}{\xi(T)} = \frac{2\sqrt{2}\,\pi H_c(T)\lambda_{\text{eff}}^2(T)}{\Phi_0}$$

Ginsburg Landau Parameter

κ << 1
Type I

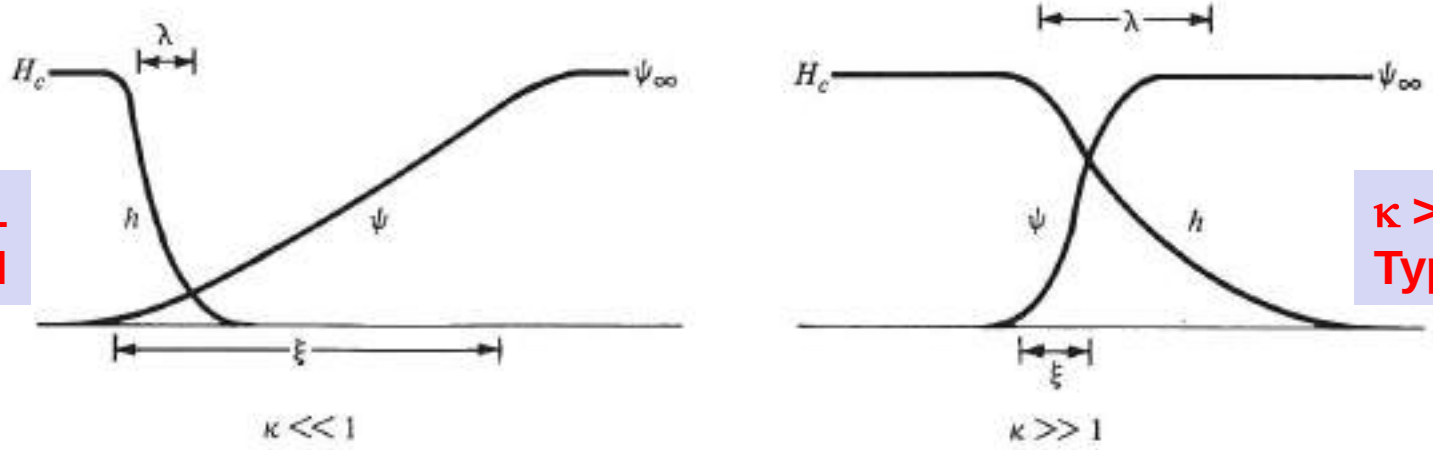

κ >> 1
Type II

FIGURE 4-2
Schematic diagram of variation of h and ψ in a domain wall. The case $\kappa \ll 1$ refers to a type I superconductor (positive wall energy); the case $\kappa \gg 1$ refers to a type II superconductor (negative wall energy).

Vortex State

In such mixed state, called the vortex state, the external magnetic field will penetrate the thin normal regions uniformly, and the field will also penetrate somewhat into the surrounding superconducting materials

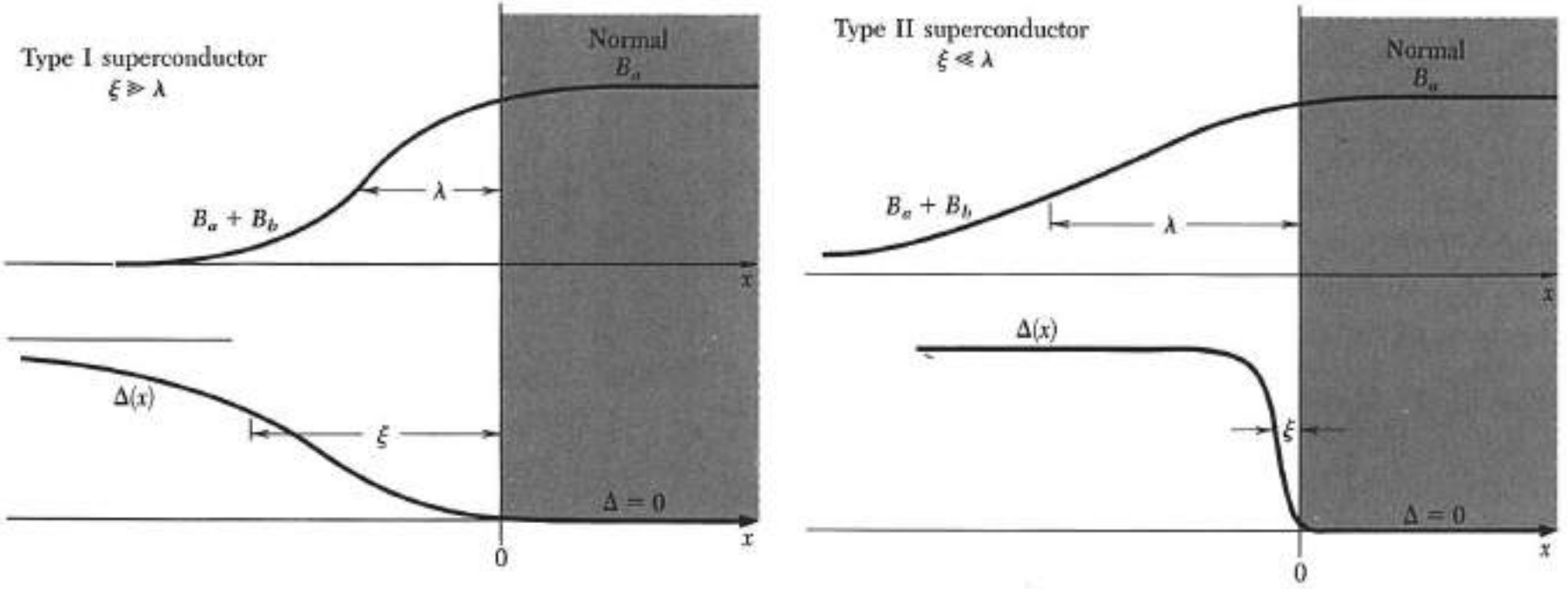

Figure 18 Variation of the magnetic field and energy gap parameter $\Delta(x)$ at the interface of superconducting and normal regions, for type I and type II superconductors. The energy gap parameter is a measure of the stabilization energy density of the superconducting state.

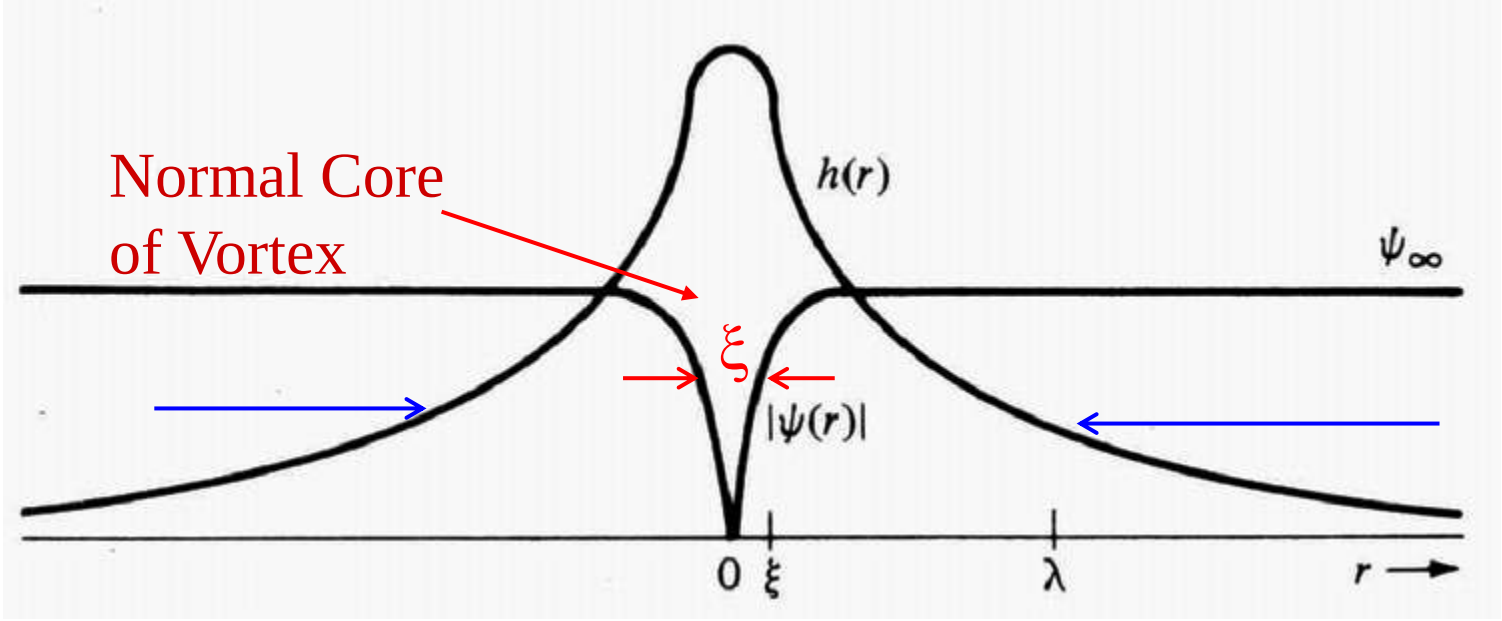

FIGURE 5-1
Structure of an isolated Abrikosov vortex in a material with $\kappa \approx 8$. The maximum value of $h(r)$ is approximately $2H_{c1}$.

$$\kappa = \lambda / \xi > 1$$

The term vortex state describes the circulation of superconducting currents in vortices throughout the bulk specimen,

Flux lattice
at 0.2K of $NbSe_2$

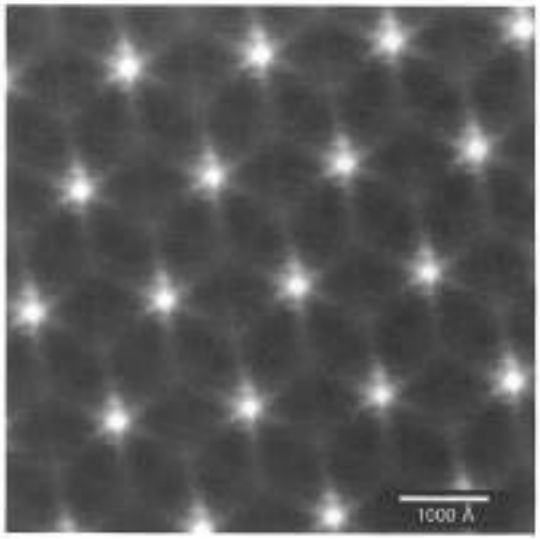

Abrikosov triangular lattice as imaged by LT-STM, H. Hess et al

Figure 19 Flux lattice in $NbSe_2$ at 1,000 gauss at 0.2K, as viewed with a scanning tunneling microscope. The photo shows the density of states at the Fermi level, as in Figure 23. The vortex cores have a high density of states and are shaded white; the superconducting regions are dark, with no states at the Fermi level. The amplitude and spatial extent of these states is determined by a potential well formed by $\Delta(x)$ as in Figure 18 for a Type II superconductor. The potential well confines the core state wavefunctions in the image here. The star shape is a finer feature, a result special to $NbSe_2$ of the sixfold disturbance of the charge density at the Fermi surface. Photo courtesy of H. F. Hess, AT&T Bell Laboratories.

The vortex state is stable when the penetration of the applied field into the superconducting material causes the surface energy become negative. A type II superconductor is characterized bv a vortex state stable over a certain range of magnetic field strength; namely, between $\boldsymbol{H}_{c1}$ and $\boldsymbol{H}_{c2}$.

Vortex Imaging of $NbSe_2$ by LT-STM

Harald F. Hess

© www.janelia.org

2H-$NbSe_2$: T_c = 7.1 K, T_{CDW} = 29 K

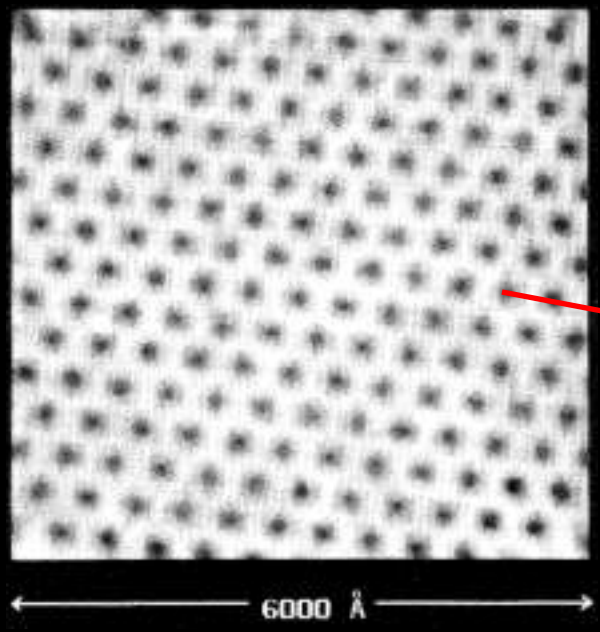

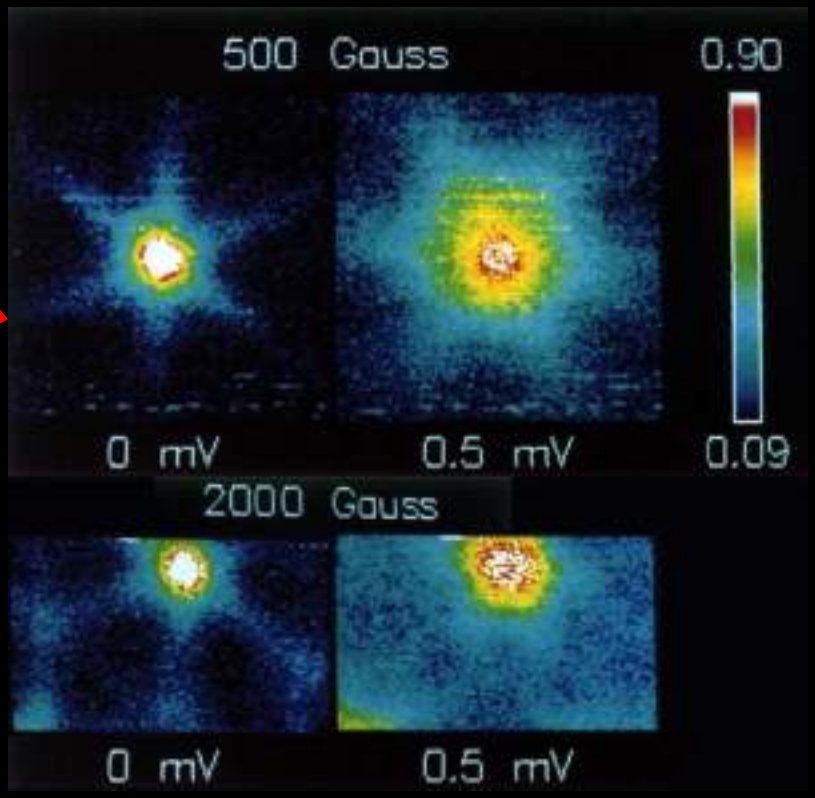

Abrikosov triangular lattice

H. F. Hess *et al.*, PRL 62, 214 (1989).
H. F. Hess *et al.*, PRL 64, 2711 (1990).

Doping *Pb* with some *In*

Type I SC becomes type II SC

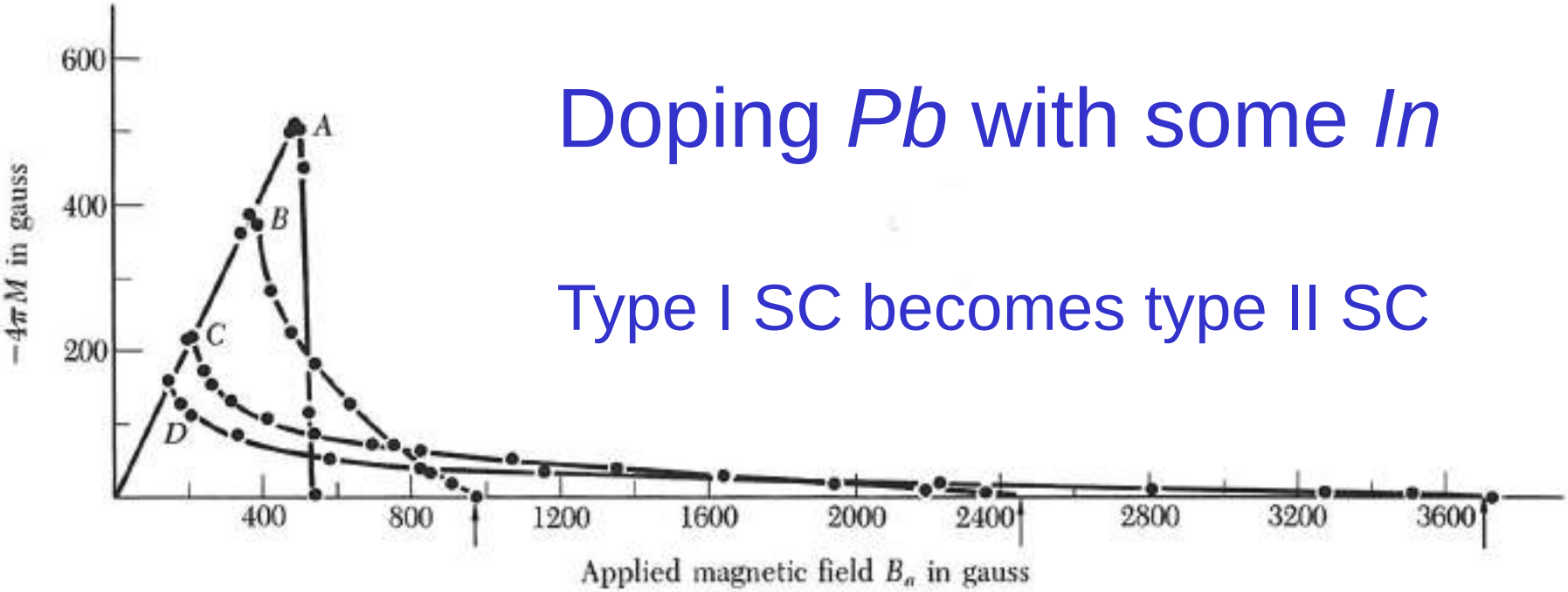

Figure 5a Superconducting magnetization curves of annealed polycrystalline lead and lead-indium alloys at 4.2 K. (*A*) lead; (*B*) lead–2.08 wt. percent indium; (*C*) lead–8.23 wt. percent indium; (*D*) lead–20.4 wt. percent indium. (After Livingston.)

Measured by pulsed magnetic field

Chevrel Phase (Ternary Sulfides)

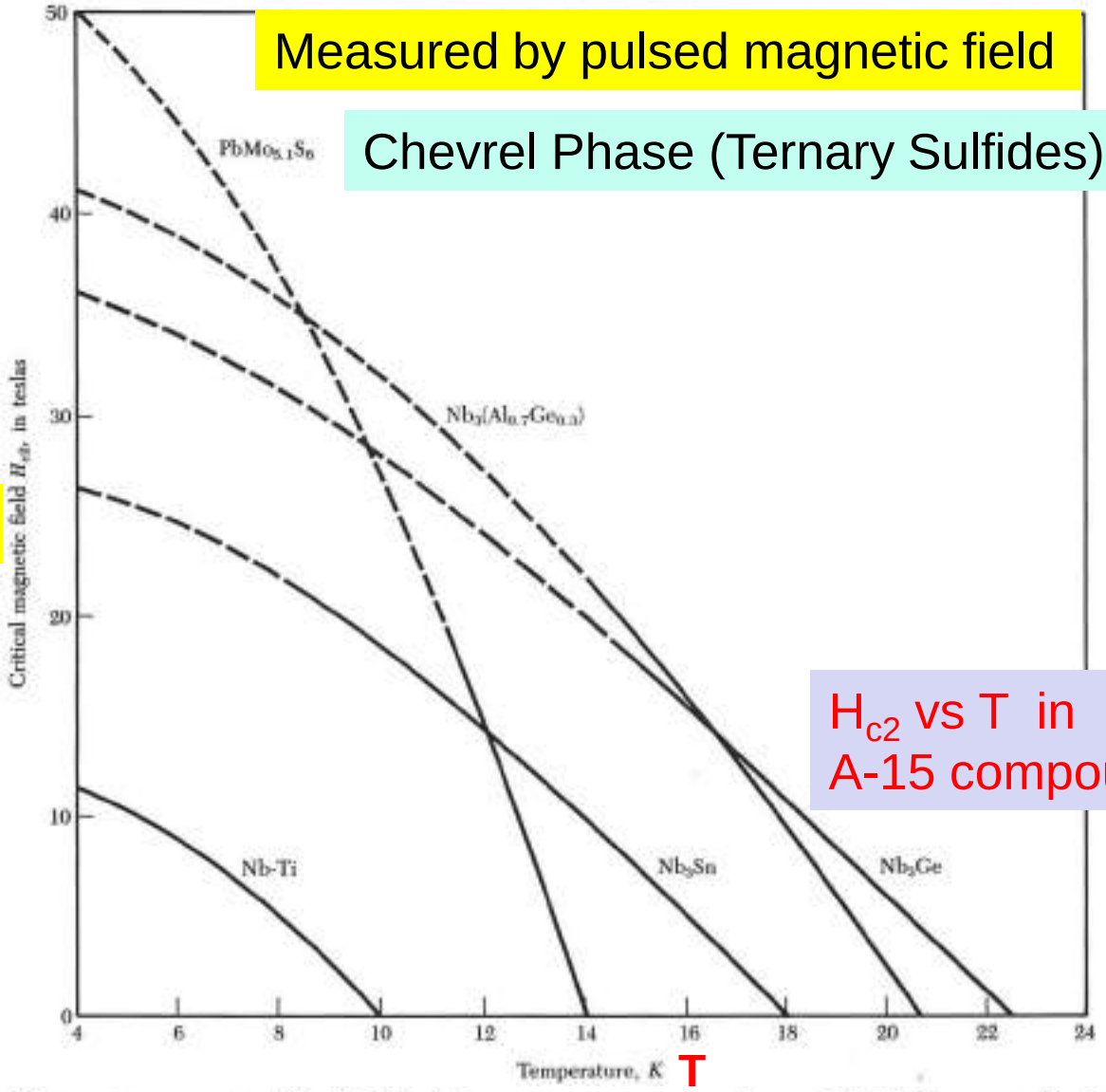

H_{c2}

T

H_{c2} vs T in A-15 compound

Figure 5b Stronger magnetic fields than any now contemplated in practical superconducting devices are within the capability of certain Type II materials. These materials cannot be exploited, however, until their critical current density can be raised and until they can be fabricated as finely divided conductors. (Magnetic fields of more than about 20 teslas can be generated only in pulses, and so portions of the curves shown as broken lines were measured in that way.)

Entropy S vs T for Aluminum

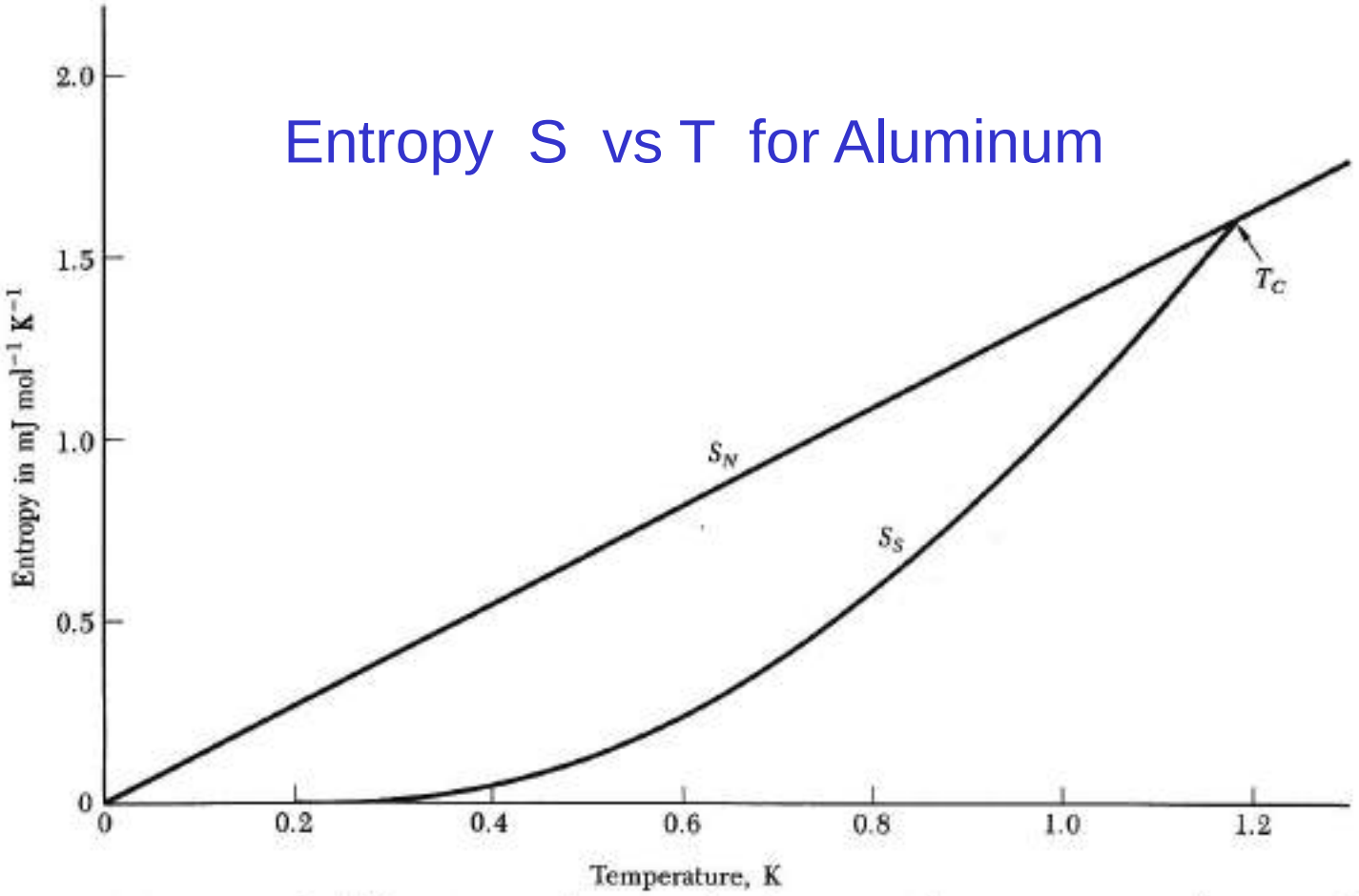

Figure 6 Entropy S of aluminum in the normal and superconducting states as a function of the temperature. The entropy is lower in the superconducting state because the electrons are more ordered here than in the normal state. At any temperature below the critical temperature T_c the specimen can be put in the normal state by application of a magnetic field stronger than the critical field.

The small entropy change must mean that only a small fraction (of the order of 10^{-4}) of the conduction electrons participate in the transition to the ordered superconducting state.

Free energy vs T for Aluminum

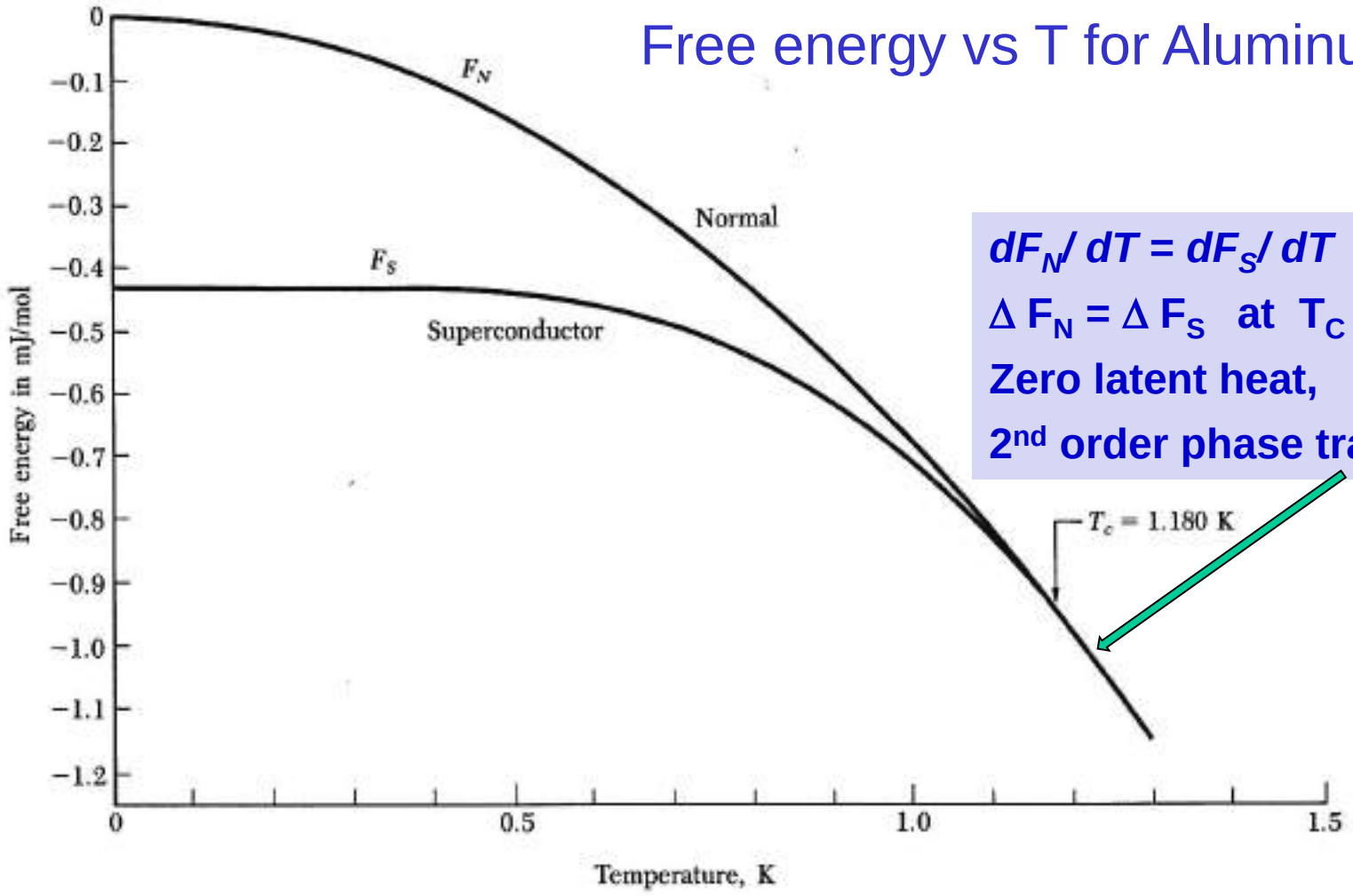

$dF_N/dT = dF_S/dT$ at T_C

$\Delta F_N = \Delta F_S$ at T_C

Zero latent heat,

2nd order phase transition

So that the phase transition is second order (there is no latent heat of transition at T_c).

heat capacity of an electron gas is

$$C_{el} = \frac{1}{3}\pi^2 D(\epsilon_F) k_B^2 T \qquad (34)$$

$$D(\epsilon_F) = 3N/2\epsilon_F = 3N/2\, k_B T_F \qquad (35)$$

$$\boxed{C_{el} = \frac{1}{2}\pi^2 N k_B T/T_F.} \qquad (36)$$

Compare with $C_V = 2Nk_BT/T_F$

where $\mathcal{E}_F = k_B T_F$

T_F is called the Fermi temperature,

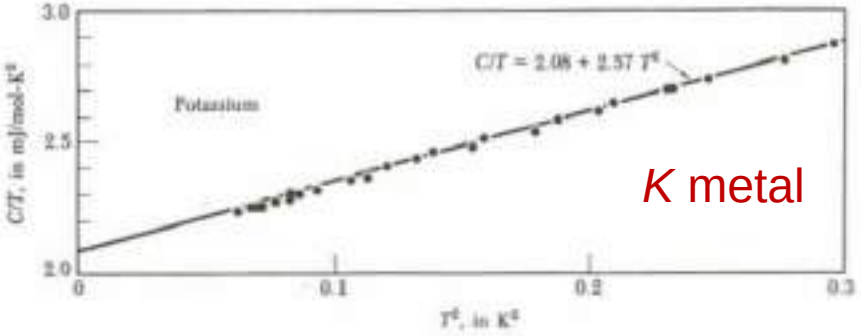

K metal

Figure 9 Experimental heat capacity values for potassium, plotted as C/T versus T^2. (After W. H. Lien and N. E. Phillips.)

$$\gamma = \frac{1}{2}\pi^2 N k_B T/T_F \quad \text{Since } \epsilon_F \propto T_F \propto 1/\text{m} \quad \therefore \gamma \propto m$$

(See Eq. 17)

At temperatures much below both the Debye temperature and the Fermi temperature, the heat capacity of metals may be written as the sum of electron and phonon contributions: $C = \gamma T + AT^3$

$$\boxed{C/T = \gamma + AT^2} \qquad (37)$$

γ , called the Sommerfeld parameter

At low T, the electronic term dominates.

Heat Capacity of Ga at low T

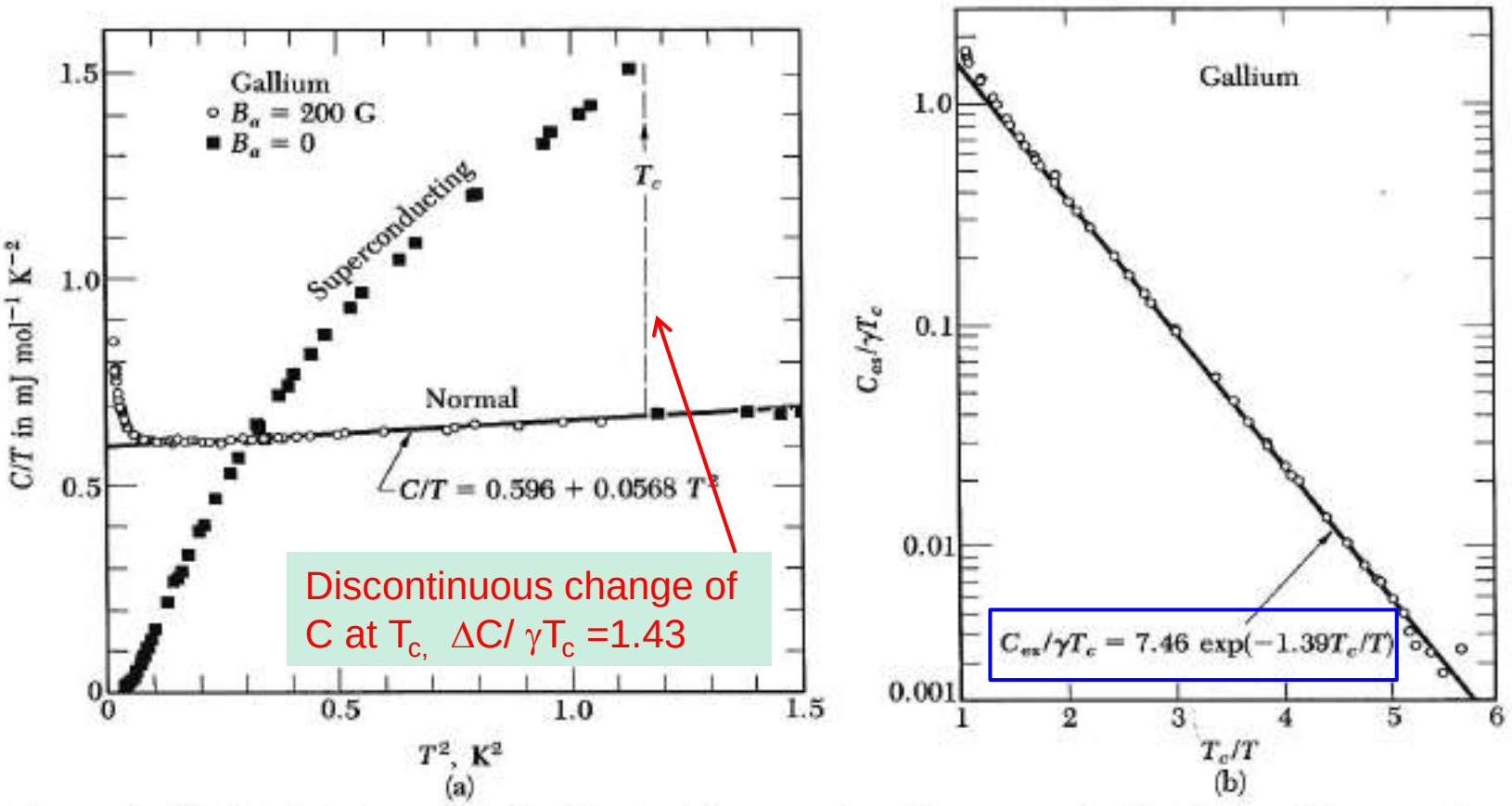

Figure 8 (a) The heat capacity of gallium in the normal and superconducting states. The normal state (which is restored by a 200 G field) has electronic, lattice, and (at low temperatures) nuclear quadrupole contributions. In (b) the electronic part C_{es} of the heat capacity in the superconducting state is plotted on a log scale versus T_c/T: the exponential dependence on $1/T$ is evident. Here $\gamma = 0.60$ mJ mol^{-1} deg^{-2}. (After N. E. Phillips.)

Electronic part of heat capacity in SC state: $C_{es}/\gamma T_c \propto a \exp(-bT_c/T)$

Proportional to -1/T, suggestive of excitation of electrons across an energy gap.

Evidence for Energy Gap in 1953

Another motivation for the BCS theory of superconductivity.

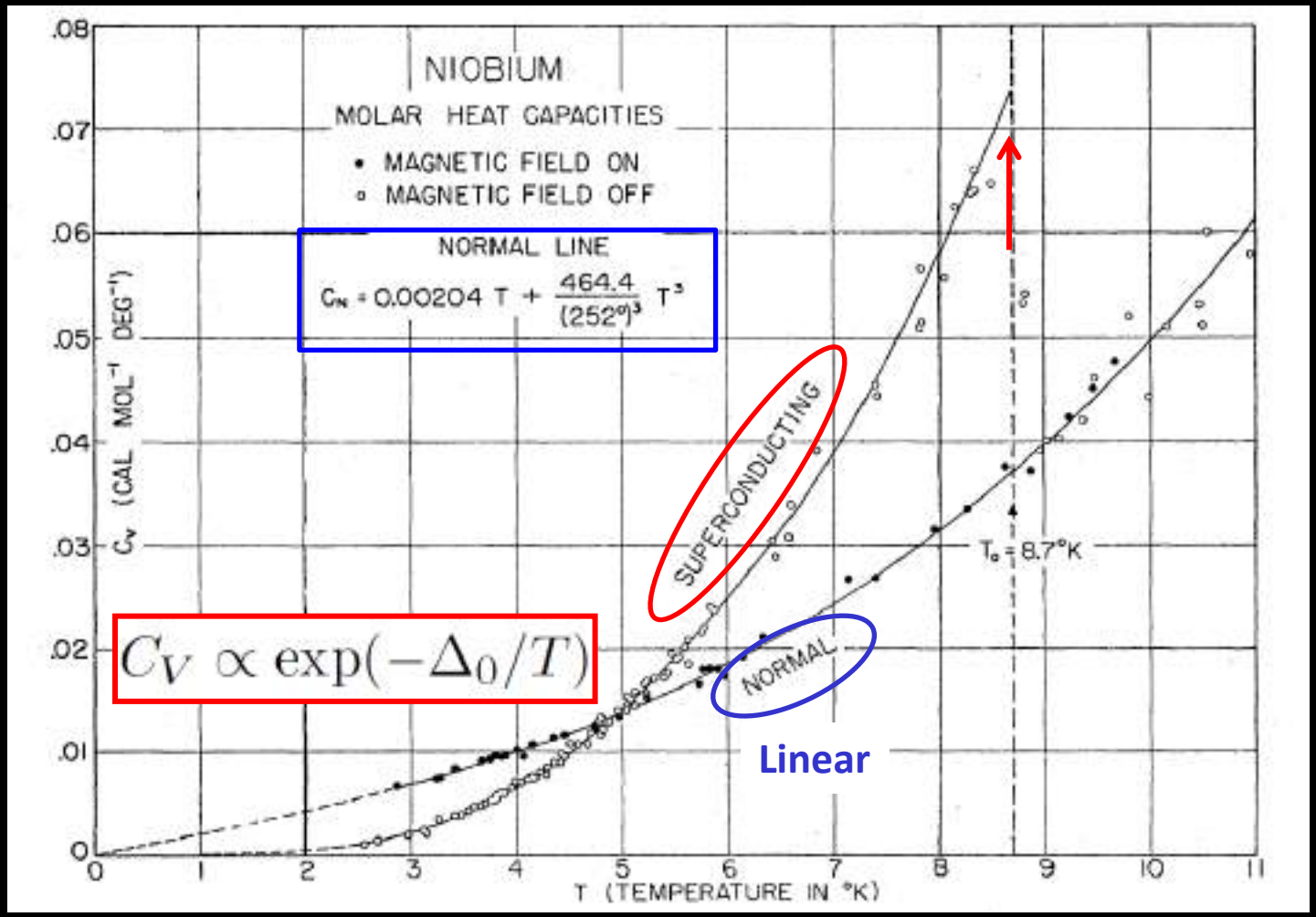

A. Brown, M. W. Zemansky, and H. A. Boorse, Phys. Rev. 92, 52 (1953)
B. B. Goodman, Proc. Phys. Soc. (London) **A66**, 217 (1953)

Energy Gap

In a superconductor the important interaction is the electron-electron interaction via phonons, which orders the electron in the k space with respect to the Fermi gas of electrons.

The exponential factor in the electron heat capacity of a superconductor Is found to be $-E_g/2k_BT$

$$C_{es} = \gamma T_c \exp(-1.76\, T_c/T)$$

The transition in zero magnetic field from the superconducting state to the normal state is observed to be a second-order phase transition.

Energy Gap of superconductors in **Table 3**

$E_g(0)/k_BT_c = 3.52$ Weak electron-phonon coupling

$E_g(0)/k_BT_c > 3.52$ Strong electron-phonon coupling

Table 3 Energy gaps in superconductors, at $T = 0$

$E_g(0)$ in 10^{-4}eV.
$E_g(0)/k_BT_c$.

$= 2\Delta$

										Al	Si
										3.4	
										3.3	
Sc	Ti	V	Cr	Mn	Fe	Co	Ni	Cu	Zn	Ga	Ge
		16.							2.4	3.3	
		3.4							3.2	3.5	
Y	Zr	Nb	Mo	Tc	Ru	Rh	Pd	Ag	Cd	In	Sn (w)
		30.5	2.7						1.5	10.5	11.5
		3.80	3.4						3.2	3.6	3.5
La fcc	Hf	Ta	W	Re	Os	Ir	Pt	Au	Hg (α)	Tl	Pb
19.		14.							16.5	7.35	27.3
3.7		3.60							4.6	3.57	4.38

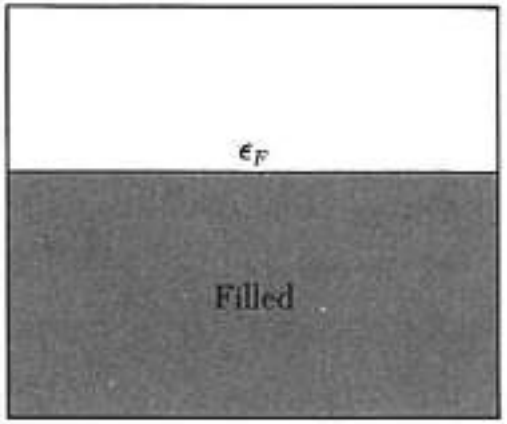

Normal
(a)

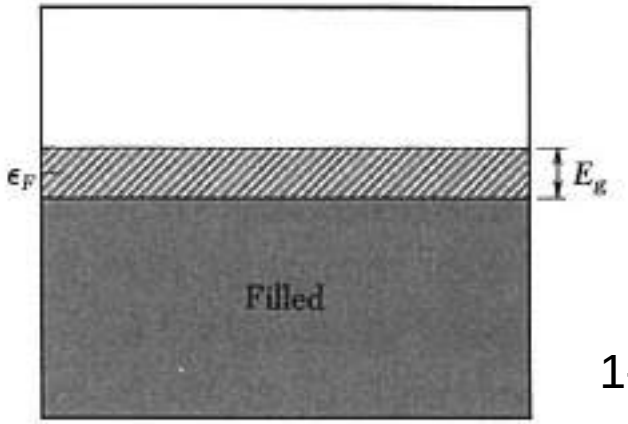

Superconductor
(b)

$E_g \sim 10^{-4}\ \varepsilon_F$

1-5 meV 3-10 eV

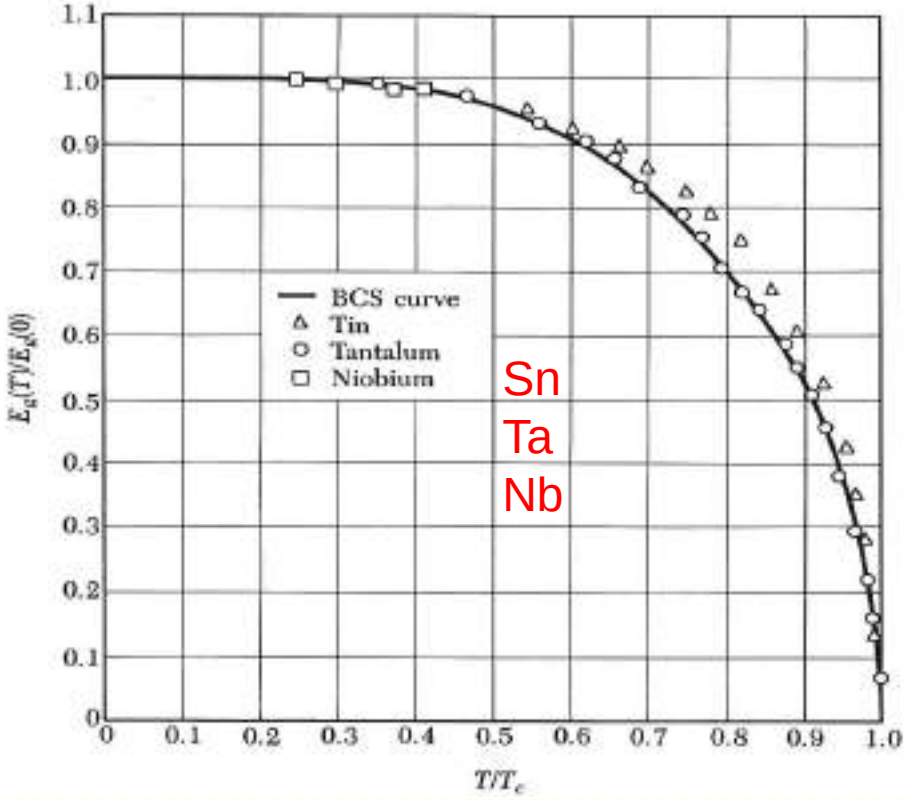

$\Delta(T)/\Delta(0) = (1 - T/T_c)^{1/2}$

Mean field theory

Figure 10 Reduced values of the observed energy gap $E_g(T)/E_g(0)$ as a function of the reduced temperature T/T_c, after Townsend and Sutton. The solid curve is drawn for the BCS theory.

$E_g(T)$ as the order parameter, goes smoothly to zero at T_c
-- second order phase transition

Isotope Effect in 1950

- Lattice vibration is a part of the SC process.
- A crucial step to a microscopic theory.

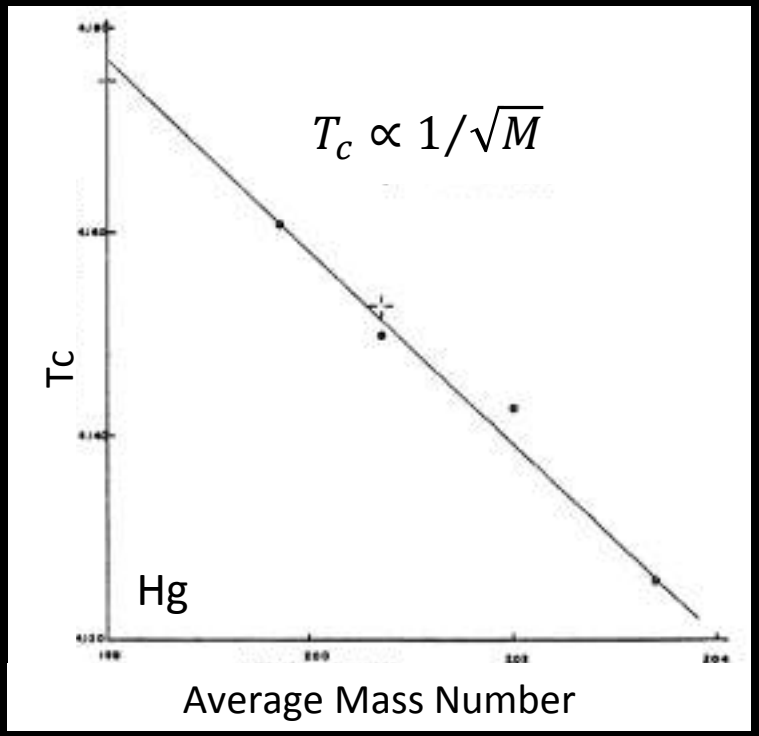

Emanuel Maxwell, Phys. Rev. 78, 477 (1950)
C.A. Reynolds et al., Phys. Rev. 78, 487 (1950)

Emanuel Maxwell

© MIT

Bernard Serin & Charles Reynolds

© Rutgers University

Isotope Effect

It has been observed that the critical temperature of superconductors varies with isotopic mass.

The experimental results within each series of isotopes may be fitted by a relation of the form

$$M^{\alpha}T_c = \text{constant} \qquad \alpha \sim 0.5$$

Table 4 Isotope effect in superconductors

Experimental values of α in $M^{\alpha}T_c$ = constant, where M is the isotopic mass.

Substance	α	Substance	α
Zn	0.45 ± 0.05	Ru	0.00 ± 0.05
Cd	0.32 ± 0.07	Os	0.15 ± 0.05
Sn	0.47 ± 0.02	Mo	0.33
Hg	0.50 ± 0.03	Nb_3Sn	0.08 ± 0.02
Pb	0.49 ± 0.02	Zr	0.00 ± 0.05

From the dependence of T_c on the isotopic mass we learn that lattice vibrations and hence electron-lattice interactions are deeply involved in superconductivity.

$\theta \propto \upsilon \propto M^{-1/2}$

$$T_c \propto \theta_{\text{Debye}} \propto M^{-1/2}, \text{ so that } \alpha = \tfrac{1}{2}$$

3. The penetration depth and the coherence length emerge as natural consequence of the BCS theory. The London equation is obtained for magnetic fields that vary slowly in space. Thus, the central phenomenon in superconductivity, the Meissner effect, is obtained in a natural way.

penetration depth (λ) ; coherence length (ξ)

4. The electron density of orbitals $D(E_F)$ of one spin at the Fermi level, and the electron –lattice interaction U. For $UD(E_F) << 1$, the BCS theory predicts:

$$T_c = 1.14\theta \exp[-1/UD(\epsilon_F)] \quad , \quad 2\Delta / k_B T_c = 3.52$$

Where θ is the Debye temperature, and U is an attractive interaction (electron-phonon interaction).

For dirty metal (a poor conductor) → ρ(300)↑, U↑, T_c↑ (but a good SC)

5. Magnetic flux through a superconducting ring is quantized and the effective unit of charge is $2e$ rather than e.

Evidence of pairing of electrons

Perfect Conductor vs Superconductor

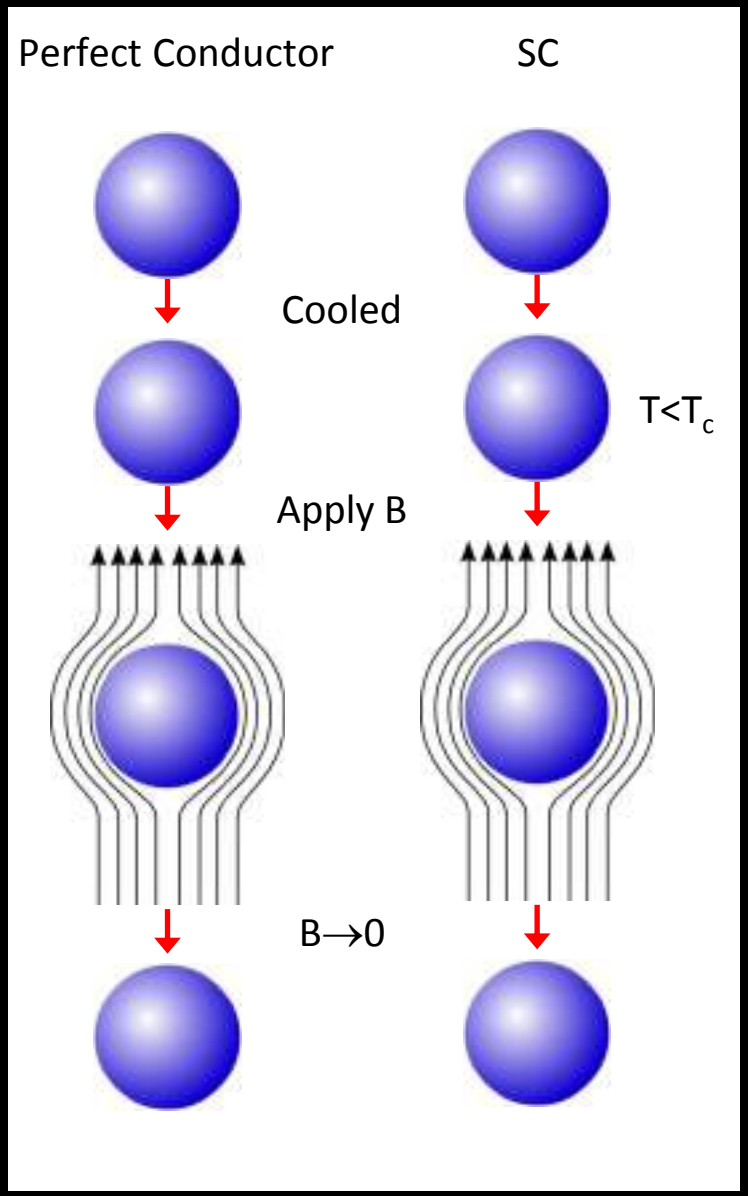

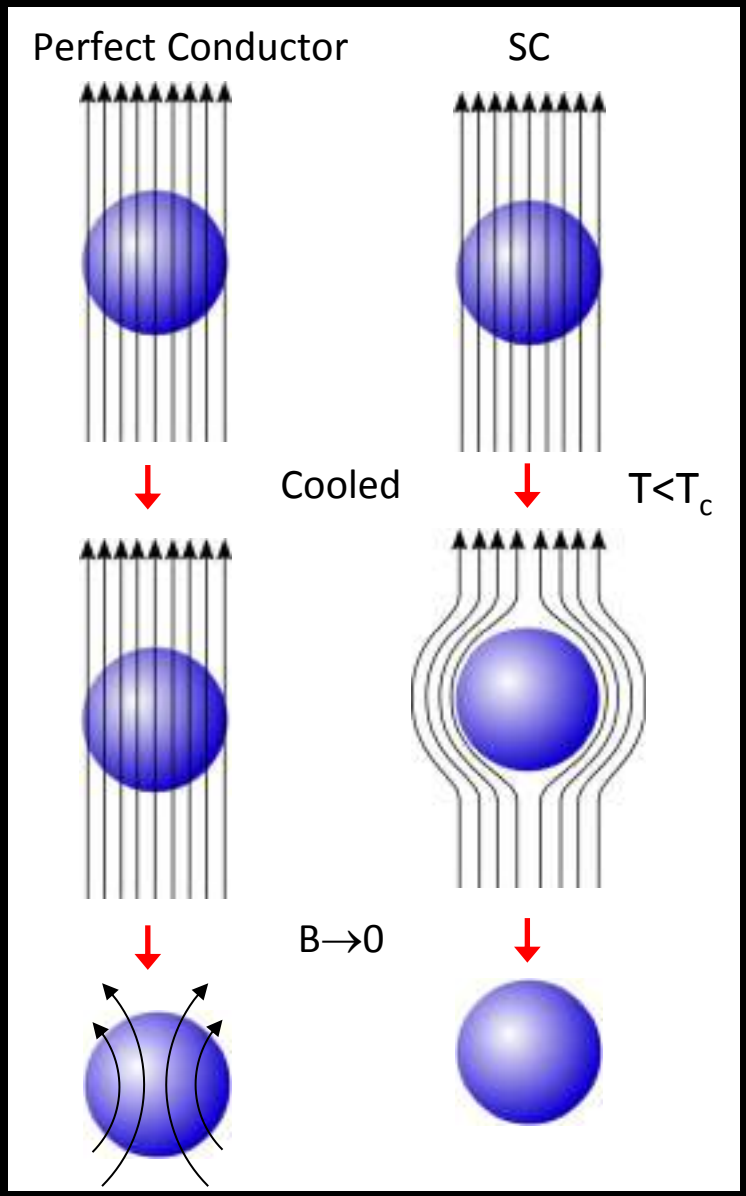

Vortex-Current Interaction

- Lorentz force on J_S due to the interaction between J_S and B.

$$f = \int J_s \times B \, d^2r = J_{tr} \times \int B \, d^2r = J_{tr} \times (\phi_0 \bar{B})$$

- Vortex motion implies that the vortex is subject to a power input per unit volume of vortex of characteristic radius r_B

$$P = \frac{f v}{\pi r_B^{\,2}} = J_{tr} \frac{\phi_0}{\pi r_B^{\,2}} v = \underbrace{J_{tr} B v}_{\text{Lorentz force per unit volume}}$$

- Vortex motion leads to dissipation! R≠0 !
- Vortex pinning is crucial for applications.

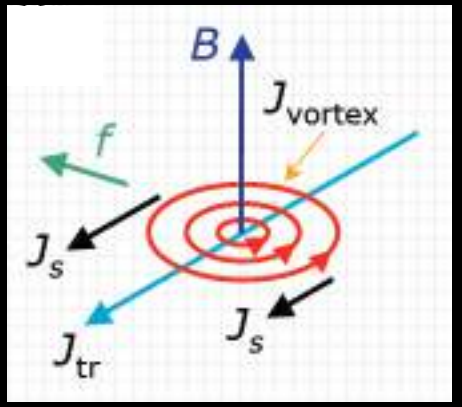

Magnus force

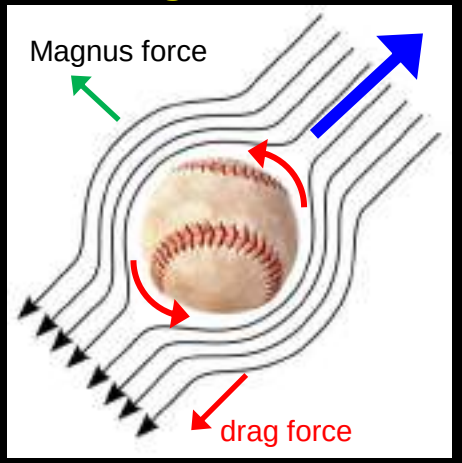

Quantum Levitation

Magnetic flux pinning is key.
Unstable for type I superconductors.

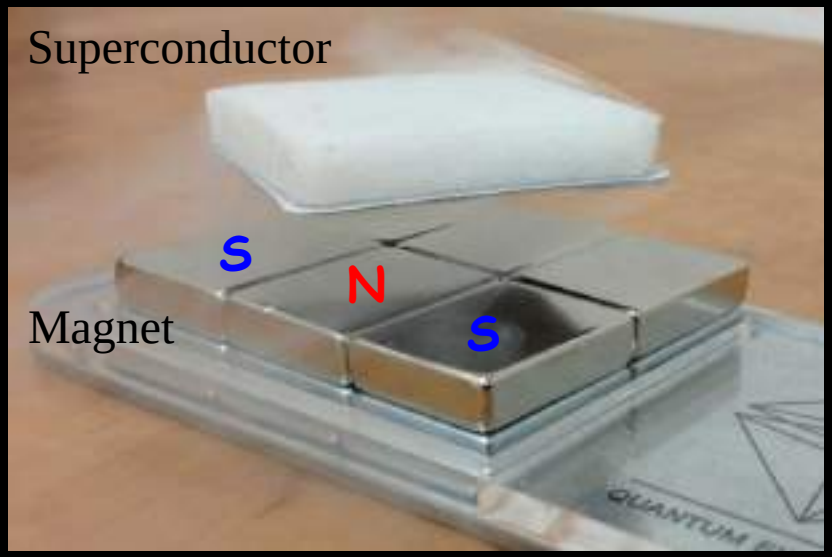

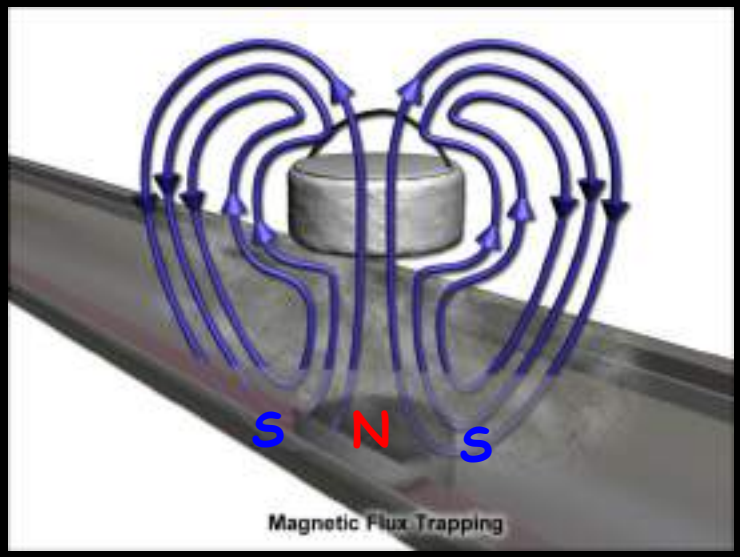

A legacy of Superconductivity

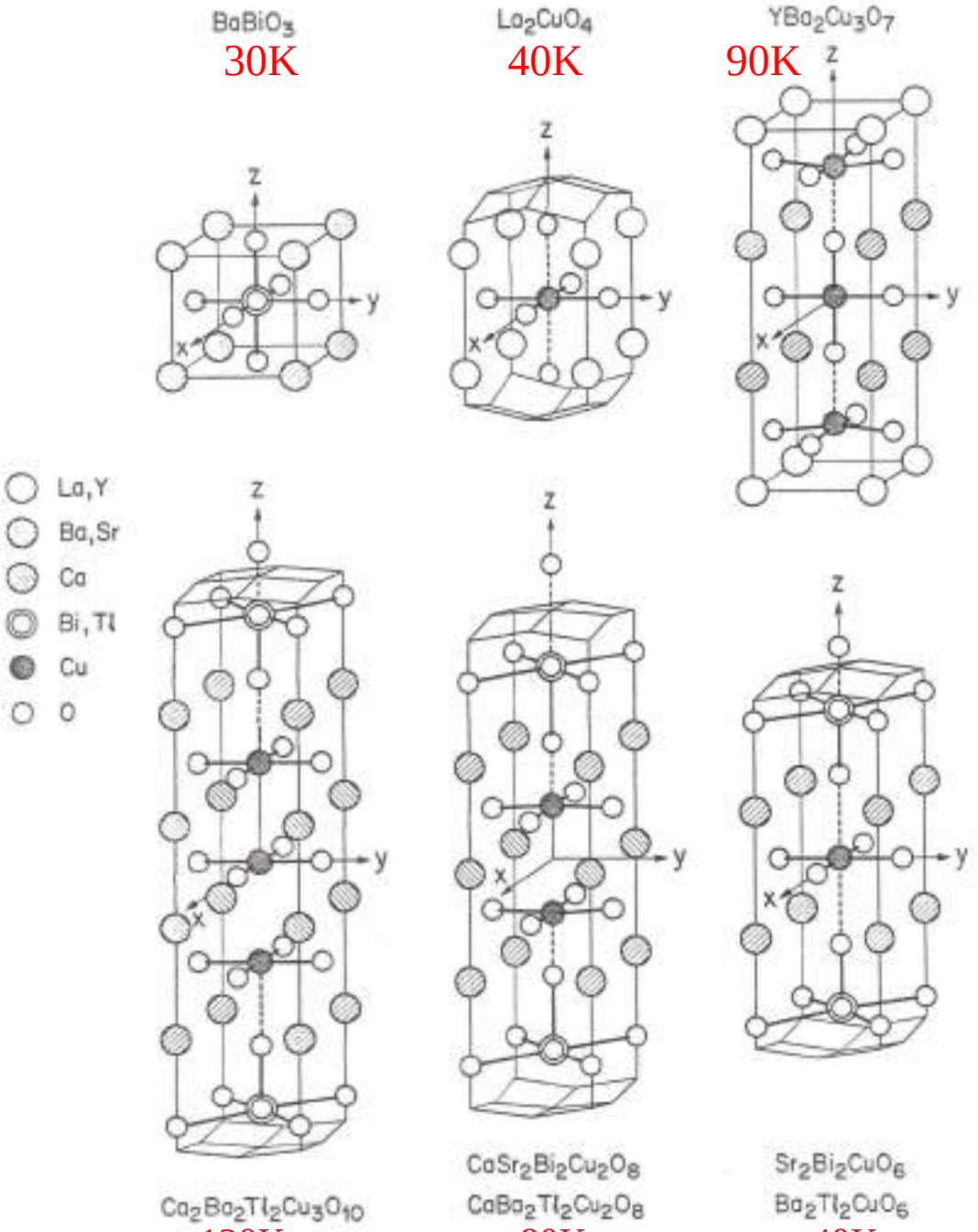
BaBiO3
30K
La2CuO4
40K
YBa2Cu3O7
90K
La,Y
Ba,Sr
Ca
Bi,Tl
Cu
O
Ca2Ba2Tl2Cu3O10
120K
CaSr2Bi2Cu2O8
CaBa2Tl2Cu2O8
80K
Sr2Bi2CuO6
Ba2Tl2CuO6
40K

THEORETICAL SURVEY

Theories of Superconductivity

1. **Phenomenological** equations: the London equations and the Landau-Ginzburg equations

   In 1950, a psuedo wave function ψ *for the SC state,* $n_s = |\psi|^2$

2. **Quantum** theory of superconductivity was given by Bardeen, Cooper, and Schrieffer (BCS).

   --Microscopic theory, 1957

   --1959, Gorkov derives a macroscopic form of BCS theory near T_c , and **the order parameter is proportional to the gap function Δ_g**

3. Subsequent work of Josephson and Anderson discovered the importance of the **phase** of the superconducting wave function.

   Josephson effect:
   - as the first case of theory leading experiment in SC !!

(1) *Thermodynamics of the Superconducting Transition*

1. The transition between the normal and superconducting state is thermodynamically reversible.

2. The critical field H_c is a quantitative measure of the free energy difference between the superconducting and normal states at constant temperature.

3. The stabilization free energy of the superconducting state with respect to the normal state can be determined by *calorimetric,* or *magnetic* measurements.

a. In the calorimetric method: From the difference of the heat capacities we can compute the free energy difference, which is the stabilization free energy of the superconducting state.

b. In the magnetic method: The stabilization free energy is found from the value of the applied magnetic field, that will destroy the superconducting state at constant temperature.

H_c : *Thermodynamic critical field*

Consider the work done (Fig. 11) on a superconductor, when it is brought reversibly at constant temperature from a position at infinity (where the applied field is zero) to a position **r** in the field of a permanent magnet:

$$W = -\int_0^{B_a} \mathbf{M} \cdot d\mathbf{B}_a \ , \qquad (3)$$

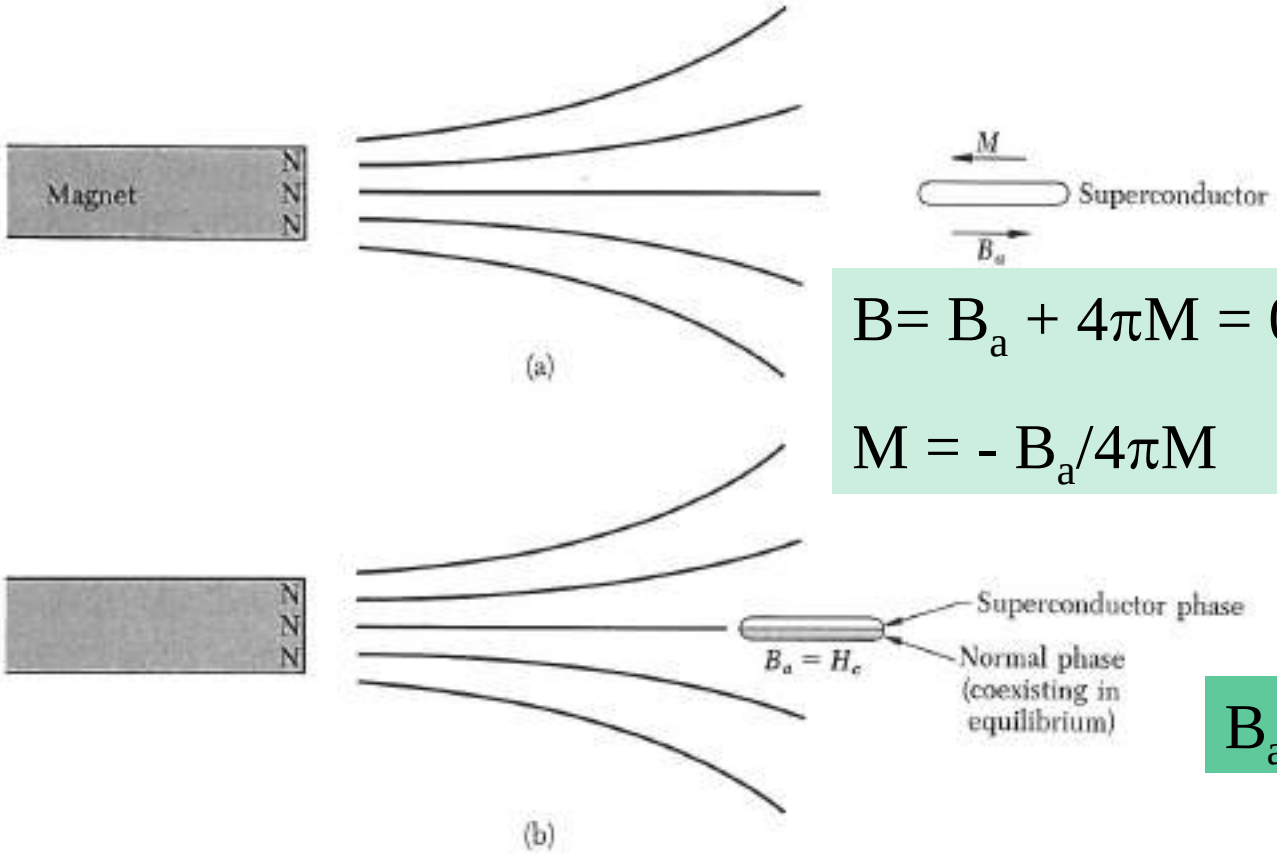

$B = B_a + 4\pi M = 0$, inside SC

$M = - B_a/4\pi M$

$B_a = H_c$

Figure 11 (a) A superconductor in which the Meissner effect is complete has $B = 0$, as if the magnetization were $M = -B_a/4\pi$, in CGS units. (b) When the applied field reaches the value B_{ac}, the normal state can coexist in equilibrium with the superconducting state. In coexistence the free energy densities are equal: $F_N(T, B_{ac}) = F_S(T, B_{ac})$.

The thermodynamic identity for the process is

$$d\boldsymbol{F} = -\mathbf{M}\cdot d\boldsymbol{B}_a \,, \qquad (4)$$

For a superconductor with **M** related to $\boldsymbol{B}_a$ by (1) $M = (-1/4\pi)B_a$

$$d\boldsymbol{F}_S = \frac{1}{4\pi}\, \boldsymbol{B}_a \; d\boldsymbol{B}_a \quad ; \qquad (5)$$

The increase in the free energy density of the superconductor is

$$\boldsymbol{F}_S(\boldsymbol{B}_a) - \boldsymbol{F}_S(0) = \boldsymbol{B}_a^{\,2} / 8\pi \; ; \qquad (6)$$

Now consider a normal nonmagnetic metal. Then M = 0 the energy of the normal metal is independent of field. At the critical field we have

$$\boldsymbol{F}_N(\boldsymbol{B}_{ac}) = \boldsymbol{F}_N(0) \;\; . \qquad (7)$$

At the critical value $\boldsymbol{B}_{ac}$ of the applied magnetic field the energies are equal in the normal and superconducting states:

$$\boldsymbol{F}_N(\boldsymbol{B}_{ac}) = \boldsymbol{F}_S(\boldsymbol{B}_{ac}) = \boldsymbol{F}_S(0) + \boldsymbol{B}_a^{\,2} / 8\pi \; . \qquad (8)$$

$$\Delta F \equiv F_N(0) - F_S(0) = B_{ac}^2 / 8\pi \,, \qquad (9)$$

Where ΔF is the stabilization free energy density of the superconducting state.

At a finite temperature the normal and superconducting phases are in equilibrium, when the magnetic field is such that their free energies **F = U - TS** are equal.

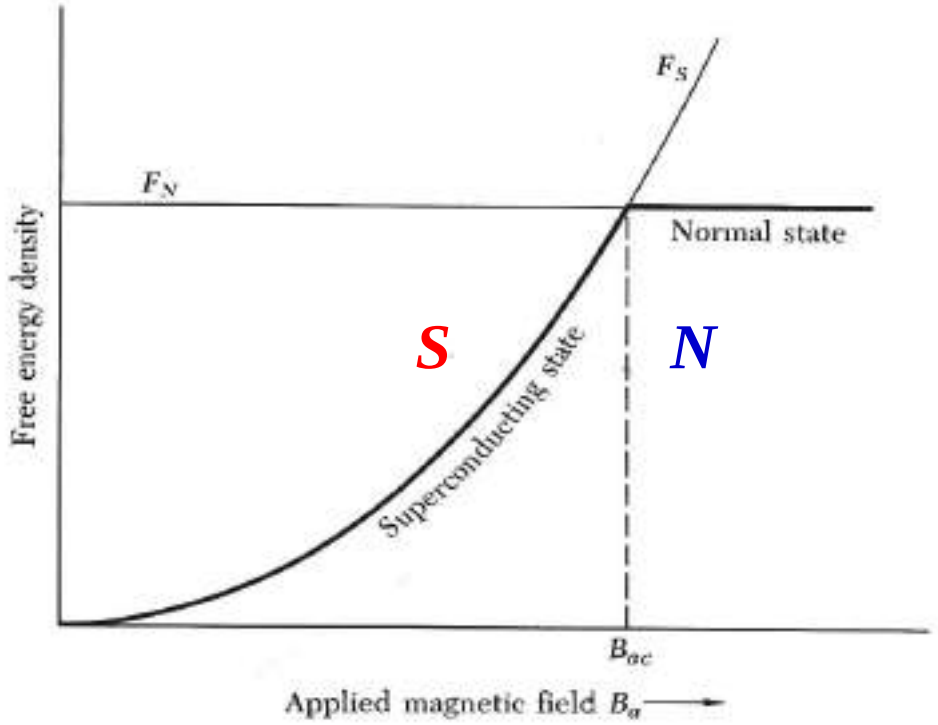

Figure 12 The free energy density F_N of a nonmagnetic normal metal is approximately independent of the intensity of the applied magnetic field B_a. At a temperature $T < T_c$ the metal is a superconductor in zero magnetic field, so that $F_S(T, 0)$ is lower than $F_N(T, 0)$. An applied magnetic field increases F_s by $B_a^2/8\pi$, in CGS units, so that $F_S(T, B_a) = F_S(T, 0) + B_a^2/8\pi$. If B_a is larger than the critical field B_{ac} the free energy density is lower in the normal state than in the superconducting state, and now the normal state is the stable state. The origin of the vertical scale in the drawing is at $F_S(T, 0)$. The figure equally applies to U_S and U_N at $T = 0$.

Free energy vs T for Aluminum

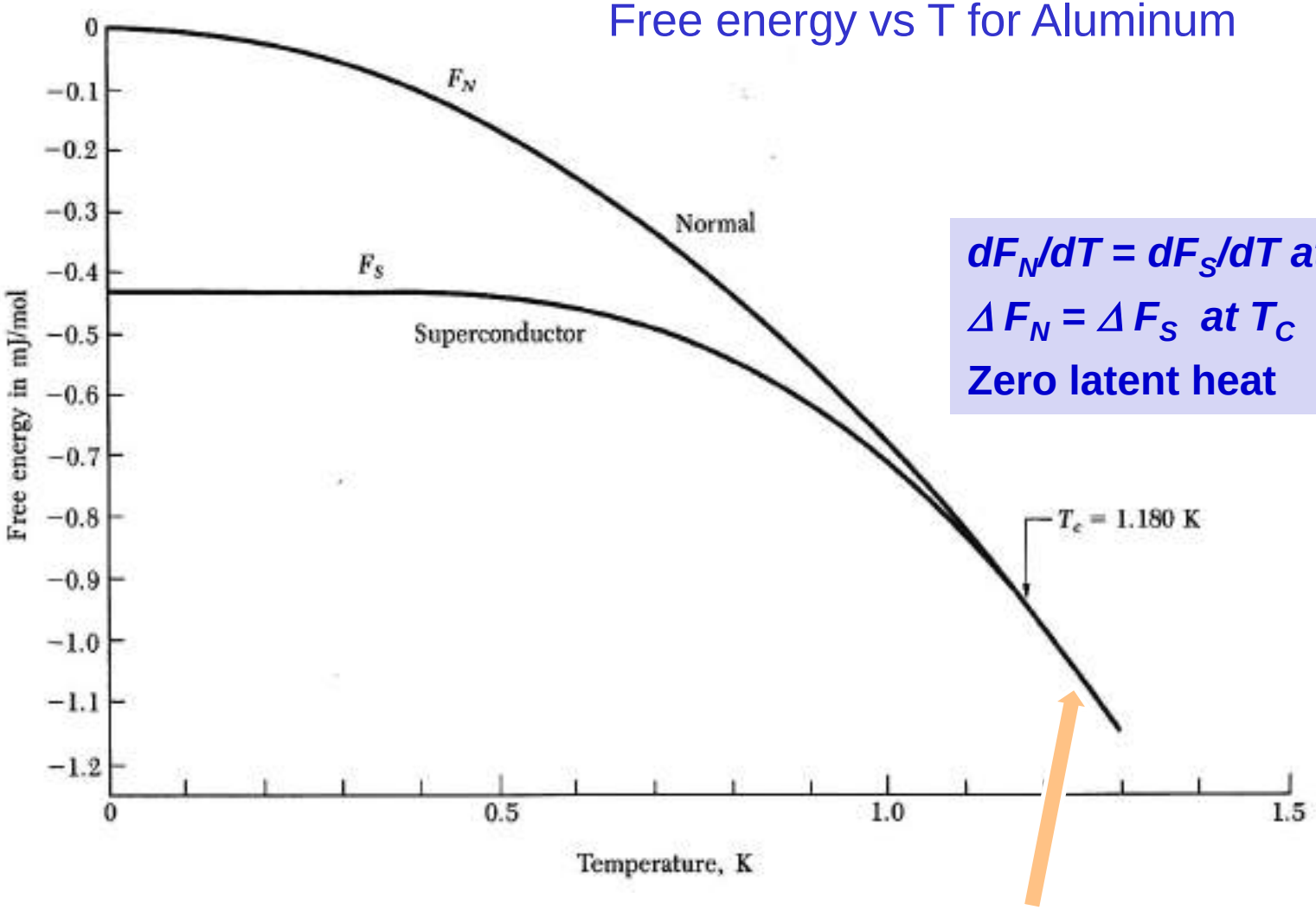

$dF_N/dT = dF_S/dT$ at T_C

$\Delta F_N = \Delta F_S$ at T_C

Zero latent heat

So that the phase transition is second order.
(There is no latent heat of transition at T_c).

(2) London Equation

Electrical conduction in the normal state of a metal is described by Ohm's law. $J = \sigma E$

We postulate that in the superconducting state the current density is directly proportional to the vector potential **A** of the local magnetic field **B,**

$$\mathbf{j} = - \frac{c}{4\pi\lambda_L^2} \mathbf{A}$$

The concept of "Local Field"

➡ ***London Equation***

Since B = curl A

$$\text{curl } \mathbf{j} = - \frac{c}{4\pi\lambda_L^2} \mathbf{B} \quad ;$$

$$\text{curl } \mathbf{B} = (4\pi/c)\, \mathbf{j}$$

from ***Maxwell Equation***

$$\text{curl curl } \mathbf{B} = - \nabla^2 \mathbf{B} = (4\pi/c)\, \text{curl } \mathbf{j}$$

$$\nabla^2 \mathbf{B} = \mathbf{B}/\lambda_L^{\,2}$$

$$\boldsymbol{B}(x) = \boldsymbol{B}(0) \exp(- x / \lambda_L) ,$$

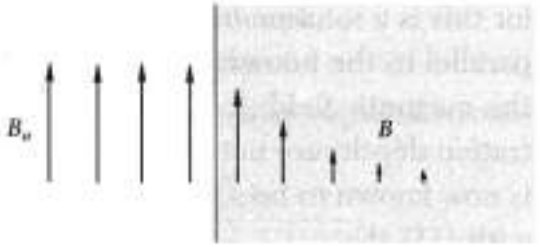

$$\boldsymbol{B}(x) = \boldsymbol{B}(0)\exp(-x/\lambda_L)\,,$$

Figure 13 Penetration of an applied magnetic field into a semi-infinite superconductor. The penetration depth λ is defined as the distance in which the field decreases by the factor e^{-1}. Typically, $\lambda \simeq 500$ Å in a pure superconductor.

Table 5 Calculated intrinsic coherence length and London penetration depth, at absolute zero

Metal	Intrinsic Pippard coherence length ξ_0, in 10^{-6} cm	London penetration depth λ_L, in 10^{-6} cm	λ_L/ξ_0
Sn	23.	3.4	0.16
Al	160.	1.6	0.010
Pb	8.3	3.7	0.45
Cd	76.	11.0	0.14
Nb	3.8	3.9	1.02

After R. Meservey and B. B. Schwartz.

Type I SC

Type II SC

See slide #24

$\lambda_L = (mc^2/4\pi nq^2)^{1/2}$; London Penetration Depth

An applied magnetic field B_a will penetrate into a thin film fairly uniformly, if the thickness is much less than λ_L; thus in a thin film the Meissner effect is not complete. In a thin film, the induced field is much less than B_a.

(3) *Coherence Length*

1. **Coherence length** is a measure of the distance within which the SC electron concentration cannot change drastically in a spatially varying magnetic field**.**
2. The **coherence length** is a measure of the range over which we should average **A** to obtain **j.**
3. It is also a measure of **the minimum spatial extent** of a transition layer between normal and SC.

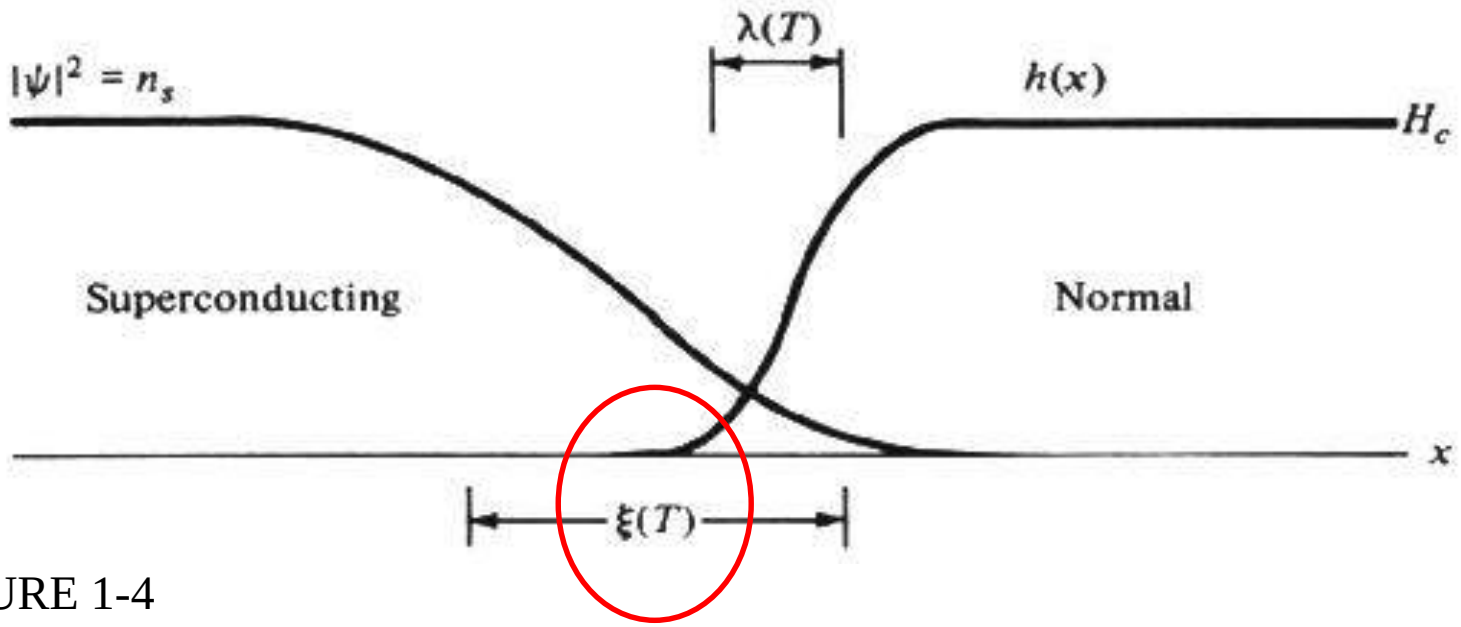

FIGURE 1-4
Interface between superconducting and normal domains in the intermediate state.

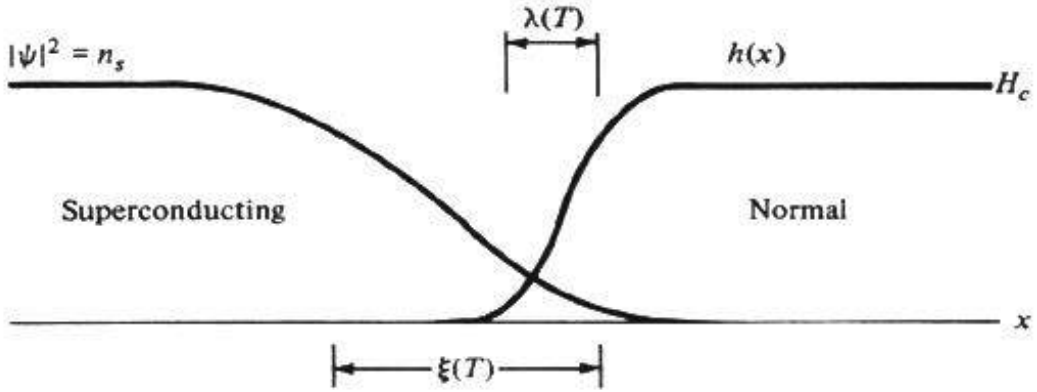

FIGURE 1-4
Interface between superconducting and normal domains in the intermediate state.

$$\kappa = \frac{\lambda_{\text{eff}}(T)}{\xi(T)} = \frac{2\sqrt{2}\,\pi H_c(T)\lambda_{\text{eff}}^2(T)}{\Phi_0}$$

Ginsburg Landau Parameters Tinkham, eq. (4-27)

κ << 1 Type I

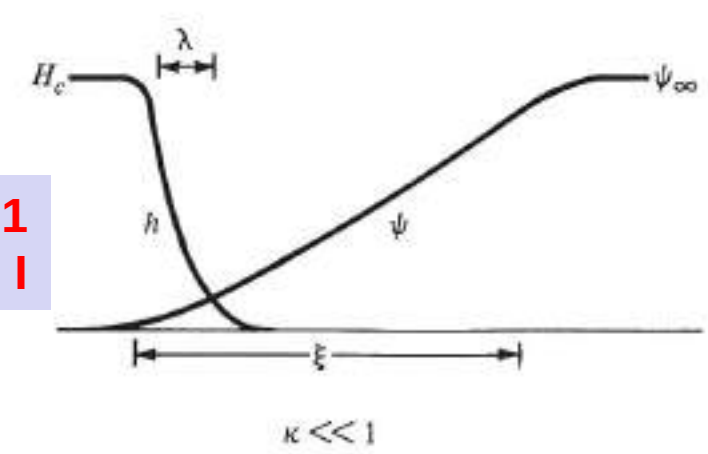

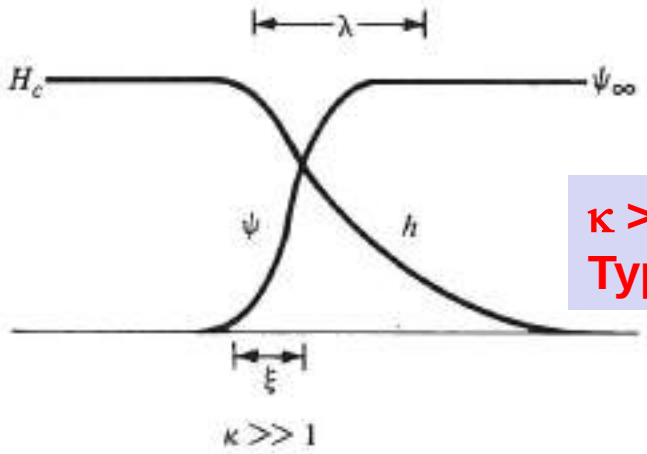

κ >> 1 Type II

FIGURE 4-2
Schematic diagram of variation of h and ψ in a domain wall. The case $\kappa \ll 1$ refers to a type I superconductor (positive wall energy); the case $\kappa \gg 1$ refers to a type II superconductor (negative wall energy).

Any spatial variation in the state of an electronic system requires extra kinetic energy. It is reasonable to restrict the spatial variation of ***j (r)*** in such a way that the extra energy is less than the stabilization energy of the SC state.

$$\varphi(x) = 2^{-1/2}\,(e^{i(k+q)x} + e^{ikx})$$

Whereas $\psi^*\psi$ is modulated with the wavevector $\boldsymbol{q}$

$$\varphi^*\varphi = \tfrac{1}{2}(e^{-i(k+q)x} + e^{-ikx})(e^{i(k+q)x} + e^{ikx})$$
$$= \tfrac{1}{2}(2 + e^{iqx} + e^{-iqx}) = 1 + \cos qx \ . \qquad (15b)$$

$$\int dx\ \varphi^* \left(-\frac{\hbar^2}{2m}\frac{d^2}{dx^2}\right)\varphi = \frac{1}{2}\left(\frac{\hbar^2}{2m}\right)[(k+q)^2 + k^2] \cong \frac{\hbar^2}{2m}k^2 + \frac{\hbar^2}{2m}kq$$

E_g

The increase of the energy required to modulate is $\boldsymbol{\hbar^2 kq/2m}$.

If this increase exceeds the energy gap $\boldsymbol{E_g}$, superconductivity will destroy.

We define an **intrinsic coherence length** $\boldsymbol{\xi_o}$ related to the critical modulation by $\boldsymbol{\xi_o = 1/q_o}$ at $k = k_F$.

$$\xi_0 = \hbar^2 k_F/2mE_g = \hbar v_F/2E_g \ ,$$

From the BCS theory, for a pure SC, the exact form

$$\xi_0 = 2\hbar v_F/\pi E_g \ .$$

Another derivation

$$\Delta t \cdot \Delta E \sim \hbar$$
$$\Delta x/v_F \cdot E_g \sim \hbar$$
$$\xi_o/v_F \cdot E_g \sim \hbar$$
$$\xi_o \sim \hbar v_F/E_g$$

In impure materials and in alloys the coherence length ξ is shorted than ξ_o. The coherence length and the actual penetration depth λ depends on the mean free path l of the electrons measured in the normal state; the relationships are indicted in Fig. 14. When the superconductor is very impure, with a very small l.

then $\xi \approx (\xi_o \ell)^{1/2}$

$\lambda \approx \lambda_L (\xi_o / \ell)^{1/2}$

at very small mean free path ℓ in impure SC

so that $\lambda/\xi \approx \lambda_L / \ell$.

This is the "dirty superconductor" limit.

The ratio λ/ξ is denoted by κ .

Figure 14 Penetration depth λ and the coherence length ξ as functions of the mean free path ℓ of the conduction electrons in the normal state. All lengths are in units of ξ_0, the intrinsic coherence length. The curves are sketched for $\xi_0 = 10\lambda_L$. For short mean free paths the coherence length becomes shorter and the penetration depth becomes longer. The increase in the ratio $\kappa\lambda/\xi$ favors type II superconductivity.

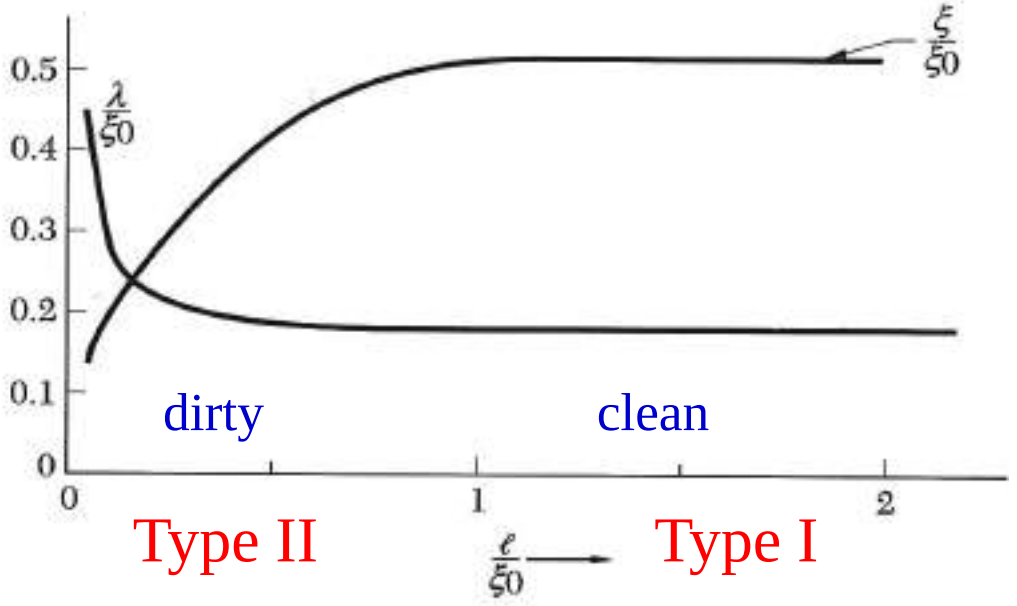

(4) *BCS Theory of Superconductivity*

1. The Cooper Pair :

The "BCS wave function" is composed of particle pairs $\boldsymbol{k}\uparrow$ and $-\boldsymbol{k}\downarrow$, when treated by the BCS theory, gives the familiar electronic superconductivity observed in metals, and exhibits the energy gaps of Table 3. This pairing is known as ***s*-wave pairing** ($l = 0$) .

Postulated by Cooper in 1956

- A weak attraction can bind pairs of electrons into a bound state
- The Fermi sea of electrons is unstable against the formation at least one bound pair, regardless how weak the interaction is, so long it is attractive.
- The lowest energy state to have the **total zero momentum**, so that two electrons must have **equal** and **opposite momenta**.
- Introduce $V_{kk'} = -V$ for all k out to a cut-off energy $\hbar\omega_c$ away from E_f , and $V_{kk'} = 0$ for k beyond $\hbar\omega_c$.

$$E \sim 2E_F - 2\hbar\omega_c e^{-2/N(0)V} \qquad \Delta = 2E_F - E = 2\hbar\omega_c e^{-2/N(0)V} > 0$$

- The contribution to the energy of the attractive potential outweights the excess kinetic energy, leading to a binding energy regardless how small V is.

Origin of the Attractive Interaction:

2. The electron-lattice-electron interaction leads to an ***energy gap*** of the observed magnitude. The indirect interaction proceeds when one electron interacts with the lattice and deforms it; a second electron sees the deformed lattice and adjust itself to take advantage of the deformation to lower its energy. Thus the second electron interacts with the first electron via the **lattice deformation.**

e.g. the mattress theory

- In 1950 **Frohlich** first suggested ***the electron phonon interaction*****:**
  The physical idea is that the first electron polarizes the medium by attractive positive ions; these excessive positive ions, in turn, attract the second electron, giving an ***effective attractive*** interaction between the electrons.
- If this attractive interaction is strong enough to override the repulsive screened Coulomb interaction, it gives rise to a ***net attractive*** interaction, and the **superconductivity** results.
- The cut-off frequency $\hbar\omega_c$ of the Cooper pair's attraction is expected to be of the order of the Debye frequency, $\hbar\omega_D$, as a measure of the ***stiffness*** of the lattice.

Superconducting Ground State

Normal state

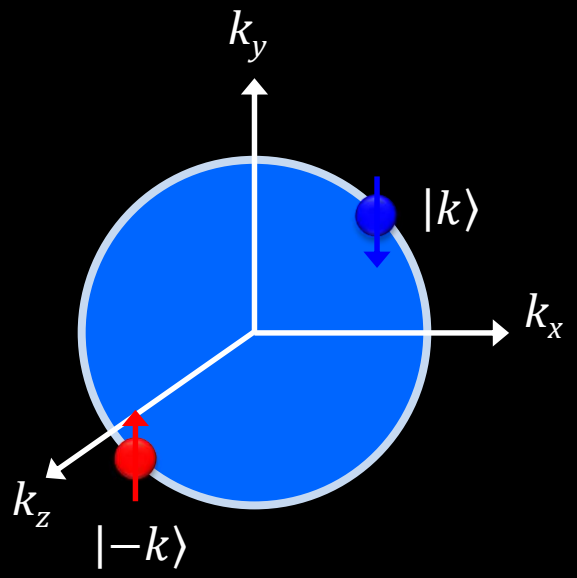

Cooper Pairs

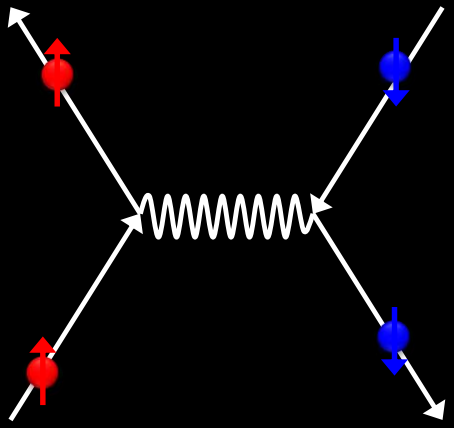

Exchange boson:
Lattice Vibration Mode

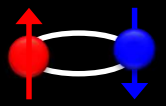

- Spin singlet
- L=0; S=0
- Binding energy: Δ

Superconducting ground state

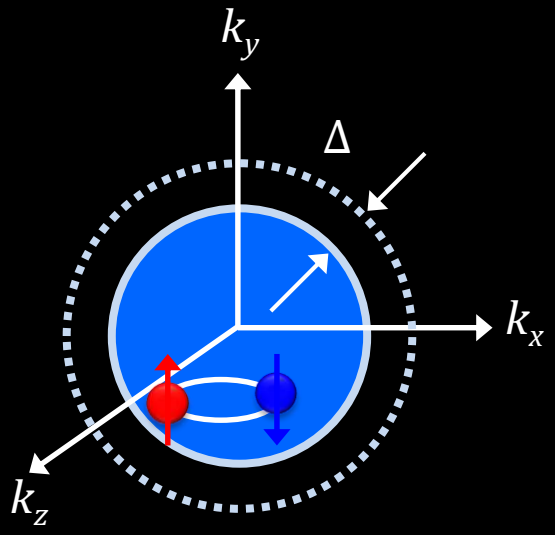

Superconducting Ground States

SC Ground State

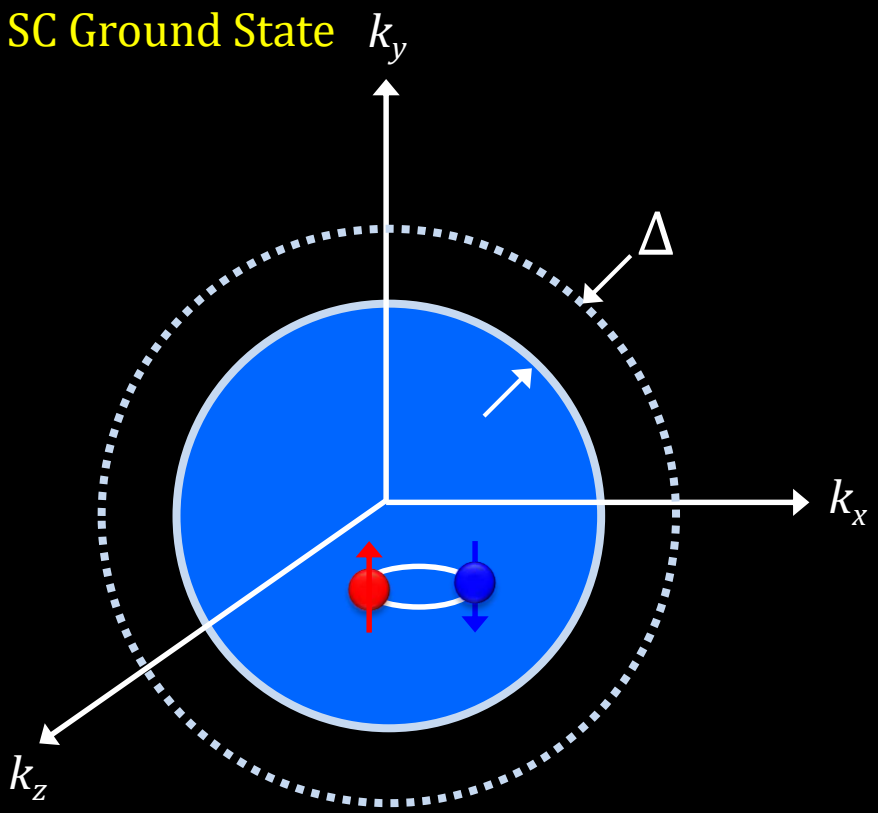

$$\Psi_{BCS} = \prod_k \left(u_k + v_k c^*_{k\uparrow} c^*_{-k\downarrow} \right) | 0 >$$

u_k and v_k : coherence factor

BCS, Phys Rev 108, 1175 (1957)

Superconducting Energy Gap in 1960

Ivar Giaever

Nobel Prize in 1973

Tunneling junction

S I N

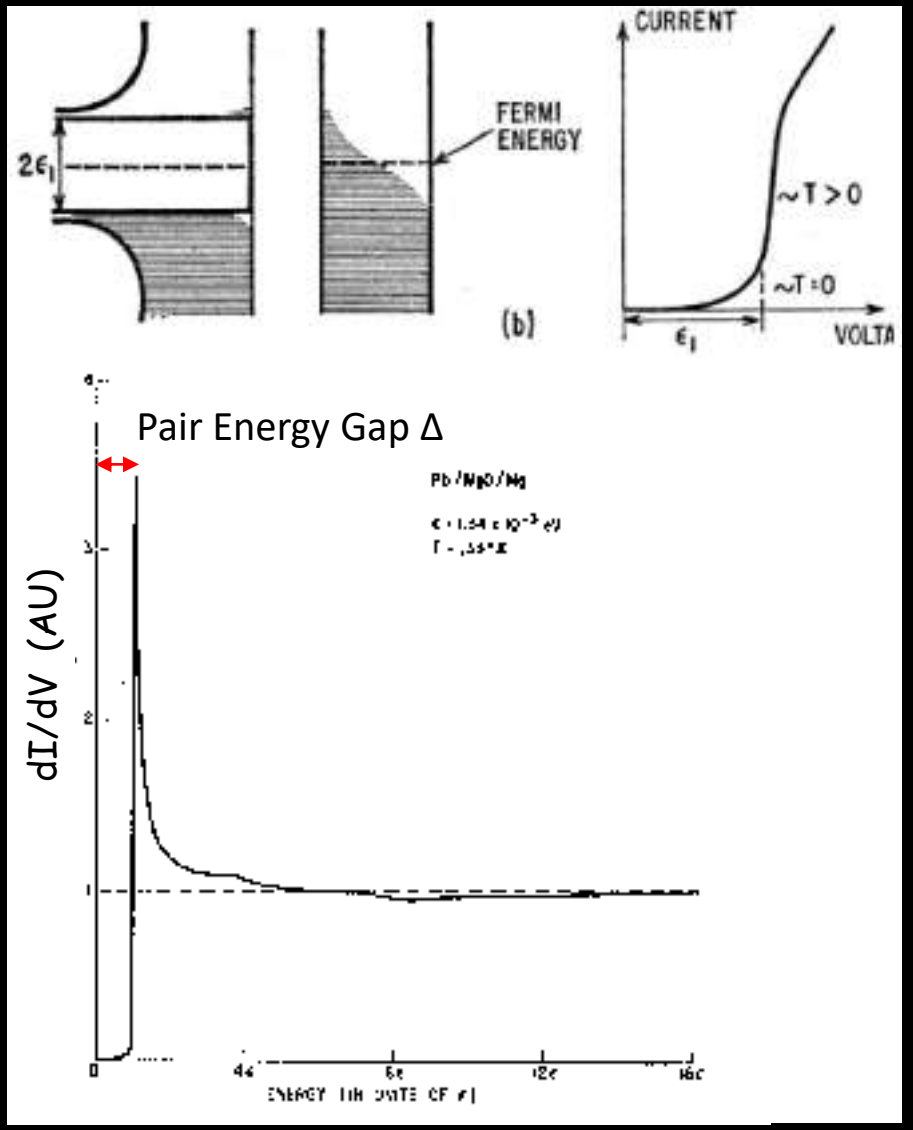

I. Giaever, Phys. Rev. Lett. 5, 147 (1960)
I. Giaever, Phys. Rev. 126, 941 (1962)

(5) *BCS Ground State*

1. The BCS theory shows that, with an appropriate attractive interaction between electrons, the new ground state is superconducting, and is separated by a finite energy E_g from its lowest excited state.
2. With the attractive potential energy of the BCS state, the total energy of the BCS state will be lower with respect to the Fermi state.
3. The central feature of the BCS state is that one–particle orbitals are occupied in pairs: if an orbital with the wavevector ***k*** and **spin up** is occupied, then the orbital with the wavevector ***–k*** and **spin down** is also occupied.
4. **Cooper pairs**: they have a spin zero, and have many attributes of **bosons**.

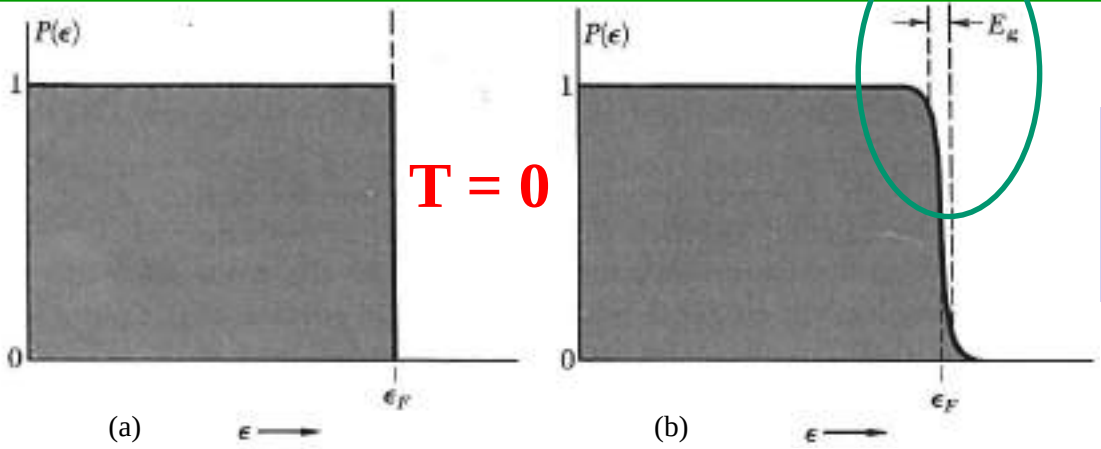

Some what like the Fermi Dirac Distribution at $T = T_c$

Non interacting Fermi gas **BCS ground state**

Figure 15 (a) Probability P that an orbital of kinetic energy ϵ is occupied in the ground state of the noninteracting Fermi gas; (b) the BCS ground state differs from the Fermi state in a region of width of the order of the energy gap E_g. Both curves are for absolute zero.

The BCS Ground State

Tinkham, Chapter 2

Singlet wave function, a vacuum state with no particles present

$$|\psi_0\rangle = \sum_{k>k_F} g_{\mathbf{k}}\, c^*_{\mathbf{k}\uparrow}\, c^*_{-\mathbf{k}\downarrow}\, |F\rangle \qquad (2\text{-}11)$$

Creation operator C_k^*
Annihilation operator C_k

where $|F\rangle$ = Fermi sea filled up to k_F

Using a **Hartree self consistent field**, or **a mean field theory**

the BCS Ground state wave function

$$|\psi_G\rangle = \prod_{\mathbf{k}=\mathbf{k}_1,\ \ldots,\ \mathbf{k}_M} (u_{\mathbf{k}} + v_{\mathbf{k}}\, c^*_{\mathbf{k}\uparrow}\, c^*_{-\mathbf{k}\downarrow})\, |\phi_0\rangle \qquad (2\text{-}14)$$

where $u_k^2 + v_k^2 = 1$, *and* $u_k = e^{i\phi} v_k$

The pairing Hamiltonian

$$\mathscr{H} = \sum_{\mathbf{k}\sigma} \epsilon_{\mathbf{k}}\, n_{\mathbf{k}\sigma} + \sum_{\mathbf{k}\mathbf{l}} V_{\mathbf{k}\mathbf{l}}\, c^*_{\mathbf{k}\uparrow}\, c^*_{-\mathbf{k}\downarrow}\, c_{-\mathbf{l}\downarrow}\, c_{\mathbf{l}\uparrow} \qquad (2\text{-}20)$$

The gap equation

$$\Delta_{\mathbf{k}} = -\frac{1}{2} \sum_{\mathbf{l}} \frac{\Delta_{\mathbf{l}}}{E_{\mathbf{l}}} V_{\mathbf{k}\mathbf{l}} = -\frac{1}{2} \sum_{\mathbf{l}} \frac{\Delta_{\mathbf{l}}}{(\Delta_{\mathbf{l}}^2 + \xi_{\mathbf{l}}^2)^{1/2}} V_{\mathbf{k}\mathbf{l}} \qquad (2\text{-}30)$$

$E_k = (\Delta_k^2 + \xi_k^2)^{1/2}$ ***Quasi-particle excitation energy***

$$V_{\mathbf{kl}} = \begin{cases} -V & \text{if} \quad |\xi_{\mathbf{k}}| \quad \text{and} \quad |\xi_{\mathbf{l}}| \leq \hbar\omega_c \\ 0 & \text{otherwise} \end{cases} \tag{2-31}$$

$$\Delta_{\mathbf{k}} = \begin{cases} \Delta & \text{for} \quad |\xi_{\mathbf{k}}| < \hbar\omega_c \\ 0 & \text{for} \quad |\xi_{\mathbf{k}}| > \hbar\omega_c \end{cases} \tag{2-32}$$

in weak coupling limit

$$\Delta = \frac{\hbar\omega_c}{\sinh\left[1/N(0)V\right]} \approx 2\hbar\omega_c e^{-1/N(0)V} \tag{2-34}$$

The BCS Pairing occupation number

$$v_{\mathbf{k}}^2 = \frac{1}{2}\left(1 - \frac{\xi_{\mathbf{k}}}{E_{\mathbf{k}}}\right) = \frac{1}{2}\left[1 - \frac{\xi_{\mathbf{k}}}{(\Delta^2 + \xi_{\mathbf{k}}^2)^{1/2}}\right] \tag{2-35}$$

$$u_{\mathbf{k}}^2 = \frac{1}{2}\left(1 + \frac{\xi_{\mathbf{k}}}{E_{\mathbf{k}}}\right) = 1 - v_{\mathbf{k}}^2$$

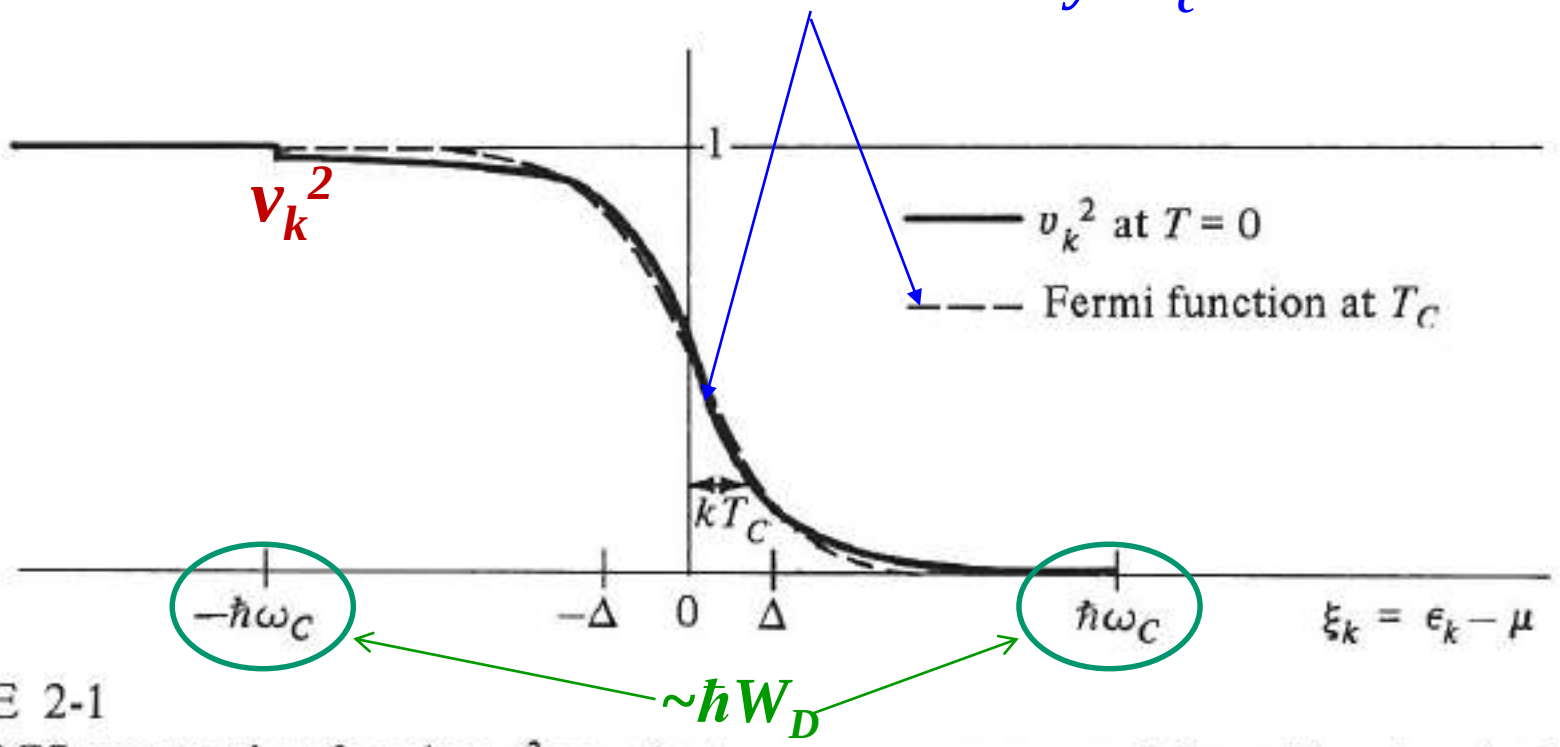

FIGURE 2-1
Plot of BCS occupation fraction v_k^2 vs. electron energy measured from the chemical potential (Fermi energy). To make the cutoffs at $\pm\hbar\omega_c$ visible, the plot has been made for a strong-coupling superconductor with $N(0)V = 0.43$. For comparison, the Fermi function for the normal state at T_c is also shown on the same scale, using the BCS relation $\Delta(0) = 1.76kT_c$.

$$\omega_C \sim \omega_D >> \Delta = 1.76\ kT_c$$

Superconducting Excited States

SC Ground State

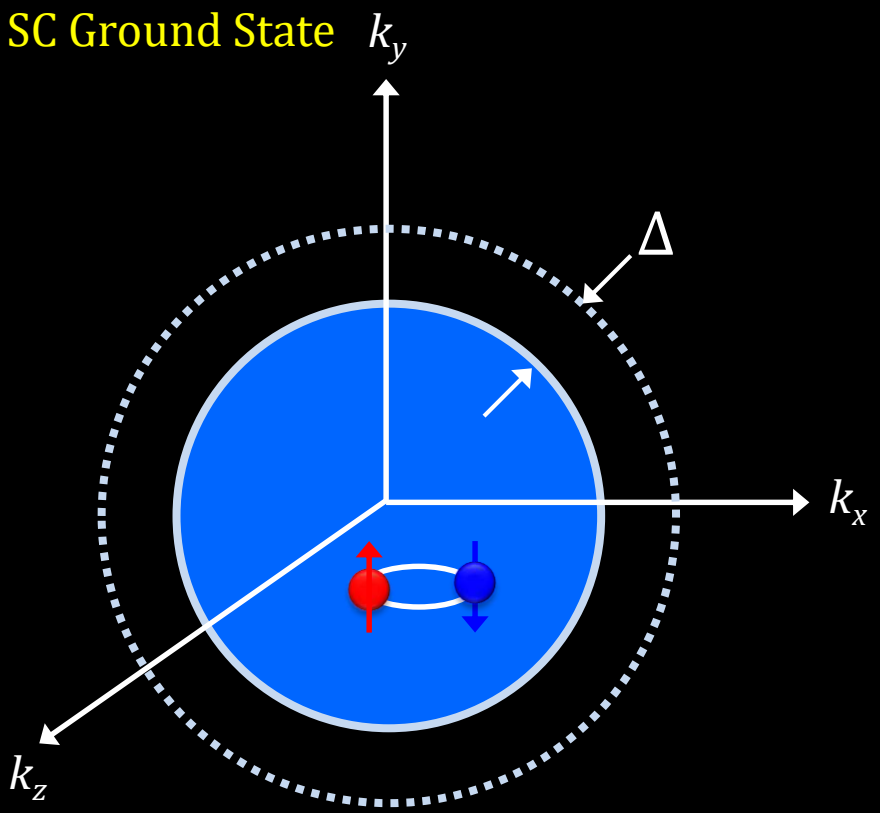

SC Excited States

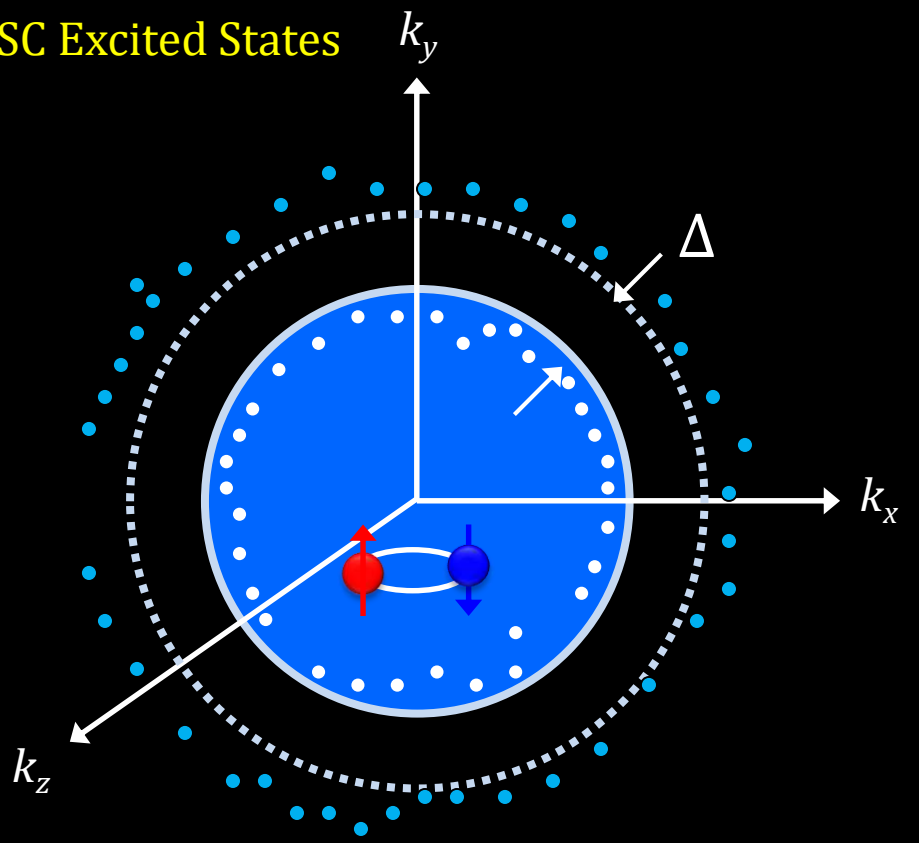

$$\Psi_{BCS} = \prod_k \left(u_k + v_k c^*_{k\uparrow} c^*_{-k\downarrow} \right) | 0 >$$

u_k and v_k : coherence factor

BCS, Phys Rev 108, 1175 (1957)

Bogoliubov quasiparticle

$$\gamma^*_{k\uparrow} = u_k c_{k\uparrow} + v_k c^*_{-k\downarrow}$$

Bogoliubov, Nuovo Cimento 7, 794 (1958)

Superconducting Excited States

$$E_{\pm}(\vec{k}) = \pm\sqrt{\varepsilon(\vec{k})^2 + \Delta(\vec{k})^2}$$

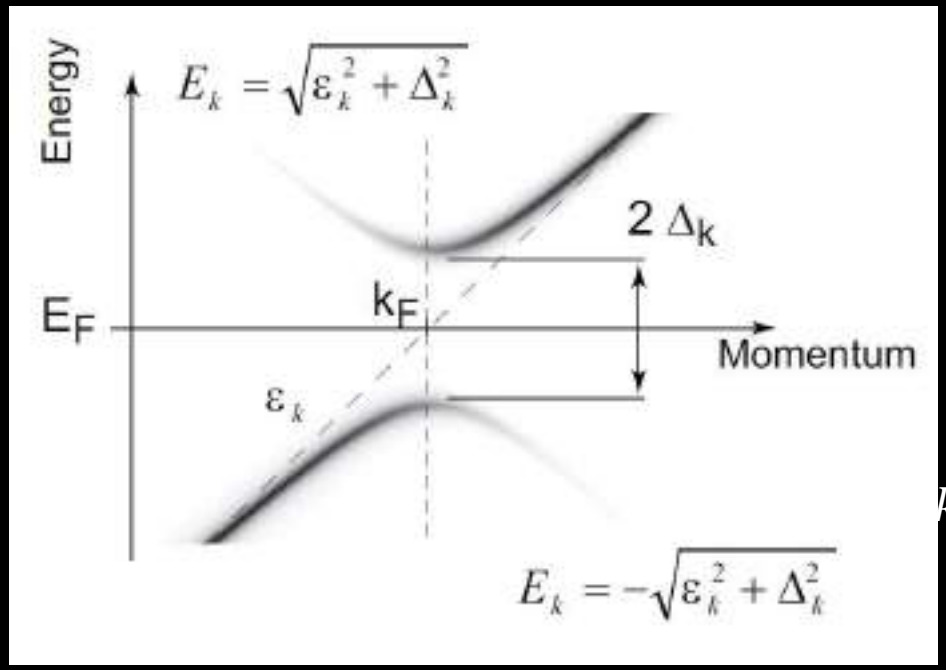

SC Excited States

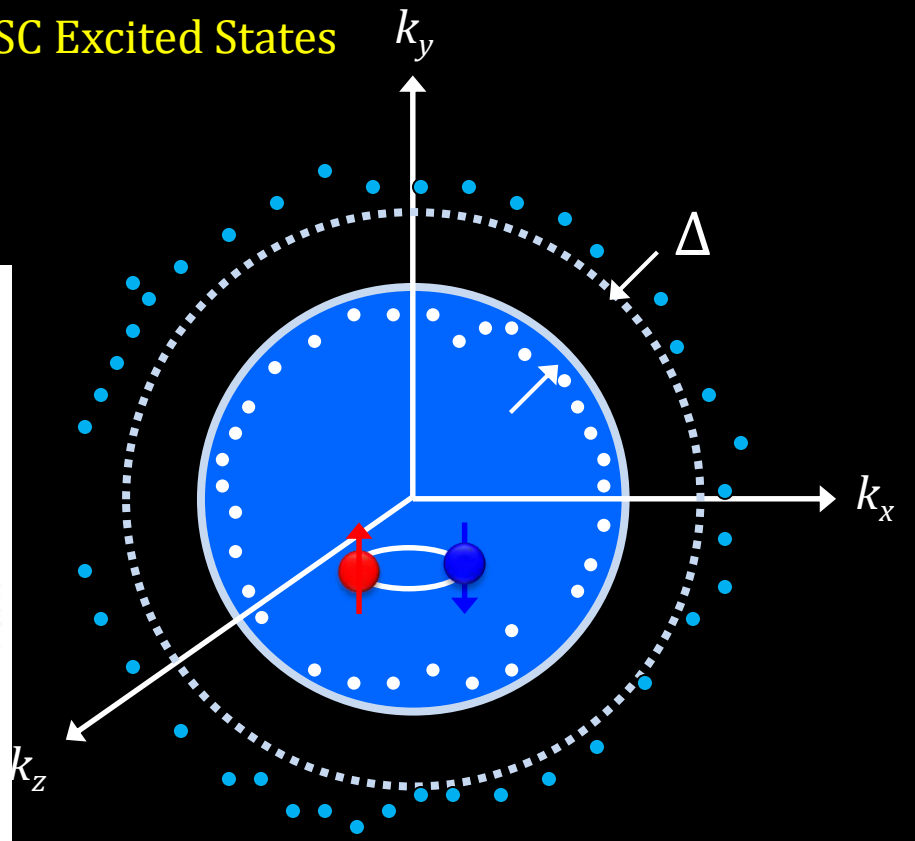

Bogoliubov quasiparticle

$$\gamma^*_{k\uparrow} = u_k c_{k\uparrow} + v_k c^*_{-k\downarrow}$$

Bogoliubov, Nuovo Cimento 7, 794 (1958)

Superconducting Excited States

Superconducting energy gap=2Δ
(T=0)

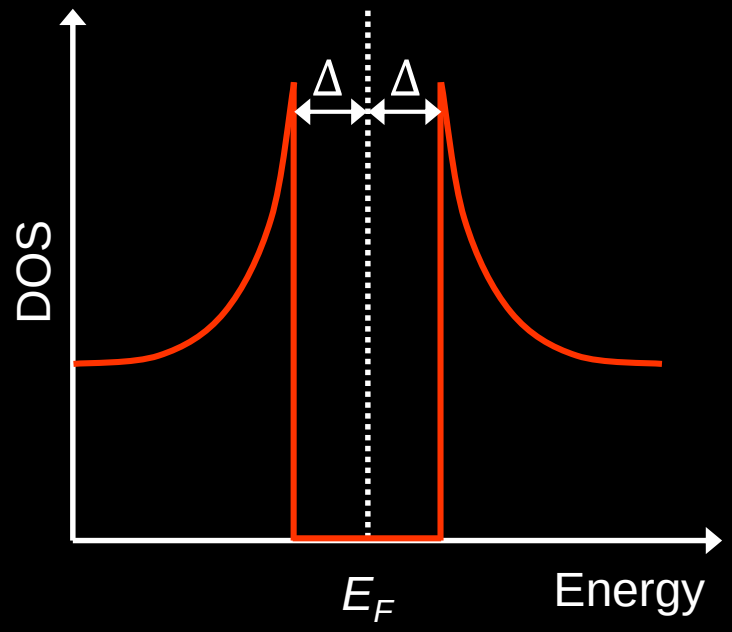

SC Excited States

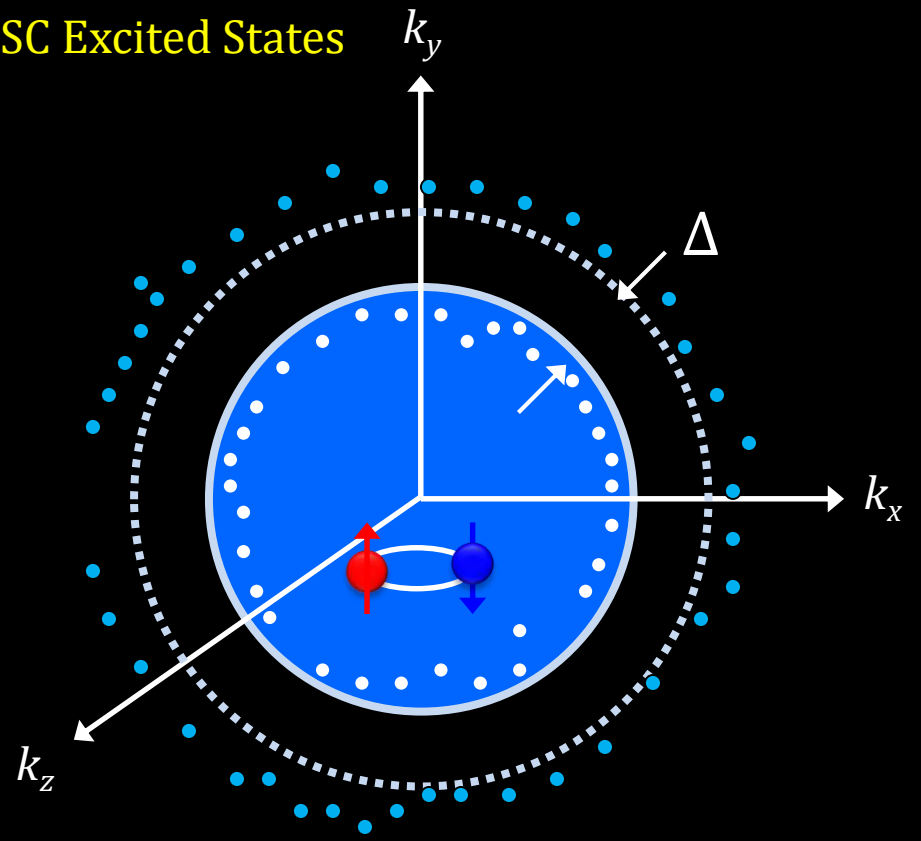

Bogoliubov quasiparticle

$$\gamma^*_{k\uparrow} = u_k c_{k\uparrow} + v_k c^*_{-k\downarrow}$$

Bogoliubov, Nuovo Cimento 7, 794 (1958)

Superconducting Gap

Pair wave function : $\Psi_{kss'} = \langle \Psi_{BCS} | c_{-ks'} c_{ks} | \Psi_{BCS} \rangle = g(k)\, \chi_{ss'}$

Spin part : $\chi_{ss'}$ $\quad (\uparrow\downarrow - \downarrow\uparrow) \quad S = 0$

$(\uparrow\uparrow, \uparrow\downarrow + \downarrow\uparrow, \downarrow\downarrow) \quad S = 1$

Orbital part : $g(k)$ $\quad \psi(\mathbf{r}) \propto \sum_{\mathbf{k}} \frac{\Delta(\mathbf{k})}{\sqrt{\epsilon(\mathbf{k})^2 + \Delta(\mathbf{k})^2}} \exp(-i\mathbf{kr})$

Spin	Orbital
anti-symmetric ($S = 0$)	symmetric (s, d, ...)
symmetric ($S = 1$)	anti-symmetric (p, f, ...)

$l = 0$: s wave (conventional SC)

$l = 1$: p wave (superfluid ^{3}He)

$l = 2$: d wave (cuprate SC)

If $l > 0$, $\psi(0) = 0$

→ { repulsive interaction

$\Delta(k)$ must change its sign

Gap Equation

$$\Delta(\mathbf{k}) = -\frac{1}{2}\sum_{\mathbf{q}} V(\mathbf{q}) \frac{\Delta(\mathbf{k})}{\sqrt{\epsilon(\mathbf{k}+\mathbf{q})^2 + \Delta(\mathbf{k}+\mathbf{q})^2}} \tanh \frac{\sqrt{\epsilon(\mathbf{k}+\mathbf{q})^2 + \Delta(\mathbf{k}+\mathbf{q})^2}}{2k_B T}$$

Pairing interaction

In conventional BCS, $V(\mathbf{q}) = -|V| < 0$: Δ is always positive.

If $V(\mathbf{q} = \mathbf{Q}) > 0$ plays a role, $\Delta(\mathbf{k})$ and $\Delta(\mathbf{k}+\mathbf{Q})$ have a different sign.

s wave

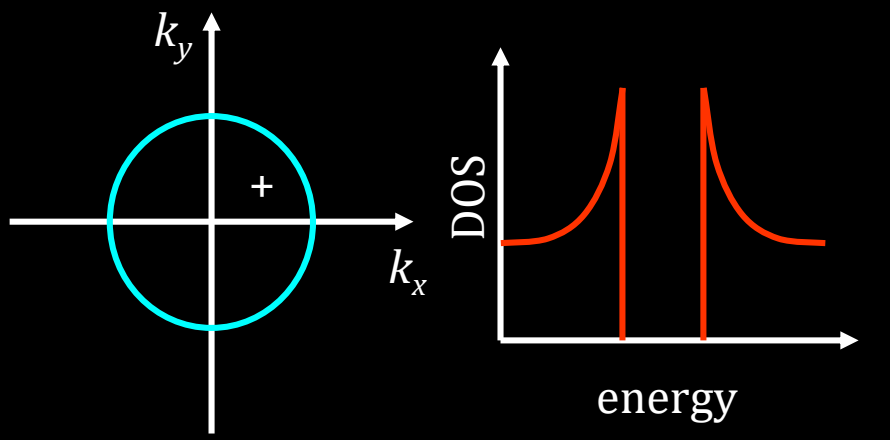

d wave

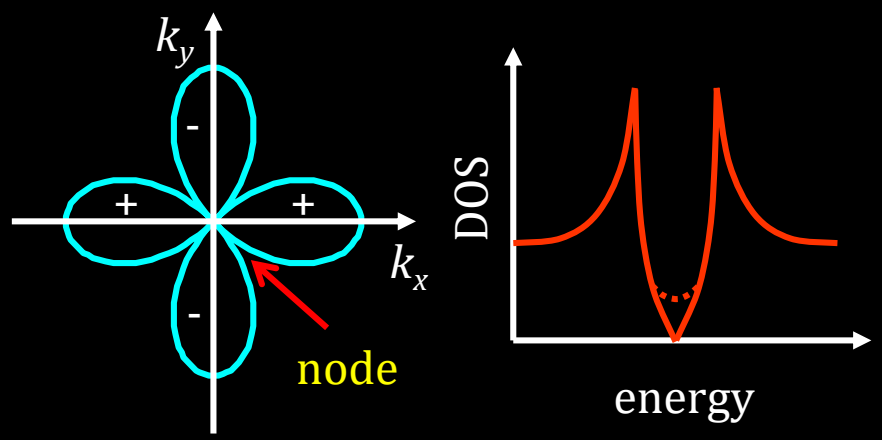

BCS theory:

$$\Delta = 2\hbar\omega_c e^{-2/N(0)V}$$
$$kT_c = 1.14\hbar\omega_c e^{-2/N(0)V}$$

$\Delta(0)/kT_c = 2/1.14 = 1.76$, weak el-ph coupling

If $\Delta(0)/kT_c > 2$, strong el-ph coupling

$\beta = 1/kT$

$$\frac{1}{V} = \frac{1}{2}\sum_k \frac{\tanh(\beta E_k/2)}{E_k}$$

(2-50)

Determines the temperature dependence of $\Delta(T)$

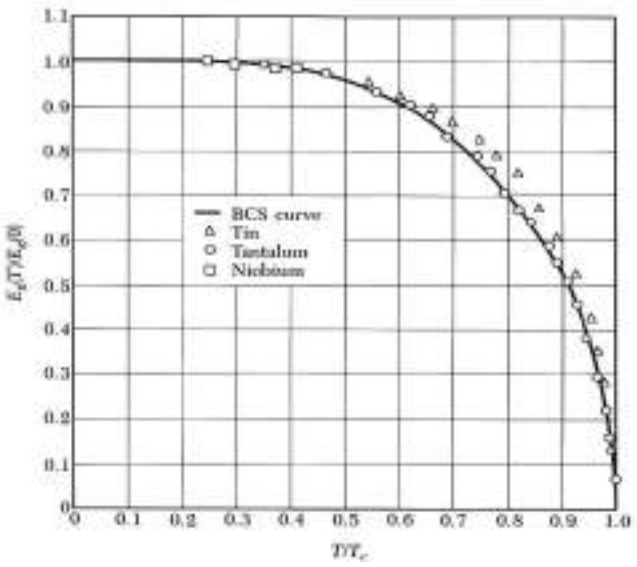

$$\Delta(T)/\Delta(0) \sim 1.74\,(1 - T/T_c)^{1/2}$$
at $T \sim T_c$

In the mean field theory,
Δ_k is the order parameter !

2-6.1 Determination of T_c

The critical temperature T_c is the temperature at which $\Delta(T) \to 0$. In this case, $E_{\mathbf{k}} \to |\xi_{\mathbf{k}}|$, and the excitation spectrum becomes the same as in the normal state. Thus, T_c is found by replacing $E_{\mathbf{k}}$ with $|\xi_{\mathbf{k}}|$ in (2-50) and solving. After changing the sum to an integral, taking advantage of the symmetry of $|\xi_{\mathbf{k}}|$ about the Fermi level, and changing to a dimensionless variable of integration, this condition becomes

$$\frac{1}{N(0)V} = \int_0^{\beta_c \hbar \omega_c/2} \frac{\tanh x}{x}\, dx$$

This integral can be evaluated and yields $\ln(A\beta_c \hbar \omega_c)$, where $A = 2\gamma/\pi \approx 1.13$, γ here being Euler's constant. Consequently,

$$kT_c = \beta_c^{-1} = 1.13 \hbar \omega_c e^{-1/N(0)V}. \qquad (2\text{-}51)$$

Comparing this with (2-34), we see that

$$\frac{\Delta(0)}{kT_c} = \frac{2}{1.13} = 1.764 \qquad (2\text{-}52)$$

so that the gap at $T = 0$ is indeed comparable in energy to kT_c. The numerical factor 1.76 has been tested in many experiments and found to be reasonable. That is, experimental values of 2Δ for different materials and different directions in k space generally fall in the range 3.0 to $4.5kT_c$, with most clustered near the BCS value of $3.5kT_c$.

2-6.2 Temperature Dependence of the Gap

Given (2-50), or its integral equivalent

$$\frac{1}{N(0)V} = \int_0^{\hbar\omega_c} \frac{\tanh \frac{1}{2}\beta(\xi^2 + \Delta^2)^{1/2}}{(\xi^2 + \Delta^2)^{1/2}} d\xi \qquad (2\text{-}53)$$

$\Delta(T)$ can be computed numerically. For weak-coupling superconductors, in which $\hbar\omega_c/kT_c \gg 1$, $\Delta(T)/\Delta(0)$ is a universal function of T/T_c which decreases monotonically from one at $T = 0$ to zero at T_c, as shown in Fig. 2-2. Near $T = 0$, the temperature variation is exponentially slow, since $e^{-\Delta/kT} \approx 0$, so that the hyperbolic tangent is very nearly unity and insensitive to T. Physically speaking, Δ is nearly constant until a significant number of quasi-particles are thermally excited. On the other hand, near T_c, $\Delta(T)$ drops to zero with a vertical tangent, approximately as

$$\frac{\Delta(T)}{\Delta(0)} \approx 1.74\left(1 - \frac{T}{T_c}\right)^{1/2} \qquad T \approx T_c \qquad (2\text{-}54)$$

The variation of the order parameter Δ with the square root of $(T_c - T)$ is characteristic of all mean-field theories. For example, $M(T)$ has the same dependence in the molecular-field theory of ferromagnetism.

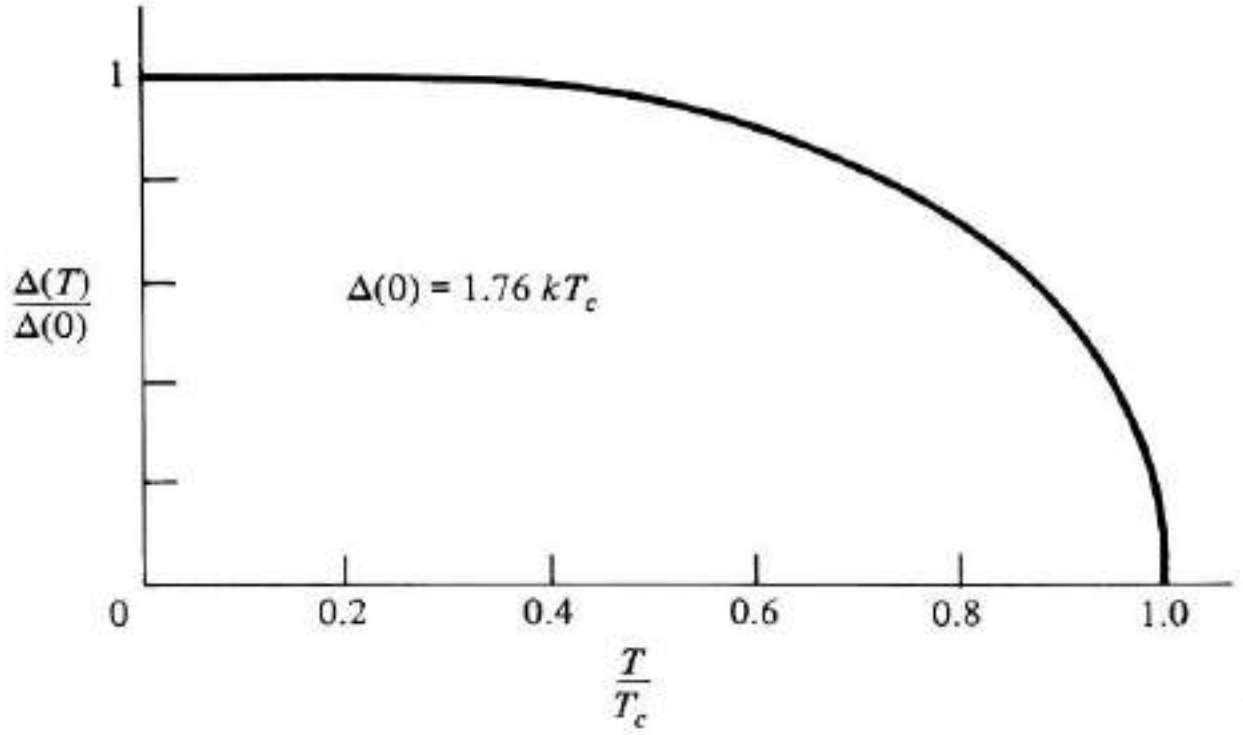

FIGURE 2-2
Temperature dependence of the energy gap in the BCS theory. Strictly speaking, this universal curve holds only in the weak-coupling limit, but it is a good approximation in most cases.

Low temperature Superconductors

-- Mediated by *electron phonon coupling*

-- *In strong electron phonon coupling, modified by Elishberg et al*

W. McMillian's formula for T_c

$$T_c = \frac{\Theta_D}{1.45} \exp\left\{ - \left[\frac{(1+\lambda_{ep})}{\lambda_{ep} - \mu^*(1+0.62\lambda_{ep})} \right] \right\}$$

λ : electron phonon coupling constant

μ^* : Coulomb repulsion of electrons

$\lambda \propto N(0) < I^2 > / \omega^2$

Are electrons or phonons more important to give rise to high T_c ?

Important E&M properties from the BCS theory

(1) We first show that a charged boson gas obeys the London equation. Let $\psi(\mathbf{r})$ be the particle probability amplitude. We suppose that the pair concentration $n = \psi^*\psi$ = constant.

$$\psi = n^{1/2}\, e^{i\theta(\mathbf{r})} \; ; \qquad \psi^* = n^{1/2}\, e^{-i\theta(\mathbf{r})} \tag{19}$$

The phase $\theta(\mathbf{r})$ is important

$$\mathbf{v} = \frac{1}{m}\left(\mathbf{p} - \frac{q}{c}\mathbf{A}\right) = \frac{1}{m}\left(-i\hbar\nabla - \frac{q}{c}\mathbf{A}\right)$$

The particle flux is given by, and from eq. (19)

$$\psi^*\mathbf{v}\psi = \frac{n}{m}\left(\hbar\nabla\theta - \frac{q}{c}\mathbf{A}\right) \tag{20}$$

that the electric current density is $\mathbf{j} = q\psi^*\mathbf{v}\psi = \dfrac{nq}{m}\left(\hbar\nabla\theta - \dfrac{q}{c}\mathbf{A}\right)$ (21)

London equation: $\operatorname{curl}\mathbf{j} = -\dfrac{nq^2}{mc}\mathbf{B}$

$$\mathbf{j} = -\frac{c}{4\pi\lambda_L^2}\mathbf{A} \; ; \tag{22}$$

London penetration depth $\lambda_L = (mC^2/4\pi nq^2)^{1/2}$

(2) Quantization of the magnetic flux through a ring is a dramatic consequence of Eq. (21). Let us take a closed path C through the interior of the superconducting material, well away from the surface (Fig. 16).

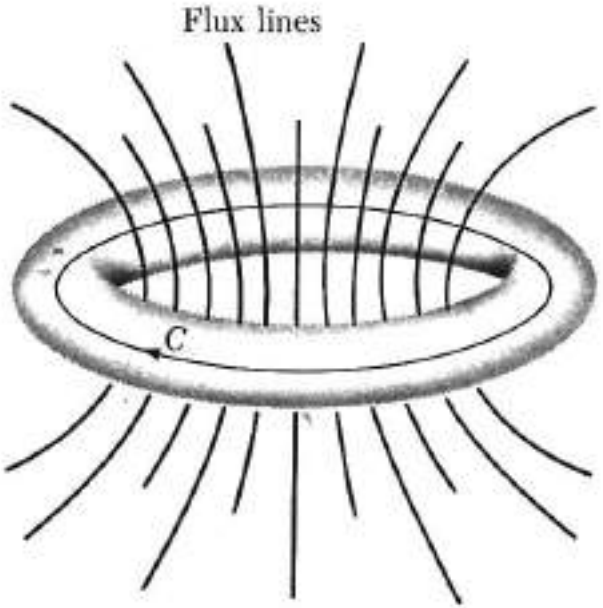

Figure 16 Path of integration C through the interior of a superconducting ring. The flux through the ring is the sum of the flux Φ_{ext} from external sources and the flux Φ_{sc} from the superconducting currents which flow in the surface of the ring; $\Phi = \Phi_{ext} + \Phi_{sc}$. The flux Φ is quantized. There is normally no quantization condition on the flux from external sources, so that Φ_{sc} must adjust itself appropriately in order that Φ assume a quantized value.

B and j are zero in the interior. from the Meissner effect

$$\hbar c \nabla \theta = q\mathbf{A} \ . \qquad \text{(23)}$$

From Eq. 20, 21

We form

$$\oint_C \nabla\theta \cdot d\boldsymbol{l} = \theta_2 - \theta_1 \qquad \text{(23)'}$$

for the change of phase on going once around the ring.

The probability amplitude ψ is measurable in the classical approximation, so that ψ must be single-valued and

$$\theta_2 - \theta_1 = 2\pi s \ , \qquad (24)$$

S is an integer

where s is an integer. By the Stokes theorem,

$$\oint_C \mathbf{A} \cdot d\boldsymbol{l} = \int_C (\text{curl } \mathbf{A}) \cdot d\boldsymbol{\sigma} = \int_C \mathbf{B} \cdot d\boldsymbol{\sigma} = \Phi \ , \qquad (25)$$

$d\boldsymbol{\sigma}$ is an element of area on a surface bounded by the curve C, and Φ is the magnetic flux through C.

$$\Phi = (2\pi\hbar c/q)s \ . \qquad (26)$$

S is an integer

Thus the flux through the ring is quantized in integral multiples of $2\pi\hbar c/q$.

Flux Quantization: The evidence of pairing of electrons !

By experiment $q = -2e$

$\Phi = \Phi_o \, \mathbf{s}$

S is an integer

$$\Phi_0 = 2\pi\hbar c/2e \cong 2.0678 \times 10^{-7} \text{ gauss cm}^2 \quad = \pi\hbar c/e$$

This unit of flux is called a **fluxoid** or **fluxon**. (27)

$\Phi = \Phi_{ext} + \Phi_{sc}$ The total flux Φ is quantized. (28)

There is normally no quantization condition on the flux from external sources, so that Φ_{sc} must adjust itself appropriately in order that Φ assume a quantized value.

Flux Quantization Theory in 1950

* We note that in order for Ψ to be a single-valued function, as required by quantum mechanics, it is necessary that the moduli of χ fulfill a kind of quantum condition:

$$\langle \chi \rangle = \oint \bar{p}_e \cdot ds = Kh$$

where K must be an integer. This means that there exists a universal unit for the fluxoid:

$$\Phi_1 = hc/e \simeq 4 \cdot 10^{-7} \text{ gauss} \cdot \text{cm}^2$$

~ 2 larger

Fritz London

Superconducting ring

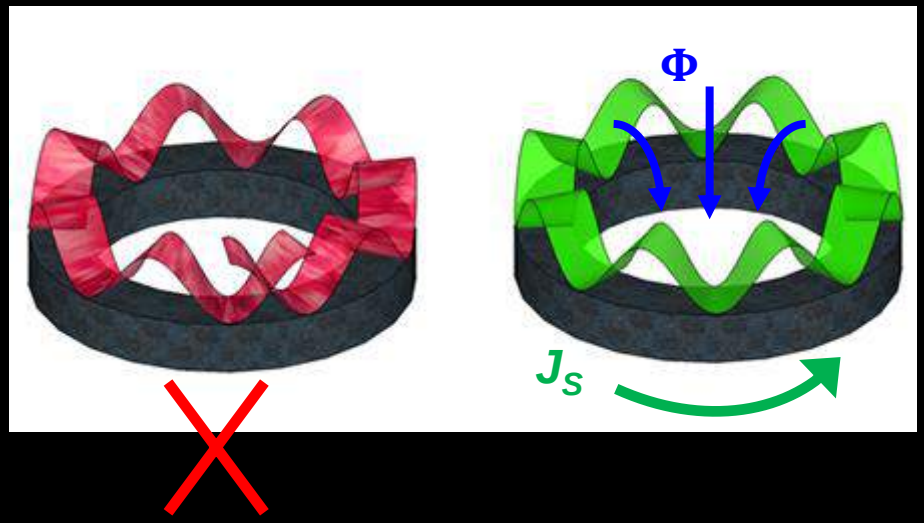

Superfluids, Macroscopic Theory of Superconductivity, Structure of Matter Vol. 1 (Wiley, New York, 1950)

Flux Quantization Experiments in 1961

Bascom Deaver

© APS

William Fairbank

© Duke Univ.

$|\Phi| = n\,{}^{hc}/_{2e} = n\Phi_0$,

where $\Phi_0 = 2.0 \times 10^{-15} Tesla - m^2$

Each vortex carries one flux quanta

SC carriers are 2e !

Confirmation of Cooper pairs !

Robert Doll

Martin Näbauer

© Walther-Meißner-Institute

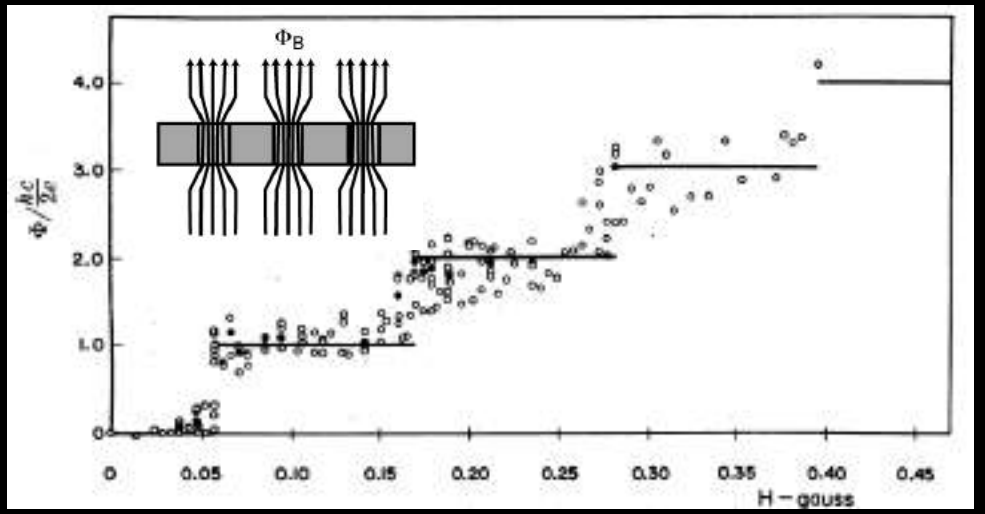

B. D. Deaver and W. M. Fairbank, PRL 7, 43 (1961)
R. Doll and M. Näbauer, PRL 7, 51 (1961)

(3) *Duration of Persistent Currents*

A fluxoid cannot leak out of the ring and thereby reduce the persistent current unless by a thermal fluctuation a minimum volume of the superconducting ring is momentarily in the normal state.

The probability per unit time that a fluxoid will leak out is the product

$$P = (\text{attempt frequency})(\text{activation barrier factor}) \ . \qquad (28)$$

The activation barrier factor is $\exp(-\Delta F/k_B T)$, where the free energy of the barrier is

$$\Delta F \approx (\text{minimum volume})(\text{excess free energy density of normal state}) \ .$$

$$\Delta F \approx R\xi^2 H_c^2/8\pi \ . \qquad (29)$$

$$\exp(-\Delta F/k_B T) \approx \exp(-10^8) \approx 10^{-(4.34\times 10^7)} \qquad (29')$$

The characteristic frequency with which the minimum volume can attempt to change its state must be of order of $E_g/\hbar$. If $E_g = 10^{-15}$ erg, the attempt frequency is $\approx 10^{-15}/10^{-27} \approx 10^{12}\ \text{s}^{-1}$. The leakage probability (28) becomes

$$P \approx 10^{12} 10^{-4.34\times 10^7}\ \text{s}^{-1} \approx 10^{-4.34\times 10^7}\ \text{s}^{-1} \ .$$

The reciprocal of this is a measure of the time required for a fluxoid to leak out, $T = 1/P = 10^{4.34\times 10^7}$ s.

The age of the universe is only 10^{18} s, so that a fluxoid will never leak out in the age of the universe, under our assumed conditions. Accordingly, the current is maintained.

(4) *Type II Superconductors*

1. A good type I superconductor excludes a magnetic field until superconductivity is destroyed suddenly, and then the field penetrates completely.
2. (a) A good type II superconductor excludes the field completely up to a field H_{c1} .

   (b) Above H_{c1} the field is partially excluded, but the specimen remains electrically super conducting.

   (c) At a much higher field, H_{c2} , the flux penetrates completely and superconductivity vanishes.

   (d) An outer **surface** layer of the specimen may remain superconducting up to a still higher field H_{c3} .
3. An important difference in a type I and a type II superconductor is in the mean free path of the conduction electrons in the normal state.

$$\textbf{type I, with } k = \lambda/\xi < 1$$

$$\textbf{type II, with } k = \lambda/\xi > 1$$

1. A superconductor is type I if the surface energy is always positive as the magnetic field is increased, for $H < H_c$
2. It is type II SC, if the surface energy becomes negative, as the magnetic field is increased. for $H_{c1} < H < H_{c2}$

The free energy of a bulk superconductor is increased when the magnetic field is expelled. However, a parallel field can penetrate a very thin film nearly uniformly (Fig.17), only a part of the flux is expelled, and the energy of the superconducting film will increase only slowly as the external magnetic field is increased.

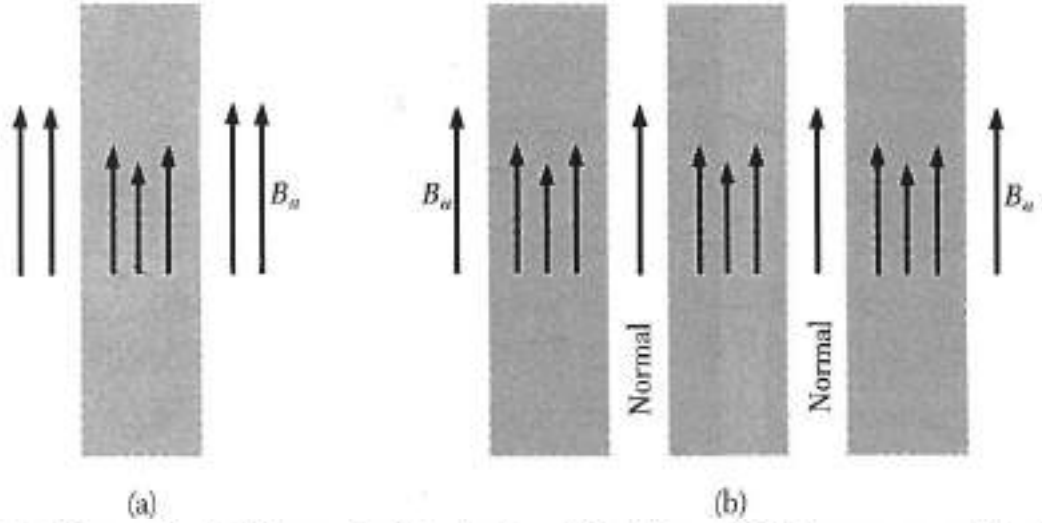

Figure 17 (a) Magnetic field penetration into a thin film of thickness equal to the penetration depth λ. The arrows indicate the intensity of the magnetic field. (b) Magnetic field penetration in a homogeneous bulk structure in the mixed or vortex state, with alternate layers in normal and superconducting states. The superconducting layers are thin in comparison with λ. The laminar structure is shown for convenience; the actual structure consists of rods of the normal state surrounded by the superconducting state. (The *N* regions in the vortex state are not exactly normal, but are described by low values of the stabilization energy density.)

Vortex State

In such a mixed state, called the vortex state, the external magnetic field will penetrate the thin normal regions uniformly, and the field will also penetrate somewhat into the surrounding superconducting material

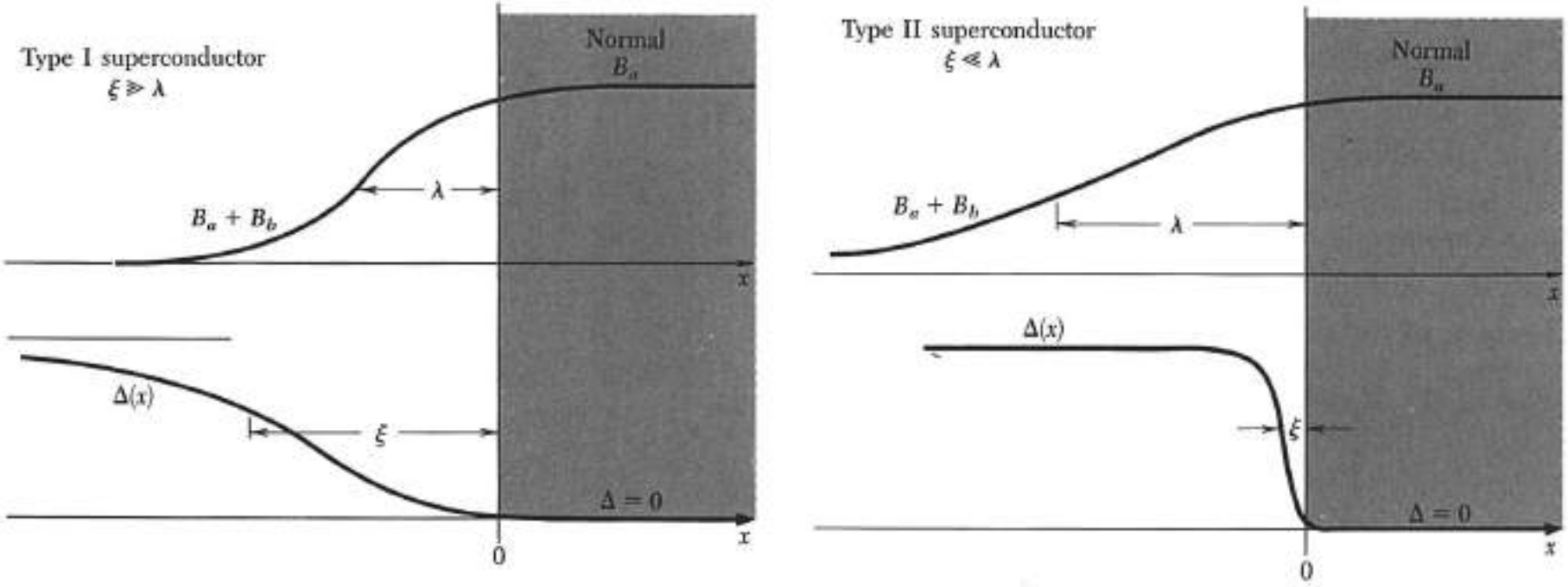

Figure 18 Variation of the magnetic field and energy gap parameter $\Delta(x)$ at the interface of superconducting and normal regions, for type I and type II superconductors. The energy gap parameter is a measure of the stabilization energy density of the superconducting state.

The term **vortex** state describes the circulation of superconducting currents in vortices throughout the bulk specimen.

Flux lattice of $NbSe_2$ at 0.2K

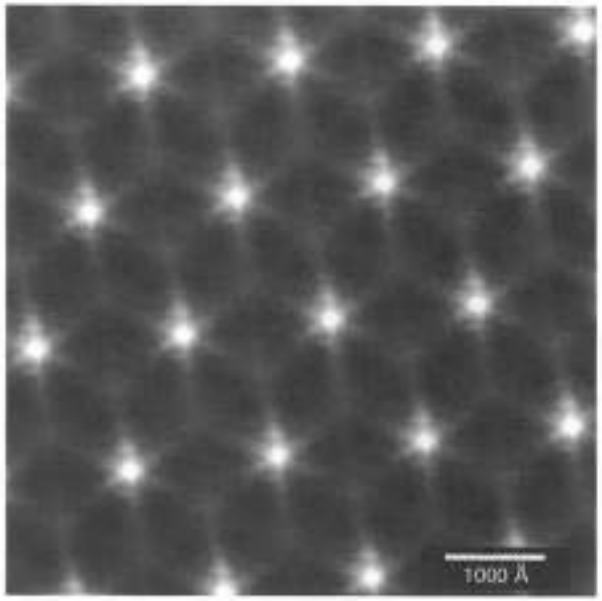

Abrikosov triangular lattice, as imaged by LT-STM, H. Hess et al

Figure 19 Flux lattice in $NbSe_2$ at 1,000 gauss at 0.2K, as viewed with a scanning tunneling microscope. The photo shows the density of states at the Fermi level, as in Figure 23. The vortex cores have a high density of states and are shaded white; the superconducting regions are dark, with no states at the Fermi level. The amplitude and spatial extent of these states is determined by a potential well formed by $\Delta(x)$ as in Figure 18 for a Type II superconductor. The potential well confines the core state wavefunctions in the image here. The star shape is a finer feature, a result special to $NbSe_2$ of the sixfold disturbance of the charge density at the Fermi surface. Photo courtesy of H. F. Hess, AT&T Bell Laboratories.

The vortex is stable when the penetration of the applied field into the superconducting material causes the surface energy become negative. A type II superconductor is characterized by a vortex state stable over a certain range of magnetic field strength; namely, between H_{c1} and H_{c2} .

VOLUME 59, NUMBER 22 PHYSICAL REVIEW LETTERS 30 NOVEMBER 1987

Observation of Hexagonally Correlated Flux Quanta In $YBa_2Cu_3O_7$

P. L. Gammel, D. J. Bishop, G. J. Dolan, J. R. Kwo, C. A. Murray,
L. F. Schneemeyer, and J. V. Waszczak
AT&T Bell Laboratories, Murray Hill, New Jersey 07974
(Received 26 August 1987)

The high-resolution Bitter pattern technique has been used to reveal the magnetic structure of single-crystal samples of high-T_c superconductor $YBa_2Cu_3O_7$ at 4.2 K. Typical patterns consist of hexagonally correlated, singly quantized vortices of flux $hc/2e$. That is, the structures are comparable to those that would be observed in conventional type-II superconductors under similar conditions.

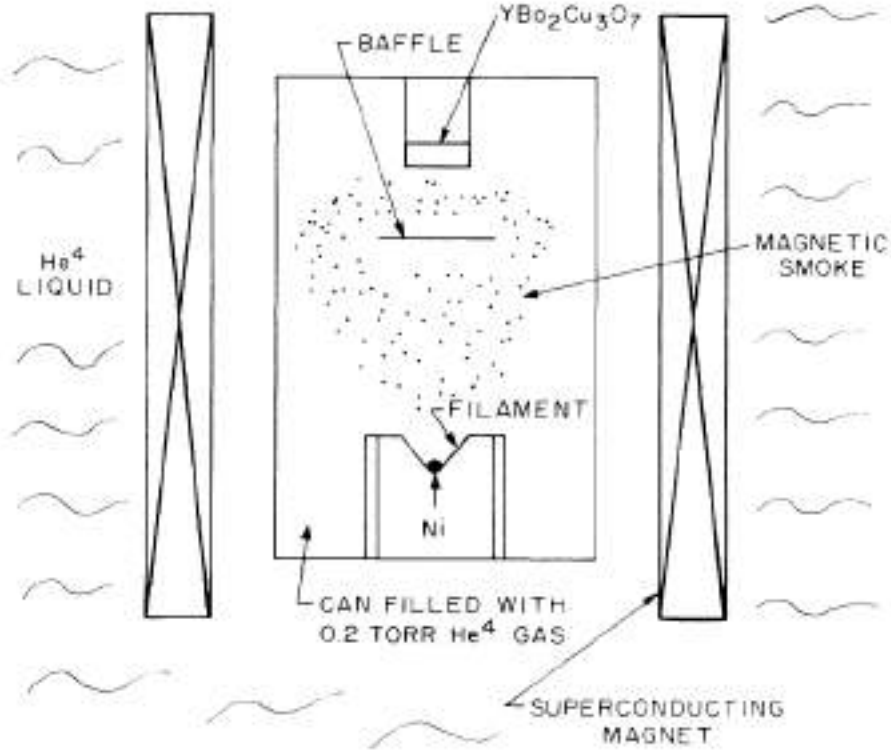

FIG. 1. Sketch of the decoration apparatus.

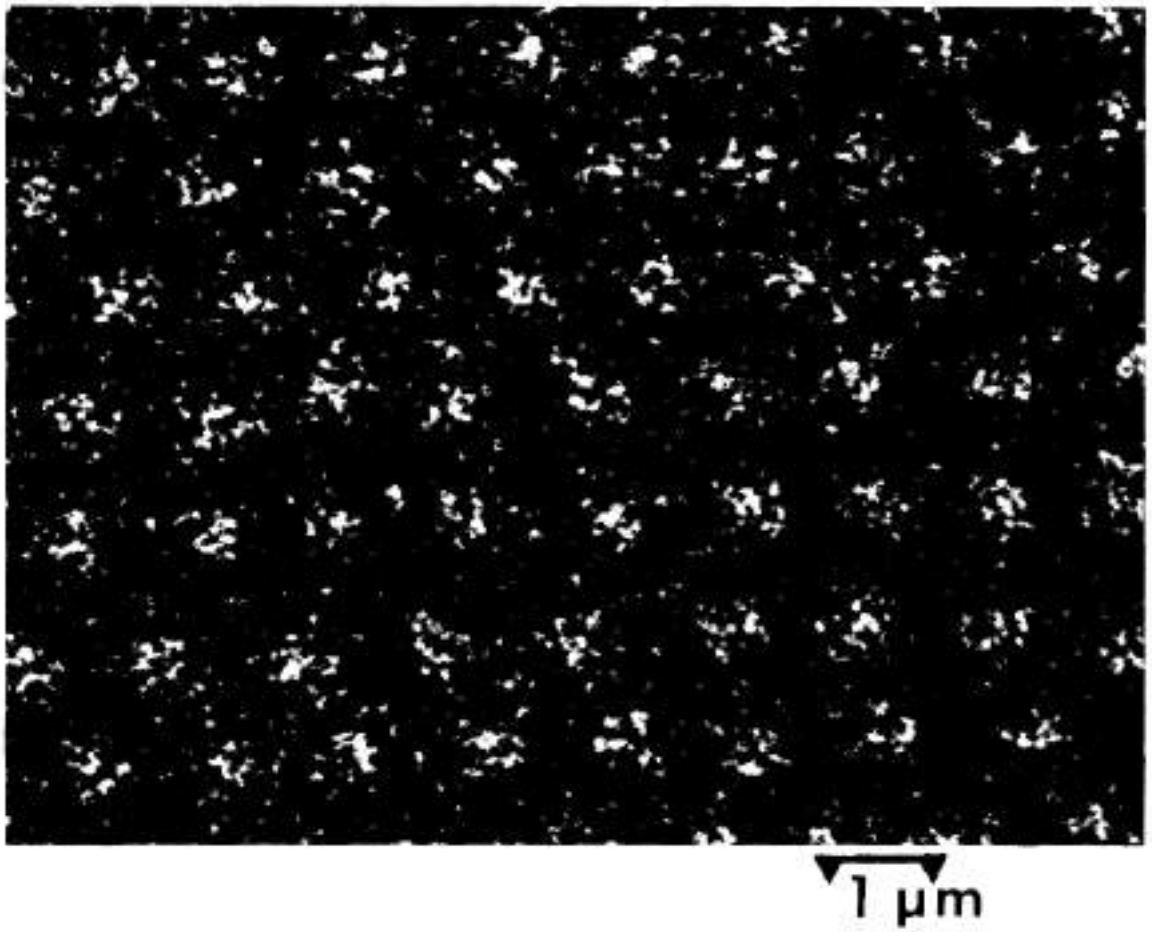

FIG. 2. Flux spots in a $YBa_2Cu_3O_7$ sample decorated after cooling in a field of 13 G.

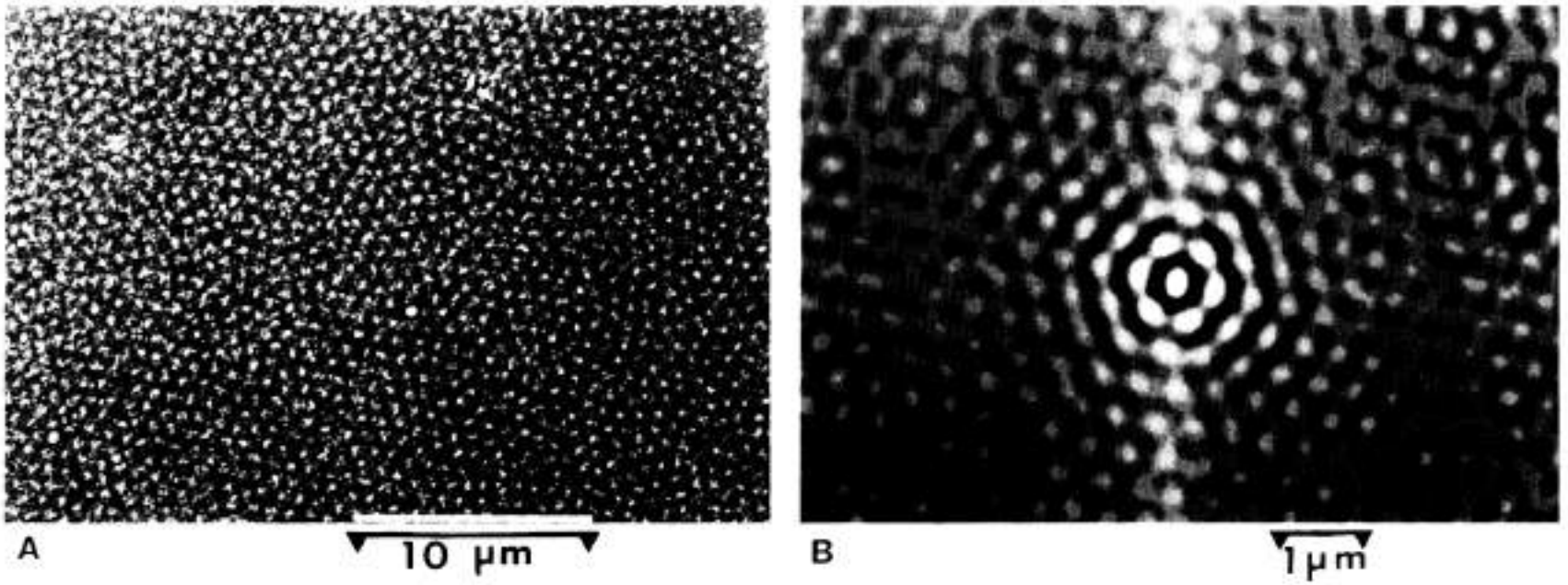

FIG. 3. (a) Typical area of a sample cooled in a 52-G field. (b) Central portion of the autocorrelation function of the pattern in (a).

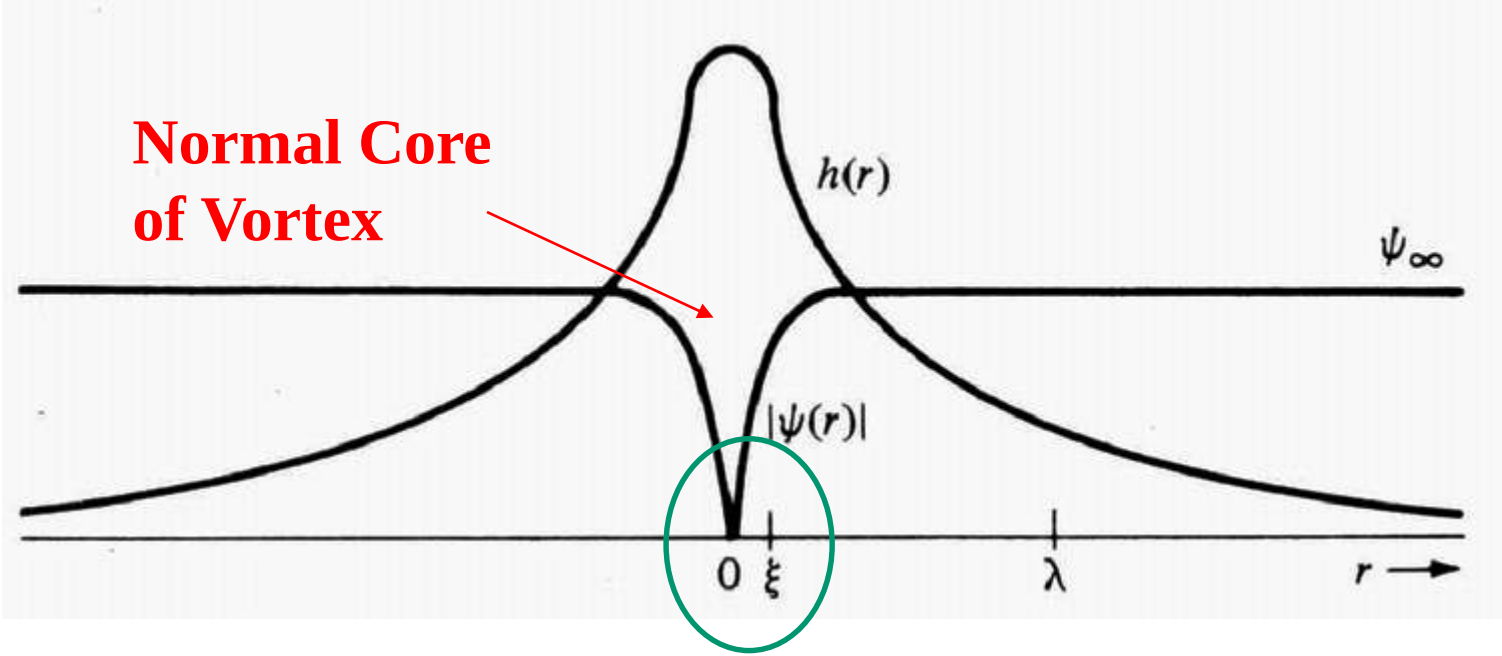

FIGURE 5-1
Structure of an isolated Abrikosov vortex in a material with $\kappa \approx 8$. The maximum value of $h(r)$ is approximately $2H_{c1}$.

Estimation of H_{c1} and H_{c2}

The field will extend out from the normal core a distance $\boldsymbol{\lambda}$ into the superconducting environment. The flux thus associated with a single (first) core is $\pi\lambda^2 H_{c1}$, and this must be equal to the flux quantum Φ_0.

$$\boldsymbol{H_{c1} \approx \Phi_0/\pi\lambda^2} \qquad (30)$$

This is the field for nucleation of a single fluxoid.

The external field penetrates the specimen almost uniformly,
with small ripples on the scale of the fluxoid lattice.
Each (last) core is responsible for carrying a flux of the order of $\pi\xi^2 H_{c2}$,

$$\boldsymbol{H_{c2} \approx \Phi_0/\pi\xi^2} \qquad (31)$$

The larger the ratio λ/ξ , the larger is the ratio of H_{c2} to H_{c1}.

The estimate H_{c1} in terms of H_c , we consider the stability of the vortex state at absolute zero in the impure limit $\xi < \lambda$; here $\kappa > 1$ are the coherence length is short in comparison with the penetration depth.

We estimate in the vortex state the stabilization energy of a fluxoid core viewed as a normal metal cylinder which carries an average magnetic field B_a. The radius is of the order of the coherence length, as the thickness of the boundary between **N** and **S** phases.

$$f_{\text{core}} \approx \frac{1}{8\pi} H_c^2 \times \pi\xi^2 \ , \qquad (32)$$

But there is also a decrease in magnetic energy because of the penetration of the applied field B_a into the superconducting material around

$$f_{\text{mag}} \approx -\frac{1}{8\pi} B_a^2 \times \pi\lambda^2 \ . \qquad (33)$$

$$f = f_{\text{core}} + f_{\text{mag}} \approx \tfrac{1}{8}(H_c^2\xi^2 - B_a^2\lambda^2) \ . \qquad (34)$$

The threshold field for a stable fluxoid is at $f = 0$, or, with H_{c1} written for B_a,

$$H_{c1}/H_c \approx \xi/\lambda \ . \sim 1/\kappa \qquad (35)$$

The threshold field divides the region of positive surface energy from the region of negative surface energy.

for $H < H_{c1}$, $f > 0$; for $H > H_{c1}$, $f < 0$

(30) + (35) $\quad \pi\xi\lambda H_c \approx \Phi_0 \qquad (36)$

(30) + (31) $\quad (H_{c1}H_{c2})^{1/2} \approx H_c \qquad (37a)$

(31) + (37a) $\quad H_{c2} \approx (\lambda/\xi)H_c = \kappa H_c \qquad (37b)$

Superconducting Energy Gap in 1960

Ivar Giaever

Nobel Prize in 1973

Tunneling junction

S I N

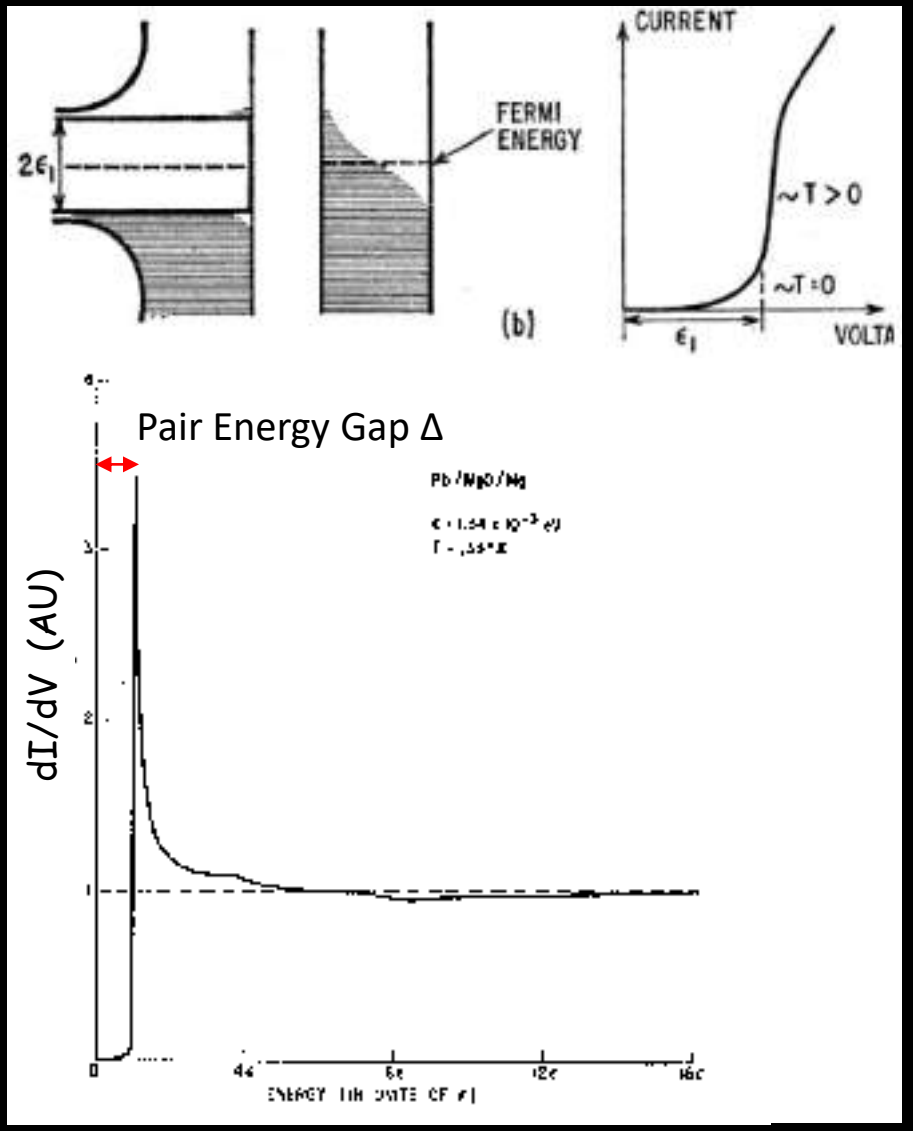

Ivar Giaever, Phys. Rev. Lett. 5, 147 (1960)
I. Giaever, Phys. Rev. 126, 941 (1962)

Single Particle Tunneling

If the barrier is sufficiently thin (less than 10 or 20Å) there is a significant probability that an electron which impinges on the barrier will pass from one metal to the other: this is called tunneling.

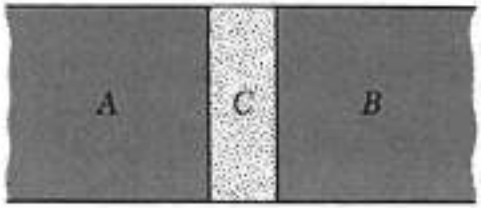

Figure 20 Two metals, *A* and *B*, separated by a thin layer of an insulator *C*.

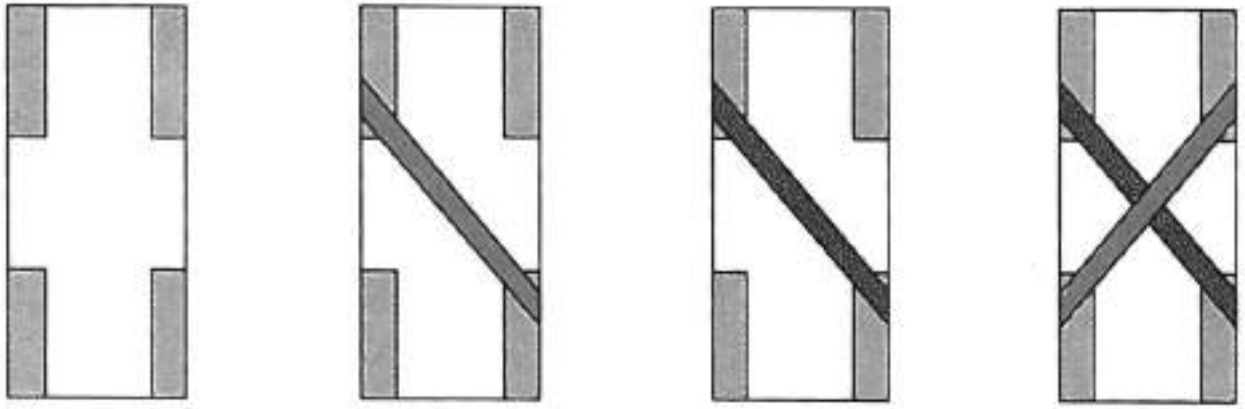

Figure 21 Preparation of an $Al/Al_2O_3/Sn$ sandwich. (a) Glass slide with indium contacts. (b) An aluminum strip 1 mm wide and 1000 to 3000 Å thick has been deposited across the contacts. (c) The aluminum strip has been oxidized to form an Al_2O_3 layer 10 to 20 Å in thickness. (d) A tin film has been deposited across the aluminum film, forming an $Al/Al_2O_3/Sn$ sandwich. The external leads are connected to the indium contacts; two contacts are used for the current measurement and two for the voltage measurement. (After Giaever and Megerle.)

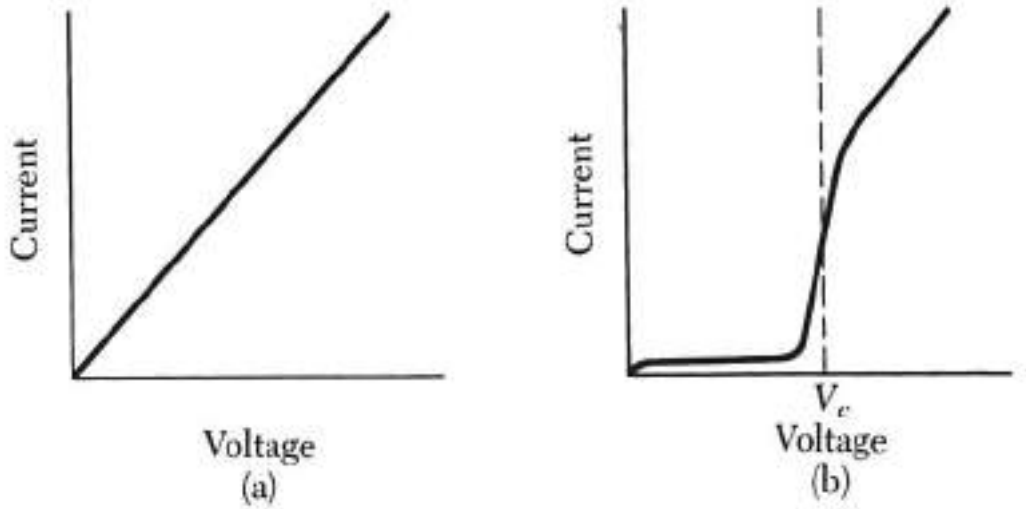

N-N tunneling **S-N tunneling**

Figure 22 (a) Linear current-voltage relation for junction of normal metals separated by oxide layer; (b) current-voltage relation with one metal normal and the other metal superconducting.

1. When both metals are normal conductors, the current-voltage relation of it is Ohmic at low voltages,

2. Giaever (1960) discovered that if one of the metals becomes superconducting, the current-voltage characteristic changes from the straight line of Fig. 22a to the curve shown in Fig. 22b.

Giaever Tunneling

In the superconductor there is an energy gap centered at the Fermi level. At absolute zero no current can flow until the applied voltage is

$$V = E_g/2e = \Delta/e.$$

$N(E) = E/(E^2-\Delta^2)^{1/2}$

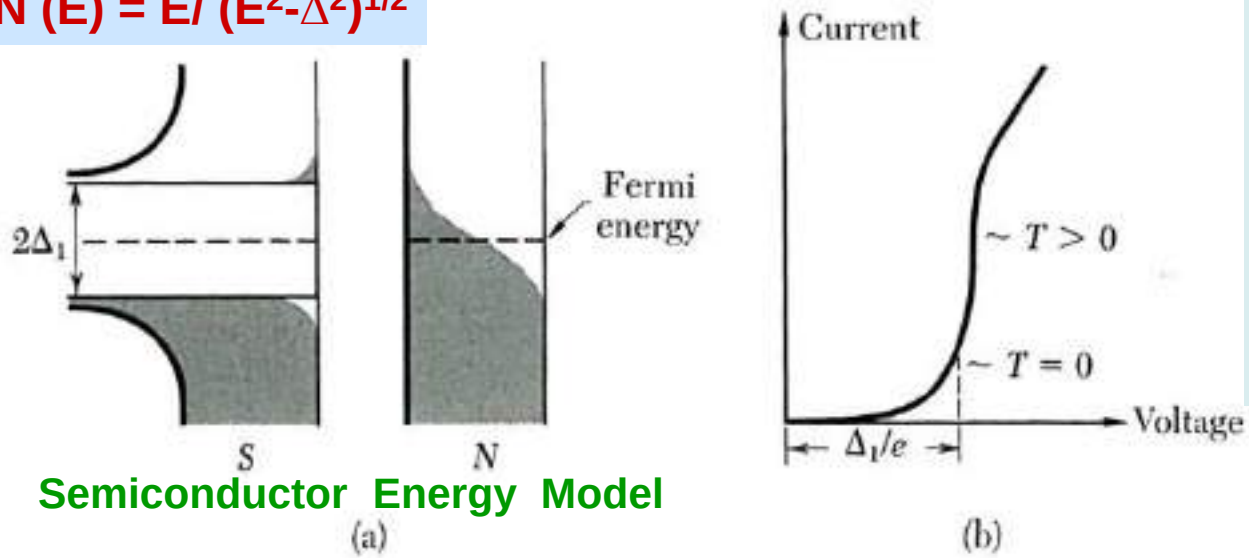

Semiconductor Energy Model

S-N tunneling

At T = 0, **I** is finite when E > Δ,

At T > 0, **I** is > 0 even for E < Δ

Figure 23 The density of orbitals and the current-voltage characteristic for a tunneling junction. In (a) the energy is plotted on the vertical scale and the density of orbitals on the horizontal scale. One metal is in the normal state and one in the superconducting state. (b) I versus V; the dashes indicate the expected break at $T = 0$. (After Giaever and Megerle.)

The current starts when $eV = \Delta$. At finite temperatures, because of electrons in the superconductor that are thermally excited across the energy gap.

Superconducting Tunneling and Application

by L. Solymar

Chapter 4
&
Chapter 5
&
Chapter 6

Semiconductor Model

4.3 Junctions between identical superconductors

The energy diagram for $T = 0°K$ is shown in Fig. 4.4. All energy levels are filled up to $E_F - \Delta$. In thermal equilibrium (Fig. 4.4 (*a*)) there is no current flowing. When a voltage $V < 2\Delta/e$ is applied there is still no current flowing because the electrons below the gap on the left have no access to empty states on the right. At $V = 2\Delta/e$ (Fig. 4.4 (*b*)) there is a sudden rise in current because electrons on the left suddenly gain access to the states above the gap on the right. The corresponding current–voltage characteristic is shown in Fig. 4.4 (*c*).

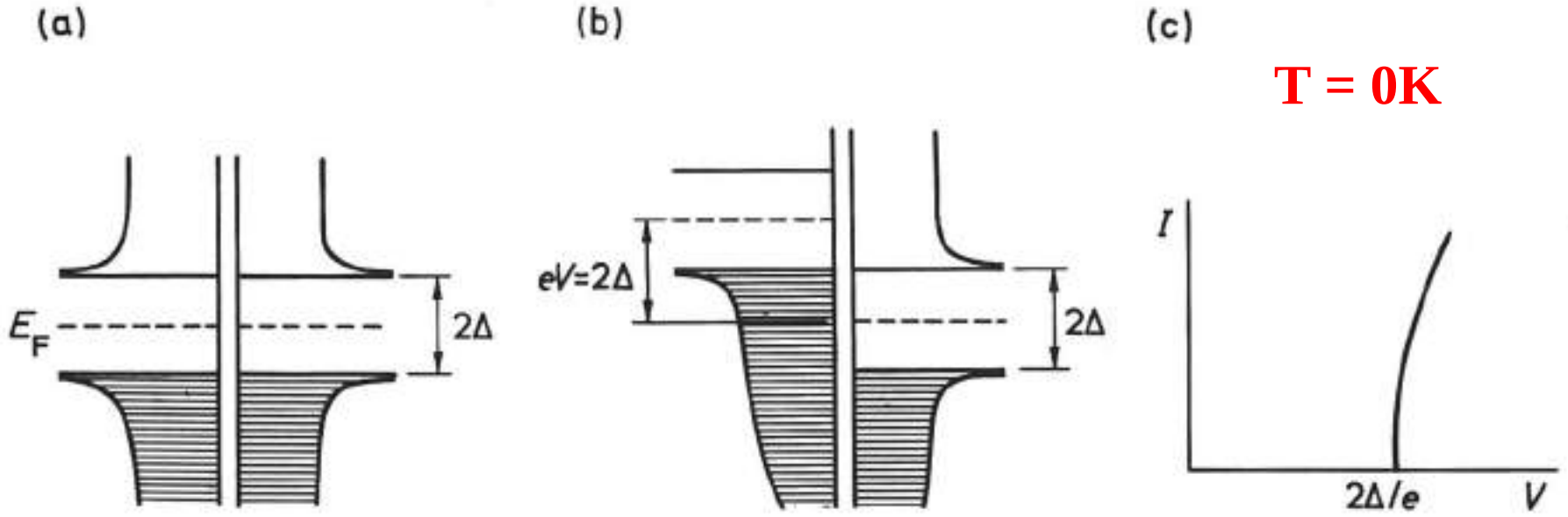

Fig. 4.4 The energy diagram of an SS junction; (*a*) $V = 0$, (*b*) $V = 2\Delta/e$, (*c*) the I–V characteristic at $T = 0$.

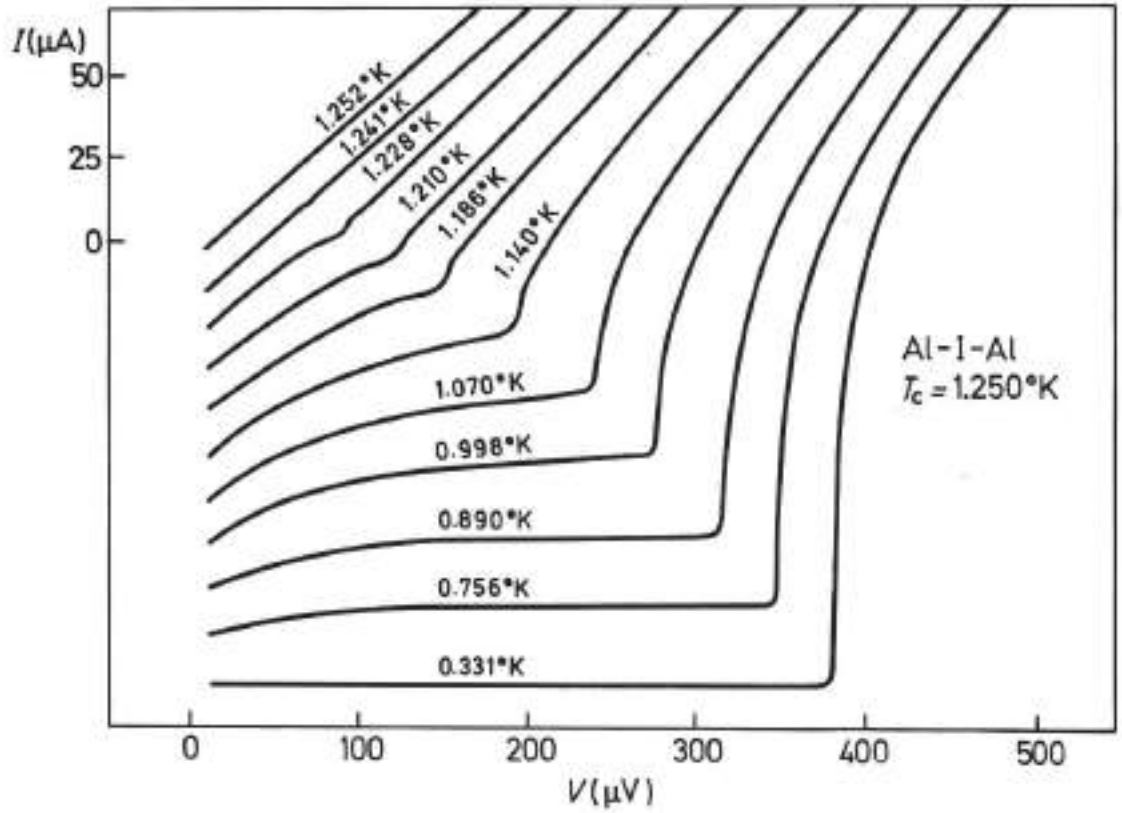

I-V temperature dependence of S/I/S junctions

T_c = 1.250K

For finite temperatures there will be some rounding off* of the sharp features of Fig. 4.4 (*c*) which, of course, depends on the actual temperature (how near it is to the critical). A very neat set of experimental results (Fig. 4.5) by Blackford and March [99] shows the temperature dependence of the current–voltage characteristic for an aluminium–aluminium oxide–aluminium junction. At 1·252°K aluminium is in the normal state and the characteristic is linear. At 1·241°K (a mere 9 millidegrees below the critical temperature) there is already some sign of the energy gap, and it becomes clearly discernible at 1·228°K. As the temperature decreases the knee in the curves moves to higher and higher voltages (corresponding to higher and higher energy gaps). The characteristic at $T = 0{\cdot}331$°K is practically identical to that at 0°K.

4.4 Junctions between superconductors of different energy gap

In the same way as the previously discussed case of identical superconductors, at $T = 0°K$ no current flows until the applied voltage is sufficiently large to bring the bottom of the gap on the left in line with the top of the gap on the right. This occurs at an applied voltage of $V = (\Delta_1 + \Delta_2)/e$ as shown in Fig. 4.6 (*a*). The current–voltage characteristic (Fig. 4.6 (*b*)) is similar to that shown in Fig. 4.4 (*c*) with the sole difference that the current starts rising at a voltage corresponding to the arithmetical mean of the gap energies.

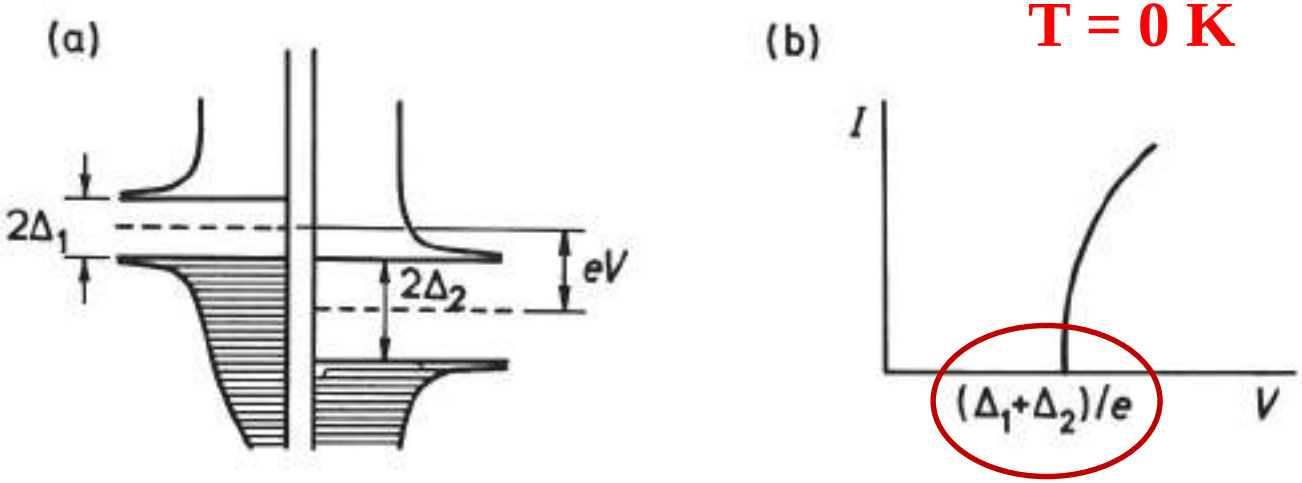

Fig. 4.6 Energy diagram and *I–V* characteristic of an S_1S_2 junction at $T = 0$.

T > 0K

At finite temperatures we may still assume that the normal electron states above the larger gap are empty but there are some thermally excited normal electrons in the smaller-gap superconductor as shown in Fig. 4.7 (*a*) for the case of thermal equilibrium.

Applying a voltage the current will start to flow immediately and will increase with increasing voltage (Fig. 4.7 (*e*)) until $V = (\Delta_2 - \Delta_1)/e$. The energy diagram for this case is shown in Fig. 4.7 (*b*); at this stage all electrons above the gap on the left can tunnel across into empty states on the right. What happens when the voltage is increased further? The number of electrons capable to tunnel across is still the same but they face a smaller density of states, as shown in Fig. 4.7 (*c*), hence the current decreases. The decrease in current continues until $V = (\Delta_1 + \Delta_2)/e$. At this point (Fig. 4.7 (*d*)) electrons from below the gap on the left gain access to empty states on the right, and there is a sudden increase in current. Thus the current–voltage characteristic of Fig. 4.7 (*e*) exhibits a negative resistance in the region

$$\frac{\Delta_2 - \Delta_1}{e} < V < \frac{\Delta_2 + \Delta_1}{e} \tag{3.1}$$

S_1/ I /S_2 T > 0K

$\Delta_1 < \Delta_2$

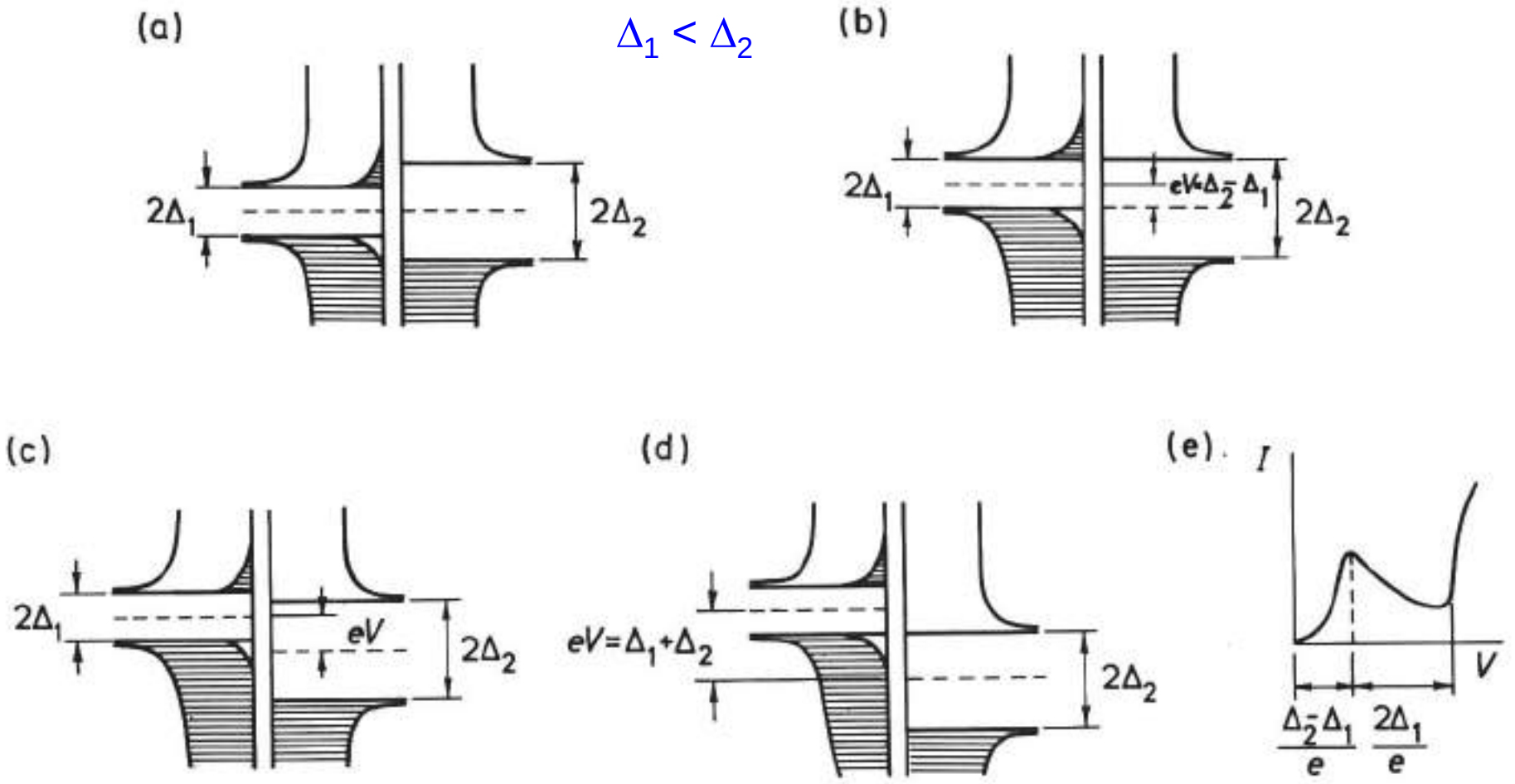

Fig. 4.7 The energy diagram and I–V characteristic of an S_1S_2 junction at finite temperature; (*a*) $V = 0$, (*b*) $V = (\Delta_2 - \Delta_1)/c$, (*c*) $(\Delta_2 - \Delta_1)/e < V < (\Delta_2 + \Delta_1)/e$, (*d*) $V = (\Delta_1 + \Delta_2)/e$, (*e*) the I–V characteristic.

The appearance of a negative resistance was reported simultaneously by Nicol *et al.* [46] and Giaever [45]. A very convincing characteristic presented by the latter author for an Al–Al_2O_3–Pb junction is shown in Fig. 4.8.

The experimentally found dependence [100] of the negative resistance on temperature is shown in Fig. 4.9 for a Sn–SnO–Pb junction. The current–voltage characteristic turns nonlinear when lead becomes superconducting and the negative resistance appears as soon as tin becomes superconducting as well. The negative resistance may be clearly seen down to 2·39°K but not at 1·16°K. Experimentally the negative resistance always disappears at sufficiently low temperatures but that may be due to insufficient accuracy of measurement and to nonideal circumstances.

The presence of a maximum and minimum in the characteristic gives further help in diagnostic measurements aimed at determining the width of the energy gaps. In addition, the negative resistance may be used in devices which will be discussed in more detail in Section 7.1.

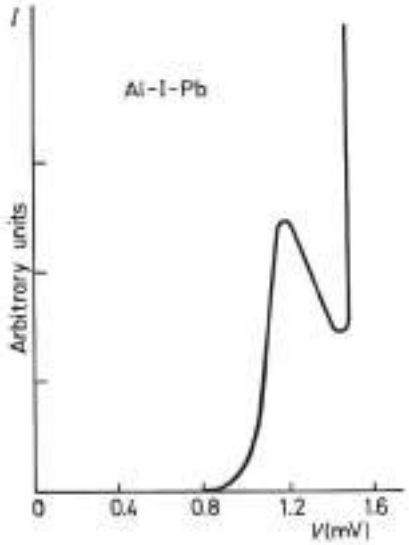

Fig. 4.8 The *I–V* characteristic of an Al–I–Pb junction, both Al and Pb superconducting. After Giaever [45].

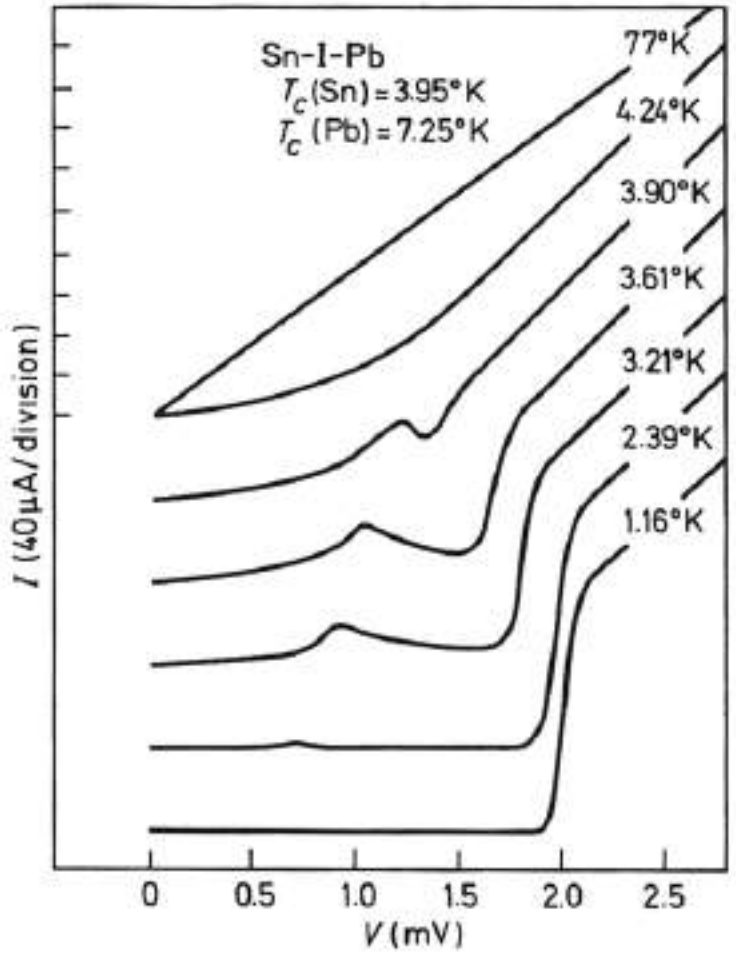

Fig. 4.9 *I–V* characteristics of an Sn–I–Pb junction.

Point contact junctions. These were developed by Levinstein and Kunzler [122, 123] in the form shown in Fig. 4.21. The barrier is prepared by heavily anodising a freshly etched tip of Al, Nb, Ta, etc. The diameter of the junction at the point of contact was estimated to be less than 10 μm. Tunnelling characteristics were observed in a large resistance range from 10^2 to 10^5 ohm.

The advantage of point contacts is that tunnelling measurements can be made on materials not accessible in thin film form. Furthermore, the tunnelling is generally from one single crystal to another since the grain size of the material both in the tip of the point contact and in the bulk is considerably larger than the contact area. Notable success of the point contact technique was to obtain the correct value for the energy gap of Nb_3Sn where thin film measurements consistently gave the wrong value.

was mostly on bulk samples

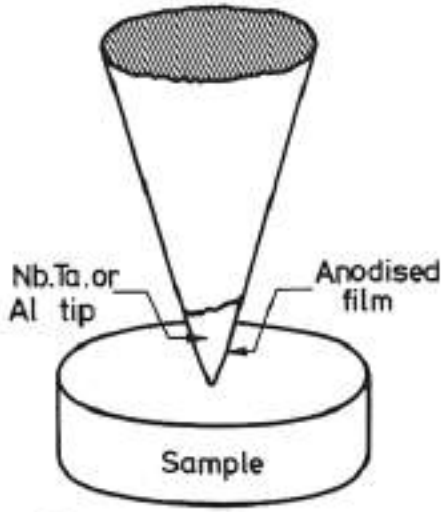

Lead to the invention of STM in 1982 !

Fig. 4.21 Point contact junction. After Levinstein and Kunzler [122].

Josephson Superconductor Tunneling

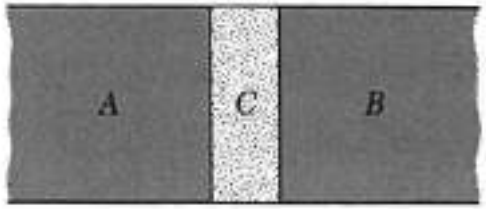

S-I-S
S-N-S

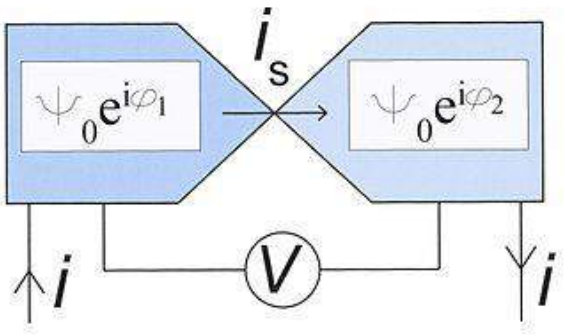

Such a junction is called a weak link.

1. **DC Josephson effect**: A ***dc*** current flows across the junction in the absence of any electric or magnetic field.
2. **AC Josephson effect**: A ***dc*** voltage applied across the junction causes ***rf*** current oscillations across the junction.

   An ***rf*** voltage applied with the ***dc*** voltage can then cause a ***dc*** current across the junction.
3. **Macroscopic long-range quantum interference**: A ***dc*** magnetic field applied through a superconducting circuit containing two junctions causes the maximum supercurrent to show interference effects as a function of magnetic field intensity. SQUID

DC Josephson Effect

Our discussion of Josephson junction phenomena follows the discussion of flux quantization, let both superconductors be identical.

$$i\hbar\frac{\partial\psi_1}{\partial t} = \hbar T\psi_2 \ ; \qquad i\hbar\frac{\partial\psi_2}{\partial t} = \hbar T\psi_1 \ . \tag{38}$$

Here $\hbar T$ represents the effect of the electron-pair coupling or transfer interaction across the insulator; T has the dimensions of a rate or frequency. It is a measure of the leakage of ψ_1 into the region 2, and of ψ_2 into the region 1.

Let $\psi_1 = n_1^{1/2}\, e^{i\theta_1}$ and $\psi_2 = n_2^{1/2}\, e^{i\theta_2}$. Then

$$\frac{\partial\psi_1}{\partial t} = \tfrac{1}{2}n_1^{-1/2}\, e^{i\theta_1}\frac{\partial n_1}{\partial t} + i\psi_1\frac{\partial\theta_1}{\partial t} = -iT\psi_2 \ ; \tag{39}$$

$$\frac{\partial\psi_2}{\partial t} = \tfrac{1}{2}n_2^{-1/2}\, e^{i\theta_2}\frac{\partial n_2}{\partial t} + i\psi_2\frac{\partial\theta_2}{\partial t} = -iT\psi_1 \ . \tag{40}$$

We multiply (39) by $n_1^{1/2}\, e^{-i\theta_1}$ to obtain, with $\delta \equiv \theta_2 - \theta_1$,

$$\frac{1}{2}\frac{\partial n_1}{\partial t} + in_1\frac{\partial\theta_1}{\partial t} = -iT(n_1n_2)^{1/2}\, e^{i\delta} \ . \tag{41}$$

We multiply (40) by $n_2^{1/2}\, e^{-i\theta_2}$ to obtain

$$\frac{1}{2}\frac{\partial n_2}{\partial t} + in_2\frac{\partial\theta_2}{\partial t} = -iT(n_1n_2)^{1/2}\, e^{-i\delta} \ . \tag{42}$$

Now equate the real and imaginary parts of (41) and similarly of (42):

eq (41); eq(42)

For the real part

$$\frac{\partial n_1}{\partial t} = 2T(n_1 n_2)^{1/2} \sin \delta \; ; \qquad \frac{\partial n_2}{\partial t} = -2T(n_1 n_2)^{1/2} \sin \delta \; ; \tag{43}$$

For the imaginary part

$$\frac{\partial \theta_1}{\partial t} = -T\left(\frac{n_2}{n_1}\right)^{1/2} \cos \delta \; ; \qquad \frac{\partial \theta_2}{\partial t} = -T\left(\frac{n_1}{n_2}\right)^{1/2} \cos \delta \; . \tag{44}$$

If $n_1 \cong n_2$ as for identical superconductors 1 and 2, we have from (44) that

$$\frac{\partial \theta_1}{\partial t} = \frac{\partial \theta_2}{\partial t} \; ; \qquad \boxed{\frac{\partial}{\partial t}(\theta_2 - \theta_1) = 0} \; . \tag{45}$$

The phase difference is time independent !

$$\frac{\partial n_2}{\partial t} = -\frac{\partial n_1}{\partial t} \; . \tag{46}$$

the current J of superconductor pairs across the junction depends on the phase difference δ as

$$\boxed{J = J_0 \sin \delta = J_0 \sin (\theta_2 - \theta_1) \; ,} \tag{47}$$

J ∝ dN/dt

where J_0 is proportional to the transfer interaction T. The current J_0 is the maximum zero-voltage current that can be passed by the junction. With no applied voltage a dc current will flow across the junction (Fig. 24), with a value between J_0 and $-J_0$ according to the value of the phase difference $\theta_2 - \theta_1$. This is the **dc Josephson effect.**

Josephson Current

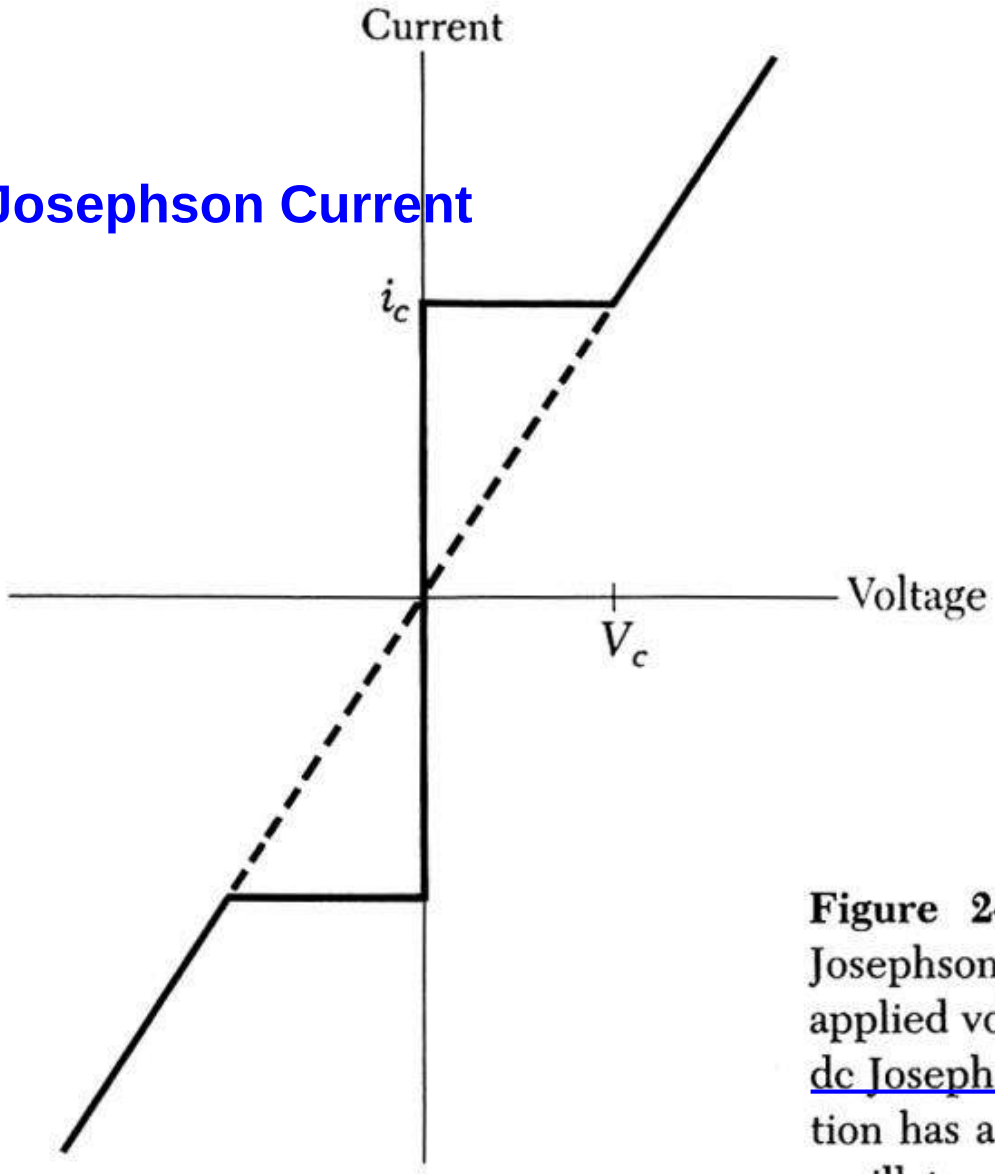

Figure 24 Current-voltage characteristic of a Josephson junction. Dc currents flow under zero applied voltage up to a critical current i_c: this is the dc Josephson effect. At voltages above V_c the junction has a finite resistance, but the current has an oscillatory component of frequency $\omega = 2eV/\hbar$: this is the ac Josephson effect.

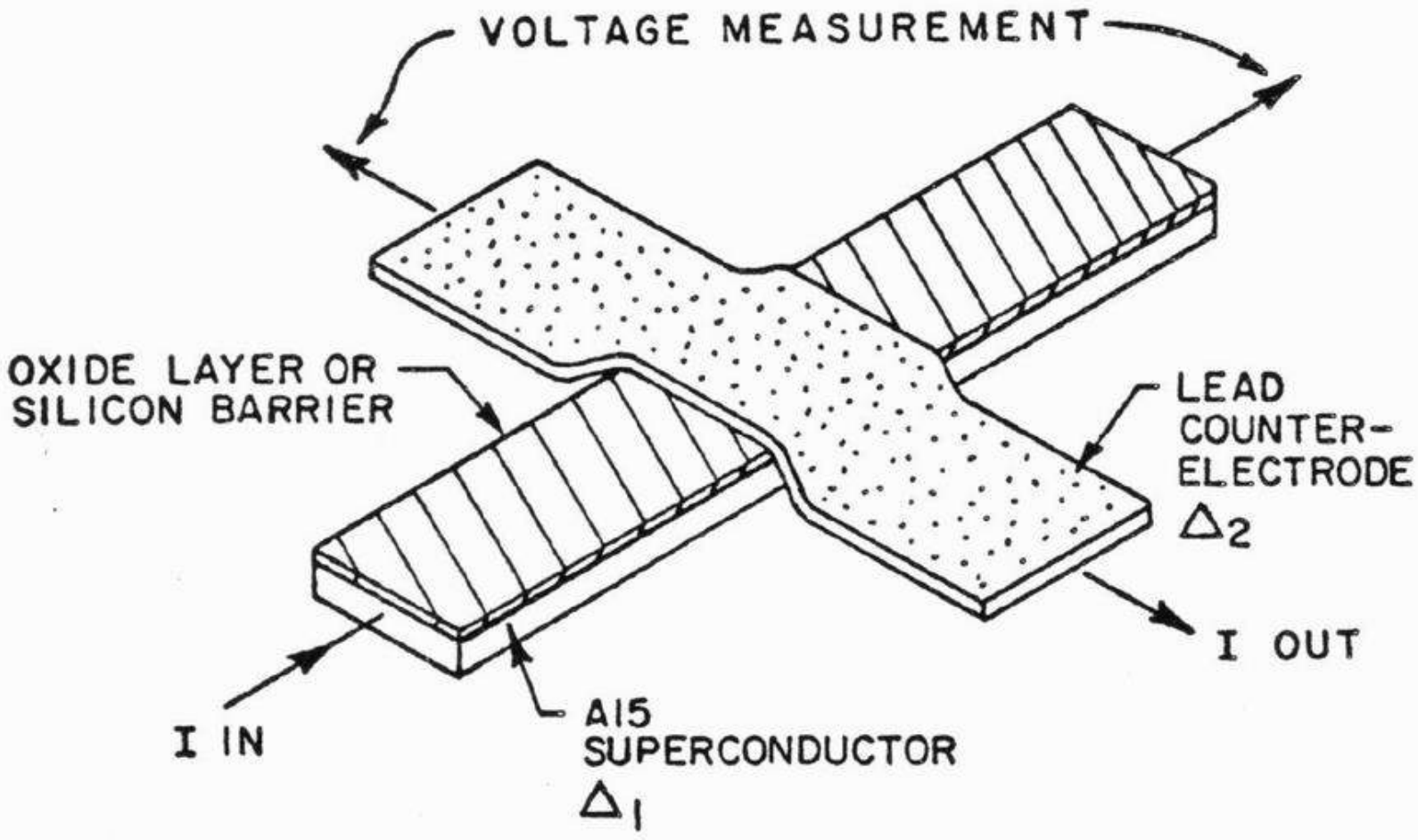

FIG. 1.1--(a) The geometry of our oxide layer tunnel junctions.

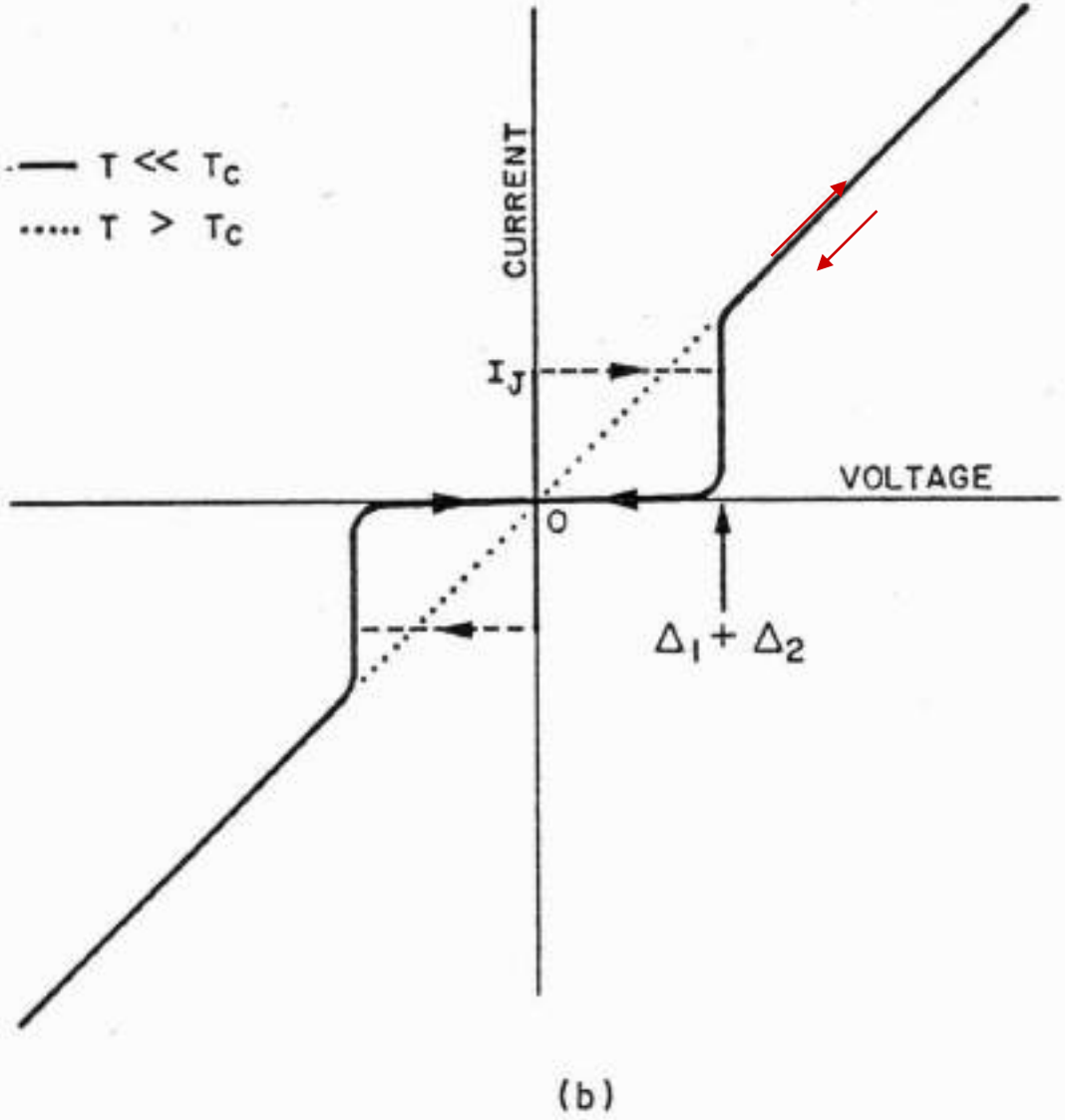

(b)

A two-terminal device !

(b) An idealized current-voltage characteristic showing quasiparticle (Giaever) and pair (Josephson) tunneling through the barrier.

AC Josephson Effect

Under a dc voltage V

We can say that a pair on one side is at potential energy $-eV$ and a pair on the other side is at eV.

$$i\hbar\,\partial\psi_1/\partial t = \hbar T\psi_2 - eV\psi_1; \qquad i\hbar\,\partial\psi_2/\partial t = \hbar T\psi_1 + eV\psi_2 \ . \tag{48}$$

Follow Eq. 41

$$\frac{1}{2}\frac{\partial n_1}{\partial t} + in_1\frac{\partial\theta_1}{\partial t} = ieVn_1\hbar^{-1} - iT(n_1n_2)^{1/2}\,e^{i\delta} \ . \tag{49}$$

This equation breaks up into the real part

$$\partial n_1/\partial t = 2T(n_1n_2)^{1/2}\sin\delta \ , \tag{50}$$

exactly as without the voltage V, and the imaginary part

$$\partial\theta_1/\partial t = (eV/\hbar) - T(n_2/n_1)^{1/2}\cos\delta \ , \tag{51}$$

which differs from (44) by the term $eV/\hbar$.

Follow Eq. 42

$$\frac{1}{2}\frac{\partial n_2}{\partial t} + in_2\frac{\partial\theta_2}{\partial t} = -i\,eVn_2\hbar^{-1} - iT(n_1n_2)^{1/2}\,e^{-i\delta} \ , \tag{52}$$

$$\partial n_2/\partial t = -2T(n_1 n_2)^{1/2} \sin \delta \ ; \tag{53}$$

$$\partial \theta_2/\partial t = -(eV/\hbar) - T(n_1/n_2)^{1/2} \cos \delta \ . \tag{54}$$

with $n_1 \cong n_2$,

$$\partial(\theta_2 - \theta_1)/\partial t = \partial\delta/\partial t = -2eV/\hbar \ . \tag{55}$$

relative phase of the probability amplitudes vary as

$$\delta(t) = \delta(0) - (2eVt/\hbar) \ . \tag{56}$$

$$J = J_0 \sin [\delta(0) - (2eVt/\hbar)] \ . \tag{57}$$

The phase is dependent on time.

The current oscillates with frequency

$$\omega = 2eV/\hbar \ . \tag{58}$$

This is the **ac Josephson effect**. A dc voltage of 1 μV produces a frequency of 483.6 MHz. The relation (58) says that a photon of energy $\hbar\omega = 2eV$ is emitted or absorbed when an electron pair crosses the barrier.

To be used for a precise measurement of $\hbar/e$

Macroscopic Quantum Interference.

We consider two Josephson junctions in parallel, as in Fig. 25.

$\hbar c \nabla\theta = qA$

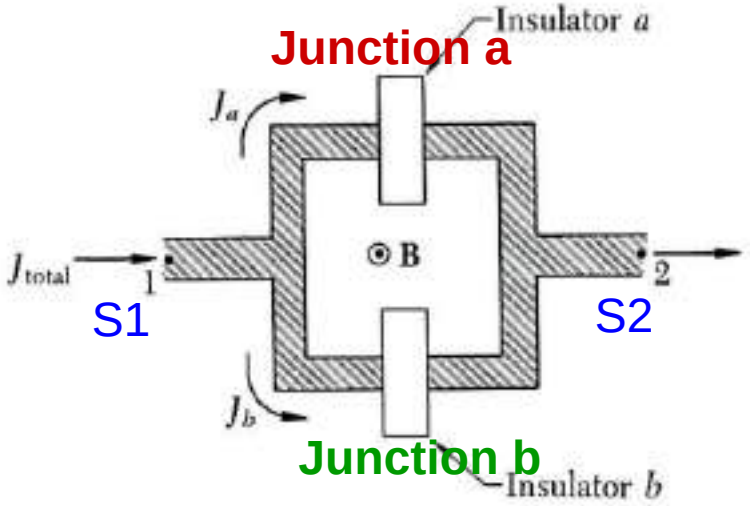

$\theta_1 - \theta_2 = (2e/\hbar c)\Phi$ eq. (59)

Figure 25 The arrangement for experiment on macroscopic quantum interference. A magnetic flux Φ passes through the interior of the loop.

Now let the flux Φ pass through the interior of the circuit.

By (59), $\delta_b - \delta_a = (2e/\hbar c)\Phi$, or

$$\delta_b = \delta_0 + \frac{e}{\hbar c}\Phi \; ; \qquad \delta_a = \delta_0 - \frac{e}{\hbar c}\Phi \; . \tag{60}$$

The total current is the sum of J_a and J_b.

$$J_{\text{Total}} = J_a + J_b = J_0\left\{\sin\left(\delta_0 + \frac{e}{\hbar c}\Phi\right) + \sin\left(\delta_0 - \frac{e}{\hbar c}\Phi\right)\right\} = 2(J_0 \sin\delta_0)\cos\frac{e\Phi}{\hbar c} \; .$$

The current varies with Φ and has maxima when

$$e\Phi/\hbar c = s\pi \; , \qquad s = \text{integer} \; . \tag{61}$$

Double slit diffraction pattern for two tunnel junctions

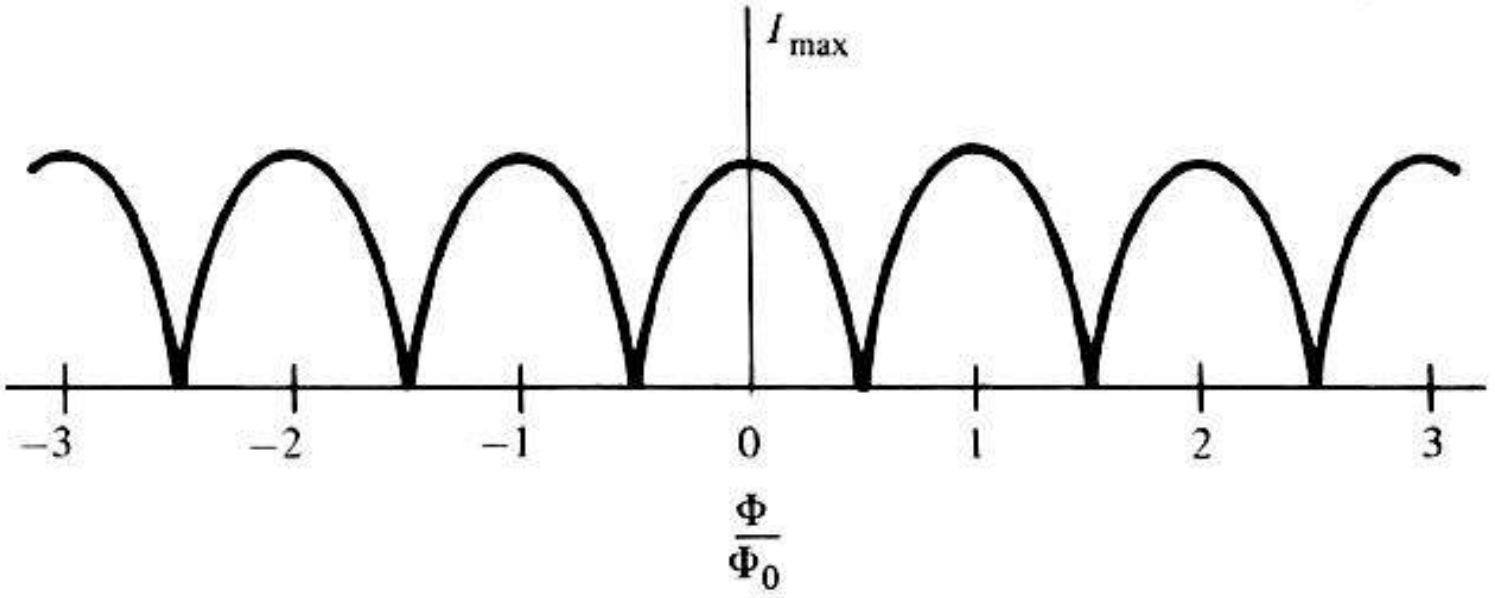

FIGURE 6-5
Dependence of maximum supercurrent through symmetrical two-junction superconducting interferometer (SQUID), shown schematically in Fig. 6-4.

Tinkham, Chapter 6, p. 203.

Single slit diffraction for single tunnel junction

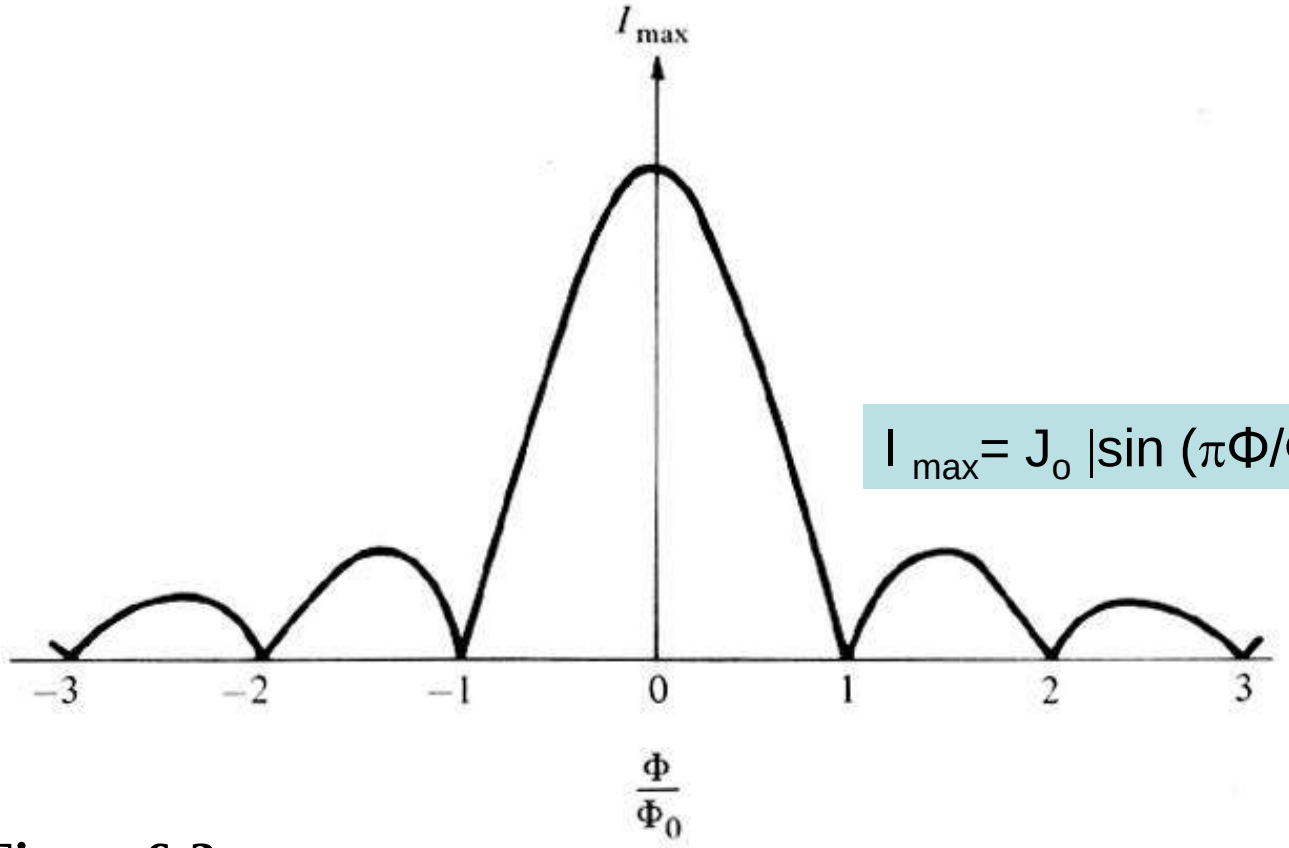

$I_{max} = J_o |\sin(\pi\Phi/\Phi_o)/\pi\Phi/\Phi_o|$

Figure 6-3

Dependence of maximum supercurrent through a **single Josephson junction** upon the flux threading the junction. The resemblance to the "single-slit" diffraction pattern of optics is evident.

Tinkham, Chapter 6, p. 199

The periodicity of the current is shown in Fig. 26.

1. The **short period** variation is produced by interference from the two junctions, as predicted by (61).
2. The **longer period** variation is a diffraction effect and arises from the finite dimensions of each junction.

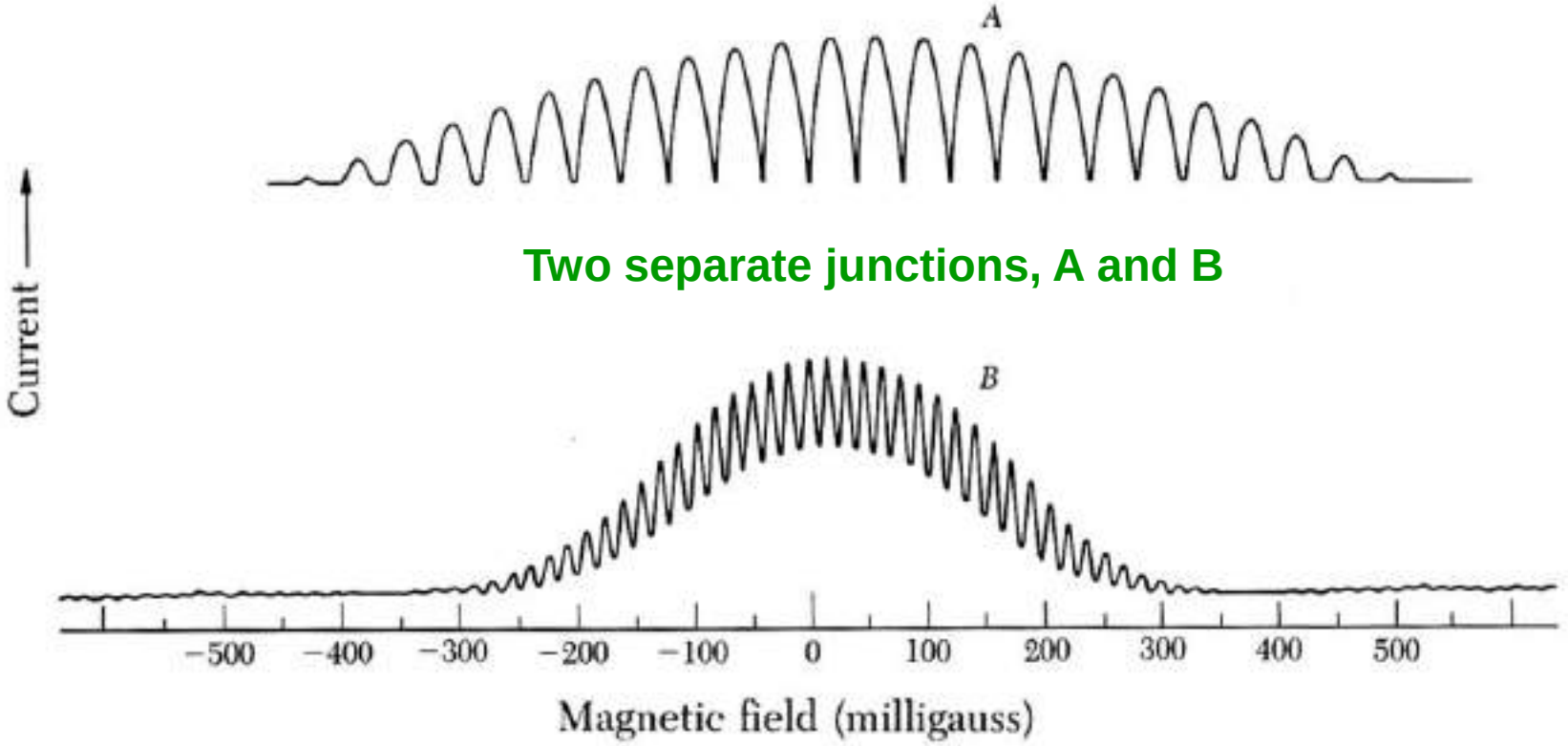

Figure 26 Experimental trace of J_{max} versus magnetic field showing interference and diffraction effects for two junctions *A* and *B*. The field periodicity is 39.5 and 16 mG for *A* and *B*, respectively. Approximate maximum currents are 1 mA (*A*) and 0.5 mA (*B*). The junction separation is 3 mm and junction width 0.5 mm for both cases. The zero offset of *A* is due to a background magnetic field. (After R. C. Jaklevic, J. Lambe, J. E. Mercereau and A. H. Silver.)

5.2 Photon-assisted tunnelling

Read the Book of Solymar

The tunnelling current may be modified by illuminating the junction with electromagnetic waves. It is easy to see that if the energy of the incident photons is in excess of 2Δ they will break up Cooper-pairs and create two electrons above the gap as shown in Fig. 5.5 (*a*). Since the number of electrons above the gap increases this way above its equilibrium value, some of these extra electrons will tunnel across the barrier (Fig. 5.5 (*b*)) creating thereby an extra current. We shall return to this problem in Section 7.2, for the moment we shall concentrate on the case when the energy of the incident photon is insufficient to break up a Cooper-pair. Influence on the tunnelling characteristics is still possible then if the photons act jointly with the applied voltage.

T = 0K

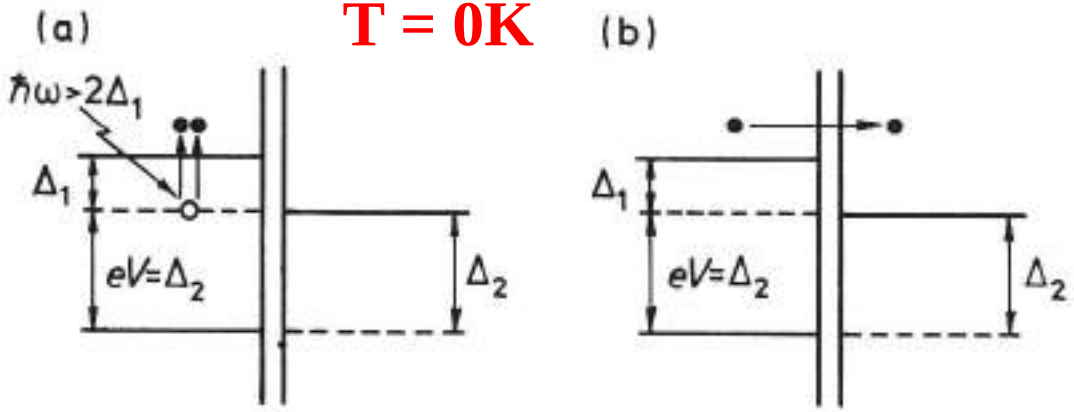

Fig. 5.5 Effect of incident photons on a tunnel junction; (*a*) a photon creates two electrons by breaking up a Cooper-pair, (*b*) one of the electrons created tunnels across.

Let us take $T = 0°K$ again and recall the case when $V = (\Delta_1 + \Delta_2)/e$. Then a Cooper-pair may break up into two electrons, one of them tunnelling across the barrier as has been shown in Fig. 4.12. If $V < (\Delta_1 + \Delta_2)/e$ no current flows. A Cooper-pair breaking up could not cause a current because the transition shown in Fig. 5.6 (*a*) with dotted lines is not permissible. However, if a photon of the right energy is available the liberated electron may follow the path shown in Fig. 5.6 (*b*) and get into an allowed state just above the gap. We may say that the electron tunnelled across the barrier by absorbing a photon, and refer to the phenomenon as photon-assisted tunnelling. The mathematical condition for the onset of tunnelling current is

$$\hbar\omega = \Delta_1 + \Delta_2 - eV. \qquad (5.1)$$

T = 0K

for $eV < \Delta_1 + \Delta_2$

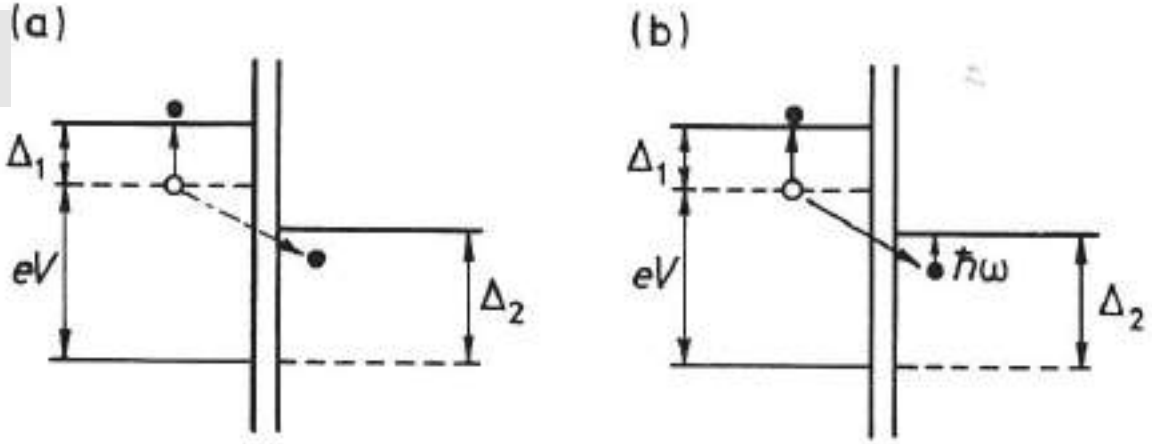

Fig. 5.6 (*a*) Tunnelling not allowed. (*b*) Tunnelling allowed if assisted by a photon.

If the energy of the photon is above this value tunnelling is still possible, though with a reduced probability because of a less favourable density of states. If the energy of the incident photon is below the value given by Equation (5.1) tunnelling may still be possible with the aid of a multi-photon process. An electron absorbing for example three photons simultaneously may tunnel across the barrier in the way shown in Fig. 5.7 (*a*). Hence we may expect sudden rises in the tunnelling characteristics whenever the condition

T = 0K

$$n\hbar\omega = \Delta_1 + \Delta_2 - eV \qquad (5.2)$$

is satisfied, that is for a series of voltages in the range $0 < V < (\Delta_1 + \Delta_2)/e$.

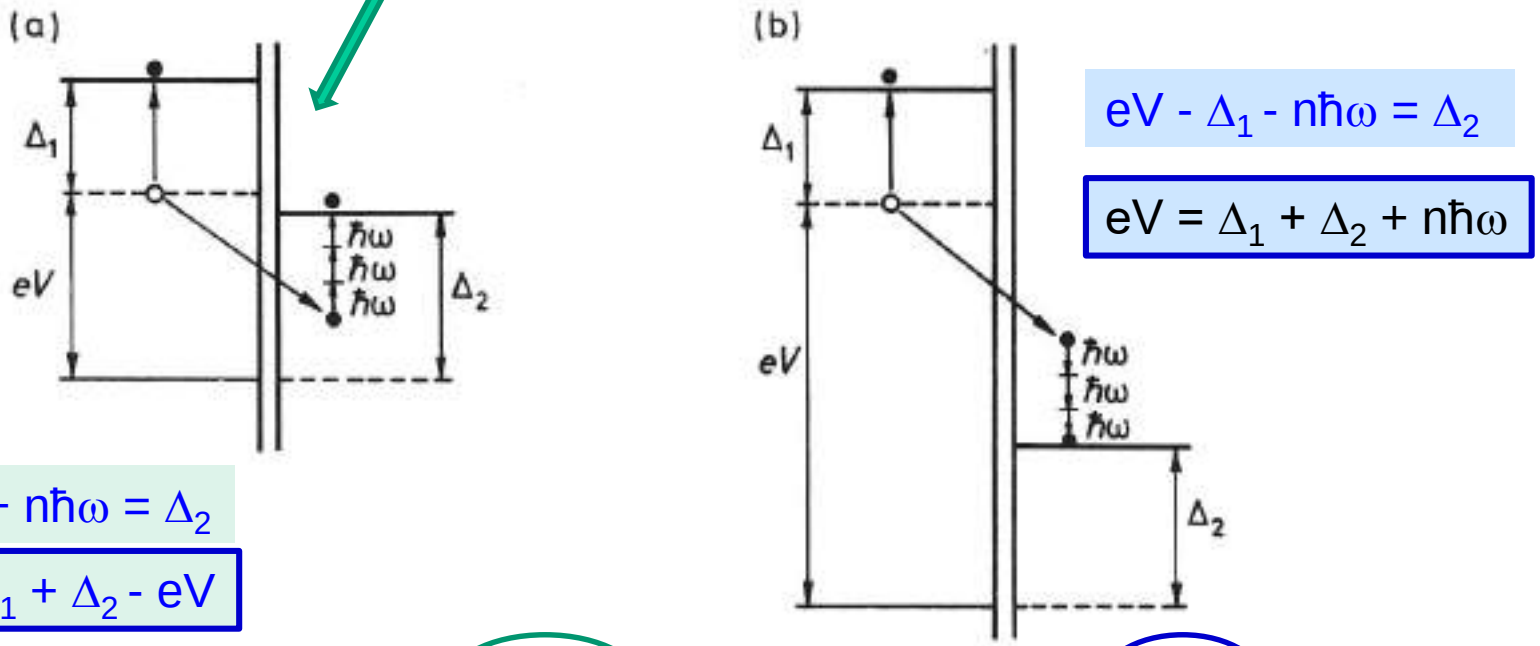

$eV - \Delta_1 + n\hbar\omega = \Delta_2$

$n\hbar\omega = \Delta_1 + \Delta_2 - eV$

$eV - \Delta_1 - n\hbar\omega = \Delta_2$

$eV = \Delta_1 + \Delta_2 + n\hbar\omega$

Fig. 5.7 Tunnelling assisted (*a*) by absorption of three photons, (*b*) by emission of three photons.

For $eV > \Delta_1 + \Delta_2$

When $V > (\Delta_1 + \Delta_2)/e$ we know that a tunnelling current will flow even in the absence of an incident electromagnetic wave. However, if photons of the right energy are available they can assist the tunnelling in this case as well, as shown in Fig. 5.7 (*b*) for a three-photon process. A Cooper-pair breaks up; one of the electrons goes into a state just above the gap on the left, and the other electron tunnels across into the superconductor on the right at an energy demanded by energy conservation (the sum of electron energies must equal the energy of the Cooper-pair). This process would occur with much higher probability if the electron could tunnel into the high density states lying just above the gap on the right. In Fig. 5.7 (*b*) this becomes energetically possible when three photons are *emitted* at the same time. Thus the mechanism of current rise is photon emission *stimulated* by input photons. For an *n*-photon emission process the current rises occur when

T = 0K

$$V_n = \frac{1}{e}(\Delta_1 + \Delta_2 + n\hbar\omega). \qquad (5.3)$$

T > 0K

For finite temperatures there is one more instance where electrons tunnel between maximum density states and that occurs at $V = (\Delta_2 - \Delta_1)/e$, as shown in Fig. 5.8 (*a*). Tunnelling between those states may also be assisted by photons as shown in Figs. 5.8 (*b* and *c*) for photon absorption and emission respectively. In general, multi-photon absorptions and emissions are possible again, and thus for finite temperatures there is another set of voltages,

$$V_m = \frac{1}{e}(\Delta_2 - \Delta_1 + m\hbar\omega), \qquad m = \pm 1, \pm 2, \pm 3 \tag{5.4}$$

at which current rises can be expected.

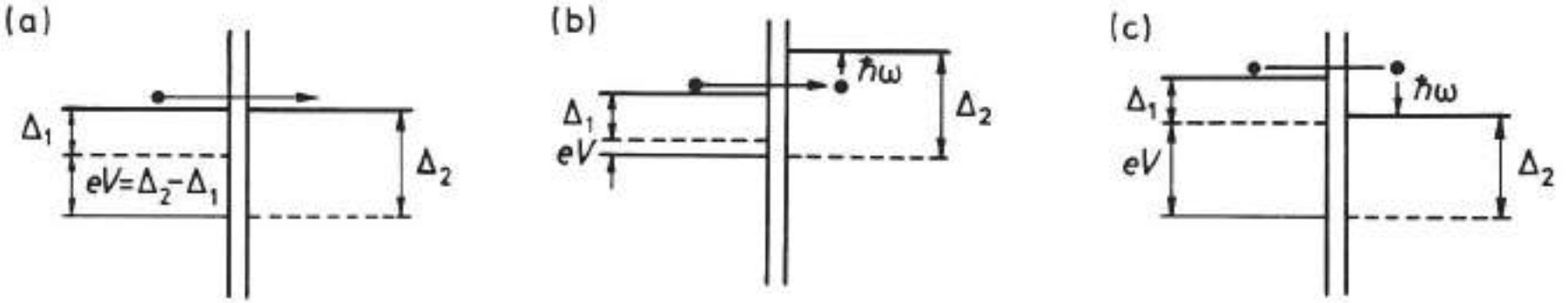

Fig. 5.8 Tunnelling between maximum density states at finite temperature (*a*) directly, (*b*) by photon absorption, (*c*) by photon emission.

The first experiments on tunnel junctions in the presence of electromagnetic waves were performed by Dayem and Martin [57] using junctions between Al and Pb, In or Sn. The frequency of the electromagnetic wave employed was 38·83 GHz so the experimental solution was to place the sample inside a cavity. The current–voltage characteristic was measured and rises in current were indeed found as may be seen in Fig. 5.9 (*a*) where the solid and dotted lines show the characteristic in the absence and presence of microwaves respectively.

Quantitative explanations were given nearly simultaneously by Tien and Gordon [58] and Cohen, Falicov and Phillips [126]. The methods in their papers were different but obtained essentially the same results. Cohen, Falicov and Phillips assumed that the magnetic field of the microwaves modulates the energy gap, whereas Tien and Gordon added an electrostatic perturbation term to the Hamiltonian. We shall follow here the latter derivation.

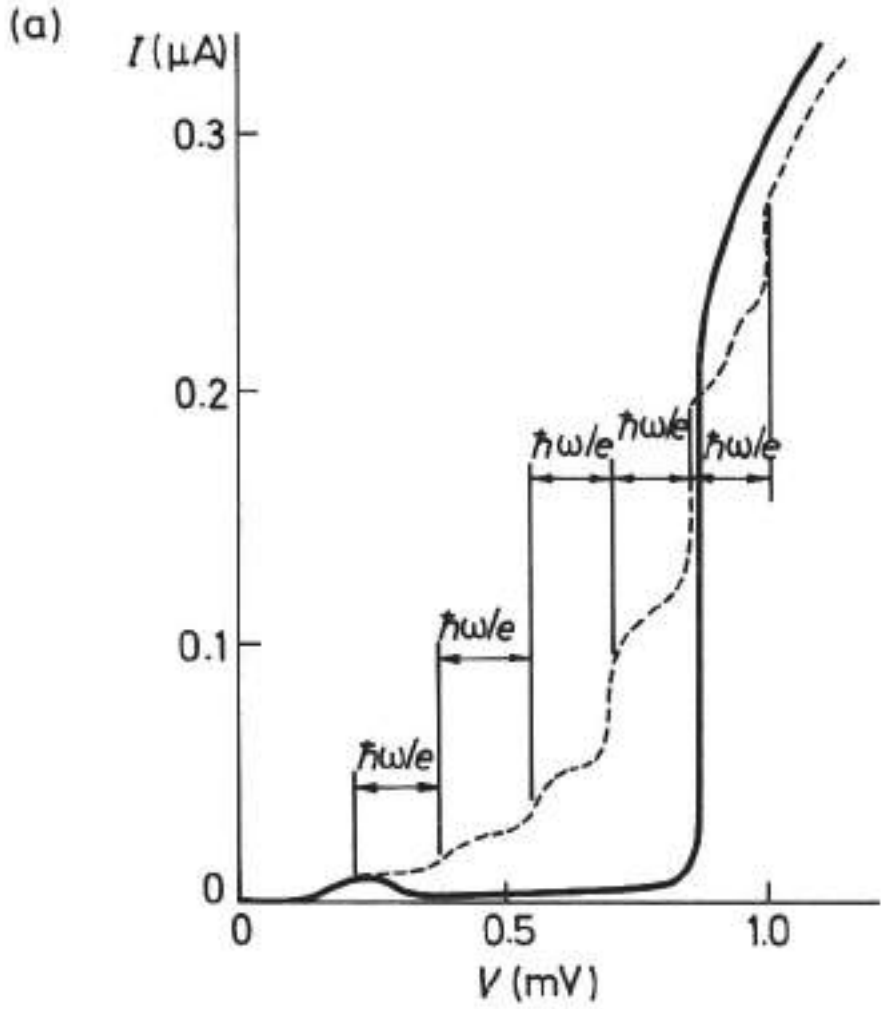

Fig. 5.9 (*a*) *I–V* characteristic of an Al–I–In junction in the absence (solid lines) and presence (dotted lines) of microwaves of frequency 38·83 GHz. Measurements by Dayem and Martin, quoted by Tien and Gordon [58].

The simplest assumption one can make is to regard the junction as a capacitance with a time-varying but spatially constant electric field between the plates. Regarding the potential of one of the superconductors (2) as the reference we may argue that the only effect of the microwave field is to add an electrostatic potential of the form

$$V_{rf} \cos \omega t \tag{5.5}$$

to the energy of the electrons in the other superconductor (1). Hence, for electrons in superconductor (1) we may use the new Hamiltonian

$$H = H_0 + eV_{rf} \cos \omega t \tag{5.6}$$

where the first term is the unperturbed Hamiltonian in the absence of microwaves.

If the unperturbed wavefunction was

$$\Psi_0(x, y, z, t) = f(x, y, z) \exp(-iEt/\hbar) \tag{5.7}$$

then the solution for the new wavefunction may be sought in the form

$$\Psi(x, y, z, t) = \Psi_0(x, y, z, t) \sum_{n=-\infty}^{\infty} B_n \exp(-in\omega t). \tag{5.8}$$

Substituting Equation (5.8) into Schrödinger's equation

$$H\Psi = i\hbar\frac{\partial\Psi}{\partial t} \tag{5.9}$$

we find

$$2nB_n = \frac{eV_{rf}}{\hbar\omega}(B_{n+1} + B_{n-1}) \tag{5.10}$$

which is satisfied by [101]

$$B_n = J_n(eV_{rf}/\hbar\omega) \tag{5.11}$$

where J_n is the n_{th} order Bessel function of the first kind. The new wavefunction is then

$$\Psi(x, y, z, t) = f(x, y, z, t)\exp(-iE\hbar/t)\sum_{n=-\infty}^{\infty} J_n(\alpha)\exp(-in\omega t), \tag{5.12}$$

where

$$\alpha = \frac{eV_{rf}}{\hbar\omega}. \tag{5.13}$$

It may be seen that in the presence of microwaves the wavefunction contains components with energies

$$E, E \pm \hbar\omega, E \pm 2\hbar\omega, \ldots \tag{5.14}$$

respectively. Without the electric field, an electron of energy E in superconductor (1) can only tunnel to the states in superconductor (2) of the same energy. In the presence of the electric field, the electron may tunnel to the states in superconductor (2) of energies E, $E \pm \hbar\omega$, $E \pm 2\hbar\omega$, etc. Let $N_{20}(E)$ be the unperturbed density of states of the superconductor (2). In the presence of microwaves we then have an effective density of states given by

$$N_2(E) = \sum_{n=-\infty}^{\infty} N_{20}(E + n\hbar\omega) J_n^2(\alpha). \tag{5.15}$$

We may now obtain the tunnelling current by substituting Equation (5.15) into the general expression Equation (2.14), yielding*

The tunneling current equation, Tinkham (2.14)

$$I = A \sum_{n=-\infty}^{\infty} J_n^2(\alpha) \int_{-\infty}^{\infty} N_1(E-eV) N_{20}(E+n\hbar\omega)[f(E-eV)-f(E+n\hbar\omega)]\,dE$$

$$= A \sum_{n=-\infty}^{\infty} J_n^2(\alpha) I_0(eV+n\hbar\omega) \tag{5.16}$$

where $I_0(eV)$ is the tunnelling current in the absence of microwaves.

In the limit $\hbar\omega \to 0$ it may be shown (see Appendix 5) that the above expression reduces to the classical value

$$I = \frac{1}{\pi} \int_{-\pi/2}^{\pi/2} I_0(V + V_{rf} \sin \omega t)\, d(\omega t). \tag{5.17}$$

The comparison between theory and experiments has a long and tangled story. The first attempt was made by Tien and Gordon [58] who could reproduce the experimental results of Dayem and Martin [57] by taking $\alpha = 2$ as shown in Fig. 5.9 (*b*). The experimental value of α (that is the voltage in the junction) was, however, not known. Estimates by Tien and Gordon indicated a discrepancy as large as an order of magnitude.

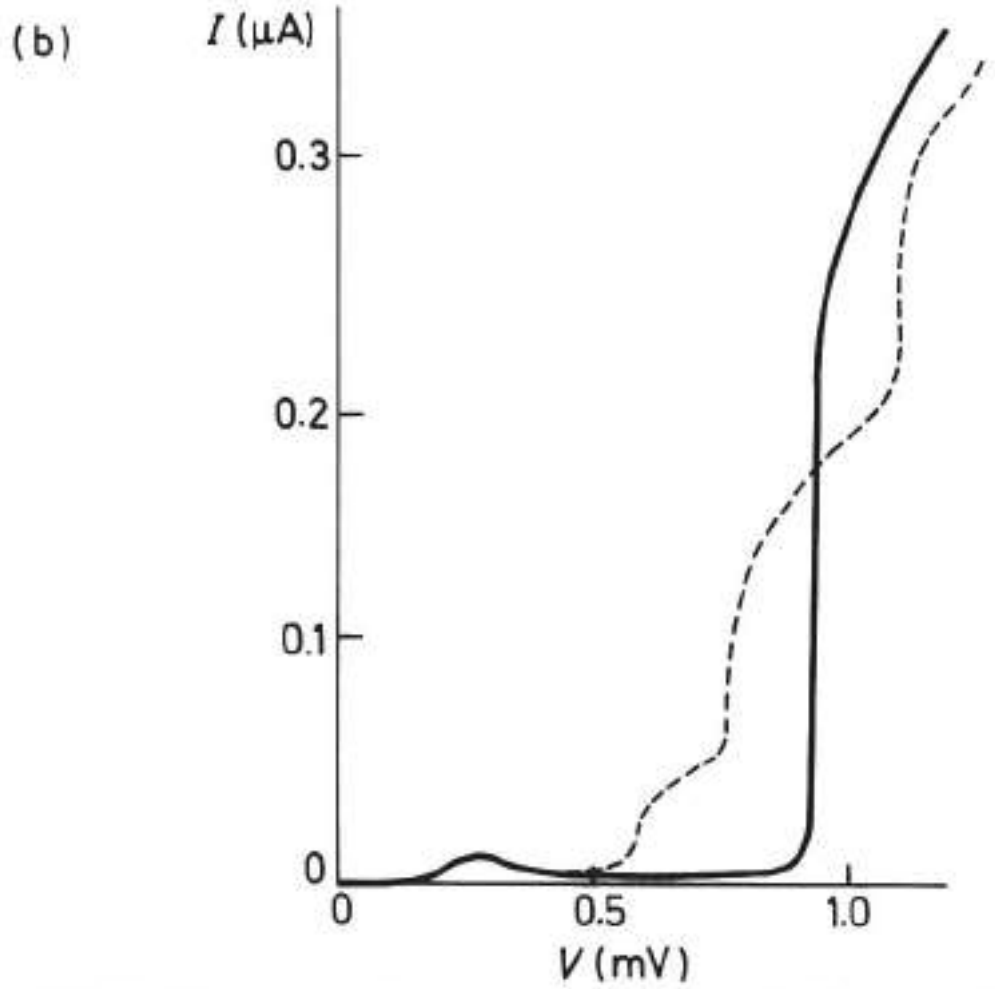

Fig. 5.9 (*b*) Theoretical curves by Tien and Gordon [58] for $\alpha = 2$.

To prove the point that it is the spatial variation which is responsible for the discrepancy, Hamilton and Shapiro [135] conducted another series of experiments on a very small (hardly overlapping in an in-line geometry) junction. The results then did agree with the Tien–Gordon theory as shown in Fig. 5.15.

Two more proofs in favour of the Tien–Gordon theory are the measurements of Hamilton and Shapiro [135] at 200 Hz where V_{rf} could be easily measured and the microwave experiments of Longacre and Shapiro [137] conducted on point contact (that is, very small) junctions.

Shapiro steps in the n^{th} order, observed in very small junctions

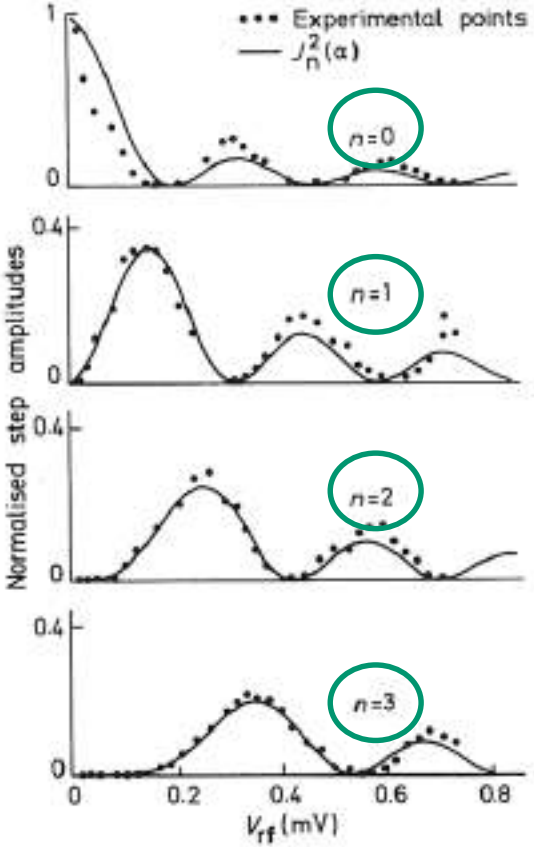

Fig. 5.15 Same as Fig. 5.14 for a very small junction. After Hamilton and Shapiro [135].

Observations of quasi-particle tunneling and Josephson behavior in $Y_1Ba_2Cu_3O_{7-x}$/native barrier/Pb thin-film junctions

J. Kwo, T. A. Fulton, M. Hong, and P. L. Gammel
AT&T Bell Laboratories, Murray Hill, New Jersey 07974

(Received 4 December 1989; accepted for publication 20 December 1989)

Low-leakage, thin-film planar tunnel junctions made of $Y_1Ba_2Cu_3O_{7-x}$/native barrier/Pb were fabricated. The $Y_1Ba_2Cu_3O_{7-x}$ films were prepared by *in situ* molecular beam epitaxy aided with an activated oxygen source. The as-grown, smooth superconducting perovskite film surface exhibits quasi-particle tunneling characteristics very similar to the etched bulk single-crystal data. The results in agreement are a linear dependence of the normal-state conductance on voltage, a gap-like structure at $\sim$20 mV, asymmetric modulations up to 50 mV, and a finite zero-bias conductance at low temperature. Junctions of lower resistance show, at temperatures below T_c of Pb, the development of a supercurrent at zero bias and associated hysteretic subgap structure, with a typical $I_cR \sim 0.5$ mV. Josephson-like behavior occurred in response to applied magnetic field and microwaves.

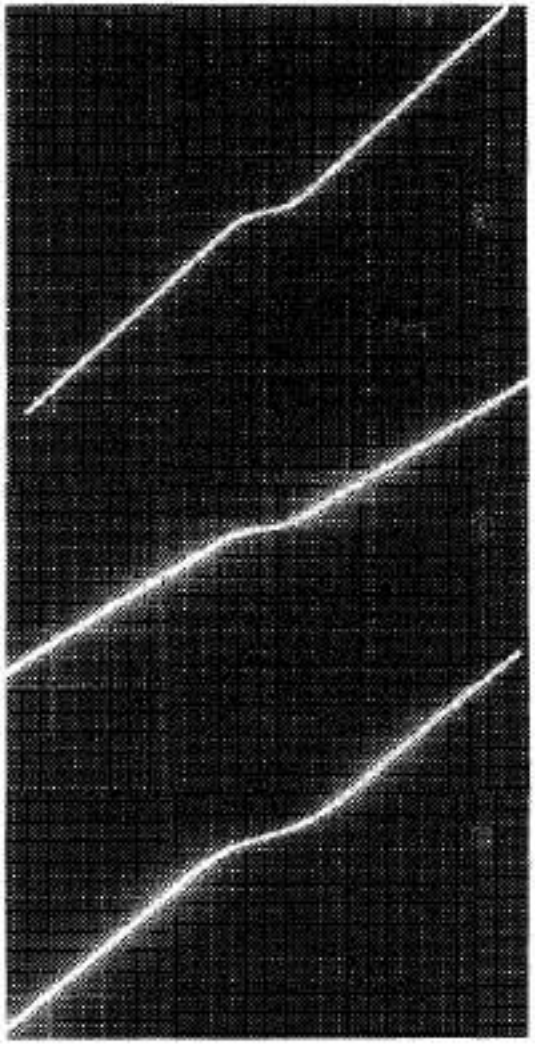

FIG. 1. Current-voltage characteristics for junctions (a), (b), and (c) at 4.2 K. The x axis (voltage) scales are 2, 2, and 1 mV per large division (pld) for (a), (b), and (c), respectively. The y axis (current) scales are 100, 250, and 250 μA pld for (a), (b), and (c), respectively.

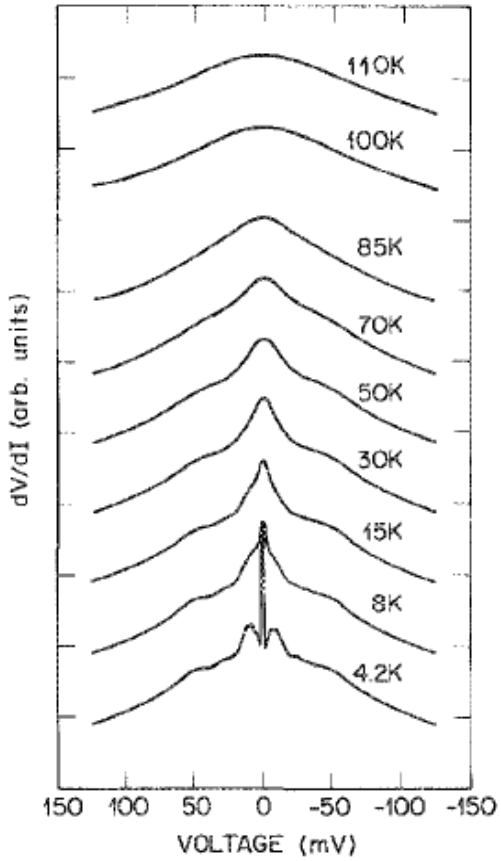

FIG. 2. Dynamic resistance $R(V)$ vs V as a function of temperature below and above T_c of a $Y_1Ba_2Cu_3O_{7-x}$ film. The zero of $R(V)$ at 4.2 K is on the base line, and the zeros of other traces are displaced progressively by one division.

Josephson current

1. Single slit diffraction pattern under B field
2. Shapiro steps in AC microwaves

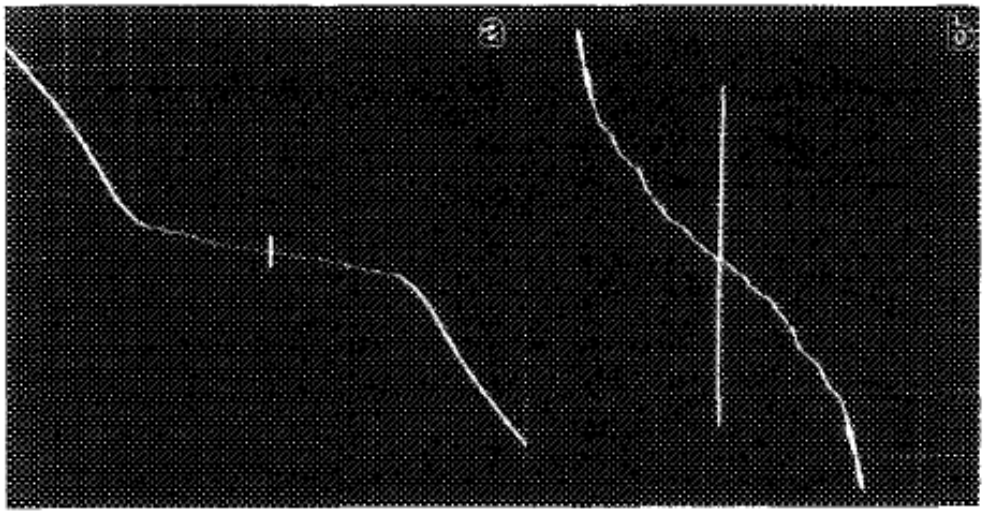

FIG. 3. Supercurrent and assoicated subgap structure at 1.5 K of a junction of R(10 mV) of 80 Ω. The x axis scale is 0.5 mV pld for (a) and (b). The y axis is (a) 10 μA pld and (b) 2 μA pld.

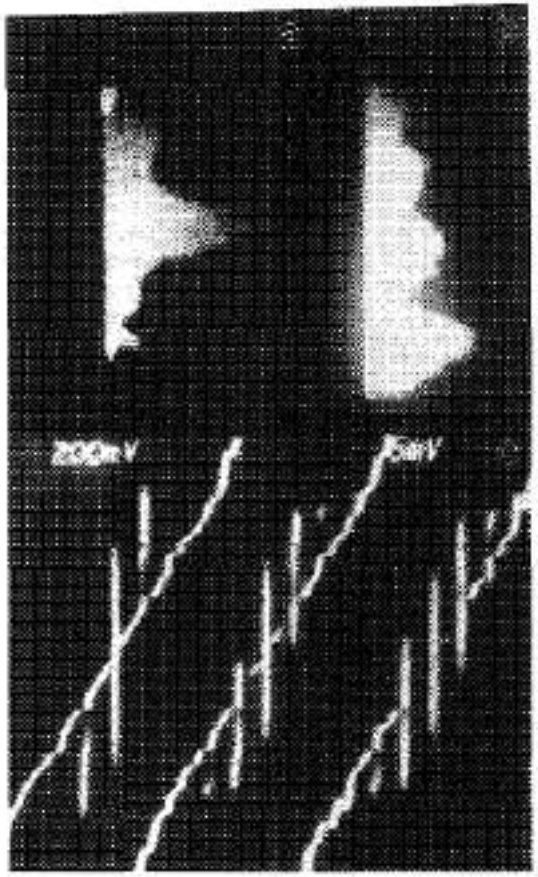

FIG. 4. Critical current (x axis, 1 μA pld) vs applied magnetic field (y axis, 1.9 G pld) for B swept (a) from negative to positive values and (b) in the opposite sense. The junction is in the $V = 0$ state where the trace is bright. (c) Occurrence of Shapiro current steps in the I-V in response to applied microwaves of 11.9 GHz. X scale is 50 μV pld and Y scale is 0.2 μA pld. Applied power is zero, intermediate, and full from left to right. The sloping steps on the leftmost trace are geometrical resonances. Shapiro steps up to $n = 2$ are visible in the right trace.

6.9 Strong coupling superconductors

The most convincing proof of the validity of the BCS theory came from tunnelling measurements but it became clear from the same measurements that some superconductors behaved somewhat differently. Giaever and Megerle [69] observed that the temperature dependence of the energy gap of lead obeyed the BCS theory only if they used the experimentally obtained value of $\Delta(0)$. The ratio $2\Delta(0)/kT_c$ was found to be 4·3, well above the BCS value of 3·52. A year later Giaever, Hart and Megerle [66] found a small but significant deviation from the BCS density of states when plotting $\sigma(V)$ as shown in Fig. 6.18. The crossover point is at about $k\theta_D$ the Debye energy suggesting immediately (low Debye energy implies strong electron–phonon interaction) the cause and the direction in which the BCS theory should be modified. In fact, more general theories were already available. Eliashberg [68] had already derived his gap equation taking into account both the electron–phonon matrix element and the phonon spectrum, but before the strategic attack upon this equation a number of tactical advances were necessary to make it sure that the experimental results were in line with the theoretical predictions. The story of these efforts is reviewed by Rowell and McMillan [165]; we shall briefly outline here the major steps in the process.

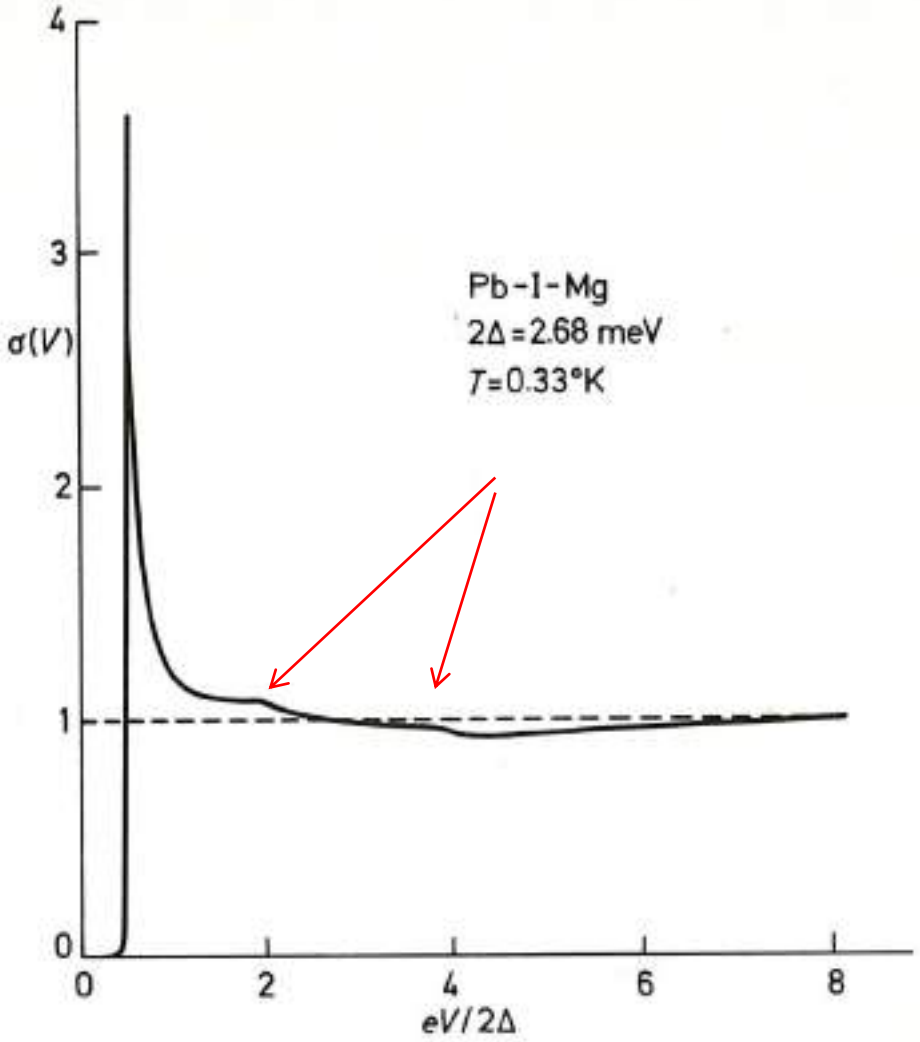

Fig. 6.18 Normalised differential conductance as a function of normalised voltage for a Pb–I–Mg junction. The structure shown in the curve signifies deviation from the BCS theory. The cross-over point corresponds to the Debye energy. After Giaever, Hart and Megerle [66].

Electron-Phonon Interaction by Tunneling Spectroscopy

William McMillan

John Rowell

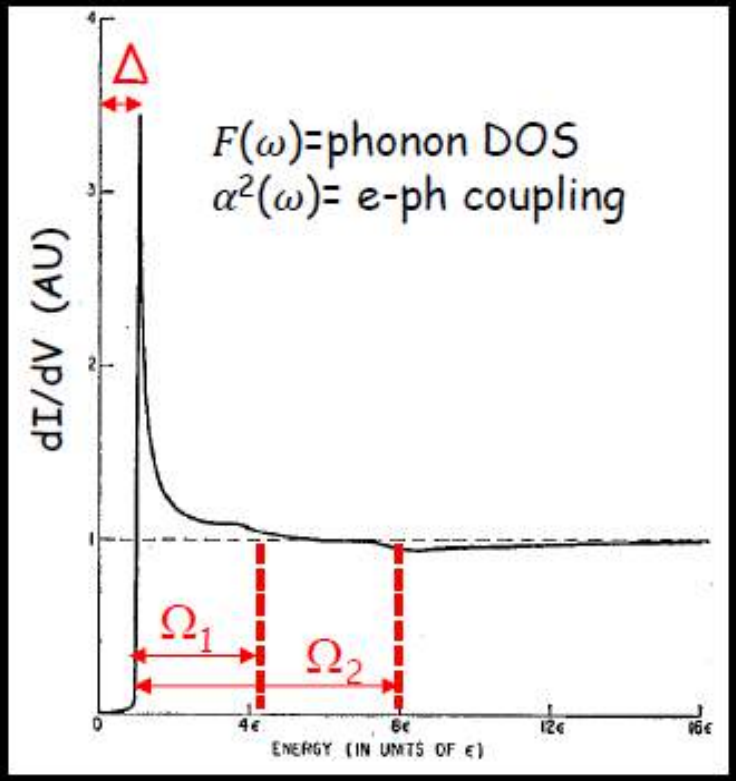

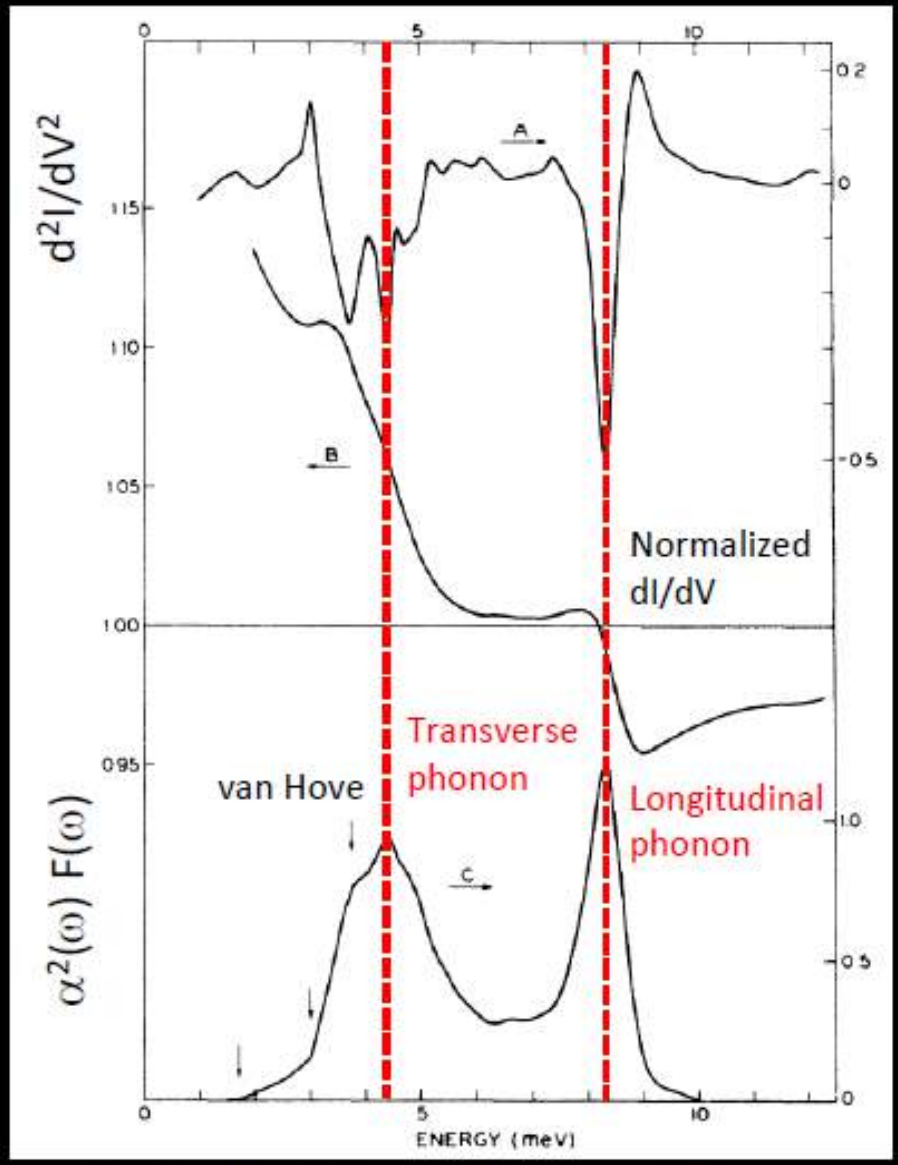

W.L. McMillan & J.W. Rowell, PRL 14, 108 (1965)

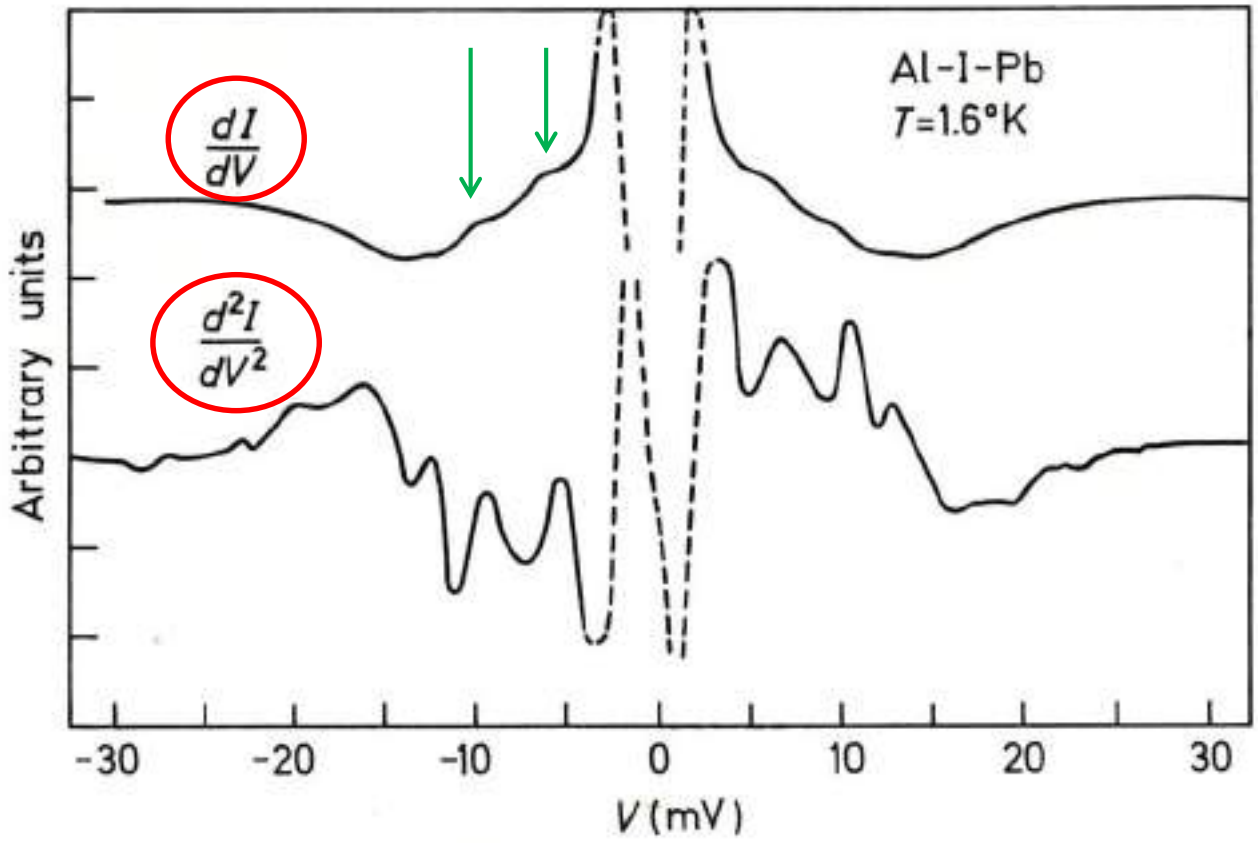

Fig. 6.19 First and second derivatives of the I–V characteristic as a function of voltage for an Al–I–Pb junction. After Rowell, Chynoweth and Phillips [219].

Morel and Anderson [218] approximated the effective phonon density by an Einstein peak at the longitudinal phonon frequency ω_L and predicted structure in the tunnelling density of states at energies $n\hbar\omega_L$. Subsequent measurements by Rowell *et al.* [219] (on Al–I–Pb junctions at 1·6°K) of the second derivative of the I–V characteristic did indeed produce the expected structure as shown in Fig. 6.19. The peak positions are given empirically by the formula

$$E_n = \Delta^1 + n\theta \tag{6.2}$$

where Δ^1 agrees roughly with the value for half the energy gap and $\theta = 3{\cdot}7$ meV is in the range of appreciable transverse phonon energies measured by neutron diffraction.

A refinement of the theory by Schrieffer *et al.* [220] was matched by further refinement of the experimental techniques [221]. By assuming the phonon density in the form of two Lorentzian peaks (representing the transverse and longitudinal phonons respectively) shown in Fig. 6.20 (*b*) and taking reasonable

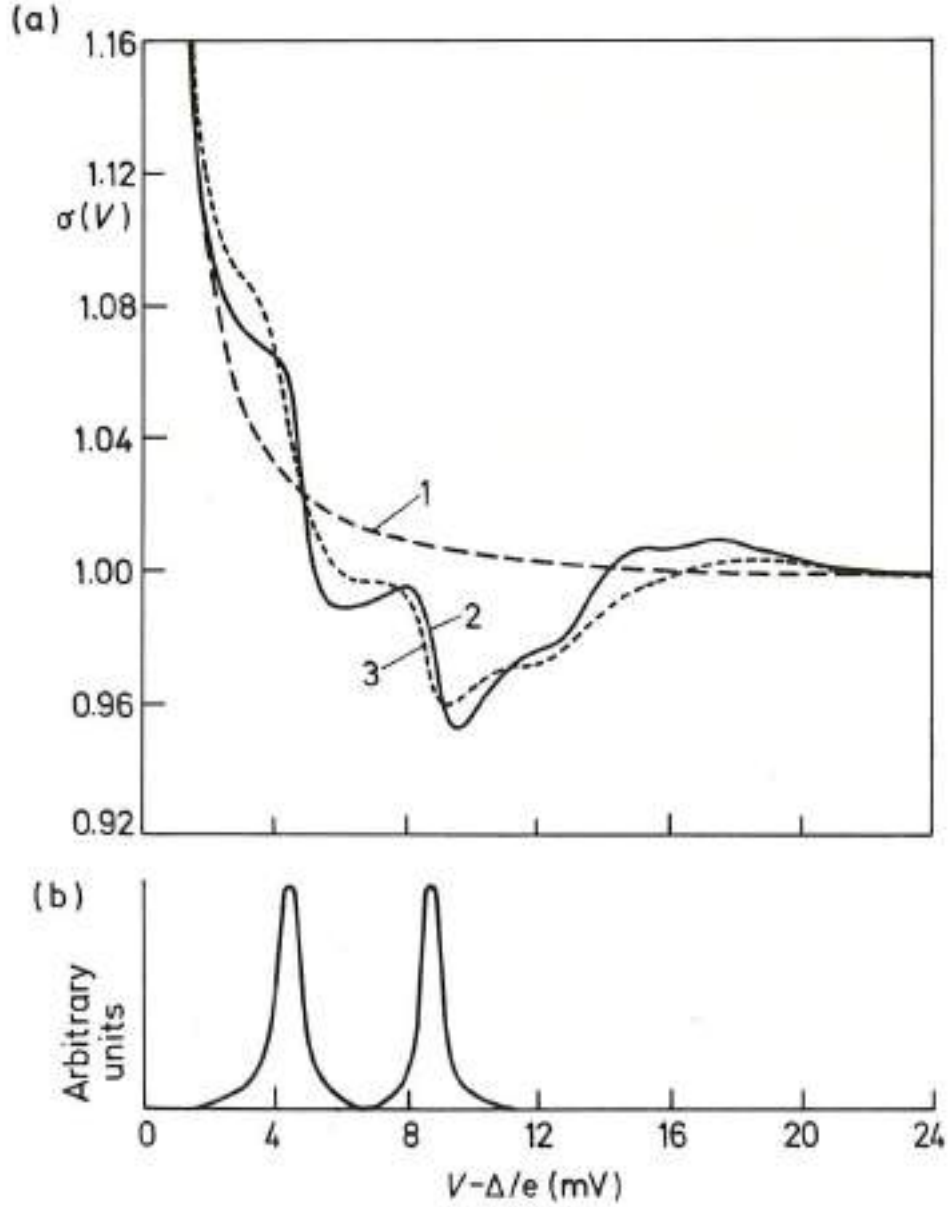

Fig. 6.20 (*a*) The normalised differential conductance as a function of voltage (zero shifted by Δ/e), 1 : BCS theory, 2 : theory by Schrieffer *et al.* [220], 3 : experimental results by Rowell, Anderson and Thomas [221]. (*b*) The phonon spectrum assumed by Schrieffer *et al.* [220].

values for α the electron–phonon coupling and μ^* the Coulomb pseudo-potential (a parameter entering the Eliashberg gap equation) a theoretical curve was obtained for $\sigma(V)$ in excellent agreement with tunnelling data (Fig. 6.20 (*a*)). Second derivative measurements [221] (Fig. 6.21) did in fact show considerably more structure for which the theory of Schrieffer *et al.* [220] could not account. These came to be identified with Van Hove singularities* measured by neutron diffraction [222]. Although the relationship of this last structure to the density of states was explained by Scalapino and Anderson [223] the conviction grew that a frontal assault on the Eliashberg equation had become feasible.

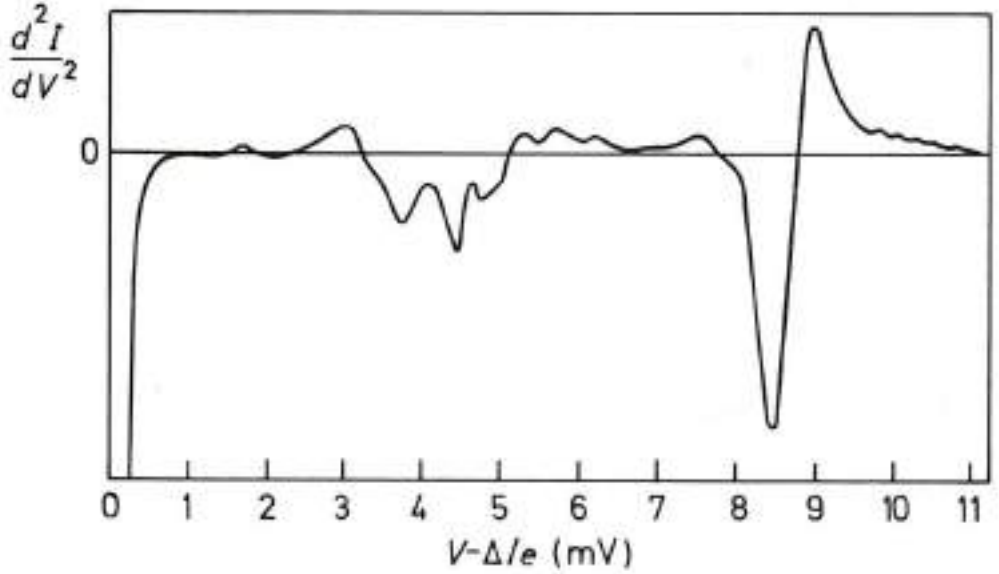

Fig. 6.21 The second derivative of the I–V characteristic as a function of voltage (zero shifted by Δ/e). Arrows indicate the voltage for Van Hove singularities on the basis of the neutron diffraction experiments of Brockhouse *et al.* [222]. After Rowell, Anderson and Thomas [221].

The method used by McMillan and Rowell [67] is based on the fact that in Eliashberg's theory the electron–phonon coupling constant weighted by the phonon density of states $\alpha^2(\omega)F(\omega)$ is uniquely related to the electronic density of states (as measured by tunnelling experiments). Hence besides working out the density of states from phonon data it is also possible to invert the Eliashberg equation and get the phonon data from the measured tunnelling characteristics. With the aid of a computer $\alpha^2(\omega)F(\omega)$ and μ^* are adjusted until the computed density of states accurately fits the measured density of states for $E < k\theta_D$. Examining the agreement for $E > k\theta_D$ the accuracy of the Eliashberg equation can be tested. The results of this rather difficult exercise may be seen in Fig. 6.22 where theory and experiments are compared. The experimental points below $E - \Delta = 11$ meV were used for determining the 'input' quantities, and the points above that are to be compared with the theory. It is remarkable that an experimental curve as complicated as that can be theoretically reproduced. McMillan and Rowell [166] conclude that our present theories of superconductivity are accurate to a few percent.*

All the experiments mentioned so far were concerned with the properties of lead. The other strong-coupling superconductor, mercury (with $2\Delta/kT_c = 4{\cdot}6$), was less thoroughly investigated but the available data [225–226] suggest similar conclusions.

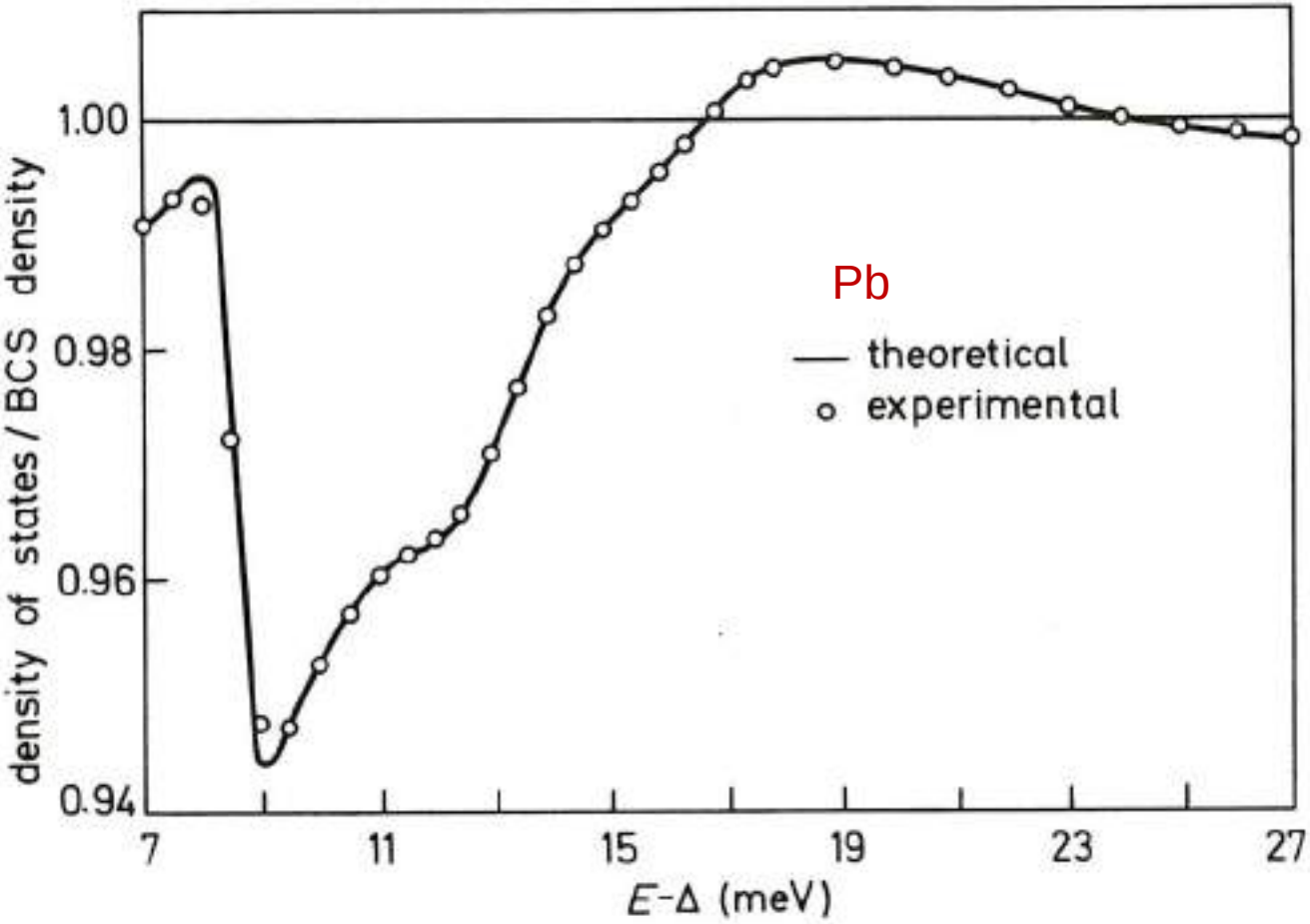

Fig. 6.22 The density of states for lead related to the BCS density of states as a function of energy (zero shifted by Δ). In the experiment the sharp drop near 9 meV is affected by thermal smearing. After McMillan and Rowell [165].

Next we shall briefly review the tunnelling experiments on lead-based alloys. The effect of a small amount of indium on the phonon spectrum was investigated by Rowell, McMillan and Anderson [227] using the inversion technique described above. The results for $\alpha^2(\omega)F(\omega)$ are shown in Fig. 6.23. The additional structure at $\hbar\omega = 9{\cdot}5$ meV is due to the presence of an 'impurity band'.** The impurity band is still present at higher indium concentrations as reported by Adler *et al.* [228]. The value of $2\Delta/kT_c$ slowly decreases with increasing indium concentration; it is 4·34 at 2 atomic percent indium reducing to 4·20 at 70 atomic percent indium.

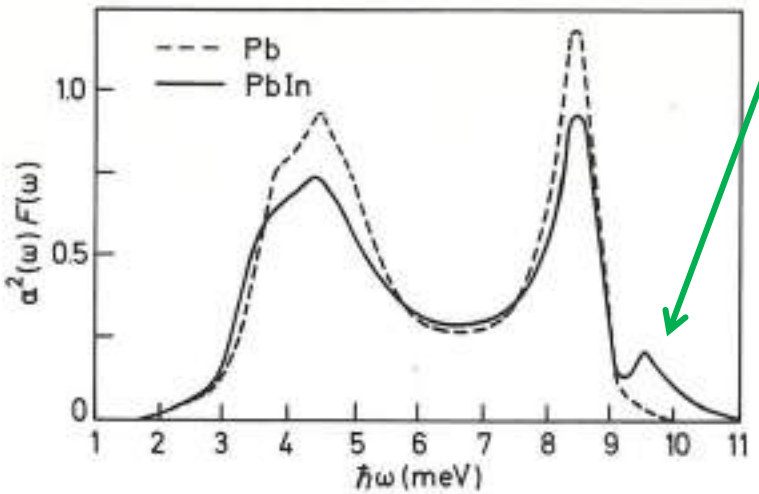

Fig. 6.23 The phonon spectrum $\alpha^2(\omega)F(\omega)$ obtained by the gap inversion technique. The localised phonon mode of the light indium impurity may be seen at about 9·5 meV. After Rowell, McMillan and Anderson [227].

Summarising, the present state of affairs is that besides thin tunnel junctions and point contacts, discussed in connection with normal electron tunnelling, we have some other geometries as well displaying the characteristic effects (like induced steps in the I–V characteristics, quantum interference, radiation, etc.).

The various geometries are shown in Fig. 8.6. The superconducting thin film bridge (Fig. 8.6 (a)) was developed by Dayem and it is often referred to as the Dayem bridge. It consists essentially of a narrow constriction of the order of $(1\ \mu\text{m})^2$ between two superconducting films.

A variation of the thin film bridge is the Notarys bridge [363] shown in Fig. 8.6 (b). This relies on the proximity effect to cause weak superconductivity. There is first a layer of normal metal evaporated, and then the superconductor forming the bridge. The 'weakness' is controlled by the relative thicknesses of the normal and superconducting layers.

The solder junction (Fig. 8.6 (c)) was developed by Clarke [338]. It is very simple to make; one simply has to dip a piece of oxidised wire into molten solder. When the solder freezes tight mechanical contact is established and the junction is ready. Its disadvantage is that the junction is not clearly defined.

The point contact junction is also widely used but not necessarily in the same form as for single particle tunnelling. Then the presence of the insulating layer is essential for displaying tunnelling characteristics. The Josephson effects may, however, be observed whether there is an insulating layer or not. If the two superconductors are in contact then we have a bridge. In actual experiments very often we do not even know whether we have a weak link or a tunnel junction. Take for example the point contact junctions developed by Zimmerman and Silver [341]. They used superconducting screws with lock nuts pressed against a superconducting surface through a Mylar spacer (Fig. 8.6(*d*)). There is no way of knowing whether there is a direct contact between the superconductors or not. All the measurements can tell us is that there is a difference in the I–V characteristics (the increase in the maximum supercurrent can be clearly observed) as more pressure is applied, leading eventually to a 'strong link', i.e. a proper short-circuit.

Weak Links

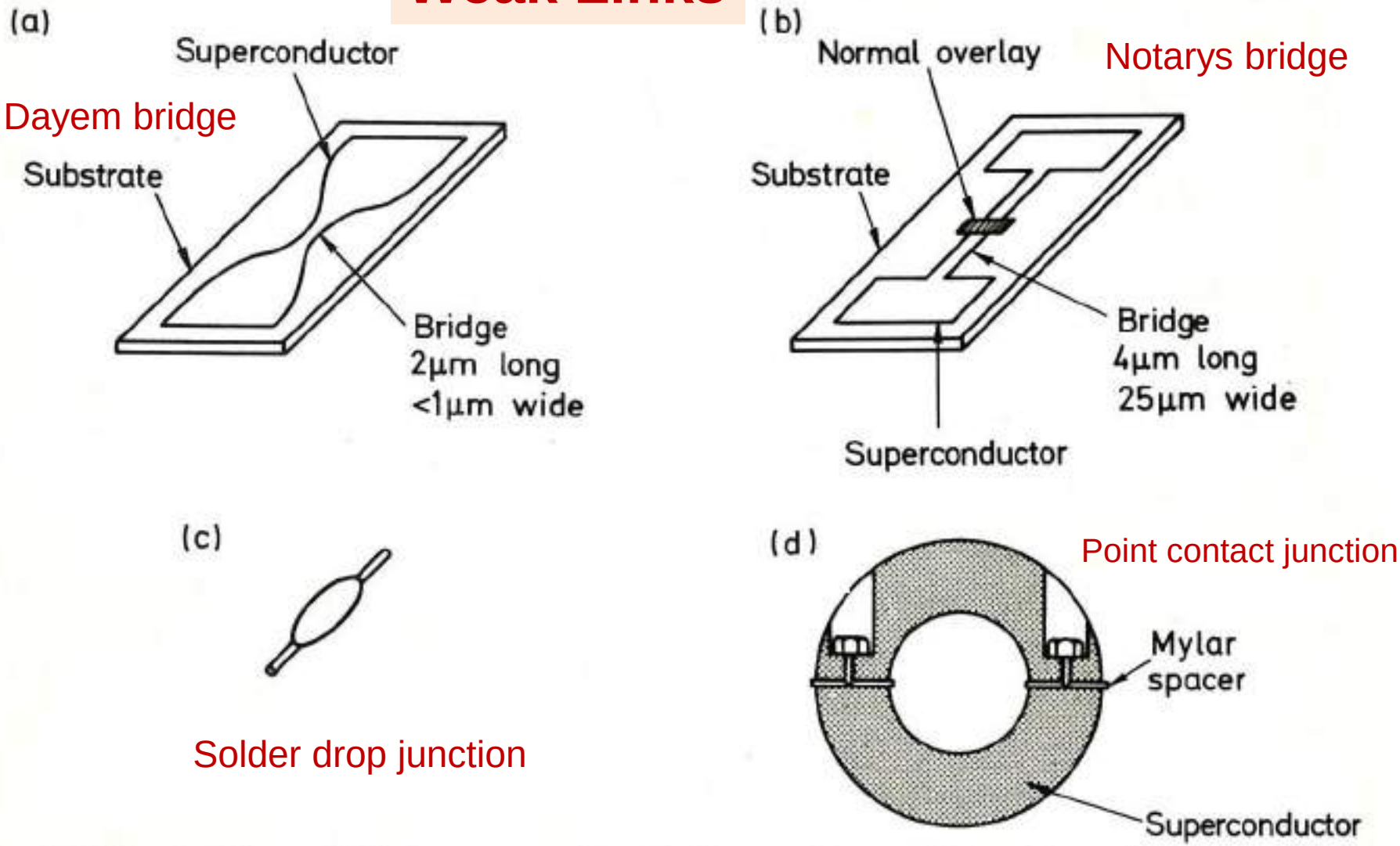

Fig. 8.6 Weak links exhibiting properties similar to those of Josephson junctions. (*a*) A superconducting thin film bridge (Dayem bridge), (*b*) a superconducting thin film bridge with a normal metal overlay (Notarys bridge), (*c*) Clarke's solder drop junction (*d*) double point-contact junction developed by Zimmerman and Silver [341].

Let us discuss now briefly that in what sense does a weak link resemble to a tunnel junction. There is no difficulty as far as the d.c. Josephson effect is concerned. At low currents there is no voltage across the weak link but as the current is increased the weak link will first turn resistive. This is because it has a smaller cross-section and thus a higher current density or (as in the Notarys bridge) it has a lower critical temperature. So we may say that it is true both for tunnel junctions and for weak links that there is no voltage up to a certain current and finite voltage above a certain current.

It is somewhat more difficult to envisage the a.c. effects. We can no longer appeal to the simple physical picture that the tunnelling Cooper pairs radiate out their energy. There is though a simple heuristic argument (due to Mercereau [364]) which can justify the presence of an a.c. supercurrent. The argument (in an abbreviated form) runs as follows.

A voltage across the weak link will effect both the normal and the superconducting electrons. The superconducting electrons will be accelerated according to Newton's Law

$$\frac{dv}{dt} = \frac{q}{m}\mathscr{E} \tag{8.7}$$

where the electric field $\mathscr{E}$ is sustained by the normal electrons. It is known, however, that when the superconducting electrons reach a certain velocity (say v_c) their density vanishes. But then there is only an electric field across the weak link which on its own cannot quench superconductivity; hence the superconducting electrons reappear and the whole process repeats itself.

Let us now make a rough calculation of the time needed to accelerate the superconducting electrons to a velocity v_c. For a constant $\mathscr{E}$ we get

$$\tau = \frac{mv_c}{q\mathscr{E}}. \tag{8.8}$$

Assuming that the electric field is constant over one coherence length (the shortest distance over which the density of superconducting electrons can change), the voltage across this region is given by

$$V = \mathscr{E}\xi \tag{8.9}$$

Expressing further the final momentum in terms of the coherence length by the relation

$$mv_c = \frac{h}{\xi} \tag{8.10}$$

where mv_c is the uncertainty in momentum, we get

$$\tau = \frac{h}{qV}$$

for the period of this 'relaxation oscillation'. Hence the angular frequency is

$$\omega = \frac{qV}{\hbar} \tag{8.11}$$

which agrees with Equation (8.3). So we managed to show (by hook or by crook) that weak links have the same radiation properties as tunnel junctions. In fact, the difference between tunnel junctions and weak links is not so much in the basic processes but rather in the circuits they represent to the outside world.

For most purposes a junction may be adequately represented by the parallel combination of an 'ideal' junction (one which carries a supercurrent only) a resistance and a capacitance. The main differences between tunnel junctions, point contacts and bridges are in the respective values of these circuit elements.

For a Josephson current of $I_J = 10\ \mu A$, the range for practical junctions is shown in Table 8.1 [365]. It is then obvious that, for example, for high frequency operation (microwaves or above) the point contact is superior to the tunnel junction. The relative values of the circuit elements play an important role in determining the I–V characeristics as well. This will be discussed in Chapter 11.

Table 8.1

	I_J	$1/G$ (*for* $V < 2\Delta$)	C
Thin film tunnel junction	10 μA	> 100 ohm	100 to 1000 pF
Point contact	10 μA	10 to 100 ohm	1 to 1000 pF
Thin film bridge	10 μA	< 1 ohm	1 pF

Circuit Representation

11.2 Capacitive loading; constant conductance

The circuit we are considering here (Fig. 11.1 (*a*)) consists of an ideal current generator feeding current into the parallel combination of a Josephson junction,

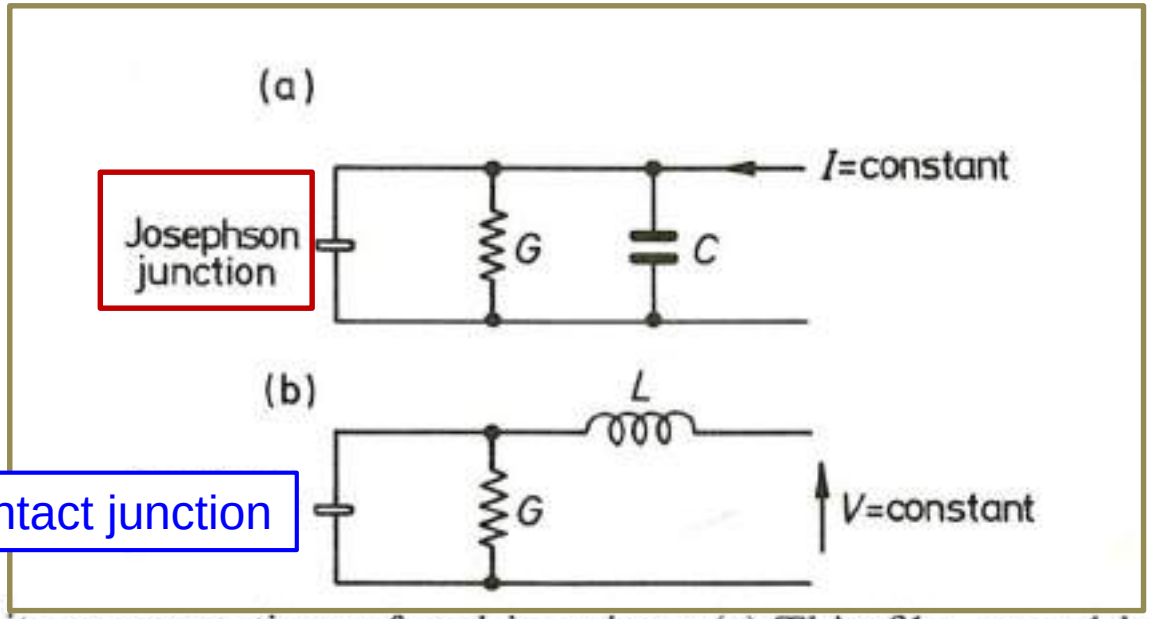

Point contact junction

Fig. 11.1 Circuit representations of real junctions. (*a*) Thin film tunnel junction made up by an 'ideal' Josephson junction (satisfying the $I = I_J \sin\phi$ relationship), an ohmic conductance and a capacitance; analysed for a constant current input. (*b*) An approximation to a point-contact junction taking account of parallel conductance and series inductance; analysed for a constant voltage input.

an ordinary ohmic-conductance and a capacitance. We have then a supercurrent

$$I_J \sin \phi \tag{11.1}$$

through the Josephson junction, an ohmic current

$$GV \tag{11.2}$$

through the conductance and a capacitive current

$$C\frac{dV}{dt} \tag{11.3}$$

through the capacitance. The sum of these three components should be equal to I, the current supplied by the generator. This is not really new. We have met all these components of current before; taking the current (more correctly the current density) in the form of Equation (9.34) and adding the displacement current, we get an equation expressing the same relationship

$$I = I_J \sin \phi + GV + C\frac{dV}{dt}. \tag{11.4}$$

Expressing the voltage with the aid of the phase (Equation (9.17)) the above equation reduces to

$\partial\phi/\partial t = qV/\hbar$

$$I = \frac{\hbar C}{q}\frac{d^2\phi}{dt^2} + \frac{\hbar G}{q}\frac{d\phi}{dt} + I_J \sin \phi. \tag{11.5}$$

Scanning Tunneling Microscope (STM)

Heinrich Rohrer & Gerd Binnig (1983)

Nobel Prize in 1986 © IBM, Zurich

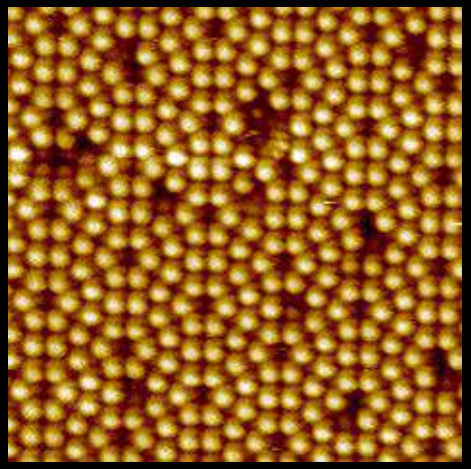

Si (111) surface 7 x 7

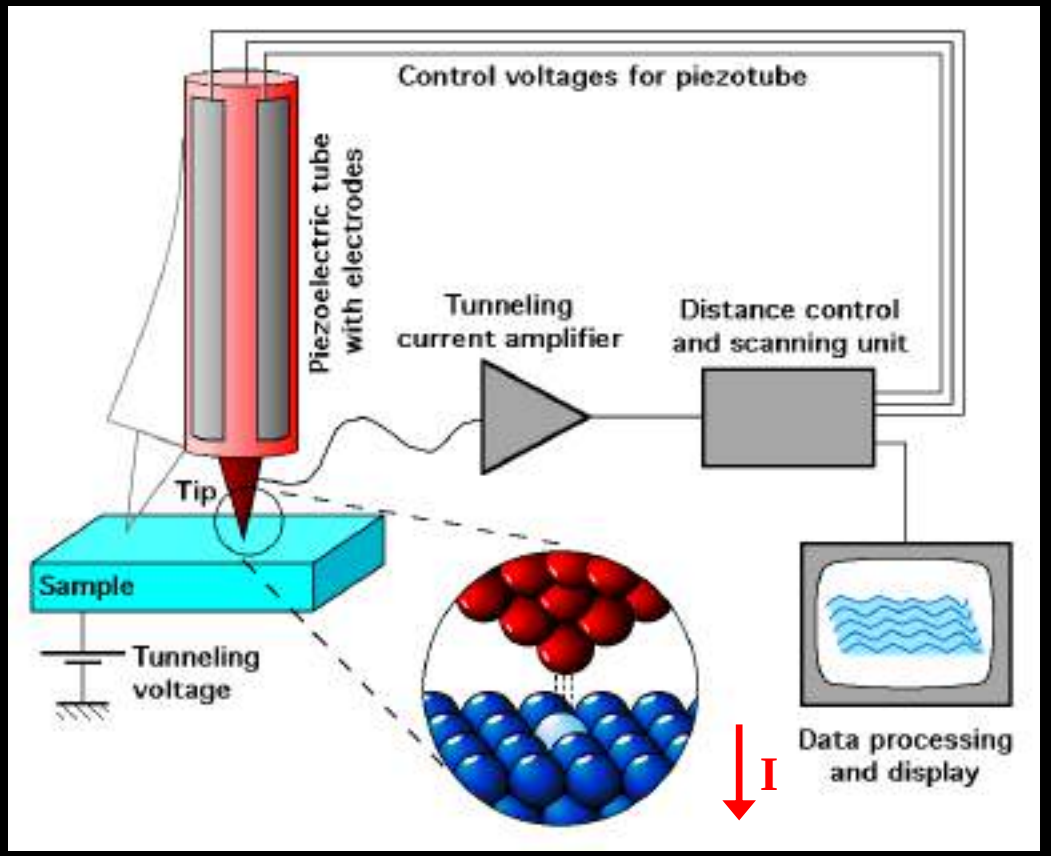

© Wikipedia

Quantum Tunneling

Erwin Schrödinger

Nobel Prize in 1933

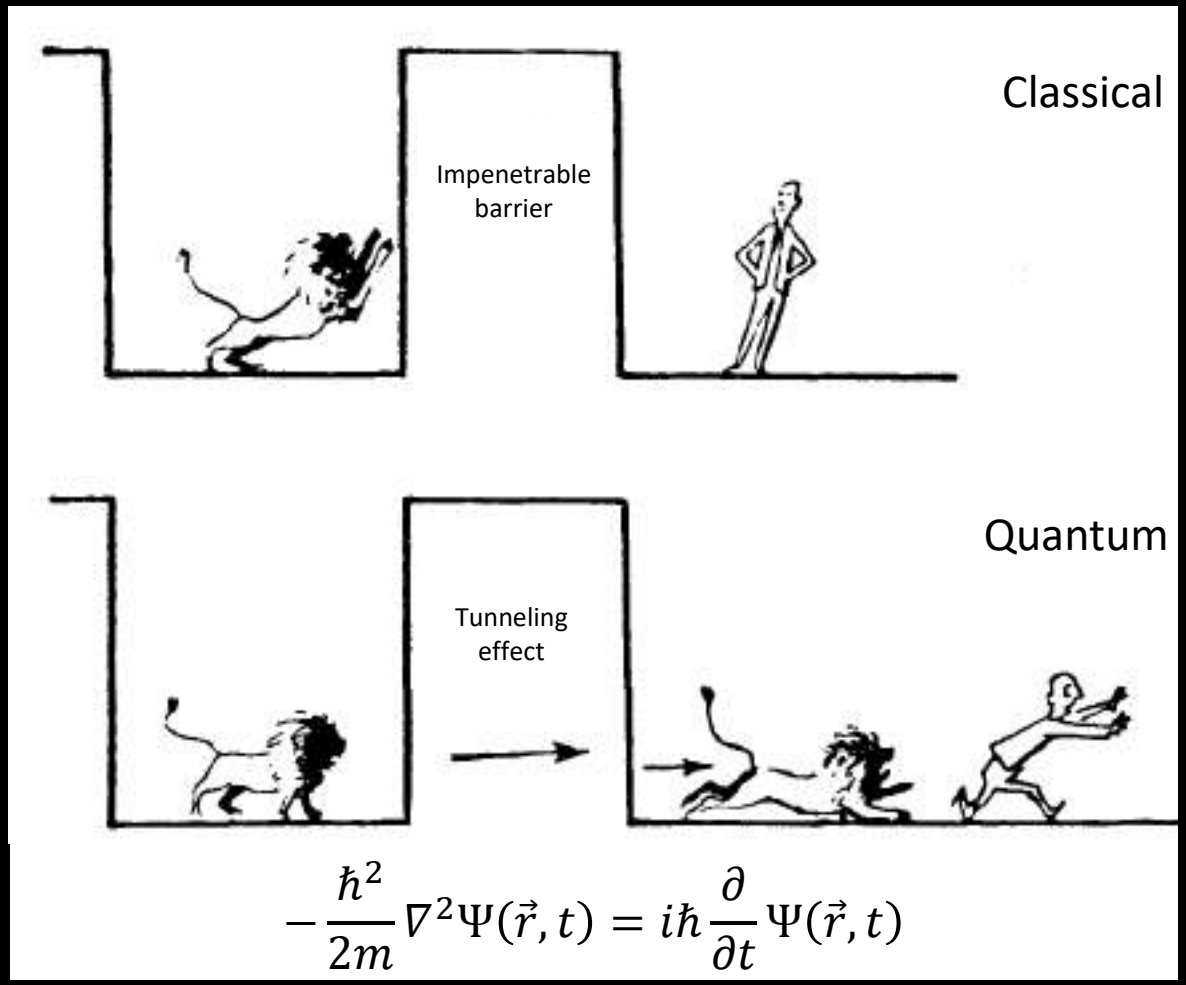

$$-\frac{\hbar^2}{2m}\nabla^2\Psi(\vec{r},t) = i\hbar\frac{\partial}{\partial t}\Psi(\vec{r},t)$$

B. Bleaney, Contemp. Phys. 25, 315 (1984)

Constant Current Topography

$$I(\vec{r}, z, V) \propto \exp(-2\kappa(\vec{r})z) \int_0^{E=eV} LDOS_{sample}(\vec{r}, E)dE$$

where $\kappa(\vec{r}) = {\sqrt{2m\emptyset(\vec{r})}}/{\hbar} \sim 1\text{Å}^{-1}$

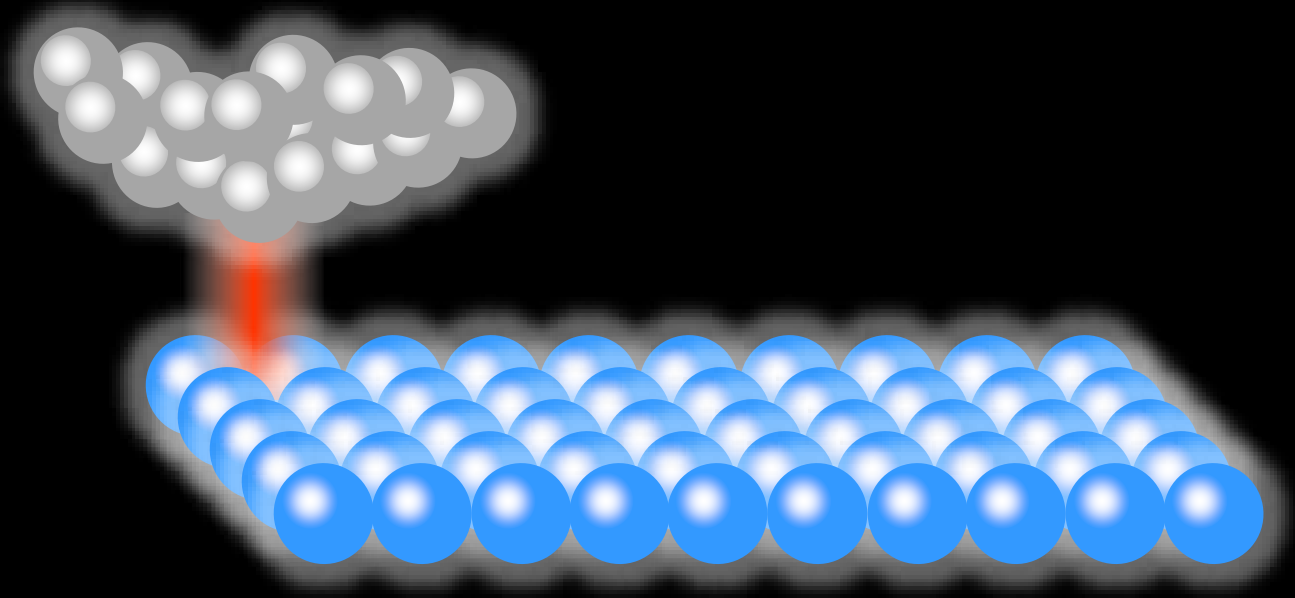

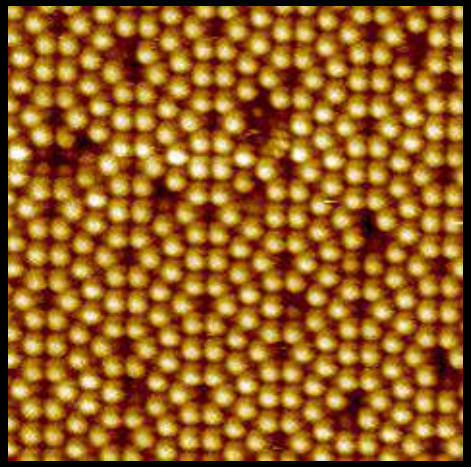

Si(111) 7x7

Tunneling current

$$I(\vec{r}, z, V) \propto \exp(-2\kappa(\vec{r})z) \int_0^{E=eV} LDOS_{sample}(\vec{r}, E)dE$$

where $\kappa(\vec{r}) = {}^{\sqrt{2m\emptyset(\vec{r})}}/_{\hbar} \sim 1\text{Å}^{-1}$

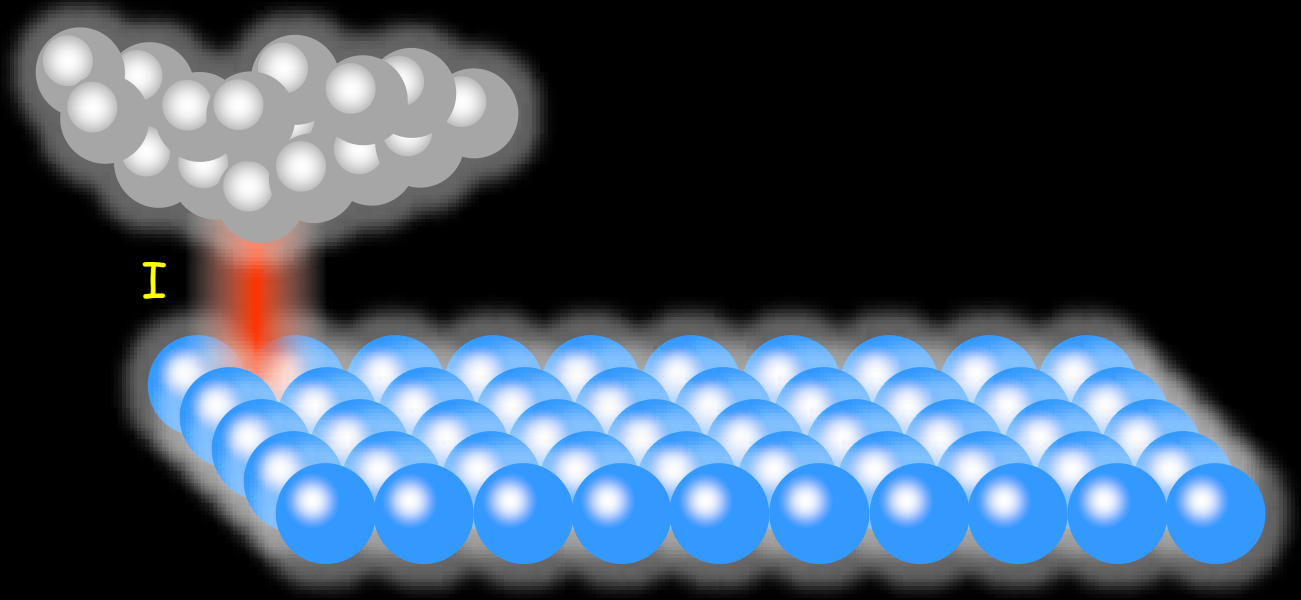

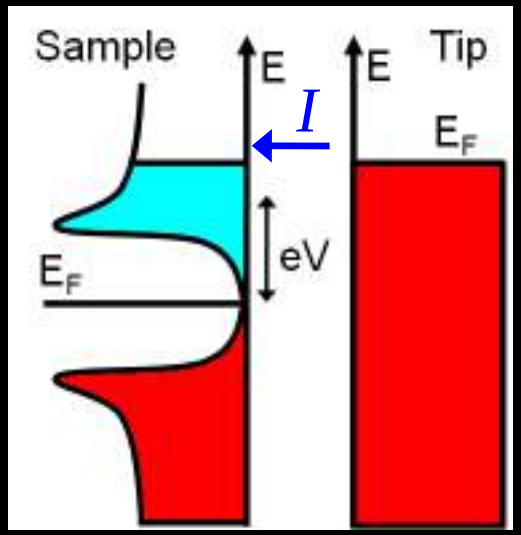

Tunneling Spectroscopy

Local Density of States : $\frac{dI}{dV}(\vec{r},V) \propto LDOS_{sample}(\vec{r},E=eV)$

$$I(V+\Delta V\sin\omega t) = I(V) + \frac{dI}{dV}\Delta V\sin\omega t + \ldots$$

Point Spectrum

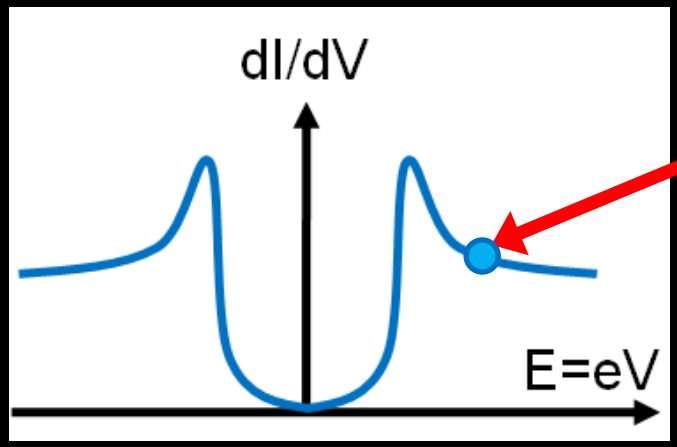

Modulation, dV

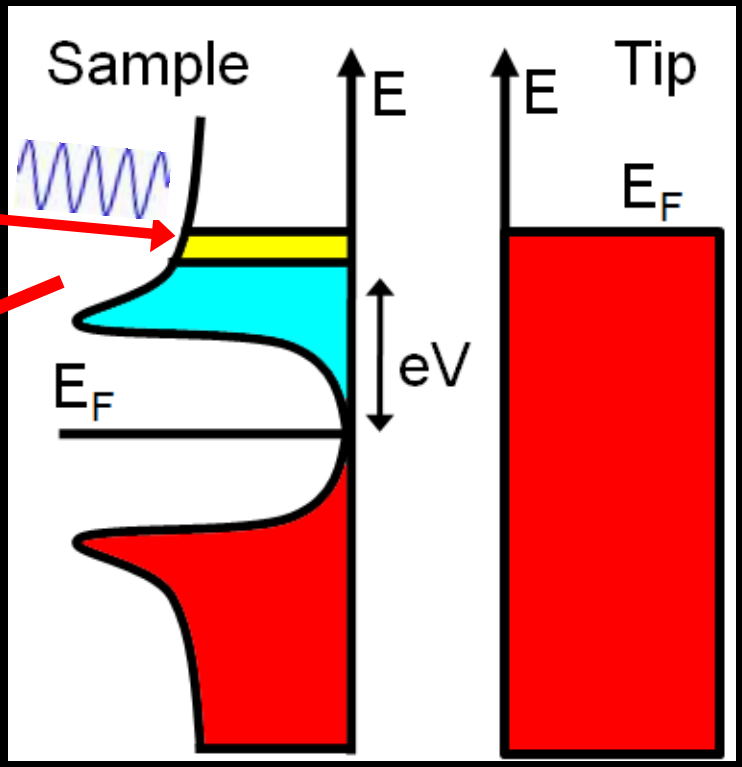

Superconducting Energy Gap by STM

Tetsuo Hanaguri

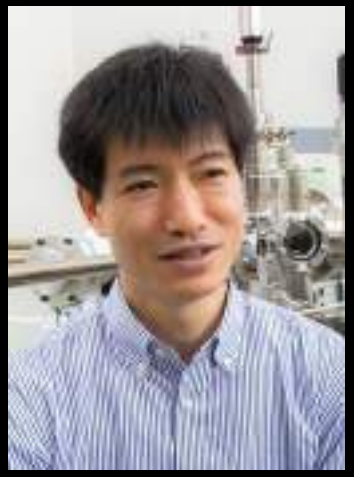

© RIKEN

Energy resolution is thermally limited.

2H-$NbSe_2$, T_c = 7.1 K, measured at $T \sim 0.4$K

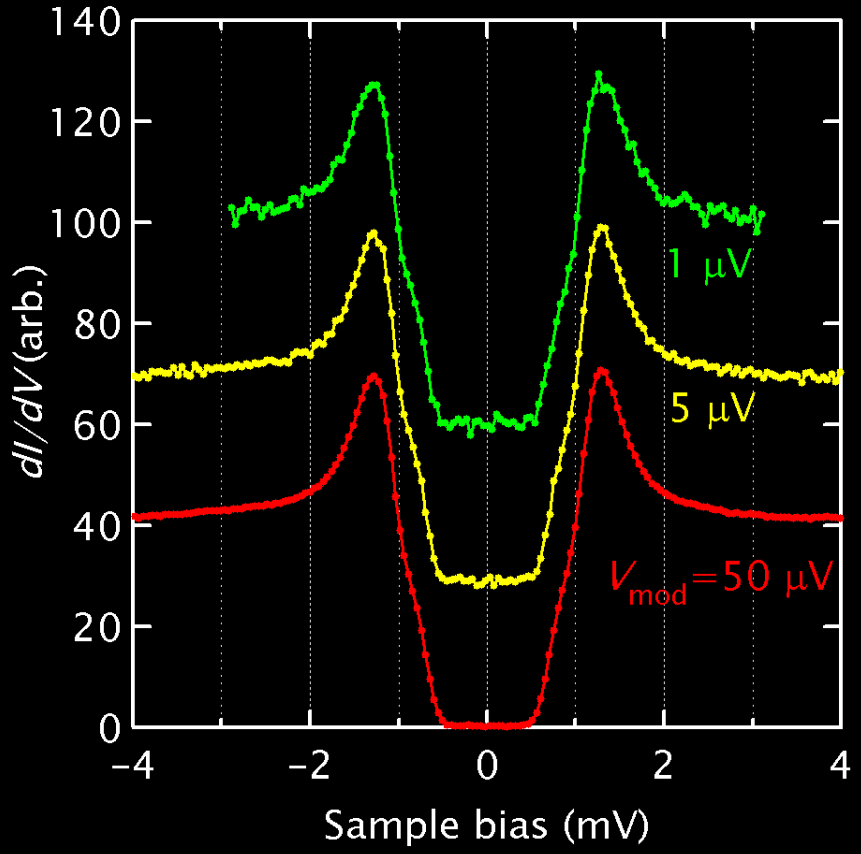

Scanning Tunneling Spectroscopy (STS) Mapping

Atomic resolution energy resolved conductance images, $g(r,E) \propto LDOS(r,E)$

Energy resolution ≤ 0.35meV at T=1.2K

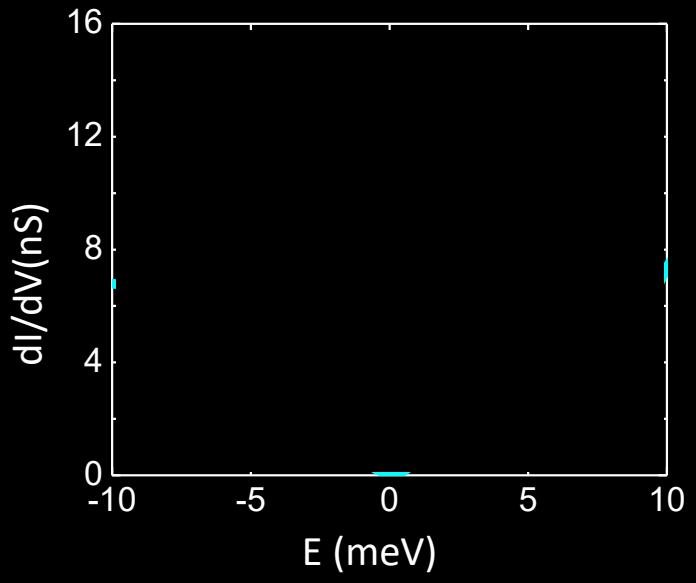

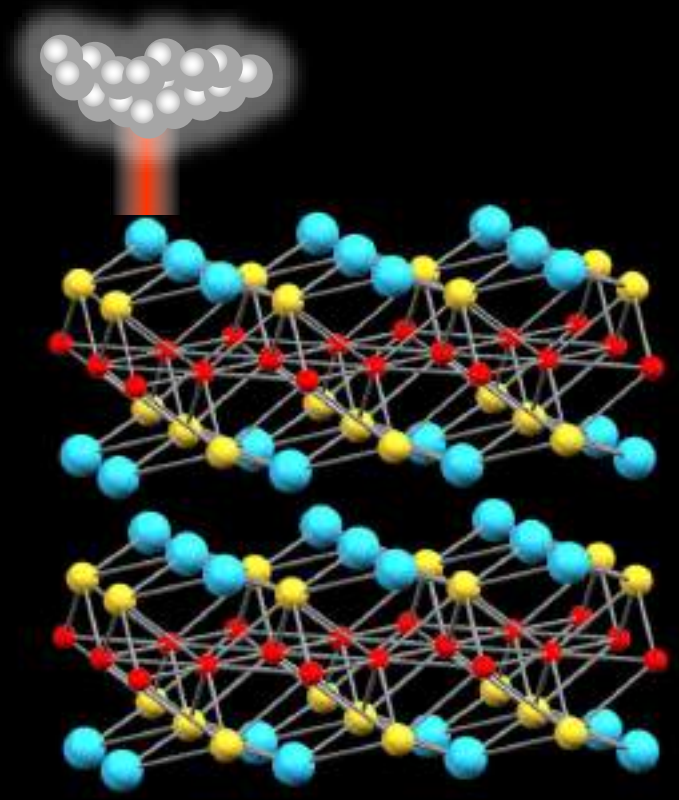

LiFeAs

Atomic Resolution Energy Resolved Images, LDOS(r,E)

~5M dI/dV(r,E):
>50ms each with S/N~100
Total measurement > 72 hours
Requires < 10^{-15} m STM-tip vibration

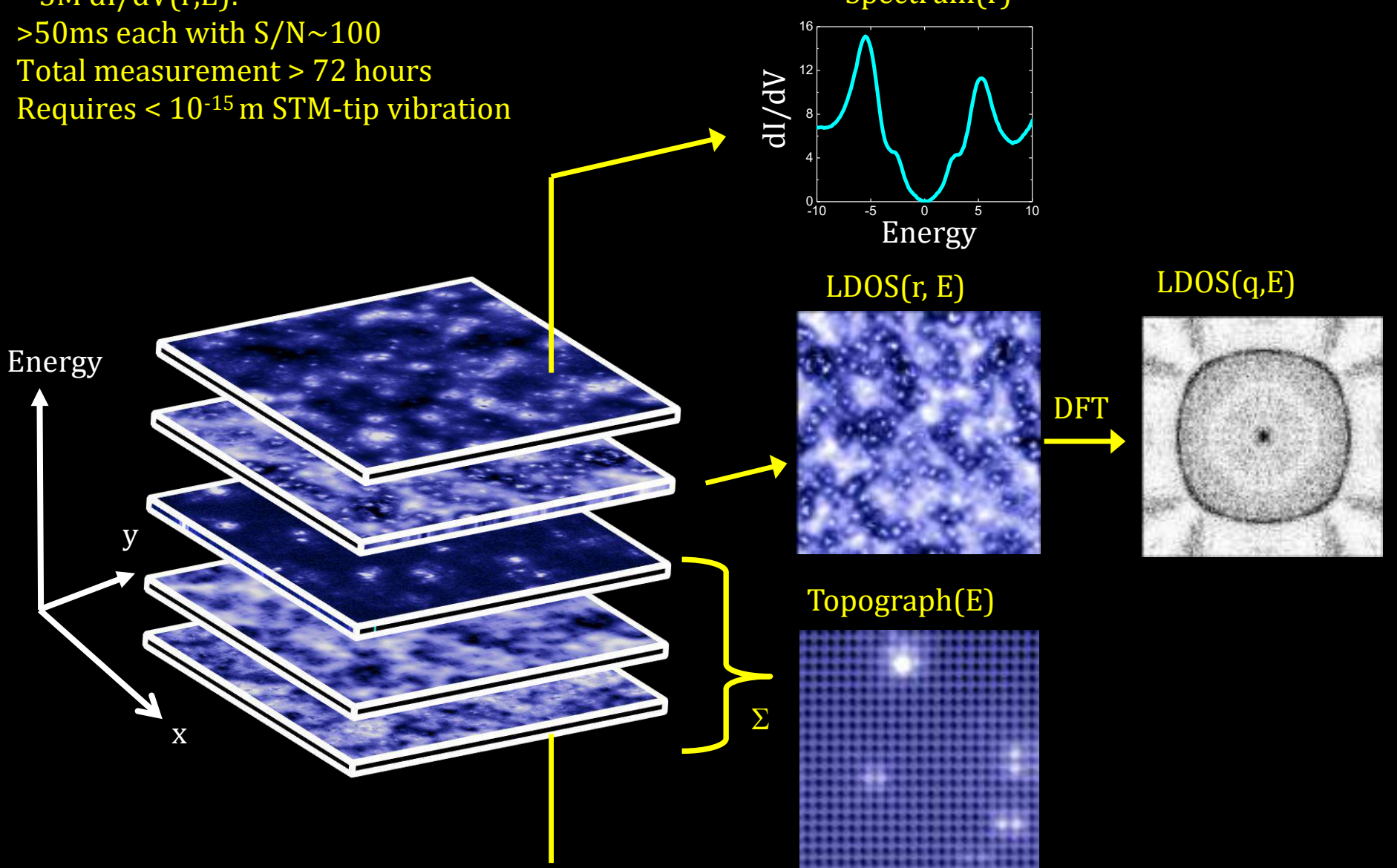

Our Resolution and Stability

STM Tip on Piezo Scanner

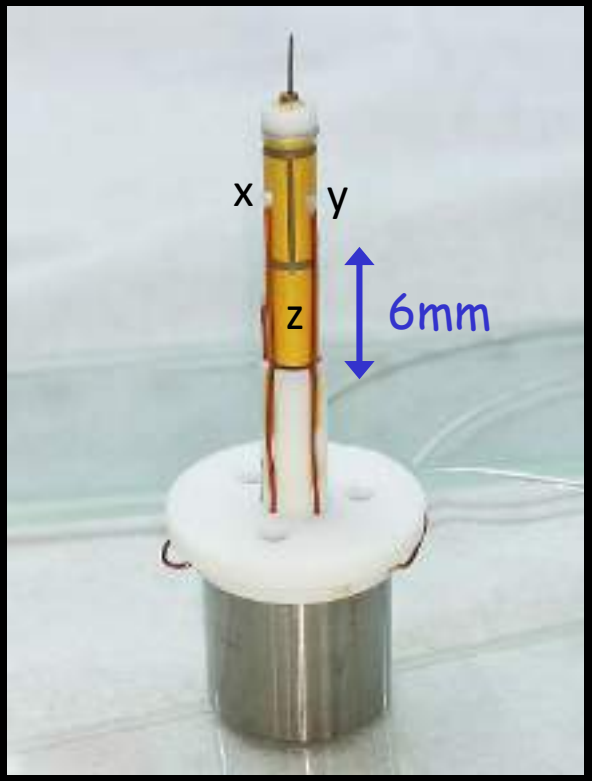

Taipei 101

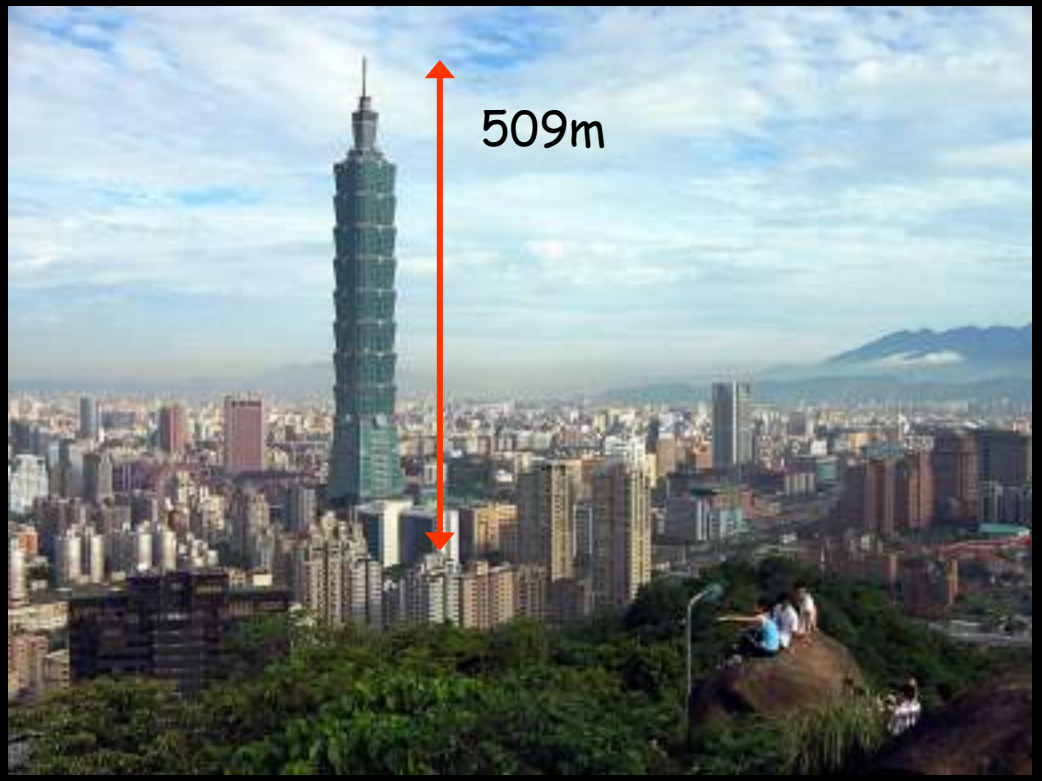

@Wikipedia

0.5pm/6mm → 42nm/509m!

Ivar Giaever

Nobel Prize 1973

The best way to do science is not to buy a big piece of expensive equipment and use it to do research. There are lots of other people who have the same big expensive equipment. The best way to do science is if you can make your own equipment, make your own thing.

- Ivar Giaever, BCS@50 Conference, 2007

愛因斯坦 (Einstein)

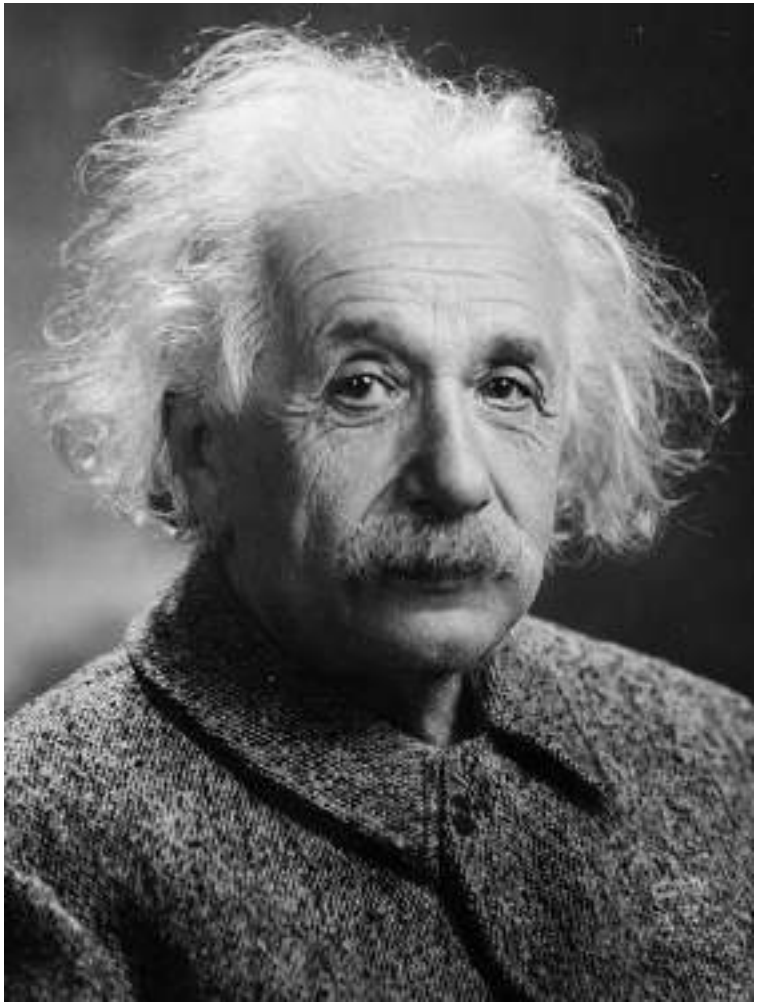

我每天提醒自己一百遍，我的生活，不管內在或是外在，都是以他人(包括活著的和逝去的)的勞動為基礎。所以我必須盡力奉獻自己，希望能以同等的貢獻，來回報長久以來(現在仍是)從他們那裡所得到的。

Nb tunnel junctions for Josephson device applications

Nb/Al/oxide/Pb junctions

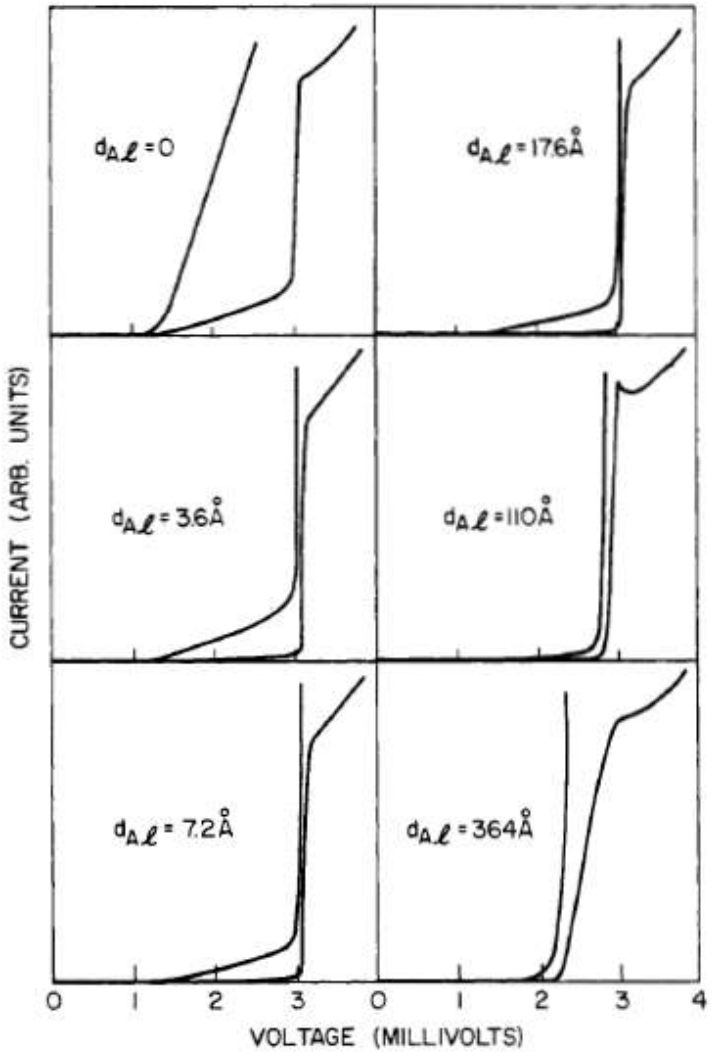

Fig. 2 Volt-ampere characteristics of Nb/Al-oxide-$Pb_{0.90}Bi_{0.10}$ junctions with different d_{Al} at $T \simeq 2^{o}K$. Expansion of the current scale ×10 is also shown. The junction without an Al overlayer was oxidized for 4 days, the rest for 20 min. All junctions have area $S \simeq 2 \cdot 10^{-3}$ cm^2.

Nb JOSEPHSON TUNNEL JUNCTIONS WITH THIN LAYERS OF Al NEAR THE BARRIER

M. Gurvitch, J. M. Rowell, H. A. Huggins,
M. A. Washington and T. A. Fulton

Bell Laboratories
Murray Hill, New Jersey 07974

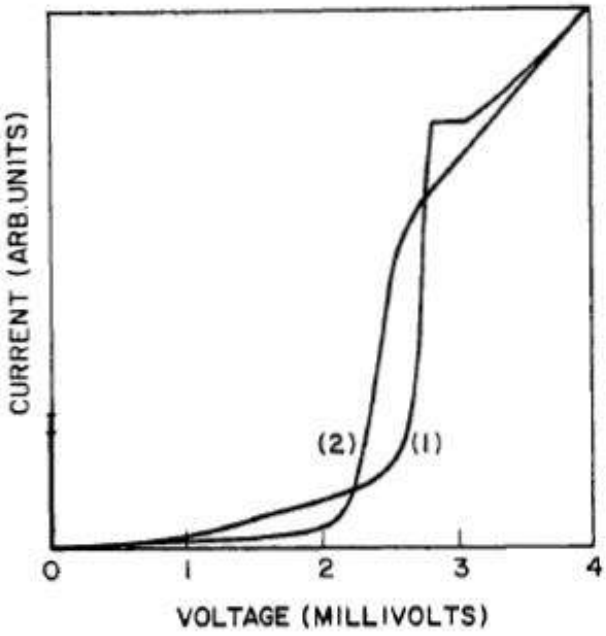

Fig. 3 Volt-ampere characteristics of Nb/Al-oxide-Nb (curve 1) and Nb/Al-oxide-Al/Nb (curve 2) junctions at $T \simeq 2^{o}K$. Both base electrodes have d_{Al} = 25Å, the top electrode of the junction with the second Al layer has d_{Al} = 32Å. Critical currents are ~50A/cm^2.

IEEE TRANSACTIONS ON MAGNETICS, VOL. MAG-19, NO. 3, MAY 1983

XPS and Tunneling Study of Air-oxidized Overlayer Structures of Nb with Thin Mg, Y and Er

J. Kwo
G. K. Wertheim
M. Gurvitch
D. N. E. Buchanan

Bell Laboratories
Murray Hill, New Jersey 07974

Artificial tunnel barrier made of oxides of thin Si, Mg, Y, and Er

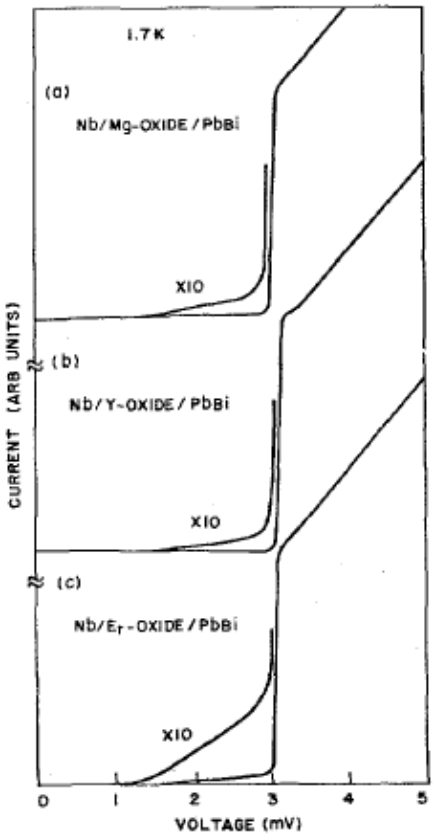

Fig. 2 Current-voltage characteristic of junctions of (a) Nb/16.6Å Mg-oxide/$Pb_{0.9}Bi_{0.1}$, R = 21.7 Ω (b) Nb/Y 8.7Å Y-oxide/$Pb_{0.9}Bi_{0.1}$, R = 181 Ω (c) Nb/Er 4.5Å Er-oxide/$Pb_{0.9}Bi_{0.1}$, R = 20 Ω The junction area is typically of $1.3 \times 10^{-2} cm^2$.

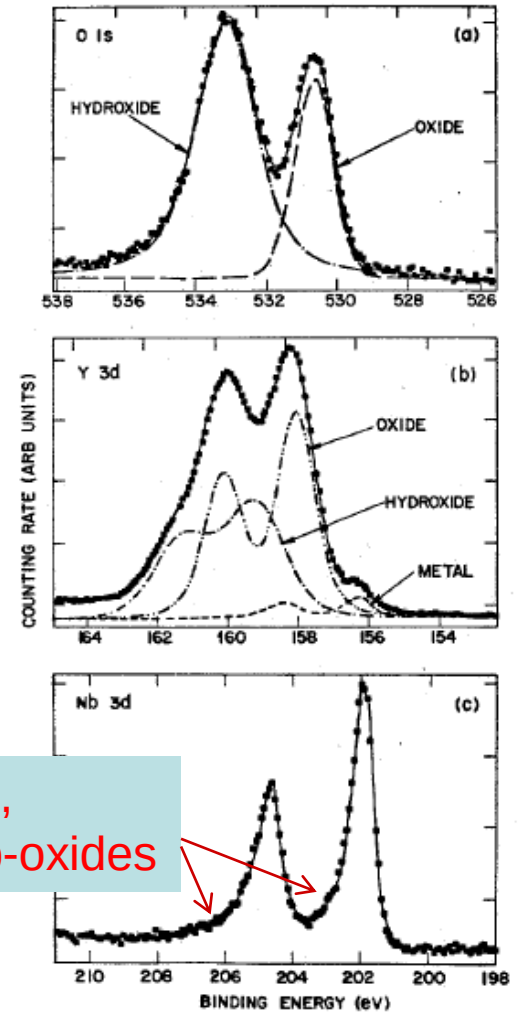

Very clean, free of sub-oxides

Fig. 3 XPS data for a sample of Nb/30Å Y overlayer
(a) O 1s
(b) Y 3d
(c) Nb 3d

References

PHYSICAL REVIEW B VOLUME 23, NUMBER 7 1 APRIL 1981

Superconducting tunneling into the *A*15 Nb_3Al thin films

J. Kwo and T. H. Geballe*

Department of Applied Physics, Stanford University, Stanford, California 94305

PHYSICAL REVIEW B VOLUME 24, NUMBER 5 1 SEPTEMBER 1981

Microscopic superconducting parameters of Nb_3Al: Importance of the band density of states

J. Kwo,* T. P. Orlando,† and M. R. Beasley‡

Department of Applied Physics, Stanford University, Stanford, California 94305

(Received 12 December 1980)

PHYSICAL REVIEW B VOLUME 24, NUMBER 4 15 AUGUST 1981

Modification of tunneling barriers on Nb by a few monolayers of Al

J. M. Rowell, M. Gurvitch, and J. Geerk*

Bell Laboratories, Murray Hill, New Jersey 07974

(Received 10 June 1981)

VOLUME 63, NUMBER 9 PHYSICAL REVIEW LETTERS 28 AUGUST 1989

Reproducible Tunneling Data on Chemically Etched Single Crystals of $YBa_2Cu_3O_7$

M. Gurvitch, J. M. Valles, Jr., A. M. Cucolo,[(a)] R. C. Dynes, J. P. Garno, L. F. Schneemeyer, and J. V. Waszczak

AT&T Bell Laboratories, Murray Hill, New Jersey 07974

(Received 26 May 1989)

Observations of quasi-particle tunneling and Josephson behavior in $Y_1Ba_2Cu_3O_{7-x}$/native barrier/Pb thin-film junctions
J. Kwo, T. A. Fulton et al, Appl. Phys. Lett. **56**, 788 (1990).

Superconductivity tunneling into the A-15 compounds

A-15 compound A_3B, with T_c = 15-23 K

With three perpendicular linear chains of ***A*** atoms on the cubic face, and B atoms are at body centered cubic site

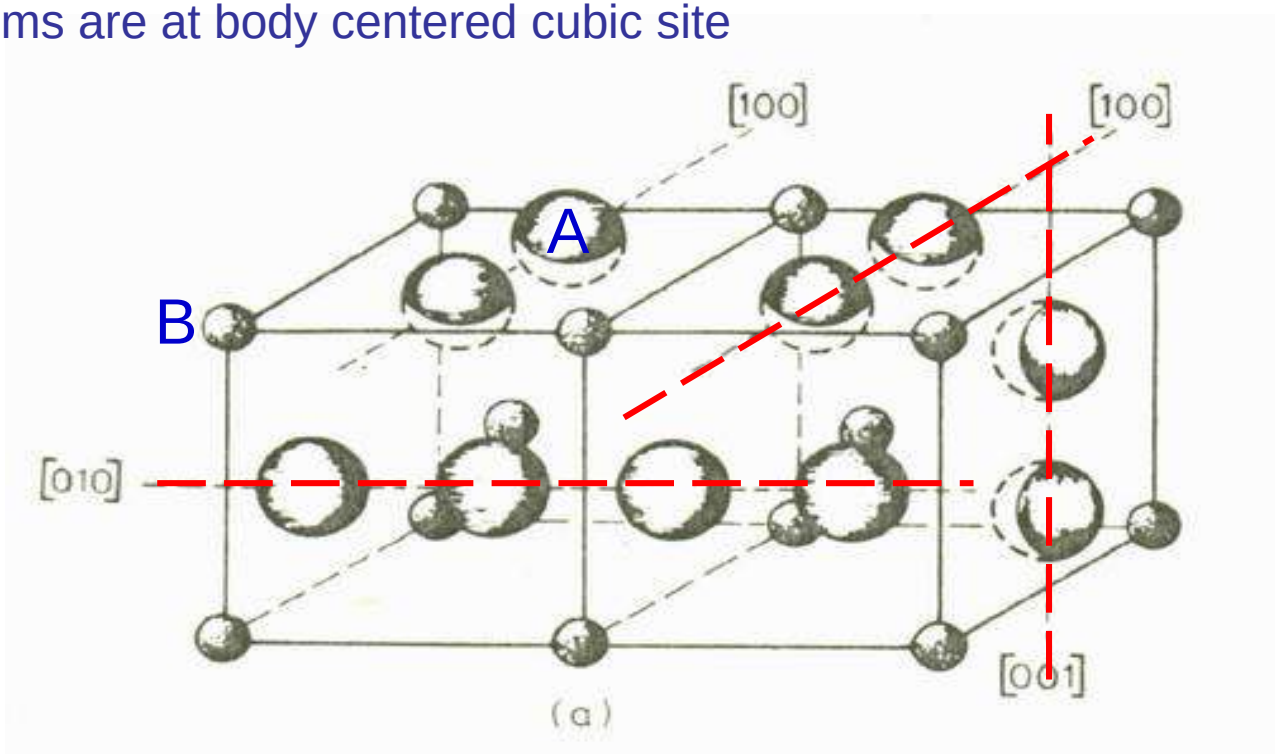

Fig. 34. (a) The position of A and B atoms in the unit cell of an A_3B compound possessing the β-W structure. (b) The Fermi surface of an A_3B compound in the tight binding, nearest neighbors approximation. There are three degenerate bands corresponding to electrons localized on the three families of chains.

1973 Nb_3Ge, 23K !

Low temperature Superconductors

-- Mediated by Electron phonon coupling

-- strong electron phonon coupling, McMillian formula for T_c

$$T_c = \frac{\Theta_D}{1.45} \exp\left\{ - \left[\frac{(1+\lambda_{ep})}{\lambda_{ep} - \mu^*(1+0.62\lambda_{ep})} \right] \right\}$$

λ : electron phonon coupling constant

μ^* : Coulomb repulsion of electrons

$\lambda \propto N(0) < I^2 > / \omega^2$

Are electrons or phonons more important?

Superconductivity tunneling into the A-15 compounds

PHYSICAL REVIEW B VOLUME 23, NUMBER 7 1 APRIL 1981

Superconducting tunneling into the *A*15 Nb_3Al thin films

J. Kwo and T. H. Geballe*
Department of Applied Physics, Stanford University, Stanford, California 94305
(Received 1 October 1980)

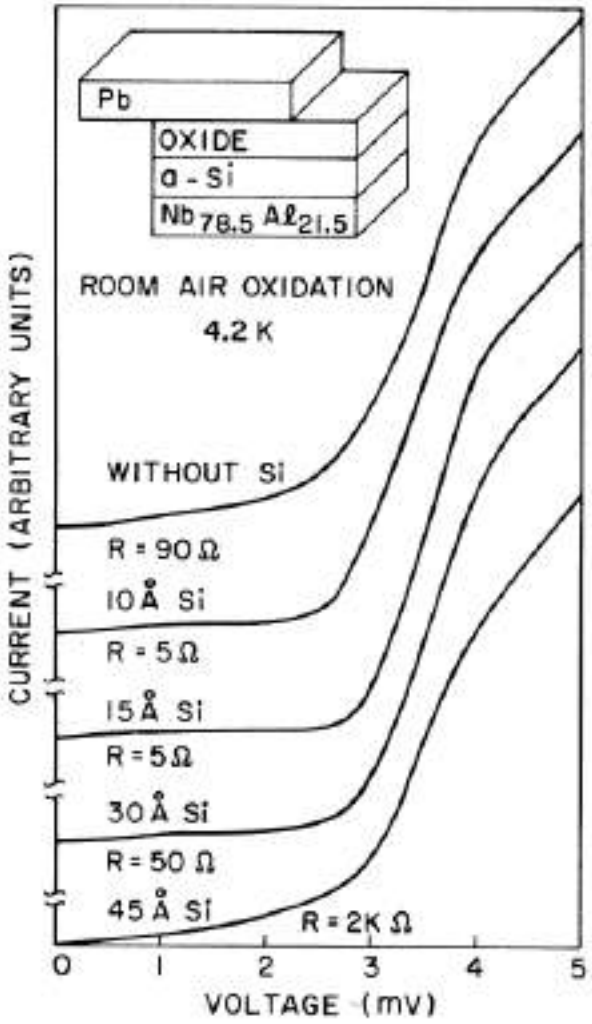

- Native Oxide of Nb is no good!
- Artificial tunnel barrier
  -- Use of a thin amorphous Si oxide 15A thick, excellent !

Current-voltage characteristics at 4.2 K of *A*15 Nb-Al (of 21.5 at. % Al) tunnel junctions with the thickness of the ***a*-Si** overlay varying from 0 to 45 A.

Tunneling as a materials diagnosis

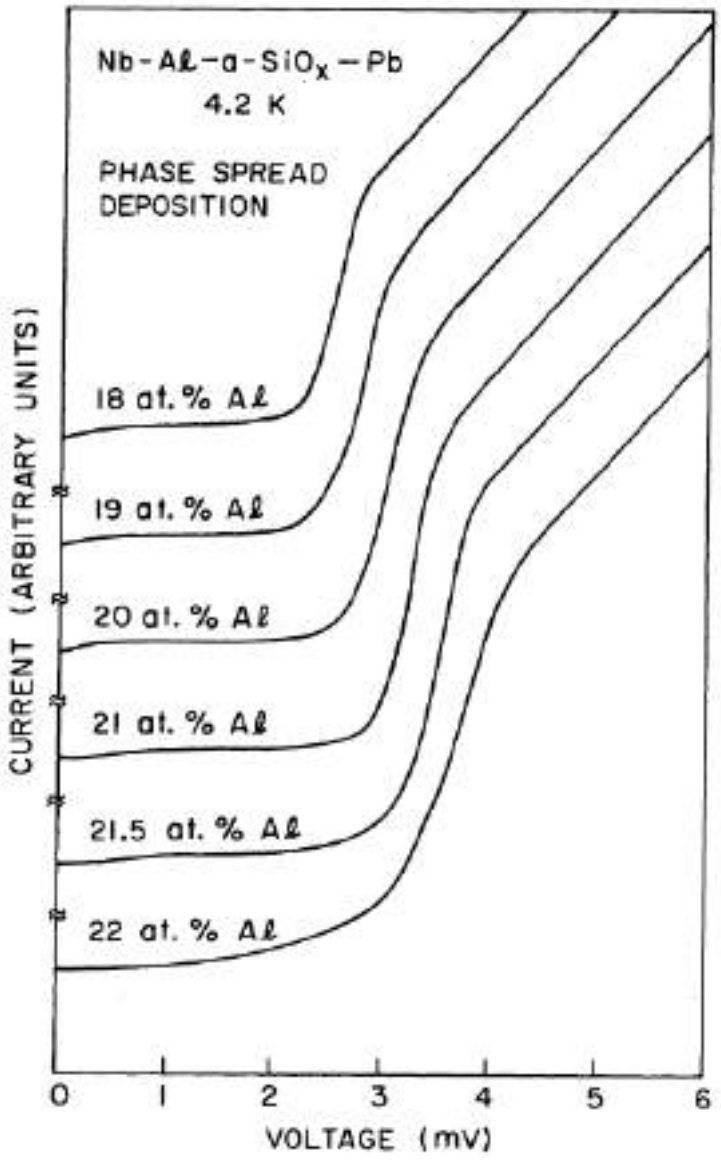

Al %↑ Tc↑

Al %↑ Δ↑

Current voltage characteristics at 4.2 K of a series of *A*15 Nb-Al junctions obtained from a phase-spread deposition at 950 °C. The thickness of the *a*-Si overlay is of 15 A. The *A*15 phase boundary is at 21.8 at. % Al.

Self-Epitaxial Growth

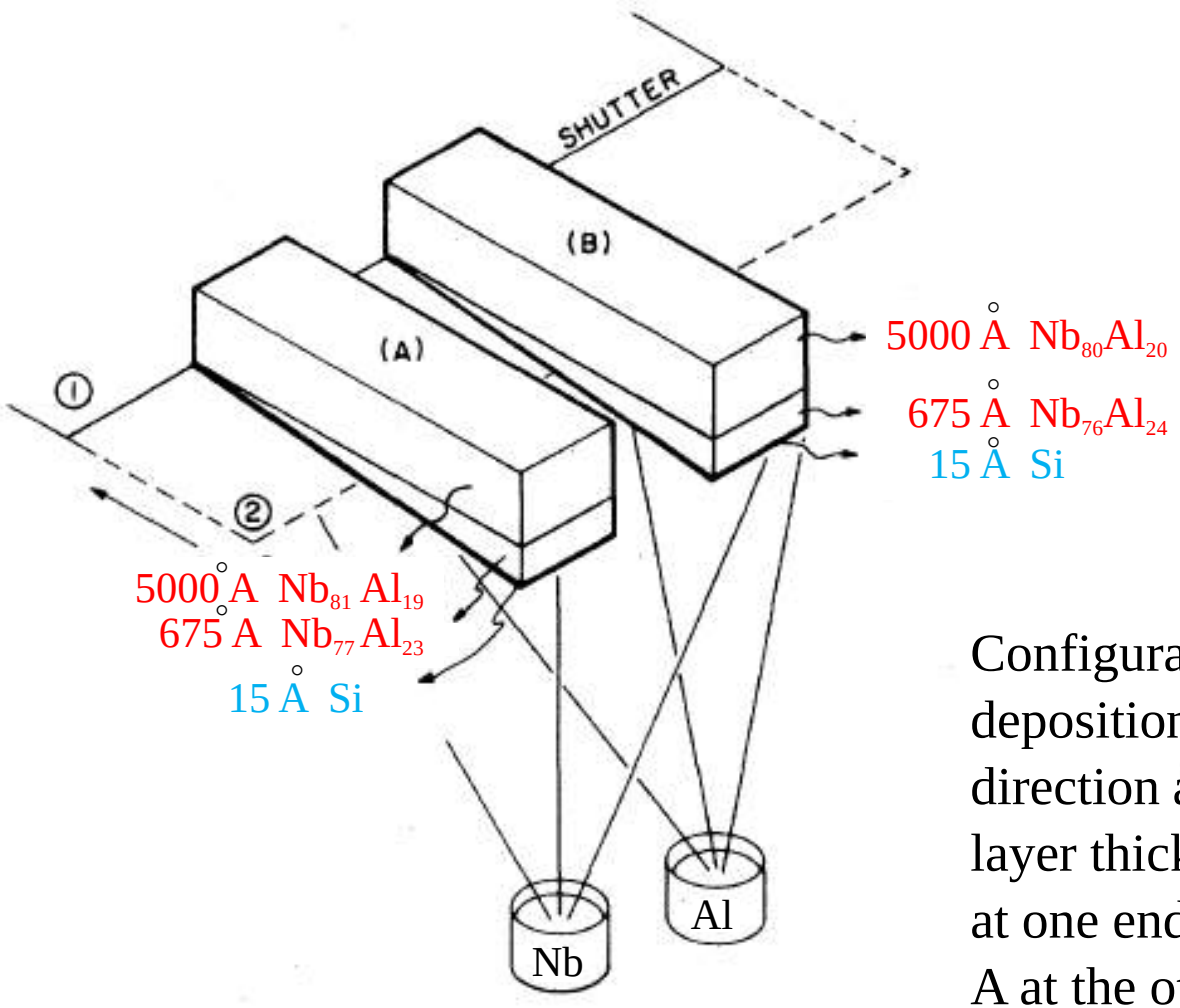

Configuration for the self-epitaxy deposition in the constant phase direction at 950 °C. The epitaxial layer thickness is varying from zero at one end of the ten substrates to 675 Å at the other end.

CONSTANT PHASE CONFIGURATION

The use of tunneling to probe the highest T_c layer via self-epitaxial growth

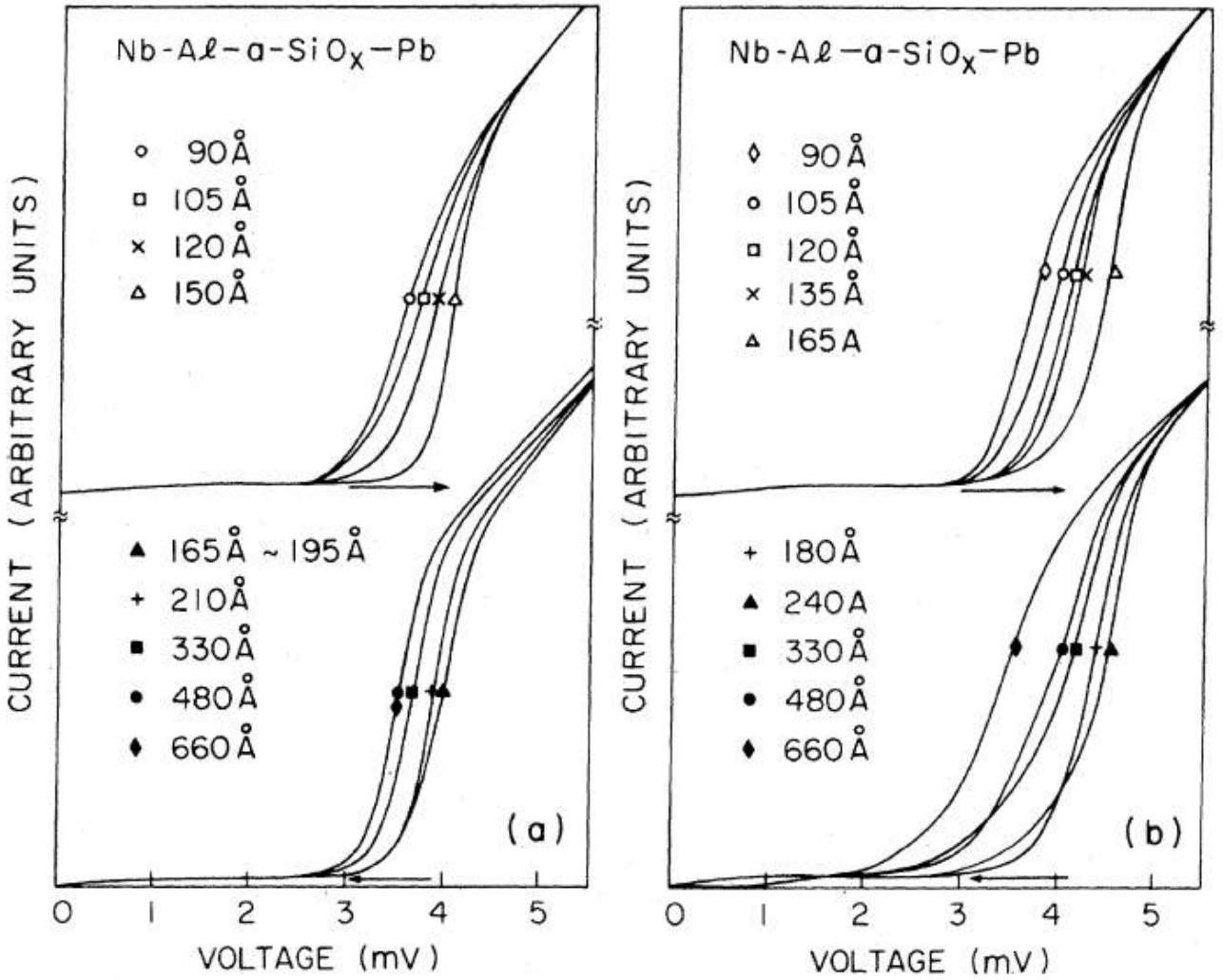

(a) Current vs voltage at 4.2 K of a series of tunnel junctions on the (*A*)-row self-epitaxial samples with epilayer thickness *d* systematically increasing from 90 to 660 A. The composition of the epilayer is of 23 at. % Al. (b) The same for the (*B*)-row self-epitaxial sample. The composition of the epilayer is of 24 at. % Al.

Electron –phonon coupling strength vs composition

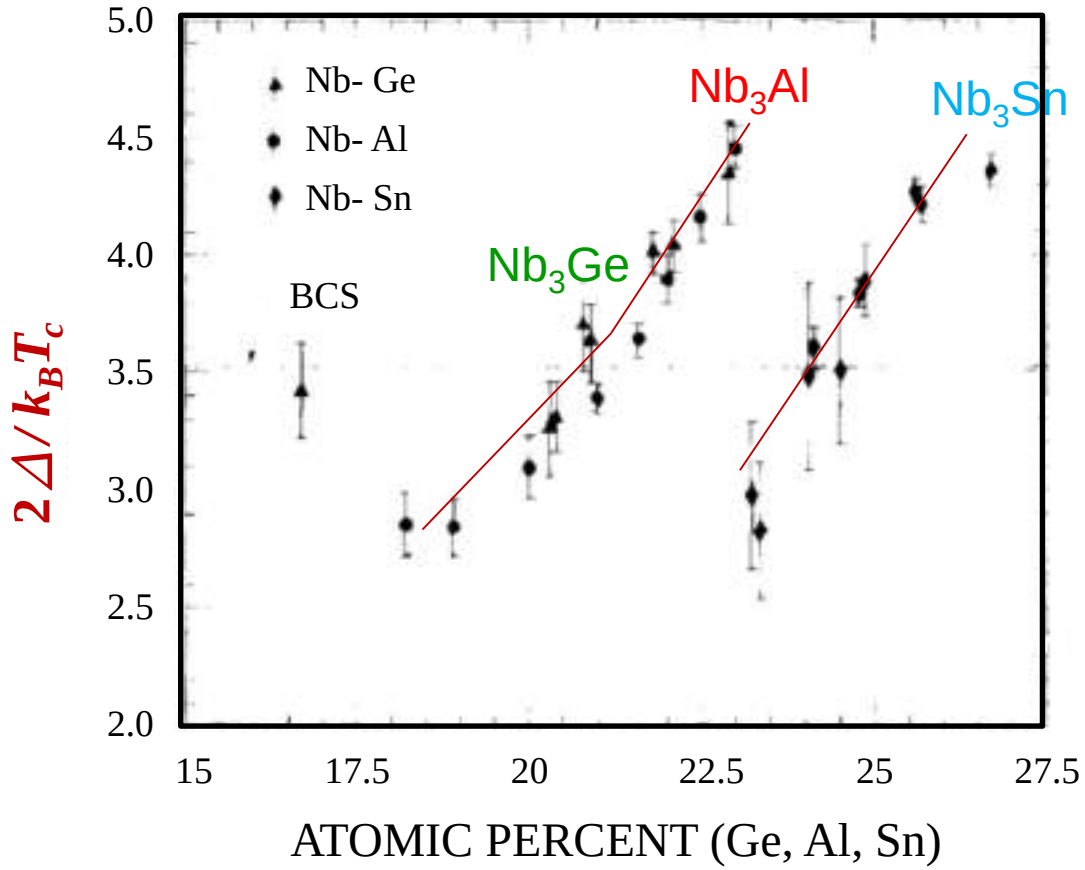

The variation with composition of the electron-photon coupling strength $\mathbf{2\Delta / k_B T_c}$ for the A15 Nb_3Sn, Nb_3Al. And Nb_3Ge.

The origin of this dramatic change of the electron phonon coupling strength of Nb_3Al with the composition approaching the *A*15 phase boundary is not well understood. An insight can be gained from referring to the analytical formula by Kresin *et al.*, [21]

$$2\Delta/k_BT_c = 3.53\,[1 + 5.3\,(T_c/\omega_o)^2\,ln\,(\omega_o/T_c)]$$

, which expresses the enhancement of the coupling strength $2\Delta/k_BT_c$ as an explicit function of the ratio T_c/ω_o, where ω_o is a characteristic Einstein phonon frequency. An analysis based on this formula shows that a change in the $2\Delta/k_BT_c$ ratio from BCS-like to a value as large as 4.4 requires a substantial increase in T_c/ω_o. Since T_c varies only modestly, from 14.0 to 16.4 K, the occurrence of phonon-mode softening, i.e., a smaller ω_o appears to be necessary to account for the large increase in T_c/ω_o. The most direct proof of this supposition is to examine the $\alpha^2F(\omega)$ functions obtained experimentally from tunneling densities of states.

Tunneling density of states and $\alpha^2 F(\omega)$

- The dynamic resistance ***dV/dI*** as a function of the bias voltage has been measured for several Nb-Al junctions of importance.
- Data of the superconducting state were taken at 1.5 K with a magnetic field ~ 1 kG applied to quench the superconductivity in Pb.
- Throughout the data reduction, a constant excess conductance, of about 2-5% of the normal-state conductance, was subtracted out from both the superconducting and the normal-state tunneling conductance.
- The reduced tunneling density of states
  $\boldsymbol{R(\omega) = N_{expt}(\omega)/N_{BCS}(\omega) - 1}$
  was then calculated.

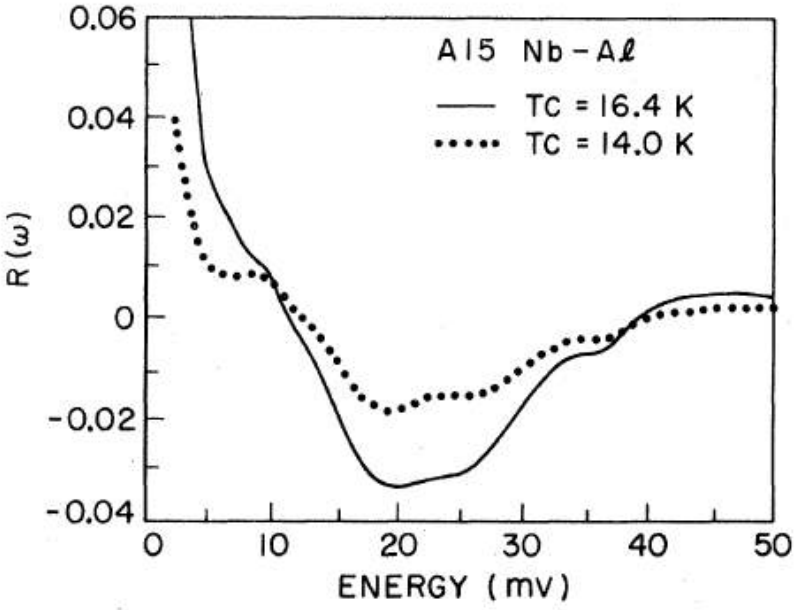

Reduced tunneling density of states $R(\omega)$ vs energy above the gap for the two Nb-Al junctions of T_c = 16.4 K, Δ =3.15 meV, and T_c = 14.0 K, Δ =2.15 meV, respectively.

- Reduced tunneling density of states R(ω)
  $R(\omega) = N_{exp}(\omega) / N_{BCS}(\omega)$ -1
- *Use R(ω) and Δ to deduce to $\alpha^2F(\omega)$ by the MR inversion program to extract* λ and μ^*
- Employ the MMR inversion program to include a normal proximity layer

- **The electron-phonon spectral function $\alpha^2 F(\omega)$** has been generated from the input data of $R(\omega)$ and $\triangle$ by **the gap-inversion analysis** for these two junctions.

- The initial method employed was the conventional McMillan-Rowell inversion program. For the junction with a T_c of 16.4 K and a $\triangle$ of 3.15 meV, that analysis gives a value of only 0.6 for the electron-phonon interaction parameter λ, and a negative value ~ -0.10 for the effective Coulomb pseudopotential μ*. The calculated T_c from these parameters is thus less than 10 K.

- Perhaps the most unphysical result using that analysis is that a high-energy cutoff of less than 30 meV had to be imposed to prevent the iterative solutions from becoming unstable. The structure between 10 and 40 meV, as associated with the Al phonons, was then left out entirely. Furthermore, shown in Fig. 7, there is a large positive offset between the experiment and the calculated $R(\omega)$'s.

Modified McMillan-Rowell (MMR) inversion analysis :

- Based on the model of **proximity-effect tunneling**, proposed by Arnold and implemented by Wolf, it has permitted an improved description, i.e., more self-consistent, of the tunneling data of such Nb and Nb_3Sn junctions within the conventional framework of the strong-coupling theory.
- In this model a thin layer of weakened superconductivity is proposed to exist between the insulating oxide and the base electrode, and it is characterized by a constant pair potential $\Delta_n << \Delta_s$ and a thickness of $d_n << \xi$.
- It is plausible that a thin proximity layer ***N*** exists between the Nb_3Al film and the *a*-Si oxide barrier. With no a priori knowledge about this proximity layer, we approximate it with Δ_n=0.
- The tunneling density of states is then, dependent on two additional parameters of $2d_n/\hbar V_F$ and d_n/l , where d_n , V_F and l are the thickness, the renormalized Fermi velocity, and the mean free path of the proximity layer, respectively.

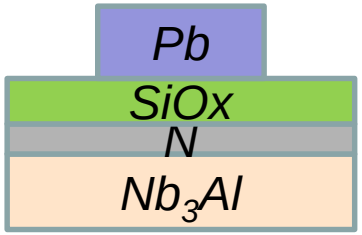

The reduced tunneling density of states $R(\omega)=N_{expt}(\omega)/N_{BCS}(\omega)-1$ was then calculated. Figure shows the $R(\omega)$'s for two particular junctions. One is a relatively weak coupled superconductor, with a T_c of 14.0 K and a gap of 2.15 meV; the other is strong coupled, of larger Al composition by 1.3 at. %, with a higher T_c at 16.4 K and a gap of 3.15 meV. A reduction in the magnitude of $R(\omega)$ is found as the Al composition is decreased, indicating a weakening in the electron-phonon coupling strength. However, the overall shapes of the two $R(\omega)$'s are rather similar, and there is no dramatic change in the positions of structures induced by phonons. Similar behavior is found in the tunneling densities of states of Nb_3Sn junctions of different T_c's and coupling strength.

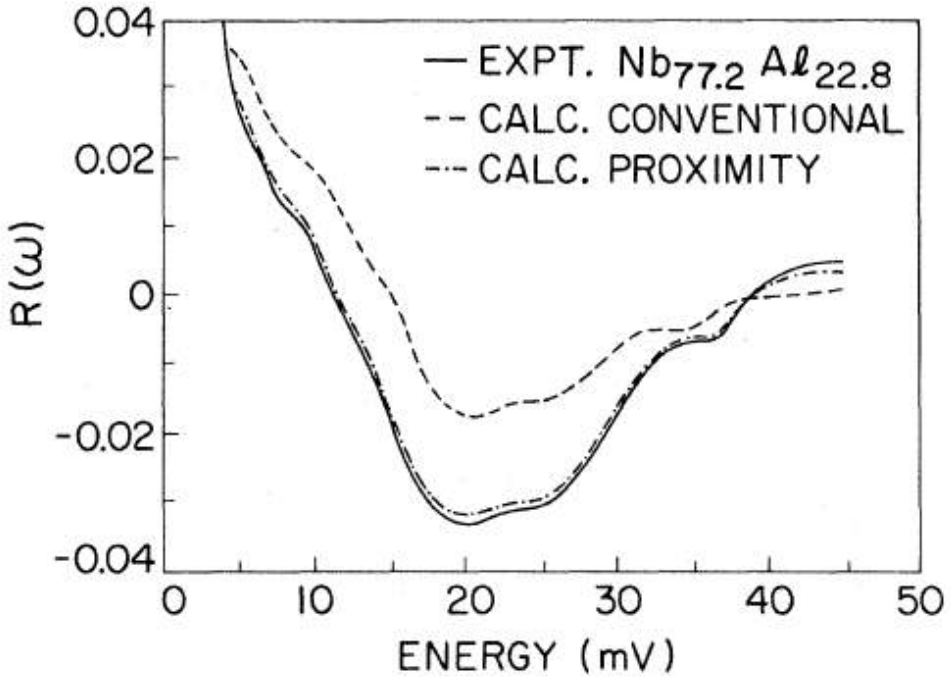

The experimental and calculated tunneling densities of states $R(\omega)$'s from both conventional (MR) and proximity inversion (MMR) analysis for the *A*15 Nb-Al junction of 22.8 at. % Al with T_c = 16.4 K, Δ =3.15 meV.

Features of the $\alpha^2 F(\omega)$ functions of these two junctions are quite similar, with a slight reduction of about 10% in the $\alpha^2 F(w)$ for the lower-T_c one.

However the strong-coupled and high-T_c junction shows a pronounced enhancement in the weightings of the low-frequency phonons, leading to smaller values of the frequency moments. In fact, the significant reduction of λ, from 1.7 to 1.2 in the lower-T_c junction, is mainly from the stiffening of phonons; i.e., $< \omega^2 >$ of larger by 20%.

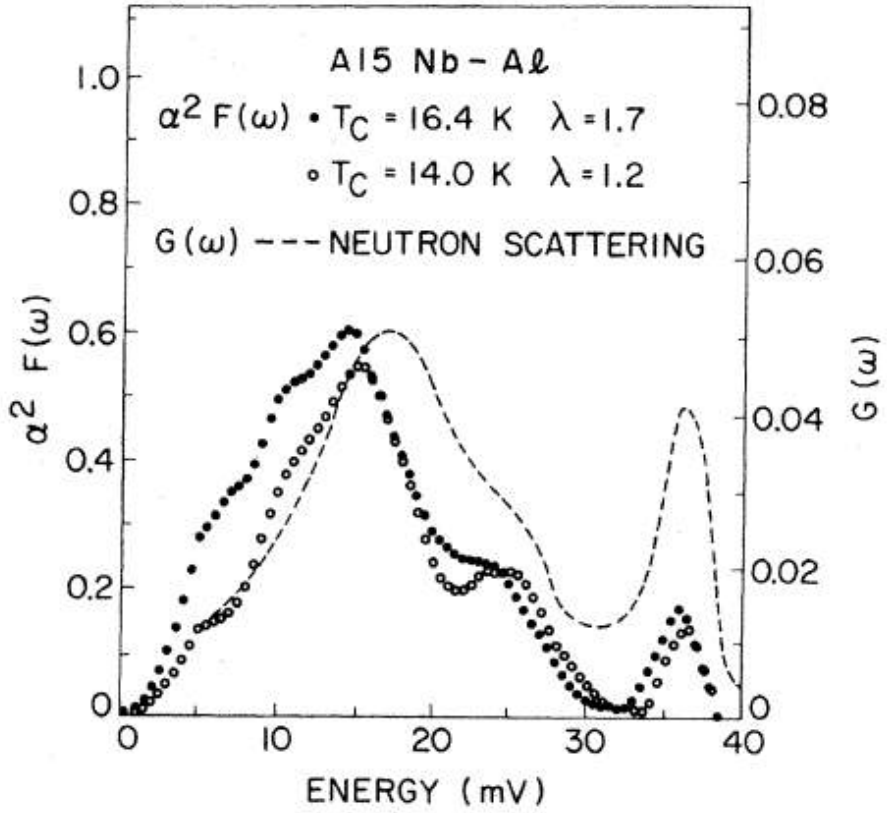

The electron phonon spectral functions $\alpha^2 F(\omega)$ for two Nb-Al junctions with $2\Delta/k_B T_c$ of 3.6 and 4.4. The data of the neutron scattering function $G(\omega)$ are after Schweiss *et al.*

TABLE I. A summary of the parameters from the proximity inversion analysis of two *A*15 Nb-Al junctions and one Nb_3Sn junction.

	Composition	T_c (K) (expt)	Δ (meV) (expt)	$\frac{2\Delta}{k_B T_c}$ (expt)	λ	μ^*	$\omega_{\log}^{b}$ (meV)	$\langle\omega\rangle^{b}$ (meV)	$\langle\omega^2\rangle^{b}$ $(\text{meV})^2$	T_c (K)[c] (calc)	$\frac{2\Delta}{k_B T_c}$ (calc)	$\frac{2d_n}{\hbar v_F^*}$ $(\text{meV})^{-1}$	$\frac{d_n}{l}$
*A*15 Nb-Al	21.5 at.% Al	14.0 ± 0.2	2.15	3.56	1.2 ± 0.05	0.13 ± 0.01	11.2	13.3	226	11.7	3.8	0.0055	0.065
	22.8 at.% Al	16.4 ± 0.1	3.15	4.45	1.7 ± 0.05	0.15 ± 0.02	9.5	11.4	181	15.1	4.3	0.006	0.055
*A*15 Nb-Sn	25.0 at.% Sn	17.7 ± 0.1	3.25	4.26	1.8 ± 0.15	0.16 ± 0.03	10.8	13.1	226	16.7	4.25	0.0097	0.13

$$T_c = \frac{\Theta_D}{1.45} \exp\left\{-\left[\frac{(1+\lambda_{ep})}{\lambda_{ep} - \mu^*(1+0.62\lambda_{ep})}\right]\right\}$$

the analytical formula by Kresin *et al.*,

$$2\Delta/k_B T_c = 3.53\,[1 + 5.3\,(T_c/\omega_o)^2 \text{ in } (\omega_o/T_c)]$$

which expresses the enhancement of the coupling strength $2\Delta/k_B T_c$ as an explicit function of the ratio T_c/ω_o, where ω_o is a characteristic Einstein phonon frequency.

$$^{a}\lambda = 2\int d\omega\omega^{-1}\alpha^2 F(\omega).$$

$$^{b}\omega_{\log} = \exp\left[\frac{2}{\lambda}\int d\omega\omega^{-1}\ln\omega\alpha^2 F(\omega)\right] .$$

$$^{c}T_c = \frac{\langle\omega\rangle}{1.2}\exp\left[\frac{-1.04(1+\lambda)}{\lambda - \mu^*(1+0.62\lambda)}\right] , \text{ see Ref. 30.}$$

$$\lambda = N(0) \langle I^2 \rangle / M\langle\omega^2\rangle$$

- The electron-phonon coupling constant λ can be expressed according to McMillan, as $\lambda = N^b(0)\langle I^2\rangle / M\langle\omega^2\rangle$

, where $N^b(0)$ and $\langle I^2\rangle$ are the electronic band density of states, and the electron-phonon matrix element, evaluated over the Fermi surface, respectively.

- The electronic parameter $N^b(0)$ (bare) can be estimated from the renormalized density of states $N^*(0)$ by specific heat experiments

$$C_{el} = 1/3\ \pi^2 N^*(0) K_B^2\ T$$

$$N^b(0)\left[\frac{\text{states}}{\text{eV spin unit cell}}\right] = \frac{17.8}{1+\lambda}\gamma^{*M}\left[\frac{\text{mJ}}{\text{cm}^3\text{K}^2}\right],$$

Also from upper critical field analysis, given that the (1+ λ) factor is known from tunneling.

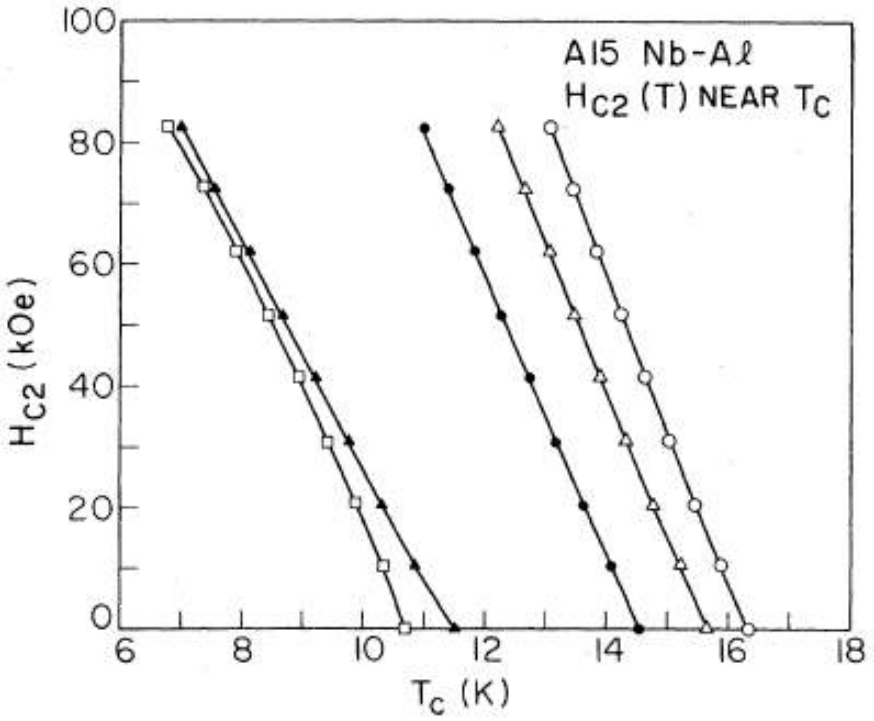

FIG. 1. Representative critical-field data near T_c of a series of *A*15 Nb-Al films measured. The lines drawn through data points are intended to serve only as a guide to the eye.

Based on the data of the critical-field slope near T_c, the general procedure of evaluating various superconducting and normal-state parameters including $N^b(0)$ is well formulated. Briefly, **the slope of critical field near T_c** including corrections for the electron-phonon interaction can be expressed as

$$\left.\frac{dH_{c2}}{dT}\right|_{T_c} = \eta_{H_{c2}}(T_c)\left[9.55\times10^{24}\gamma^{*2}T_c\left(\frac{n^{3/2}S}{S_F}\right)^{-2} + 5.26\times10^{4}\gamma^{*}\rho(\Omega\,\mathrm{cm})\right]\times[R(\gamma_{tr})]^{-1}\ \mathrm{Oe/K}\ ,$$

The electron-phonon spectral function $\alpha^2 F(\omega)$

Nb_3Sn

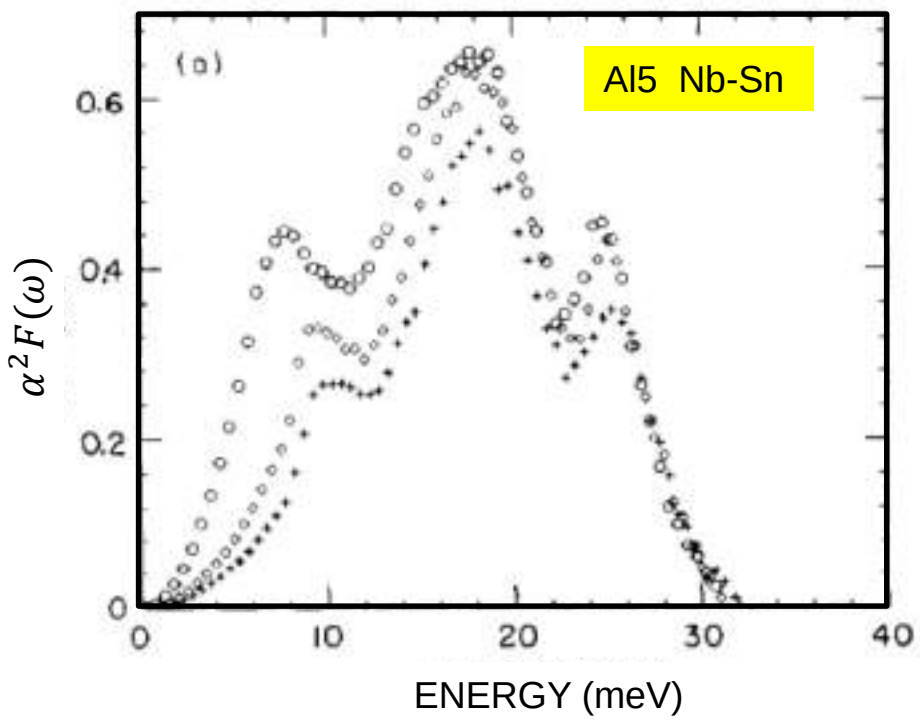

Nb_3Ge

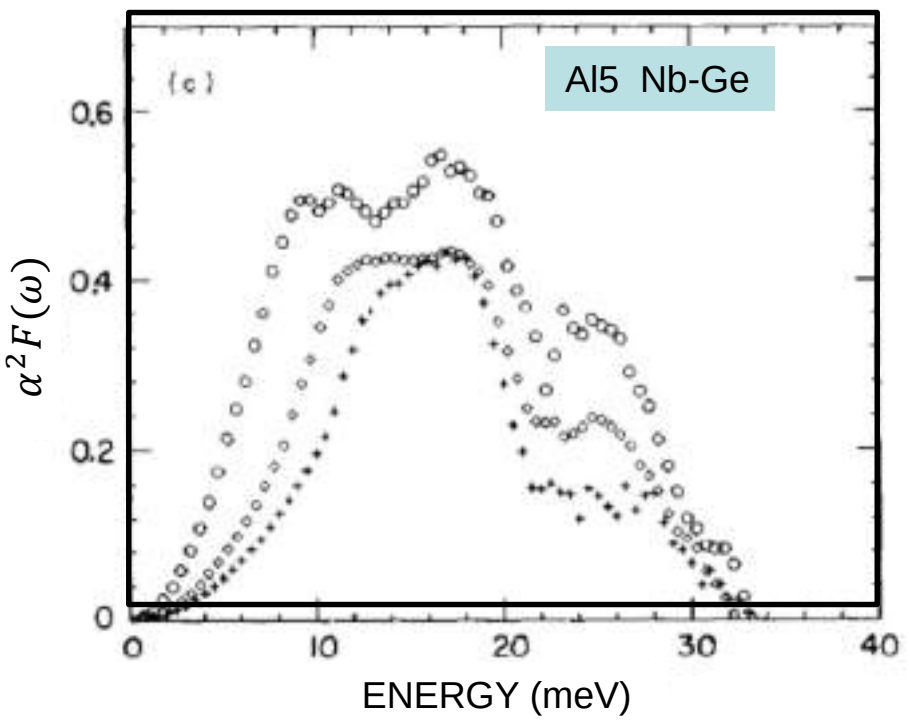

Superconducting tunneling into high temperature superconductors of $YBa_2Cu_3O_7$ crystals and films (90K)

Break-junction Tunneling on HTSC ceramics (1987)

PHYSICAL REVIEW B VOLUME 35, NUMBER 16 1 JUNE 1987

Break-junction tunneling measurements of the high-T_c superconductor $Y_1Ba_2Cu_3O_{9-\delta}$

J. Moreland, J. W. Ekin, L. F. Goodrich, T. E. Capobianco, and A. F. Clark
Electromagnetic Technology Divison, National Bureau of Standards, Boulder, Colorado 80303

J. Kwo, M. Hong, and S. H. Liou
AT&T Bell Laboratories, Murray Hill, New Jersey 07974
(Received 25 March 1987; revised manuscript received 7 May 1987)

Current-voltage tunneling characteristics in a high-critical-temperature superconducting material containing predominately $Y_1Ba_2Cu_3O_{9-\delta}$ have been measured using the break-junction technique. Sharp gap structure was observed, with the largest superconductive energy gap measured to be $\Delta = 19.5 \pm 1$ meV, assuming a superconductor-insulator-superconductor junction. This energy gap corresponds to $2\Delta/k_BT_c = 4.8$ at $T = 4$ K, for a critical temperature of 93 K (midpoint of the resistive transition).

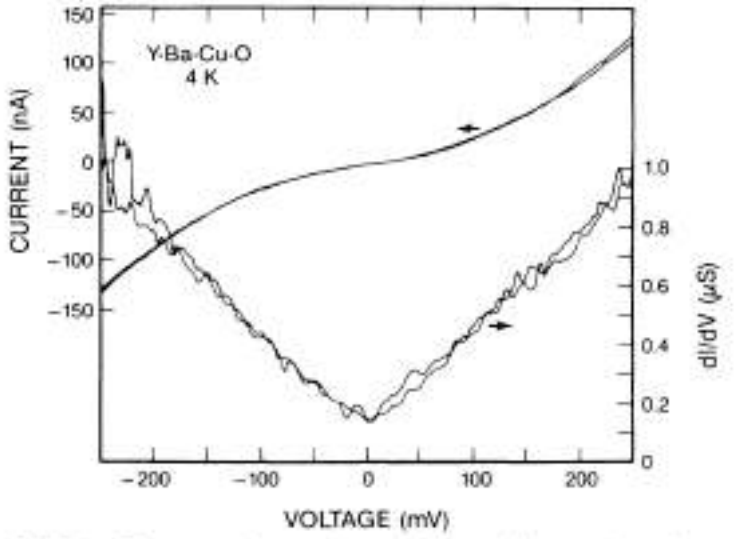

FIG. 1. Current-voltage characteristic and dynamic conductance (dI/dV) characteristic of a $Y_1Ba_2Cu_3O_{9-\delta}$ break junction immersed in liquid helium. This trace is typical of that predominately seen in the sample.

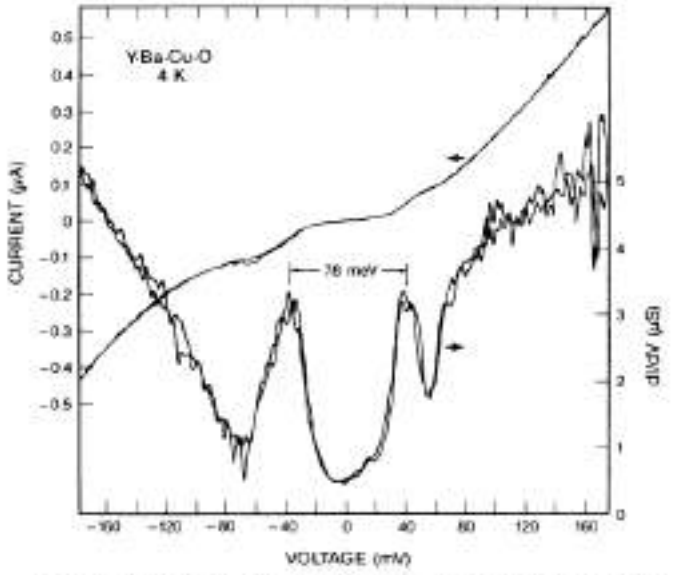

FIG. 2. Current-voltage characteristic and dynamic conductance (dI/dV) showing superconducting gap structure typical of the largest measured in the $Y_1Ba_2Cu_3O_{9-\delta}$ break-junction sample.

Reproducible Tunneling Data on Chemically Etched Single Crystals of $YBa_2Cu_3O_7$

M. Gurvitch, J. M. Valles, Jr., A. M. Cucolo,[a] R. C. Dynes, J. P. Garno, L. F. Schneemeyer, and J. V. Waszczak

AT&T Bell Laboratories, Murray Hill, New Jersey 07974

(Received 26 May 1989)

We have fabricated tunnel junctions between chemically etched single crystals of $YBa_2Cu_3O_7$ and evaporated metal counterelectrodes which exhibit reproducible characteristics. Above the bulk critical temperature of $YBa_2Cu_3O_7$, T_c, the conductance, $G(V)$, has a linear dependence with voltage and has some asymmetry. Below T_c, additional structure associated with the superconductivity appears in $G(V)$. At $T \ll T_c$ there is a reproducible, finite, zero-bias conductance which suggests that there are states at the Fermi energy in superconducting $YBa_2Cu_3O_7$. Junctions with Pb, Sn, Bi, Sb, PbBi, and Au counterelectrodes all show qualitatively similar behavior.

PACS numbers: 74.50.+r, 74.65.+n

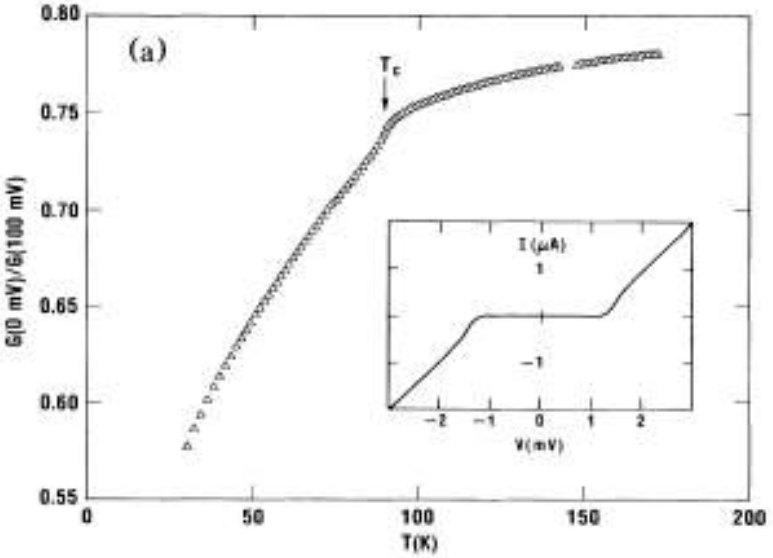

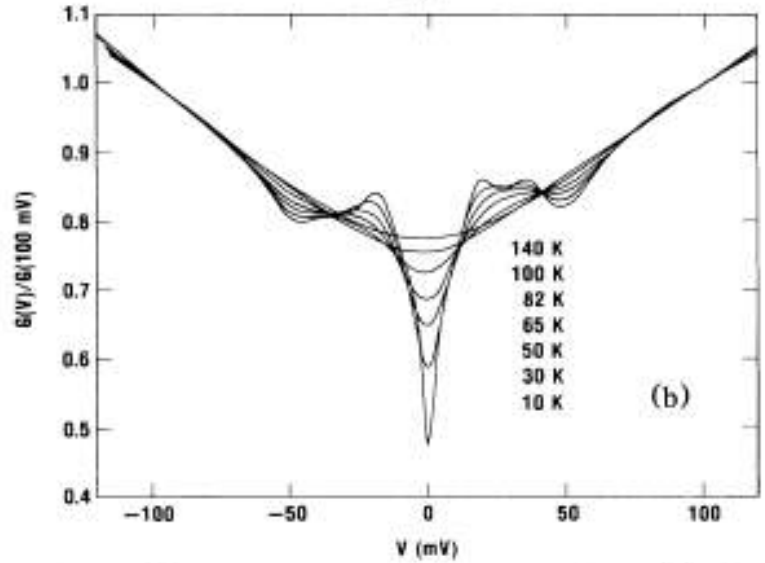

FIG. 1. (a) Temperature dependence of $G(0\text{ mV})/G(100\text{ mV})$ of a $YBa_2Cu_3O_7$/Pb junction. Inset: Current vs voltage for a typical junction for $T < 1$ K. Note the absence of leakage. (b) Voltage dependence of $G(V)/G(100\text{ mV})$ for the temperatures indicated for the junction in (a). The lowest-temperature curve has the lowest zero-bias conductance. The polarity refers to the $YBa_2Cu_3O_7$ electrode.

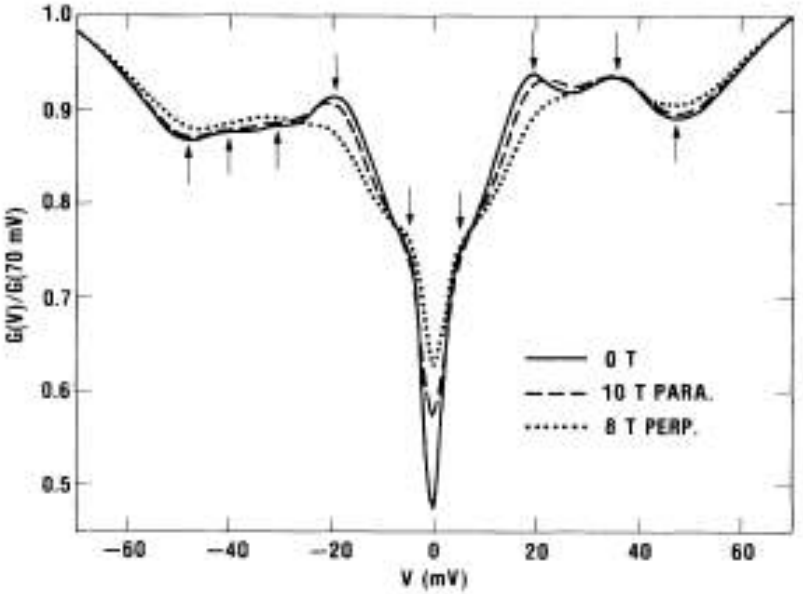

FIG. 2. $G(V)$ for $YBa_2Cu_3O_7$/Pb junction in 0 T (solid line), 10.0 T (dashed line), and 8.0 T (dotted line) magnetic fields at $T = 10$ K. Arrows indicate features which are discussed in the text.